63-2-4

PROGRESS REPORT

OF
CONTRACT NONR 3173
GEM CONTROL SYSTEMS STUDY

AP-5061-R December 7, 1962

THE GARRETT CORPORATION
AiResearch Manufacturing Division
Phoenix, Arizona

PROGRESS REPORT

OF
CONTRACT NONR 3173
GEM CONTROL SYSTEMS STUDY

AP-5061-R December 7, 1962

Prepared by B. W. Andersen
R. V. Boyle
O. A. Becker

Approved by M. C. Steele
M. C. Steele, Supvr Control Systems Analysis

W. M. Norgren
W. M. Norgren, GEM Project Engineer

THE GARRETT CORPORATION
AiResearch Manufacturing Division
Phoenix, Arizona

REPORT NO. AP-5061-R

TOTAL PAGES 135

ATTACHMENTS:

Appendix A
Appendix B
Appendix C
Appendix D

References

REV	BY	APPROVED	DATE	PAGES AND/OR PARAGRAPHS AFFECTED

MP-1208

THE GARRETT CORPORATION
AiResearch Manufacturing Division
Phoenix, Arizona

TABLE OF CONTENTS

THE GARRETT CORPORATION
AiResearch Manufacturing Division
Phoenix, Arizona

LIST OF ILLUSTRATIONS

LIST OF ILLUSTRATIONS (CONT'D)

LIST OF ILLUSTRATIONS (CONT'D)

LIST OF ILLUSTRATIONS (CONT'D)

LIST OF SYMBOLS

A_B - total base area

a - vehicle base width

a_p - displacement of ducted propellers in y direction

$\bar{a} = \frac{2y_s}{a}$

$\bar{A}$ = mean vertical displacement of water surface beneath vehicle

b - vehicle base length

$\bar{b} = \frac{2x_s}{b}$

b_w - "moment arm" of relative wind (aft of vehicle c.g.)

$\bar{B}$ - mean slope of water surface beneath vehicle

$B = P/\rho V_j^2$

$B_{io} = P_{io}/\rho V_j^2$

c_D - drag coefficient

c_L - lift coefficient

C - jet length

g - acceleration of gravity

G_i - peripheral jet width

G_{ik} - compartmentation jet width

h	-	operating height
I_x	-	moment of inertia about x axis
I_y	-	moment of inertia about y axis
I_z	-	moment of inertia about z axis
m	-	mass
P	-	pressure
P_i	-	compartment i pressure
P_o, P_t	-	total pressure
P_{io}	-	pressure that just turns the jet
Q_{fi}	-	fan i air flow
Q_i	-	jet i air flow
Q_{ik}	-	jet ik air flow
Q_f	-	total fan air flow
R	-	universal gas constant
s	-	operator denoting differentiation with respect to time
T	-	temperature
t	-	time
T_p, T_s	-	thrust of port and starboard propeller

U_x - velocity in x direction

U_y - velocity in y direction

U_{xr} - velocity of relative wind in x direction

U_{yr} - velocity of relative wind in y direction

V_w - wind velocity

V_j - jet velocity

W_c - vehicle weight

x - roll axis and body coordinate in fore-aft direction

x_a - "moment arm" of aerodynamic lift

$x_s = \frac{b + 2a}{a + b} \left(\frac{b}{4}\right)$

y - pitch axis and body coordinate in side direction

y_a - moment arm of aerodynamic lift

$y_s = \frac{a + 2b}{a + b} \left(\frac{a}{4}\right)$

Z_p - displacement from vehicle center line of ducted propellers

z - yaw axis

Z_w - water displacement

β - angle between inertial axis X and real wind

Δ - change from steady state

ζ - damping ratio

η_A - augmentation efficiency

η_Q - discharge coefficient for flow under jet

θ - pitch angle

θ_j - jet discharge angle

ρ - air density

ρ_w - water density

Σ - summation symbol

τ - time constant

ϕ - roll axis

ψ - yaw axis

ω - frequency

ω_n - natural frequency

THE GARRETT CORPORATION
AiResearch Manufacturing Division
Phoenix, Arizona

Normalized Quantities

$$\overline{T} = \frac{T}{W_c} \quad \text{(thrust)}$$

$$\overline{U}_x = \frac{U_x}{b}$$

$$\overline{U}_y = \frac{U_y}{a}$$

$$\overline{V}_w = \frac{V_w}{b}$$

$$\overline{\theta} = \frac{b}{2h}\,\theta$$

$$\overline{\phi} = \frac{a}{2h}\,\phi$$

$$\overline{Z} = \frac{Z}{h}$$

$$\overline{P}_i = \frac{A_B}{W_c} P_i$$

$$\overline{Q} = \frac{Q}{Q_{fo}} \qquad Q_{fo} = \text{steady-state flow}$$

HI GAIN AMPLIFIER

SUMMING AMPLIFIER

INTEGRATING AMPLIFIER

CONSTANT COEFFICIENT

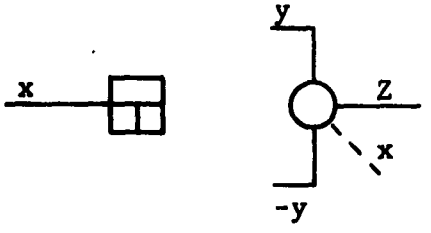

SERVO MULTIPLIER Z = xy

NONLINEAR FUNCTION GENERATOR

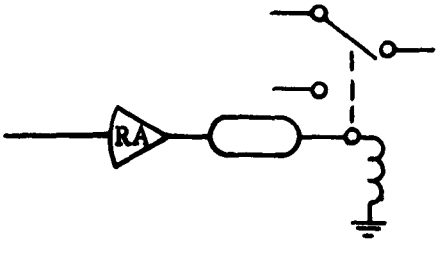

RELAY SWITCH

THE GARRETT CORPORATION
AiResearch Manufacturing Division
Phoenix, Arizona

PROGRESS REPORT OF CONTRACT NONR 3173 GEM CONTROL SYSTEMS STUDY

1.0 INTRODUCTION

This report will include a summarization of that work performed under Navy Contract NONR 3173 from November 1961, to November 1962.

The AiResearch GEM Control Systems Study as it existed early in 1962 (as reported in AP-5047-R, Reference 1) consisted of an analytical formulation upon which one could accurately predict the natural characteristics of virtually any vehicle. This formulation was incorporated into a digital computer program used to calculate the steady-state characteristics and an analog computer simulation that accurately represented the vehicle in the transient modes of pitch, roll, and heave.

It could be considered that the primary aim of the work performed since the last progress report has been to establish a complete analytical formulation of a typical ground effect machine that would be fully controllable in 6 degrees of freedom.

The initial approach was of course completely general in that it could apply to virtually any peripheral jet, compartmented-base vehicle. Upon further study, however, it was found that the analysis was growing far too complex for any practical application. However, defining a reference design vehicle and making certain valid assumptions allowed the formulation to be radically simplified.

In summary, the efforts have been extended toward the accomplishment of the following tasks:

(1) Simplification and linearization of the basic equations of pitch, roll, and heave motion. Previously, there existed in this formulation nonlinearities that were shown to have very little effect upon the response of the vehicle. These nonlinearities arose primarily from the equations describing the transient behavior of the base pressure. It is now assumed that the rate of change of base pressure is zero--i.e., the new pressure is reached instantaneously following a perturbation.

(2) Development of the remaining three equations of motion for yaw, "forward flight," and "side slip" to complete the 6-degree-of-freedom simulation.

(3) Analytically describe the forces and moments that partially comprise the above-mentioned equations of motion and the former 3 degrees of freedom, arising from aerodynamics due to relative wind.

(4) Development of an analytical representation of the water dynamics beneath a vehicle, including the all-important "hump" speed.

(5) Physically define a complete vehicle, including the power source, the air-moving equipment, and the propulsive means.

(6) Analytically describe the dynamics of the engine, fan-duct system, and propulsion propellers.

(7) A preliminary design and simulation of a suitable control system, including the characteristics of the system.

(8) Construction of pilots' controls that will provide an electrical signal to the analog computer following a control command input. This system includes a pilot display of pitch angle, roll angle, yaw angle (relative heading), yaw rate, forward velocity, side velocity, and an x-y plot of position.

(9) Generate and perform a test program in order to evaluate the over-all characteristics of the reference design vehicle.

2.0 ANALYSIS FORMULATION

The purpose of this section will be to discuss the steps leading to the analytical formulation and analog computer simulation of the Reference Design Vehicle that is controllable in 6 degrees of freedom. The appendices at the end of this report contain complete derivations of the analytics involved in the final formulation; therefore, no derivations will be presented here.

2.1 Linearization and Simplification

In order to utilize the analytics as they existed at the beginning of this phase of the study, it was first necessary to make certain assumptions in order to reduce the complexity of the over-all formulation.

2.1.1 Basic Simplifying Assumptions

(a) The base area is divided into four equal areas such that $A_i = A_B/4$. The four areas or compartments are defined by the stabilizing (compartmentation) jets and the peripheral jets. This makes possible the further assumption that at steady-state hover conditions, the pressures (P_i) in all four compartments (i) are equal.

(b) The above-mentioned base compartment pressure is an average steady-state value (P_i) plus a variation (p_i). The average steady-state value will be seen to be less than the quantity Wc/A_B by an amount that is equivalent to the vertical thrust produced by the jets.

(c) The fan air flow (Q_{fi}) is a steady-state value plus a variation (q_{fi}).

(d) The products of variable terms in the jet flow equations are neglected in the peripheral jet equations but are retained in the compartment jet equations because of relative magnitude.

(e) The effects of pitching, rolling, and heaving motions upon the compartment jet heights are neglected ($\bar{h}_{ik} = 1$).

(f) The rate of change of pressure in a compartment is zero--that is, the new pressure level is reached instantaneously following a perturbation. Previously, the simulation contained the equations for the rate of change of pressure ($\dot{P}_i$). These equations had to be integrated in order to reach the new pressure level. The rate of change of pressure was so great that the actual integration could not be done rapidly enough. For this reason the former simulation was not in real time but had been "slowed down" by a factor of 10. With the assumption that pressure reaches its new value instantaneously, the simulation is now in real time.

(g) The peripheral jets are assumed to be always underfed.

(h) The compartment jets are assumed to be always overfed.

Equations (A-38), (A-39), and (A-40) are the general equations of motion for heave, roll, and pitch. It is noted that they have not only been simplified using the above assumptions but also that they have been normalized and linearized to a certain degree.

At this point the base configuration of the reference design was introduced, and the equations for the rate of change of pressure ($\dot{\bar{p}}_i$), flow ($\bar{Q}_i$ and $\bar{Q}_{ik}$), and body motions were written for this particular model.

In Section 3 of Appendix A the completely linear equations of motion in pitch, roll, and heave are developed. It is noted that Equations (A-92), (A-96), and (A-100) present the variations in heave, pitch, and roll due to fan flow variations and surface disturbances.

2.2 Six-Degree-of-Freedom Equations

Appendix B contains the development of the equations of motion in 6 degrees of freedom. Section 1 of Appendix B shows the general equations of motion of a body free to translate in three dimensions and rotate about 3 body-fixed axes. In order to simplify these equations, it is assumed that the origin of the body-fixed axis system coincides with the center of mass and also that the body fixed axes are the principal axes (those axes about which the products of inertia go to zero).

The primary concern of Section 2 is the analytical description of the external forces and moments that act on the vehicle in "flight." These forces and moments will arise from the following:

(1) Propeller Thrust - The reference design vehicle has as its primary source of propulsion two variable-pitch propellers mounted on the "stern" of the craft. These propellers, when manipulated together, provide thrust for forward flight and braking. When operated differentially they provide a moment about the vertical axis for yawing. The propellers also produce a pitching moment about the lateral (y) axis.

(2) Pitching and Rolling - These motions about the longitudinal and lateral axes produce forward and side forces resulting from components of lift. The force in the lateral direction due to rolling the craft will be the only force available in this direction other than aerodynamic forces.

(3) External Aerodynamics - The vehicle is subjected to a number of forces and moments arising from external aerodynamics. These aerodynamic forces become appreciable only when the vehicle travels at high speed. They are, however, analytically described over the full range of speeds. They are shown to affect the following areas:

(a) Lift - at forward speed the cushion is augmented due to an aerodynamic lift.

(b) This lift acts forward of the craft center of gravity, therefore producing a pitching moment.

(c) Stability in the yaw mode is achieved by aerodynamic forces acting aft of the center of gravity, thus producing yaw moments that tend to restore the craft to a longitudinal translation.

(d) Parasite drag or air friction produces a force that resists motion.

(e) An induced pressure occurs around the periphery of the vehicle which can be considered as a variation in the "ambient" pressure which will, in turn, produce slight variations in base pressure.

(f) Momentum drag results from a combination of forward velocity and the air flow to the fans. At forward or side flight the air mass that is directed into the fan intakes is forced to change direction, which produces a rather large drag force on the craft.

As the exact shape and configuration of the vehicle are not established, it is pointed out that many of the parameters such as lift and drag coefficients, thrust characteristics of the propellers, and internal aerodynamics are only estimates based upon preliminary calculations by the Aerodynamics Group.

(4) Wind - To study the handling characteristics of the vehicle in a cross wind, the term "relative wind" is seen to include both the effects of flight and wind.

The final six equations of motion are full range equations such that with the proper input commands the vehicle can be maneuvered throughout a full range of operations. It is noted that these equations no longer contain the terms describing an ocean wave moving beneath the craft. The effects of these waves on a vehicle were described in the April, 1962, progress report (AP-5047-R). In the present simulation, however, it was impossible to include these terms, due to a shortage of electronic multipliers in the analog computer.

2.3 Surface Deflections, Base Pressure Variations and Effects of Water Dynamics upon Body Motions in the Transient

2.3.1 The simulation of a vehicle capable of maneuvering over water would be incomplete without a description of the water surface dynamics due to the presence of a pressure area (vehicle's cushion pressure) over the surface.

J. J. Stoker* has presented the general solution of the deflection of the water surface in a free stream flowing beneath a pressure area of a finite length. Stoker's solution is in the form of an integral of an analytic function as presented in Appendix C.

* Reference 3

In order to determine the surface displacement at discrete points over the length of the pressure area, it was necessary to integrate the function. However, integration of the function yielded not elementary functions but rather an infinite power series upon successive integration by parts. For this reason it was necessary to perform a numerical integration. After defining the integrals and their paths, Simponson's rule was applied to the functions which, with the aid of a digital computer program, yielded a set of surface shapes that were a function of the free-stream velocity and applied pressure.

This method of solution was, of course, far too complex and lengthy to be of any practical use other than as a comparison. Therefore, an equation was introduced that very closely approximated those surface shapes calculated by the computer, using the exact solution. This equation can be thought of as a traveling wave of fixed shape moving with the craft. From this equation two expressions were obtained. One gives the mean vertical displacement as a function of forward velocity, while the other gives the mean slope of the water surface as a function of forward speed.

The water slope, as it may be considered a disturbance, will be included in the pitch equation. This is the term that analytically describes the "hump" that is developed beneath and in front of a vehicle as it accelerates from hover to cruise speed.

The second of the expressions, that gives the mean displacement of the surface, will be used only as a descriptive term in a frequency-modifying term.

2.3.2 Relative wind, the combination of vehicle and wind velocities relative to the surface produces induced pressures around the periphery of a vehicle. For example, while the vehicle is traveling forward at high speeds, a high-pressure area is produced at the front of the vehicle due to the velocity "head" and a low-pressure area is created around the sides and rear of the craft. This effect, or the variation in ambient pressure around the jets causes variations in base pressure.

Section 2.0 of Appendix C presents the expressions that analytically show the effect upon body motions of these varying ambients.

2.3.3 As a vehicle pitches, rolls, or heaves while hovering or traveling at low speed, the surface of the water tends to "follow" the motion of the vehicle. This is caused, for example, when the nose pitches down and the pressure beneath the nose momentarily rises, causing an increased depression of the water surface. In effect, this produces a decrease in the "cushion spring rate" resulting in a lower natural frequency.

Section 3.0 in Appendix C presents the derivation of this frequency-modifying term for the three motion modes of pitch, roll, and heave. It should be noted that as forward speed increases, the effect of water dynamics upon body motion diminishes. The previously mentioned term for the mean displacement is seen to be a function of forward speed, and it is further noted that this term approaches zero as speed increases. Therefore, this term is used to make the frequency-modifying term a function of forward velocity as seen in Section 3.0 of Appendix C.

2.4 Reference Design Vehicle

As mentioned previously, the complete simplification, linearization, and normalization of the formulation partially depended upon defining a reference design vehicle. This section will present the following information regarding the reference design vehicle:

(a) Physical description, including shape and general configuration. (Figure 2-1)

(b) Air-moving equipment, including power supply, cushion, propulsive fans, and propellers.

(c) Control system philosophy.

(d) Summary of the parameters and functions used in simulation.

2.4.1 The base planform is rectangular and symmetrical about the x and y axes. The periphery is defined by peripheral jets that are directed down and inward at a 45° angle with the vertical. The base is divided into four equal areas by the compartmentation or stabilizing jets which are directed vertically downward. It is assumed that the center of pressure of each compartment is located at its geometric center.

The jets themselves are divided into four groups, each of which defines a compartment. The air flow to these jets is supplied by one fan located above the compartment. With this scheme the flow and subsequently the pressure in any one compartment is controlled by varying the flow to the fan itself.

The external shape of the vehicle is streamlined as much as possible with the only major obstructions being the fan inlets, cockpit, and ducted propellers mounted on the stern above the deck of the vehicle.

2.4.2 The power supply consists of a pair of gas turbine engines which drive two fans and one ducted propeller each. The engines are basically constant speed with a droop-type governor. The speed may be manually adjusted by means of a fine speed set point. This adjustment is provided so that the pilot may trim in roll and heave by adjusting the engine speed.

The "lifting" fans are radial-flow, constant-speed fans which discharge into ducts leading to the proper jets. Control of the air flow is achieved by varying inlet guide vanes directly upstream of the fans.

Propulsion is obtained by variable-pitch, ducted propellers mounted on the stern of the vehicle. Each propeller is driven at a constant speed by a separate engine.

2.4.3 Control System

The basic control system consists of the following pilot-operated components:

(a) Pitch Control - is achieved by differentially controlling the pressure in the two front compartments versus the two rear compartments. Pressure changes are achieved by varying the air flow to the compartments. Variable pitch

inlet guide vanes upstream of the fans provide control over the air flow to the fans. The pilot then can cause the vehicle to pitch by changing the position of the inlet guide vanes. Pitch trim is obtained by a separate fine adjustment of the inlet guide vanes.

(b) Roll Control - is achieved in exactly the same manner as pitch except, of course, the two port compartments are controlled differentially with the two starboard compartments. Roll trim is achieved by adjustment of the fine speed set point on the engines.

(c) Heave Control - It is not anticipated that continuous control over heave will be desirable. Therefore, control will be achieved by adjustment of the fine speed set point on the engines.

(d) Fore and Aft Speed Control - is achieved by collectively changing the pitch on the two ducted propellers. A small amount of additional fore and aft "thrust" is obtained by pitching the vehicle and thus obtaining a fore and aft component of lift.

(e) "Side Slip" Control - Translation in a side-ways direction is achieved by rolling the vehicle and thus obtaining the component of lift. This is a small force, however, since high speeds in the side direction are neither anticipated nor desirable.

(f) Yaw Control - is achieved by differentially manipulating the pitch on the ducted propellers.

2.4.4 Reference Design Parameters (See Fig. 2-1)

Physical Dimensions

A_B = 1593 ft^2

W_c = 78,140 lb

I_x = 3.086 x 10^6 lb ft^2

I_y = 8.786 x 10^6 lb ft^2

I_z = 10.0 x 10^6 lb ft^2

a = 27 feet

b = 59 feet

Z_p = 9 feet

a_p = 7 feet

$\bar{a}$ = 0.842

$\bar{b}$ = 0.657

Assumed Parameters

c_D = 0.07

c_L = 0.08

η_A = 73 percent

η_Q = 67 percent

b_w = 6 feet

x_a = 14.75 feet

y_a = 6.75 feet

THE GARRETT CORPORATION
AiResearch Manufacturing Division
Phoenix, Arizona

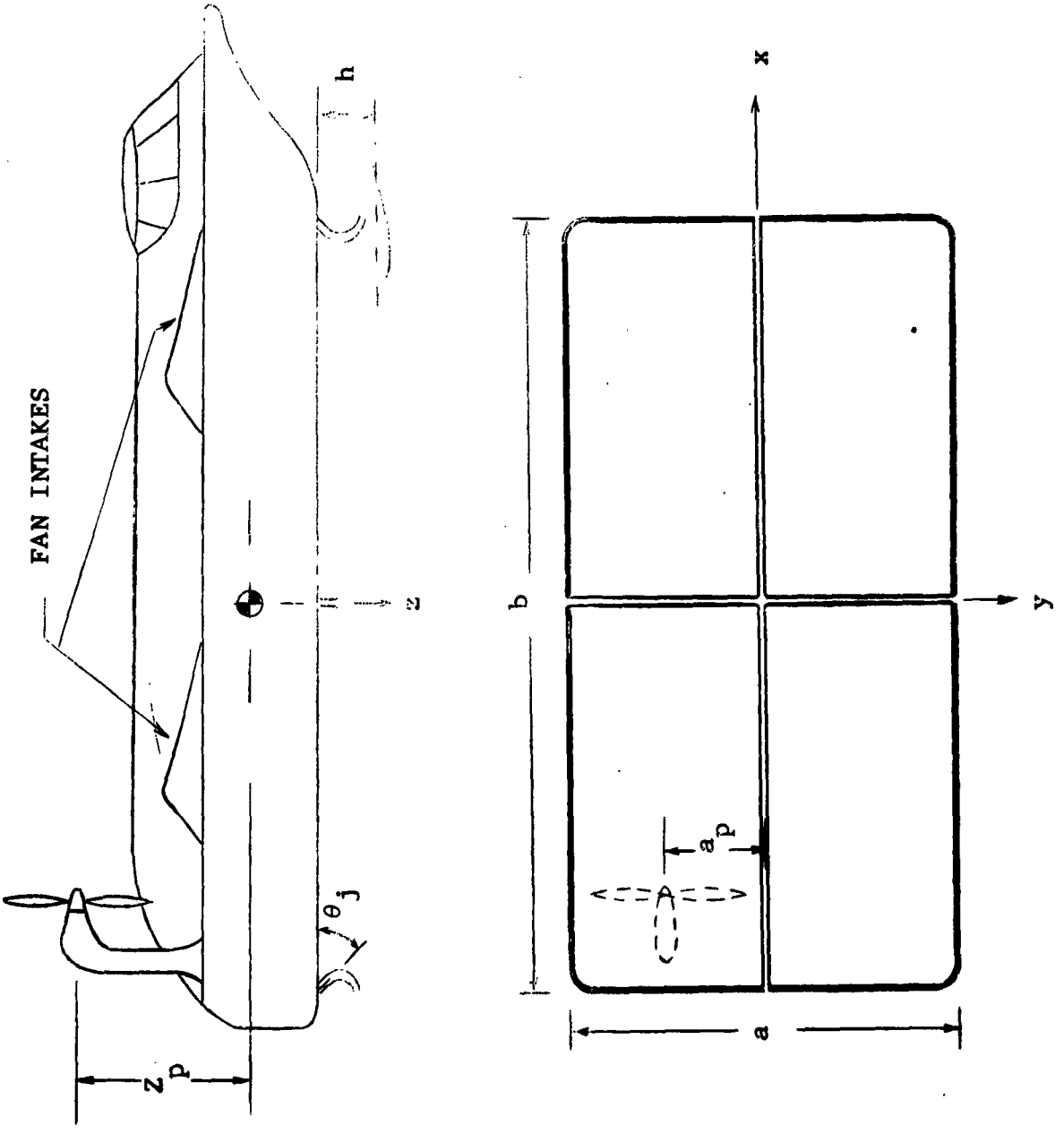

REFERENCE DESIGN VEHICLE SCHEMATIC

FIGURE 2-1

Operating Conditions (Steady State)

$h = 1.8$ feet

$P_1 = P_2 = P_3 = P_4 = 45$ lb/ft^2

$P_{io} = 40.11$ lb/ft^2

$V_j = 196.65$ ft/sec (all jets)

$\rho = 0.002425$ lb sec^2/ft^4

$Q_{f_1} = Q_{f_2} = Q_{f_3} = Q_{f_4} = 4692.9$ ft^3/sec

$Q_1 = Q_2 = Q_3 = Q_4 = 4222.9$ ft^3/sec

$Q_{12} = Q_{34} = 294.97$ ft^3/sec

$Q_{14} = Q_{23} = 543.36$ ft^2/sec

$\lambda_1 = 0.9156$ (page 8) Appendix A

$F_1 = 0.9696$ (page 5) Appendix A

$F_{zi} = 4.447$ (page 4) Appendix A

$B_{io} = 0.4277$ (page 4) Appendix A

$K_{KA} = 0.6563$ (page 14 of AP-5047-R, Appendix A)

Miscellaneous Parameters

$$\frac{\partial \bar{Q}_{fi}}{\partial \bar{P}_i} = -0.093, \qquad \frac{\partial Q_{fi}}{\partial P_i} = -9 \ \frac{ft^3/sec}{lb/ft^2}$$

(The variation of fan flow with base pressure)

$\tau_1 = 0.00426$ sec

$\tau_2 = 0.187$ sec

$\frac{W_c b^2}{8 I_y} = 3.87$

$\frac{W_c a^2}{8 I_x} = 2.307$

$\frac{a}{a+b} = 0.3139$

$\frac{b}{a+b} = 0.686$

$\frac{F_1}{K_{KA}} = 1.477$

$\frac{\lambda_1 \bar{b} g}{h} = 10.76$ 1/sec^2

$\frac{\lambda_1 \bar{a} g}{h} = 13.79$ 1/sec^2

$\frac{A_B P_o}{W_c} = 0.8162$

$\frac{1}{2} \frac{G}{h} \sin\theta_j = 0.0982$

$\left(\lambda_1 + \frac{A_B P_o}{W_c}\right) \frac{\partial \bar{Q}_{fi}}{\partial \bar{P}_i} = - 0.1633$

$\bar{F}_1 = 0.819$

THE GARRETT CORPORATION
AiResearch Manufacturing Division
Phoenix, Arizona

Pitch Equation Components (θ)

$$\omega_\theta = 5.25 \text{ rad/sec}$$

$$\zeta_\theta = 0.311$$

$$\frac{\partial\bar{\theta}}{\partial\bar{Q}_{fi}} = 0.649$$

$$\omega_\theta^2 \frac{\partial\bar{\theta}}{\partial\bar{Q}_{fi}} = 17.89 \text{ 1/sec}^2$$

$$\frac{Z_p g b W_c}{4 I_y h} = 21.12 \text{ 1/sec}^2$$

$$\frac{\omega_\theta^2 W_c}{\rho_w A_B h} = 12.06 \text{ 1/sec}^2$$

$$\frac{\rho g A_B b^4}{4 I_y h} = 23.78$$

$$\frac{c_L x_a}{b} + \frac{0.29a}{4(a+b+2a\bar{F}_1)} = 0.035$$

$$\bar{K}_\theta = 0.258\ (1 + \epsilon - \frac{2\sin\alpha}{\alpha}\cos\alpha) = 0.258\ f_1\ (U_x)$$

$$f_2\ (U_x) = 6\frac{\sin\alpha}{\alpha}\ (\frac{\sin\alpha}{\alpha} - \cos\alpha)$$

THE GARRETT CORPORATION
AiResearch Manufacturing Division
Phoenix, Arizona

Roll Equation Components (ϕ)

$$\omega_\phi = 3.93 \text{ rad/sec}$$

$$\zeta_\phi = 0.182$$

$$\frac{\partial \bar{\phi}}{\partial \bar{Q}_{fi}} = 0.5065$$

$$\omega_\phi^2 \frac{\partial \bar{\phi}}{\partial \bar{Q}_{fi}} = 7.82 \text{ 1/sec}^2$$

$$\frac{\rho g A_B a^3 b}{4 h I_x} = 6.49$$

$$\frac{c_L y_a}{a} + \frac{0.365a}{4(a+b+2b\bar{F}_1)} = 0.0335$$

$$\bar{K}_\phi = 0.247 \left(1 + \epsilon - \frac{2 \sin\alpha}{\alpha} \cos\alpha\right) = 0.247 f_1 (U_x)$$

Heave Equation Components (z)

$$\omega_z = 3.95 \text{ rad/sec}$$

$$\zeta_z = 0.307$$

$$\frac{\partial \bar{Z}}{\partial \bar{Q}_{fi}} = 0.426$$

$$\omega_z^2 \frac{\partial \bar{Z}}{\partial \bar{Q}_{fi}} = 6.647 \text{ 1/sec}^2$$

$$\bar{K}_z = 0.276 \left(1 + \epsilon - \frac{2 \sin\alpha}{\alpha} \cos\alpha\right) = 0.270 f_1 (U_x)$$

Fore-Aft Equation Components (x)

$$\frac{c_D \rho g A_B b}{2W_c} = 0.00328 \text{ 1/ft}$$

$$\frac{Q_F \rho g}{W_c} = 0.01875 \text{ 1/sec}$$

$$\frac{a}{b} = 0.458$$

$$\frac{g}{b} = 0.546 \text{ 1/sec}^2$$

$$\frac{2hg}{b^2} = 0.0333 \text{ 1/sec}^2$$

Side Slip Equation Components (y)

$$\frac{c_D \rho g A_B b}{2W_c} = 0.00328 \text{ 1/ft}$$

$$\frac{Q_F \rho g}{W_c} = 0.01875 \text{ 1/sec}$$

$$\frac{b}{c} = 2.185$$

$$\frac{2hg}{a^2} = 0.159 \text{ 1/sec}^2$$

Yaw Equation Components (ψ)

$$\frac{W_c g a_p}{2I_z} = 0.881 \text{ 1/sec}^2$$

$$\frac{c_D \rho g A_B b b_w a}{2I_z} = 0.00415$$

2.4.5 Control System Parameters

Let: α_i = inlet guide vane angle

θ_c = pitch command input angle

ϕ_c = roll command input angle

Assumed Control System Functions

Flow to Inlet Guide Vane Angle

$$q_i = \frac{\partial Q_i}{\partial \alpha_i} \alpha_i$$

$$\frac{\partial Q_i}{\partial \alpha_i} = 48 \quad \frac{ft^3/sec}{deg\ (input)}$$

Pitch

$$\alpha_1 = \frac{\partial \alpha_i}{\partial \theta_c} \frac{1}{(1 + \tau_{cp}\, s)} \theta_c$$

$$\alpha_2 = -\frac{\partial \alpha_i}{\partial \theta_c} \frac{1}{(1 + \tau_{cp}\, s)} \theta_c$$

$$\alpha_3 = -\frac{\partial \alpha_i}{\partial \theta_c} \frac{1}{(1 + \tau_{cp}\, s)} \theta_c$$

$$\alpha_4 = \frac{\partial \alpha_i}{\partial \theta_c} \frac{1}{(1 + \tau_{cp}\, s)} \theta_c$$

$$\frac{\partial \alpha_i}{\partial \theta_c} = 1.00 \frac{\text{deg (output)}}{\text{deg (input)}}$$

$$\tau_c = 0.1 \text{ sec (10 rad/sec lag)}$$

$$q_1 = \frac{48}{(1 + 0.1s)} \theta_c$$

$$q_2 = -\frac{48}{(1 + 0.1s)} \theta_c$$

$$q_3 = -\frac{48}{(1 + 0.1s)} \theta_c$$

$$q_4 = \frac{48}{(1 + 0.1s)} \theta_c$$

Roll

$$\alpha_1 = \frac{\partial \alpha_i}{\partial \phi_c} \frac{1}{(1 + \tau_{cp} s)} \phi_c$$

$$\alpha_2 = \frac{\partial \alpha_i}{\partial \phi_c} \frac{1}{(1 + \tau_{cp} s)} \phi_c$$

$$\alpha_3 = -\frac{\partial \alpha_i}{\partial \phi_c} \frac{1}{(1 + \tau_{cp} s)} \phi_c$$

$$\alpha_4 = -\frac{\partial \alpha_i}{\partial \phi_c} \frac{1}{(1 + \tau_{cp} s)} \phi_c$$

$$\frac{\partial \alpha_i}{\partial \phi_c} = 0.214 \frac{\text{deg (output)}}{\text{deg (input)}}$$

$$\tau_c = 0.1 \text{ sec (10 rad/sec lag)}$$

$$q_1 = \frac{10.3}{(1 + 0.1s)} \phi_c$$

$$q_2 = \frac{10.3}{(1 + 0.1s)} \phi_c$$

$$q_3 = -\frac{10.3}{(1 + 0.1s)} \phi_c$$

$$q_4 = -\frac{10.3}{(1 + 0.1s)} \phi_c$$

Heave

It is assumed that a change in engine speed set point is instantaneous following the pilot command (Z_c).

Yaw

Denote β as propeller pitch angle and ψ_{cp} as the pilot command

$$\frac{\partial \beta}{\partial \psi_{cp}} = 4 \frac{\text{deg (output)}}{\text{deg (input)}}$$

The control is assumed to have a 10 rad/sec lag. ($\tau_{yc} = 0.1$ sec)

Forward Velocity

Denote x_c as pilot command for forward velocity

$$\frac{\partial \beta}{\partial x_c} = 0.89 \frac{\text{deg (output)}}{\text{deg (input)}}$$

$$\tau_{xc} = 0.1 \text{ sec}$$

2.4.6 Engine and Fuel Control

The engines are shaft turbine engines with a free-type power turbine. They are in the 1300 to 1600 hp class.

In order to eliminate the complex representation of such an engine and its fuel control, it was assumed that the simplified system as shown in Figure 2-2 was sufficient for this purpose.

The particular parameters for this system are given below.

$$\frac{\partial W_f}{\partial N_e} = 0.056 \ \frac{lb/hr}{rpm}$$

$$\frac{\partial N_{GP}}{\partial W_f} = 12.3 \ \frac{rpm}{lb/hr}$$

$$\frac{\partial Q_t}{\partial N_{GP}} = 0.0447 \ \frac{ft/lb}{rpm}$$

$$\frac{\partial Q_t}{\partial N_t} = -0.008 \ \frac{ft/lb}{rpm}$$

$J = 0.905$ ft lb sec^2 (Total inertia of rotating machinery referred to output shaft of engine)

$\tau_{fc} = .05$ sec

$\tau_{GP} = 1$ sec

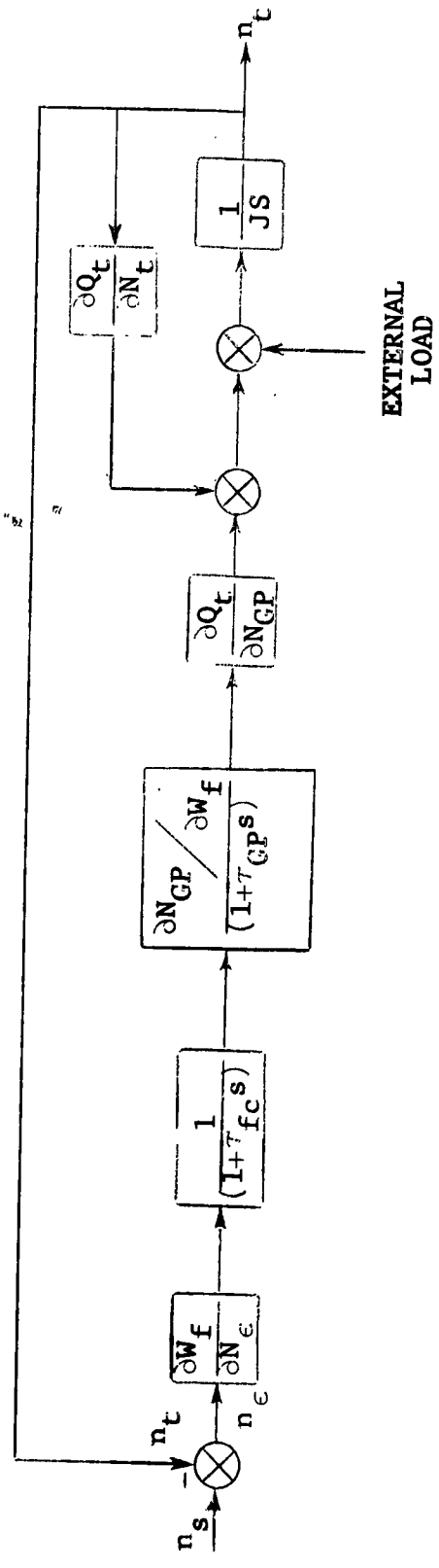

BLOCK DIAGRAM OF ASSUMED
FREE TURBINE ENGINE DYNAMICS

FIGURE 2-2

2.4.7 Miscellaneous Gains and Functions

Gains:

Load horsepower to fan flow

$$\frac{\partial HP}{\partial Q_f} = 0.1 \frac{hp}{ft^3/sec}$$

Fan flow to turbine speed

$$\frac{\partial Q_t}{\partial N_t} = 0.207 \frac{ft^3/sec}{rpm}$$

Load torque to load horsepower

$$\frac{\partial Q_L}{\partial HP} = 0.2387 \frac{ft/lb}{hp}$$

Note: This assumes constant engine speed.

Functions:

Thrust ($\bar{T}$) for a ducted propeller is a function of propeller pitch angle (β), forward velocity ($\bar{U}_x$) and engine speed (N_t). For purposes of this simulation it was assumed that $\bar{T}'$ vs $\Delta\beta$ could be represented as shown in Figure 2-3. For a given propeller pitch angle the corresponding $\bar{T}$ is then obtained from the following:

$$\overline{T} = \overline{T}' (1.9 - 0.568\ \overline{U}_x) \left[1 - \frac{\partial T}{\partial N_t} (N_t - N_{to}) \right]$$

where N_{to} is the steady state operating speed.

$$\frac{\partial \overline{T}}{\partial N_t} = 0.485 \times 10^{-5} \qquad 1/\text{rpm}$$

The shaft horsepower absorbed in producing the required thrust is given in Figure 2-4.

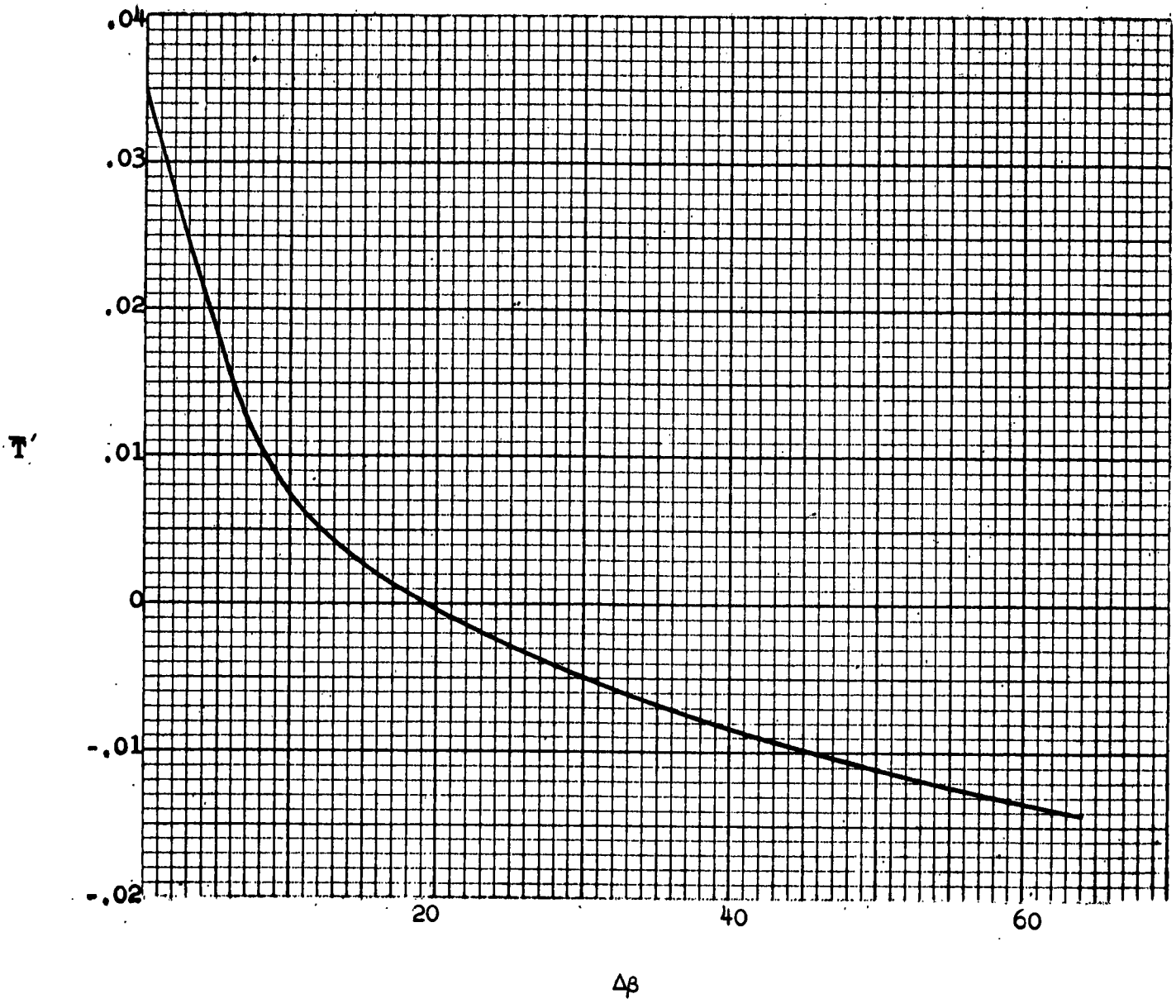

FIGURE 2-3. THRUST VS PROPELLER PITCH ANGLE

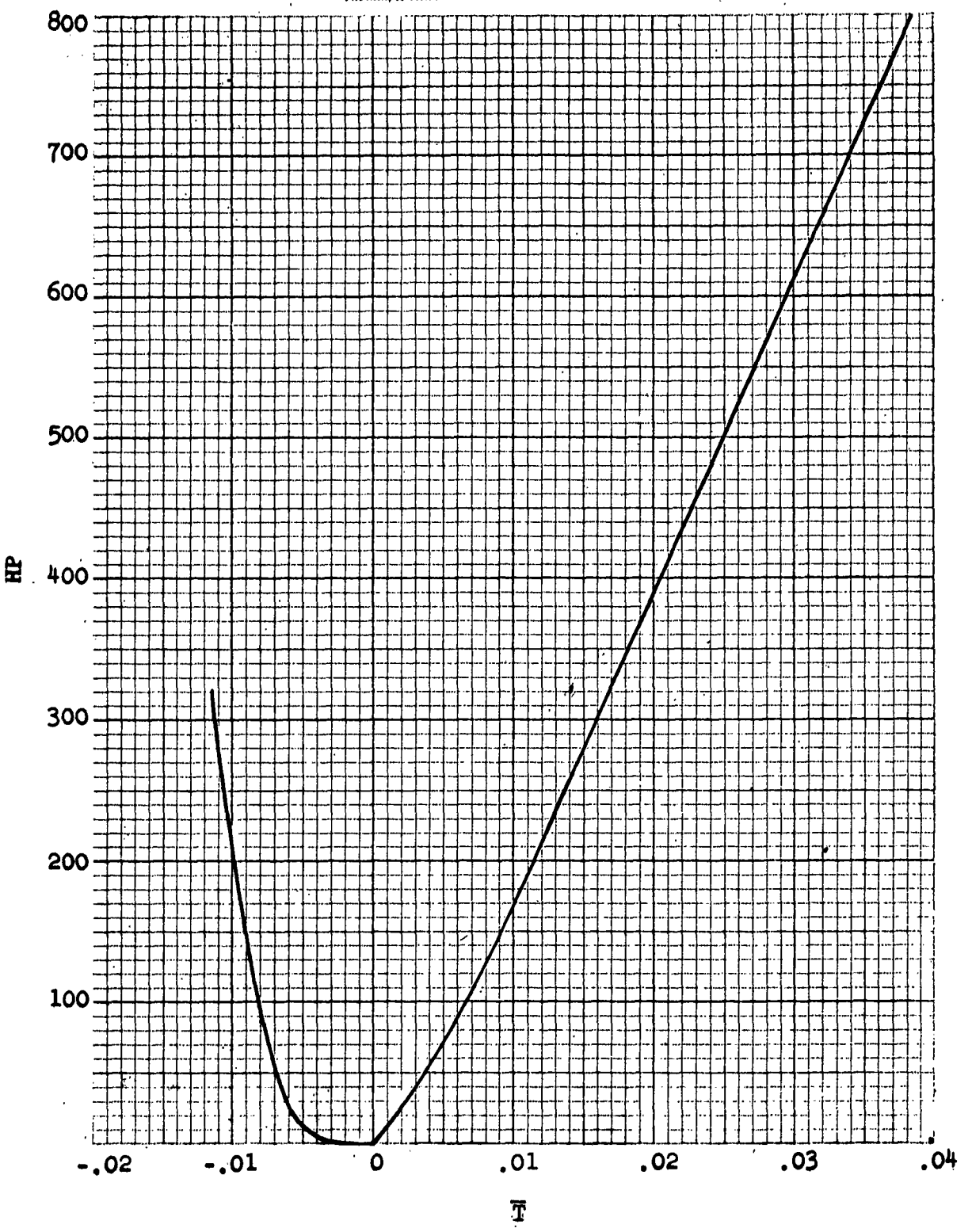

FIGURE 2-4. DRIVING HORSEPOWER VS THRUST

3.0 DESCRIPTION OF GEM CONTROL STATION DESIGN

The purpose of designing and building a GEM-control station was threefold:

1. To provide the physical means for analog simulation of GEM handling.

2. To determine the specific performance characteristics of the GEM model under study.

3. To provide a test setup for selecting the best suited control station arrangement.

The functions to be controlled by the operator are:

(a) Yaw

(b) Roll

(c) Pitch

(d) Fore and aft power

(e) Hover height

In order to satisfy point 3, a total of six control units have been incorporated in the design. Figure 3.1 shows the control station that has been designed and built to simulate the control arrangement of a cockpit.

Manual controls to serve the control functions are incorporated in a pivoted column headed by a steering wheel. To accomplish the desired control functions this device can be manipulated by

(a) Moving the entire column fore and back (Fig. 3.4)

(b) Swinging the wheel about the pivot axis of the column (Fig. 3.4)

(c) Rotating the wheel about its own axis (Fig. 3.2)

An alternative means of steering is given by a foot-operated treadle (Fig. 3.5).

Two lever type positioners have been provided to take care of the less frequently operated controls of the vehicle (Fig. 3.2).

The mechanical input signals will be converted into proportional voltage signals by 20 kΩ potentiometers which are for trimming purposes connected in series with an adjustable potentiometer of 2 kΩ.

The potentiometers are rotated by a pulley about which a wire attached to the control handle is wound. An equalizing extension spring eliminates any backlash.

The frame of the control station has been designed to accommodate any kind of seat--i.e., an ordinary chair for the operator of the simulator (Fig. 3.6).

To enable adjustment of the relative steering wheel position, the respective bars have been hinged to permit relocation of the steering wheel column (Fig. 3.3).

THE GARRETT CORPORATION
AiResearch Manufacturing Division
Phoenix, Arizona

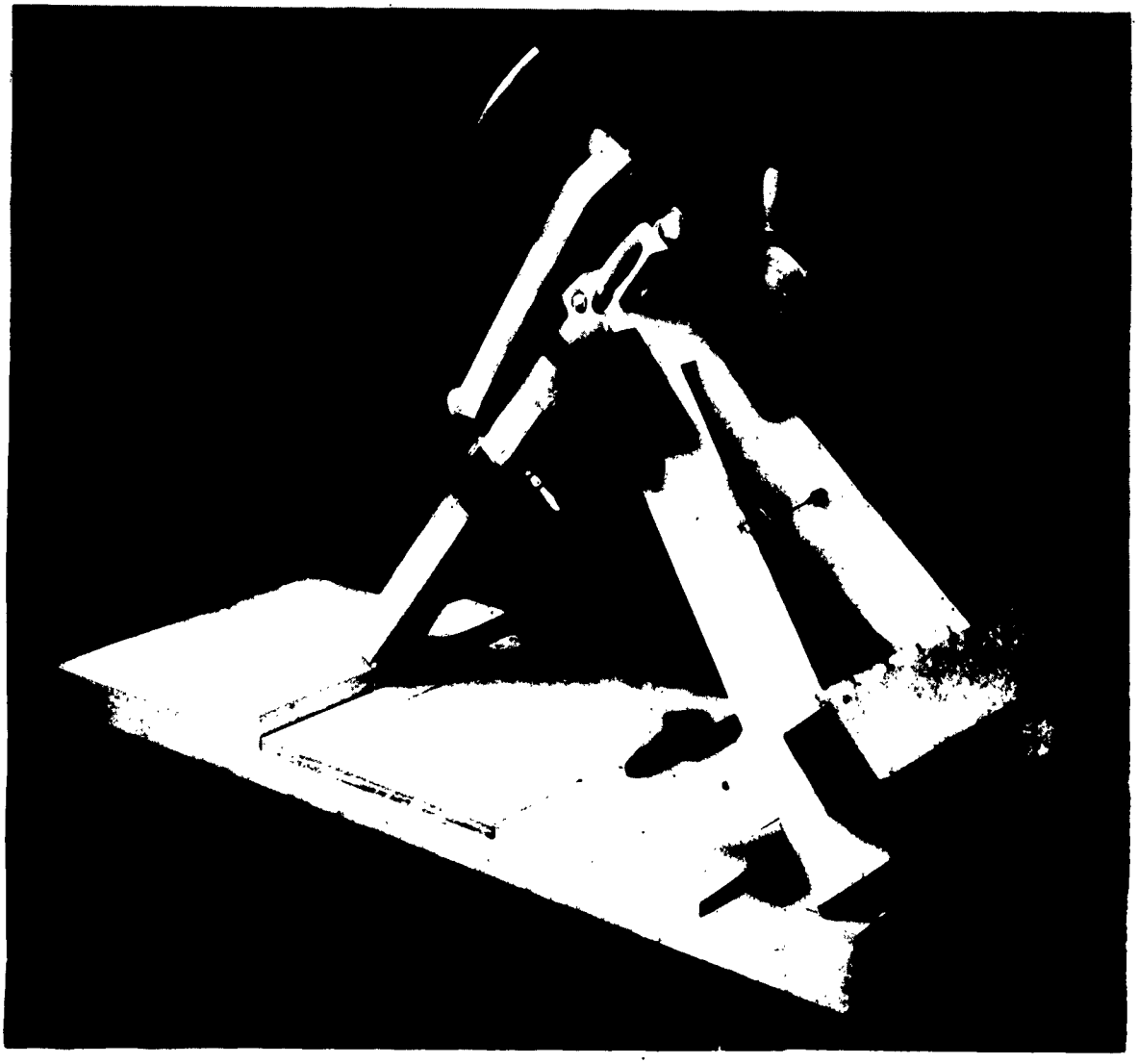

FIGURE 3-1. GEM CONTROL STATION, GENERAL VIEW

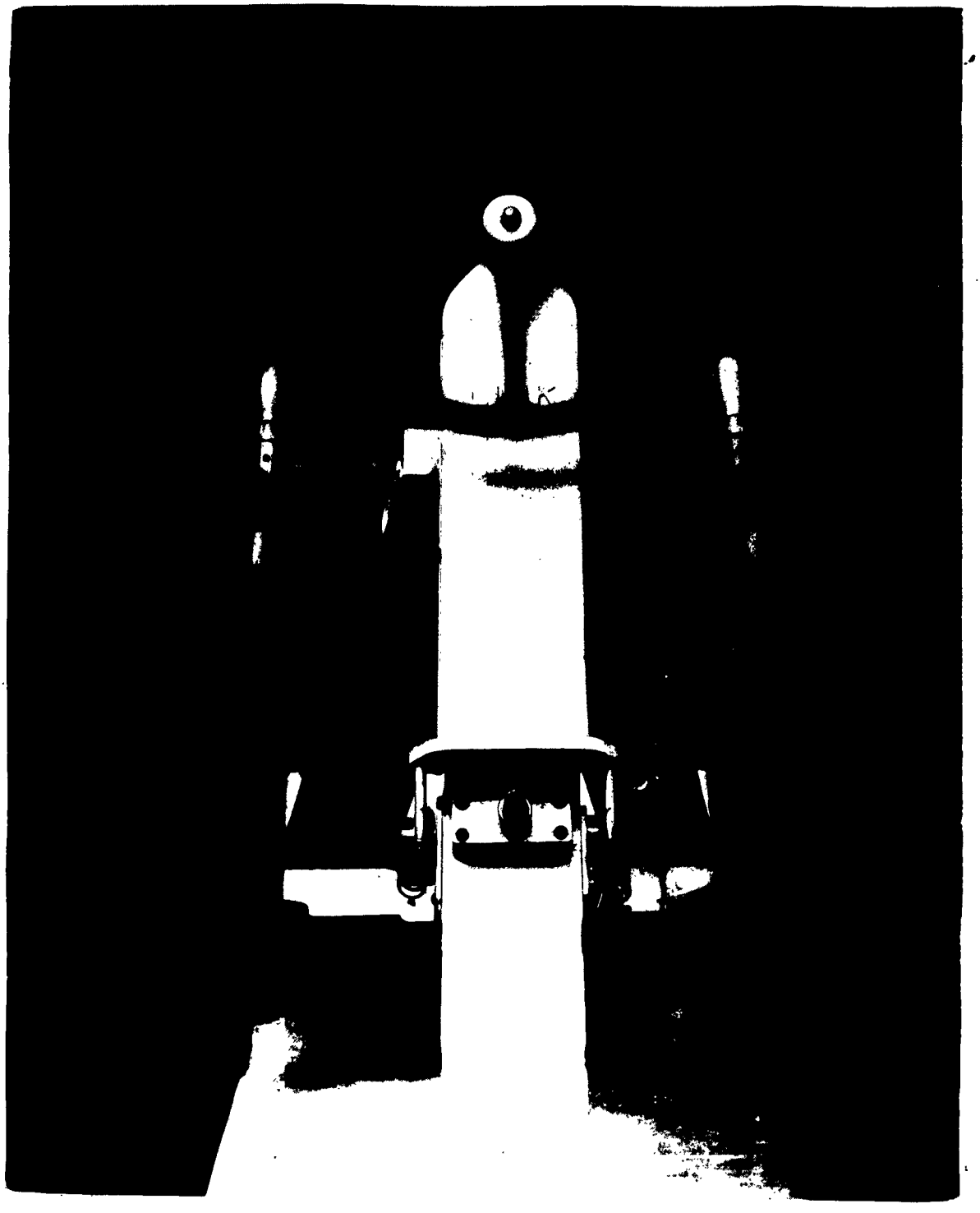

FIGURE 3-2. GEM CONTROL STATION, FRONT VIEW

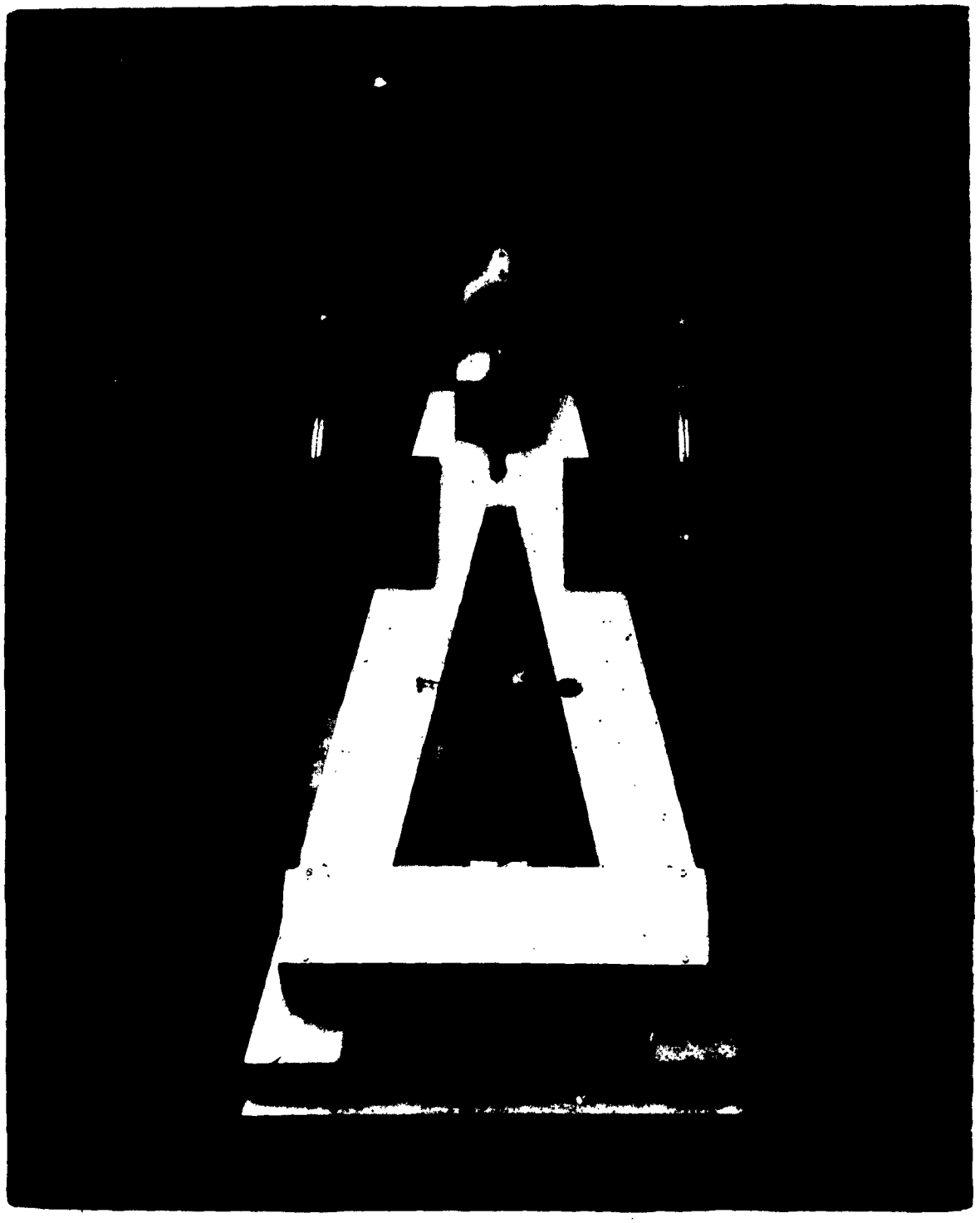

FIGURE 3-3. GEM CONTROL STATION, REAR VIEW

THE GARRETT CORPORATION
AiResearch Manufacturing Division
Phoenix, Arizona

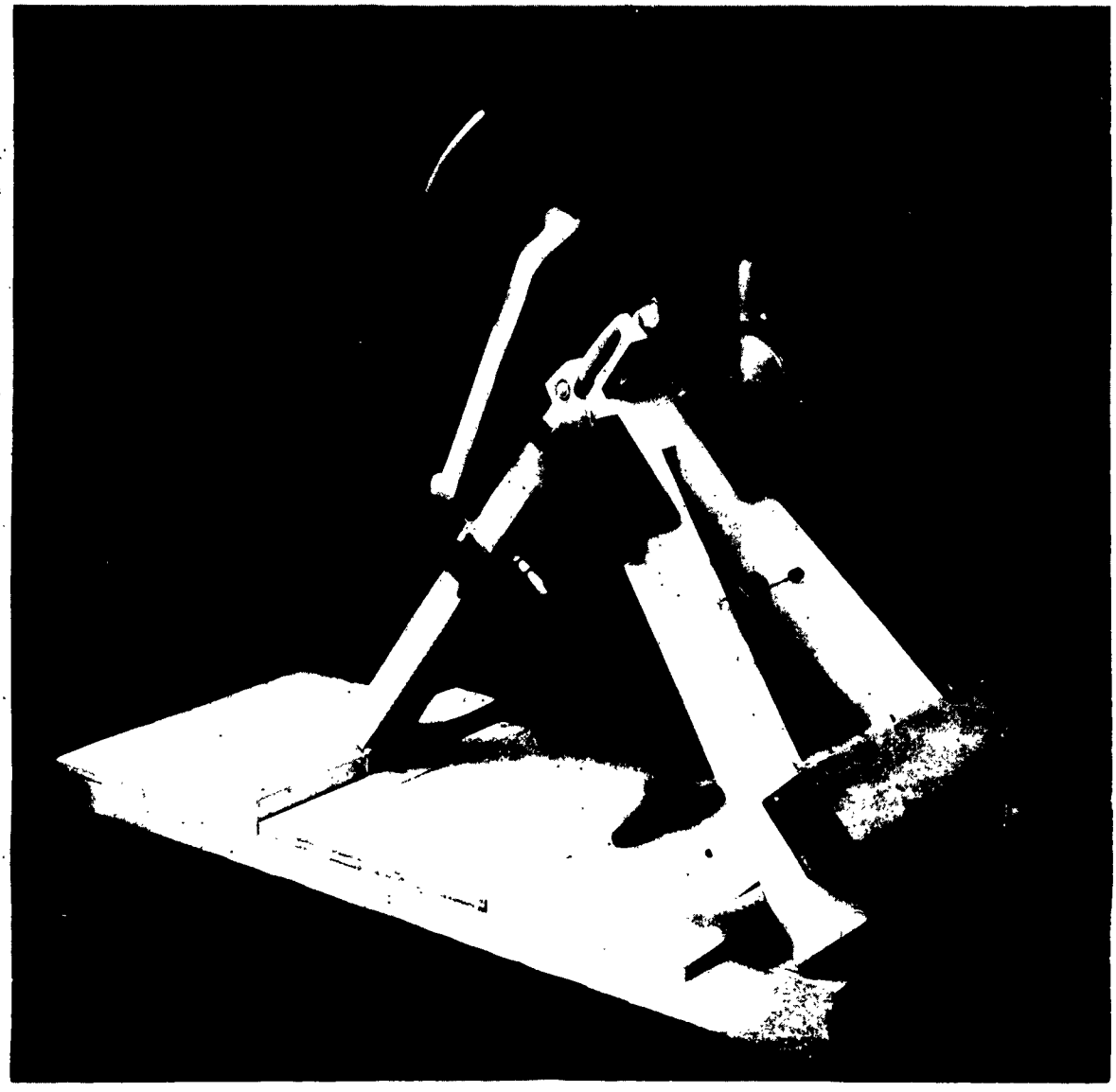

FIGURE 3-4. GEM CONTROL STATION, COLUMN MOVED BACK AND ROTATED

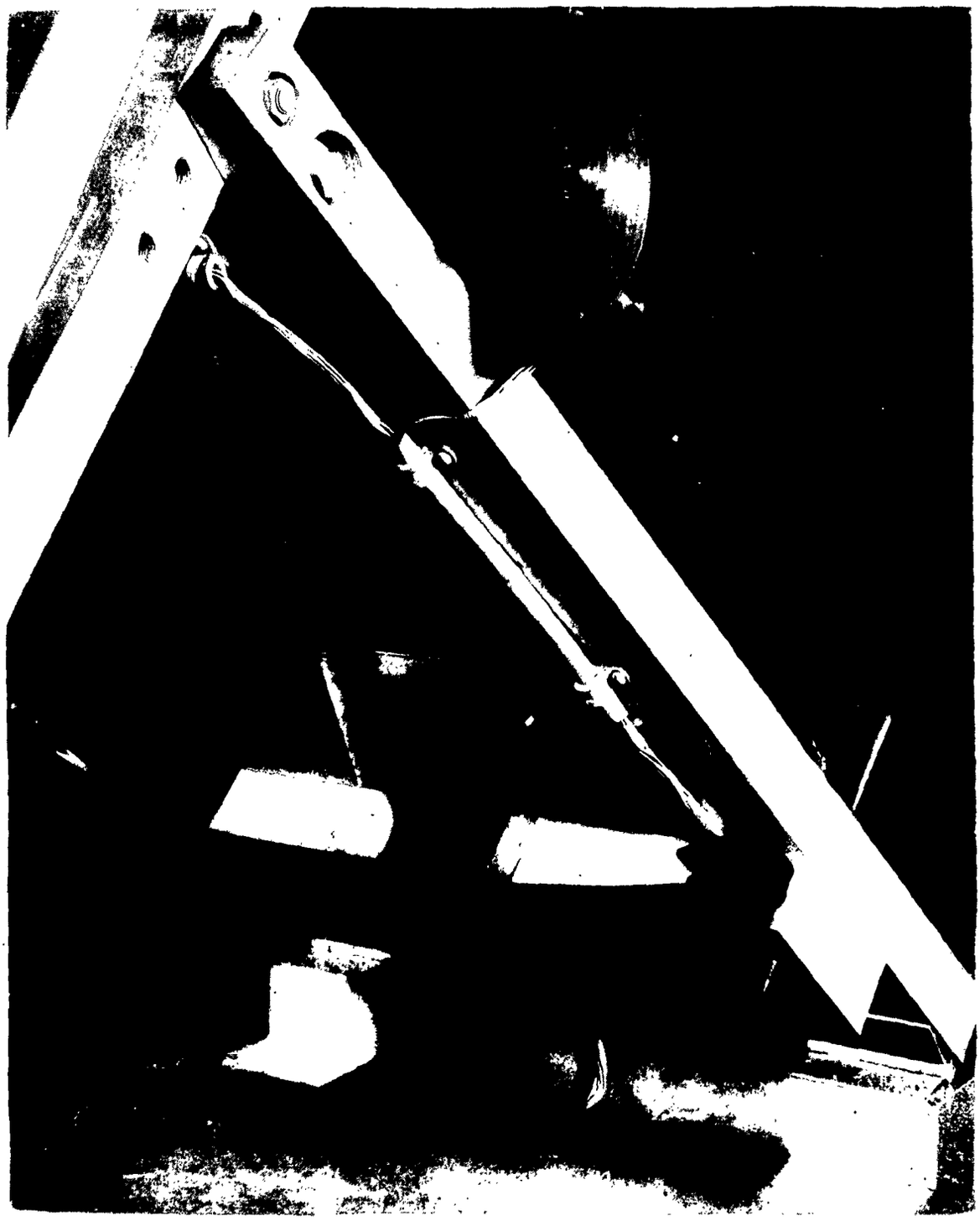

FIGURE 3-5. GEM CONTROL STATION, TREADLE CONTROL

THE GARRETT CORPORATION
AiResearch Manufacturing Division
Phoenix, Arizona

FIGURE 3-6. GEM CONTROL STATION, ANALOG COMPUTER

4.0 TEST RESULTS

The six degrees of freedom analog computer simulation of a completely controlled reference GEM has two purposes. The first is to demonstrate the analytical evaluation of GEM's generally. The second is to show what characteristics will be attained by the reference design. The vehicle characteristics have been classified under (1) natural motions, (2) response to commands, and (3) controllability.

Natural motions are the transient motions of the vehicle with locked controls following a disturbance such as a sudden change in a control imput. Response to commands means how much and how fast a given vehicle attitude or velocity changes following a control input which commands this change. Controllability means how well a human operator can drive or pilot the vehicle through a prescribed or desired maneuver.

The manner in which specific data was obtained will be discussed below as the data is presented.

4.1 Natural Motions

The natural motions that were recorded are heave, pitch, roll, and yaw motions. The condition simulated was that of a vehicle over smooth water responding to step changes in pilot commands. Particular attention was given to the coupling of forward speed to pitch, side motion to roll, and yaw to side velocity.

4.1.1 Heave

In the reference vehicle, hovering height is controlled by engine speed. This is done, in preference to inlet guide vane changing, to keep the engines at an efficient operating point. This means that the control command for a new hovering height is a change of engine speed set point.

Figure 4-1 shows some typical curves of engine speed and vehicle height following a step change in engine speed set point. It is seen that 6 to 8 seconds is required for the height to change, that there is no noticeable overshoot, and that height follows engine speed very closely. The transfer functions for the engine and vehicle show the engine speed response to set point to have a second-order lag at 0.64 radian per second with a damping ratio of 0.83. This is the slow transient seen in the traces (Figure 4-1). The vehicle response to fan flow changes has a second-order lag at 3 to 4 radians per second with a damping ratio of 0.31. Since the vehicle is faster than the engine, it would be expected to follow the engine speed rather closely--as seen in the traces. Thus, how fast vehicle height can be changed is limited by the engine response.

The traces also show the steady-state gain variation with forward velocity. The traces show the following gains in feet per 100-rpm speed change:

Velocity, fps	0	20	50
Gain, ft per 100 rpm	0.21	0.24	0.14

This change is primarily due to the change in effective water surface stiffness with forward speed.

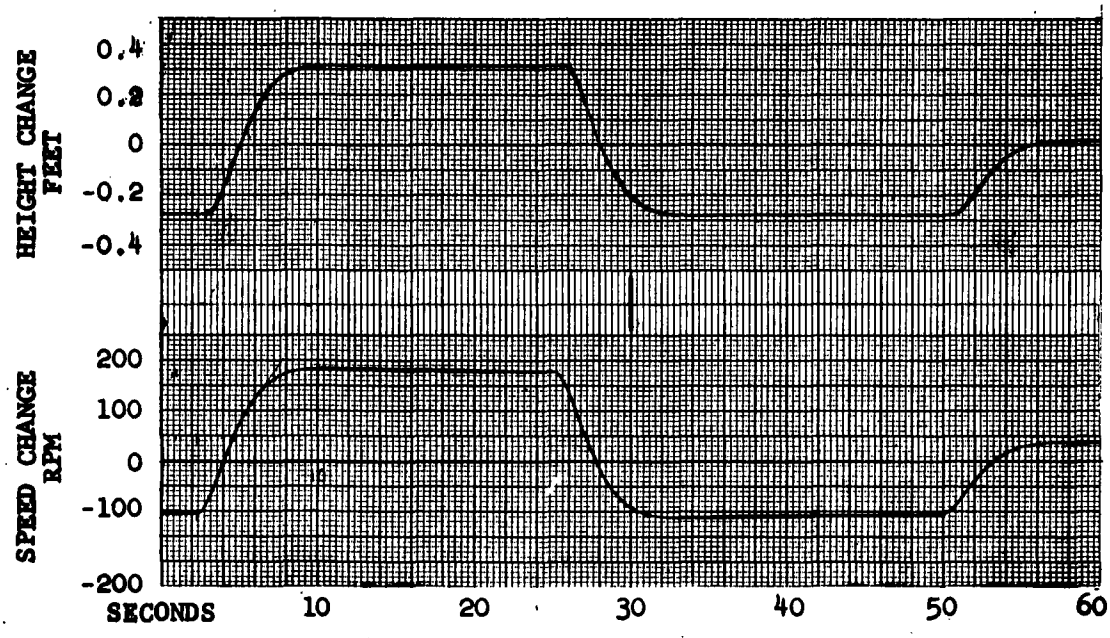

(a) HOVERING - FORWARD VELOCITY ZERO

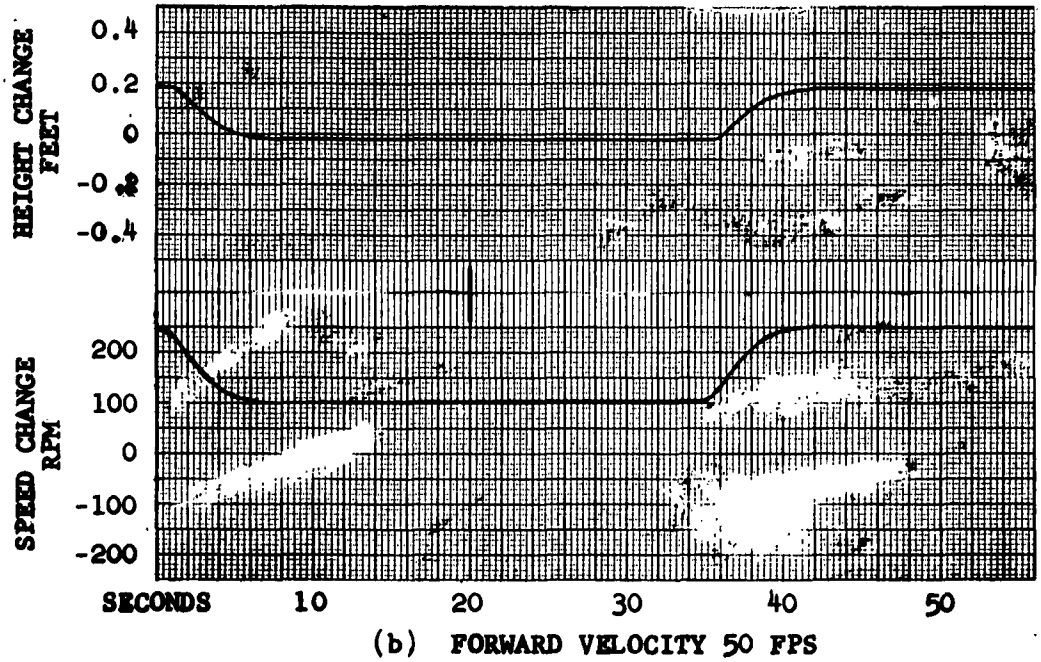

(b) FORWARD VELOCITY 50 FPS

HOVERING HEIGHT VS. TIME FOLLOWING A SPEED COMMAND

FIGURE 4-1

4.1.2 Pitch

The pilot controls pitch by means of differential inlet guide vanes. Figures 4-2(a), (b), and (c) show pitch angle, vehicle height changes, and forward velocity vs time following a pitch command. Two things can be seen from these traces. The first is the frequency and damping of pitch (and heave) oscillations. The second is the influence of pitch on forward speed.

From the traces, the natural frequencies and damping ratios appear to be the following:

Speed	0	20 fps	40 fps
ω_θ	3.93	4.7	4.62
h	0.42	-	-

The sloping curve at 20 and 40 fps as the oscillations damp out precludes any reasonable determination of the damping ratio. However, it is interesting to note that the natural pitching frequency over a hard surface with no coupling effects is 5.25 radians per second with a 0.31 damping ratio. At hover, Figure 4-2(a), the frequency is nearer the natural frequency of heave motions, which is 3.95 radians per second. At 20 and 40 fps, pitch still has a strong effect on height but the frequency is nearer that of natural pitch oscillations.

The forward-speed traces show speed to be affected by pitch. However, the effect is seen primarily as the result of prolonged pitching in one direction. The oscillations seen in both the pitch and the height traces are virtually undetectable in the

speed traces. In Figure 4-2(a) the speed change is almost linear with time when the pitch angle is constant. This is the expected result of constant acceleration, since there is virtually no aerodynamic drag below 10 fps. The slope of these curves indicates an acceleration rate of about 0.045 g when the pitch angle is about 3 degrees, or 0.052 radian. In Figure 4-2(b) and (c), accelerations are not as readily seen due to the variation of slope with time. However, where points were checked, the slope changes were found to be very nearly equal to the pitch angle changes in radians.

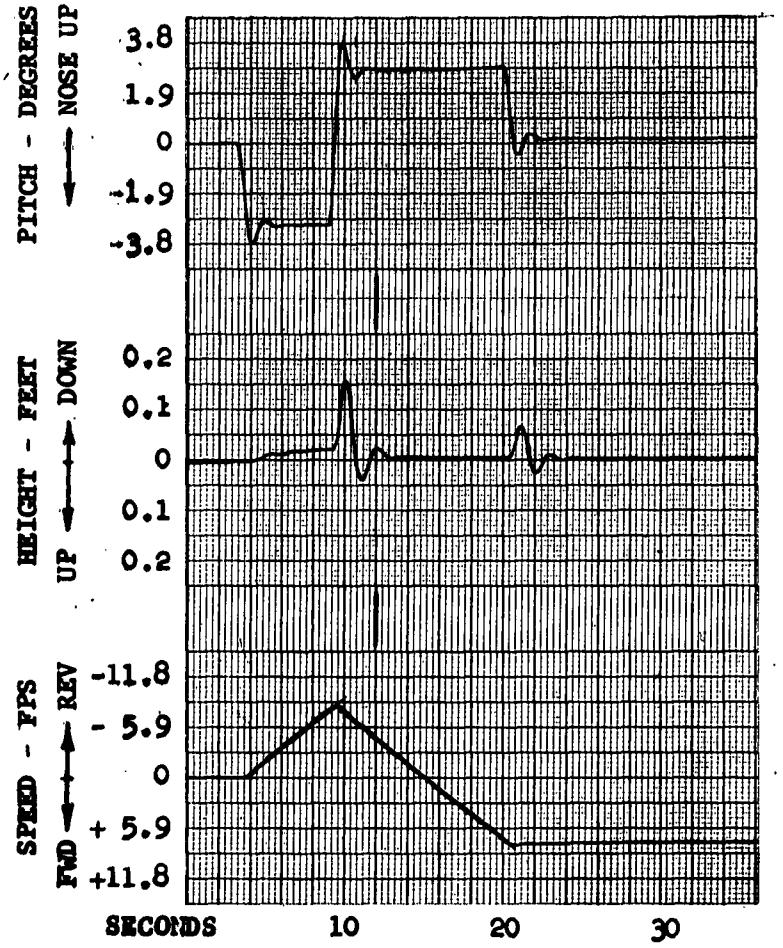

HOVER - ZERO FORWARD SPEED

PITCH AND FORWARD SPEED VS.
TIME FOLLOWING A PITCH COMMAND

FIGURE 4-2(a)

THE GARRETT CORPORATION
AiResearch Manufacturing Division
Phoenix, Arizona

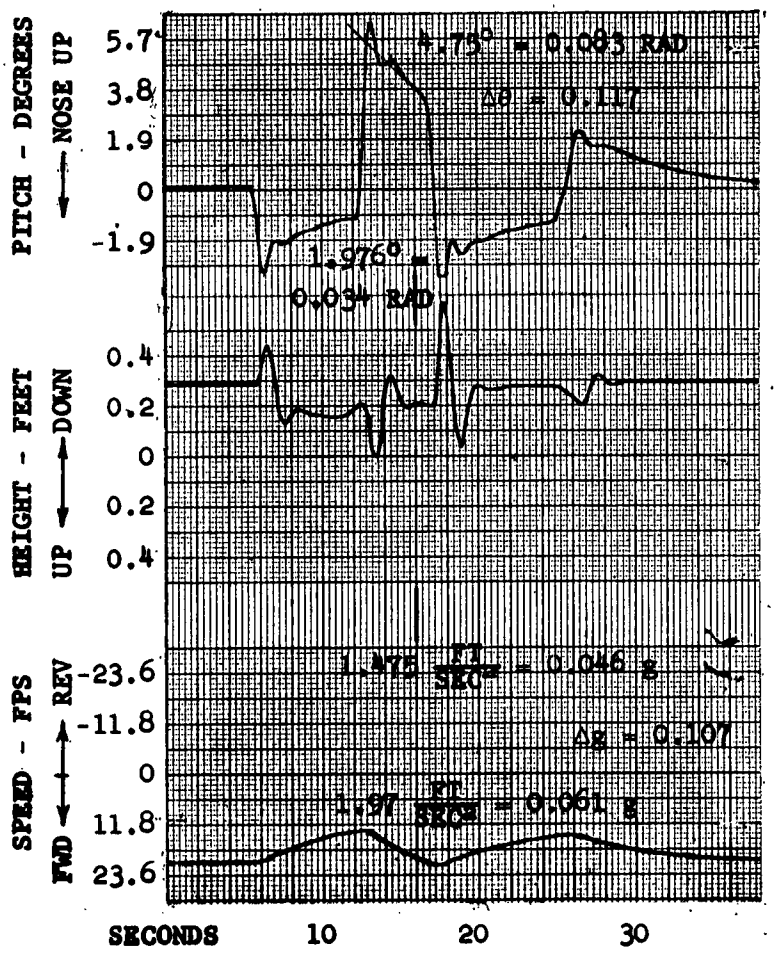

20 FPS FORWARD SPEED

PITCH AND FORWARD SPEED VS.
TIME FOLLOWING A PITCH COMMAND

FIGURE 4-2(b)

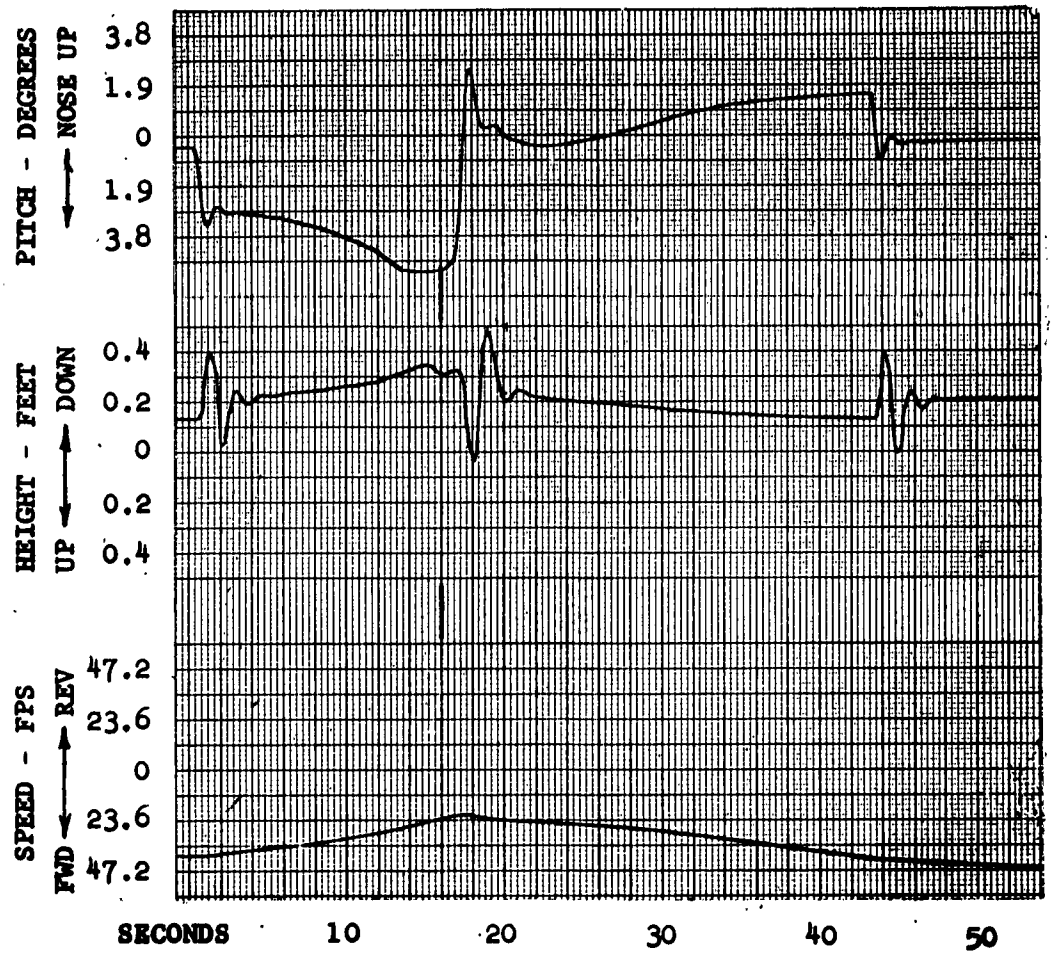

40 FPS FORWARD SPEED

PITCH AND FORWARD SPEED VS.
TIME FOLLOWING A PITCH COMMAND

FIGURE 4-2(c)

4.1.3 Roll

Figure 4-3 shows roll angle and sidewise displacement vs time as roll oscillations die out naturally. To see the oscillation of side motions due to roll oscillations it was necessary to run the traces simultaneously on two x-y plotters. The figure shown is a composite of the two plots. The run was made by putting in a full positive roll command followed by a full negative roll command and restoring the roll command to zero. As seen in the figure, this effectively "rocks the boat" with an amplitude of a few degrees. The frequency of oscillation determined from these traces (at hover) is 3.3 radians per second with 0.22 damping ratio. Over a hard surface the frequency and damping ratio would have been 3.93 radians per second and 0.18, respectively.

Figure 4-3 also shows that side motion is oscillatory when the roll angle oscillates. However, the amplitudes shown on the traces are less than 0.05 feet (0.6 inch) for the indicated roll amplitudes of about 4 degrees. As the amplitude decreases the side displacement lags the roll angle by very nearly 180°. This means that during roll motions the center of rotation is not at the center of gravity but is rather above it by the ratio of side displacement amplitude to roll amplitude. Although these amplitudes are not easily obtained from damped transient data, the center of rotation appears to be about 0.7 foot above the center of gravity. It is expected that this distance would be independent of gross weight. Theoretically, it should be g/ω_θ^2 for harmonic rolling motions. This gives 2.93 feet at the natural frequency of 3.31 radians per second.

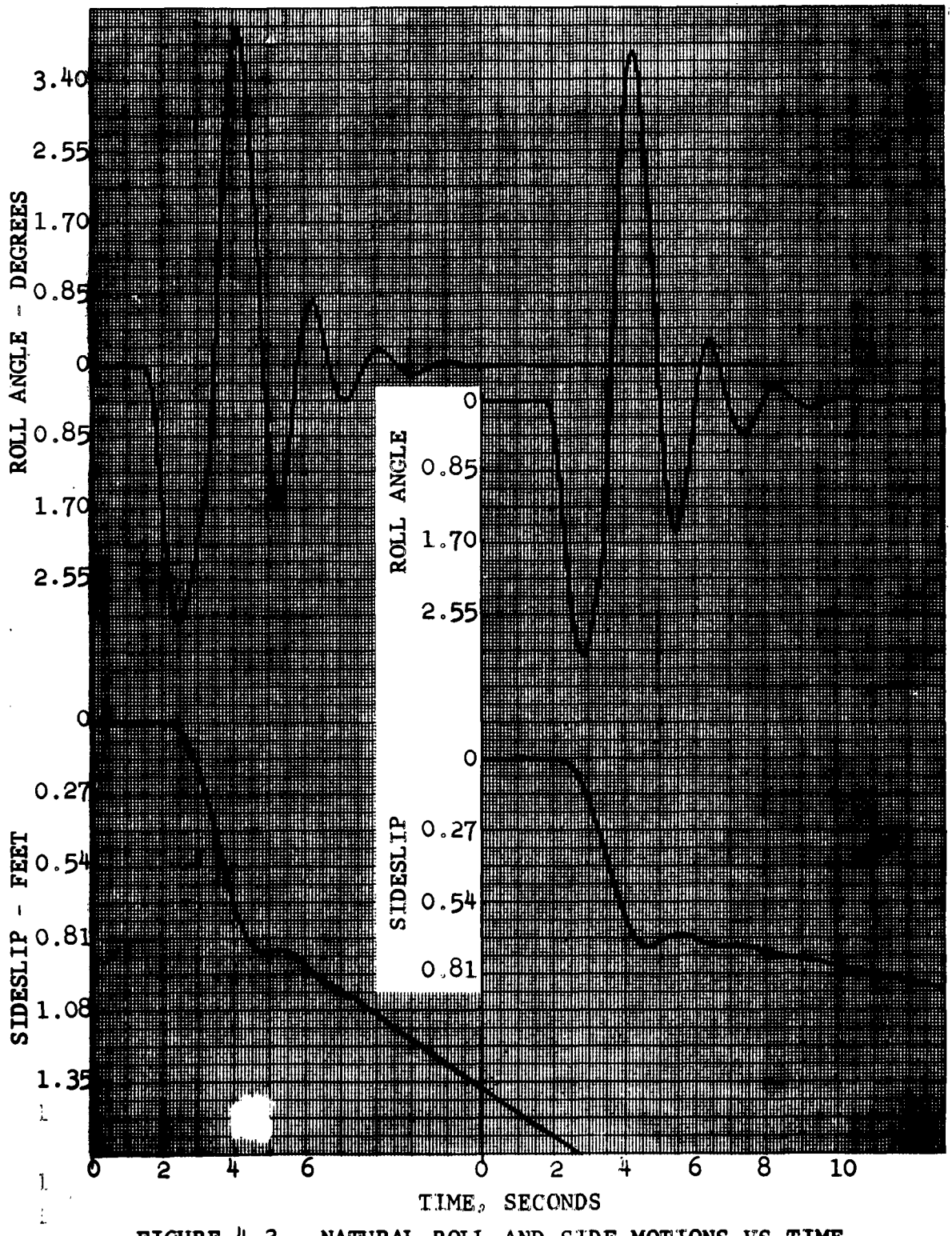

FIGURE 4-3. NATURAL ROLL AND SIDE MOTIONS VS TIME

4.1.4 Yaw

The curves shown in Figure 4-4 show the vehicle in a "fishtailing" motion. The GEM was first brought up to a steady speed and then a yaw command was given. After a suitable yaw rate was obtained, the yaw command was reduced to zero. The subsequent yaw oscillations are due to aerodynamic moment resulting from side velocity. The curves show that yaw causes a transfer of velocity from U_x to U_y and vice versa. They also show the period of oscillation to be considerably less at 100 fps than at 50 fps forward speed. At 50 fps one period of side motion (beginning at 19 fps) required about 84 seconds. At 100 fps one period of side motion (beginning at 17 fps) required only about 58 seconds. It is seen also that the period gets longer as the amplitude of side velocity decreases. This is the expected result, since the aerodynamic forces are proportional to the square of the velocity.

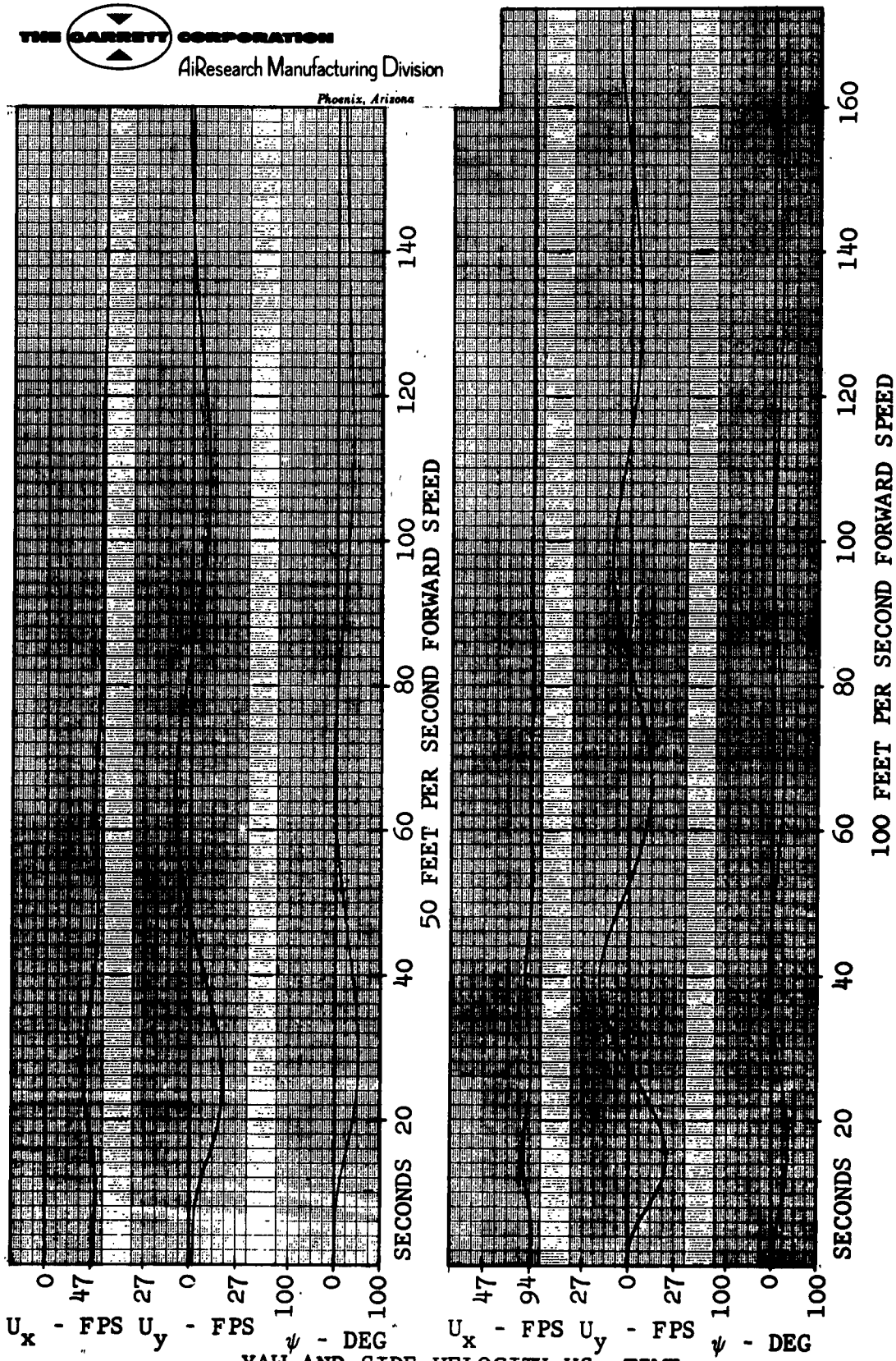

YAW AND SIDE VELOCITY VS. TIME

FIGURE 4-4

4.2 Response to Commands

4.2.1 Acceleration and Braking

The data in Table 4-1 was obtained by accelerating and braking the GEM with full forward thrust and full reverse thrust commands. A straight-line course was used.

	Speed Range	Acceleration			Braking		
	feet/second	Time (sec.)	Dist. (feet)	a_{AV} (g-units)	Time (sec.)	Dist. (feet)	a_{AV} (g-units)
WAVE IN	0 to 17.7	4.4	40	0.125	18.0	150	0.03
	0 to 47.5	16.28	460	0.09	31.8	600	0.045
	49.5 to 94.4	38.6	3000	0.035	19.6	1400	0.070
WAVE OUT	0 to 40	10.8	250	0.115	38.0	670	0.033
	0 to 74.4	27.0	1250	0.085	61.2	2000	0.038

TABLE 4-1 ACCELERATION AND BRAKING DATA

The first row in Table 4-1 shows the low-speed acceleration capability. The indication is a maximum accelerating thrust of 0.125 g, or 12.5 percent of the vehicle gross weight. This amounts to about 10,000 pounds. The maximum braking thrust is 0.03 g, or 2400 pounds. The second row, which gives acceleration and braking through the "hump" speed, indicates less average thrust for accelerating but more for braking. The effect of water surface response to vehicle motion is seen in the pitch attitude. The computer traces from which the data in Row 2 was taken are reproduced in Figure 4-5.

Consider now the pitch angle and forward-speed traces in Figure 4-5. When thrust is first applied (at zero forward speed) the water surface is essentially flat and the vehicle pitches nose down due to the thrust vector being considerably above the center of gravity. The nose-down attitude adds to the forward thrust. As speed increases, the wake develops with a wave crest forming at the nose and a trough toward the rear of the GEM. The result is a nose-up pitch attitude as the vehicle follows the surface slope. The GEM begins to pitch upward when the speed is about 16 feet per second and reaches its highest nose-up attitude (about 3 degrees) when the velocity is about 25 feet per second. This is seen to be the lowest slope or minimum acceleration point on the particular curves shown. After this the GEM gets over the hump and begins to run ahead of the wake so that it feels an increasingly flat surface. The pitch angle is essentially zero when the velocity reaches 44 feet per second. At this speed it is also seen that the slope begins to decrease as speed increases, showing that the aerodynamic drag begins to be significant. The third row in Table 4-1 shows that due to aerodynamic drag (including thrust loss due to forward speed) the average accelerating thrust from 50 to 95 feet per second is only 0.035 g, or about one fourth of that available at low speeds. Braking, however, is helped considerably at high speeds. It is seen that the vehicle can slow down twice as fast as it can accelerate from 50 to 95 feet per second.

The data in the last two rows of Table 4-1 were taken to show the extent to which water surface response affects acceleration and braking. It is seen that the average acceleration from 0 to 40 feet per second is 0.09 g compared with 0.115 g when the surface response is included. The figures in these two rows may be taken as "over land" values.

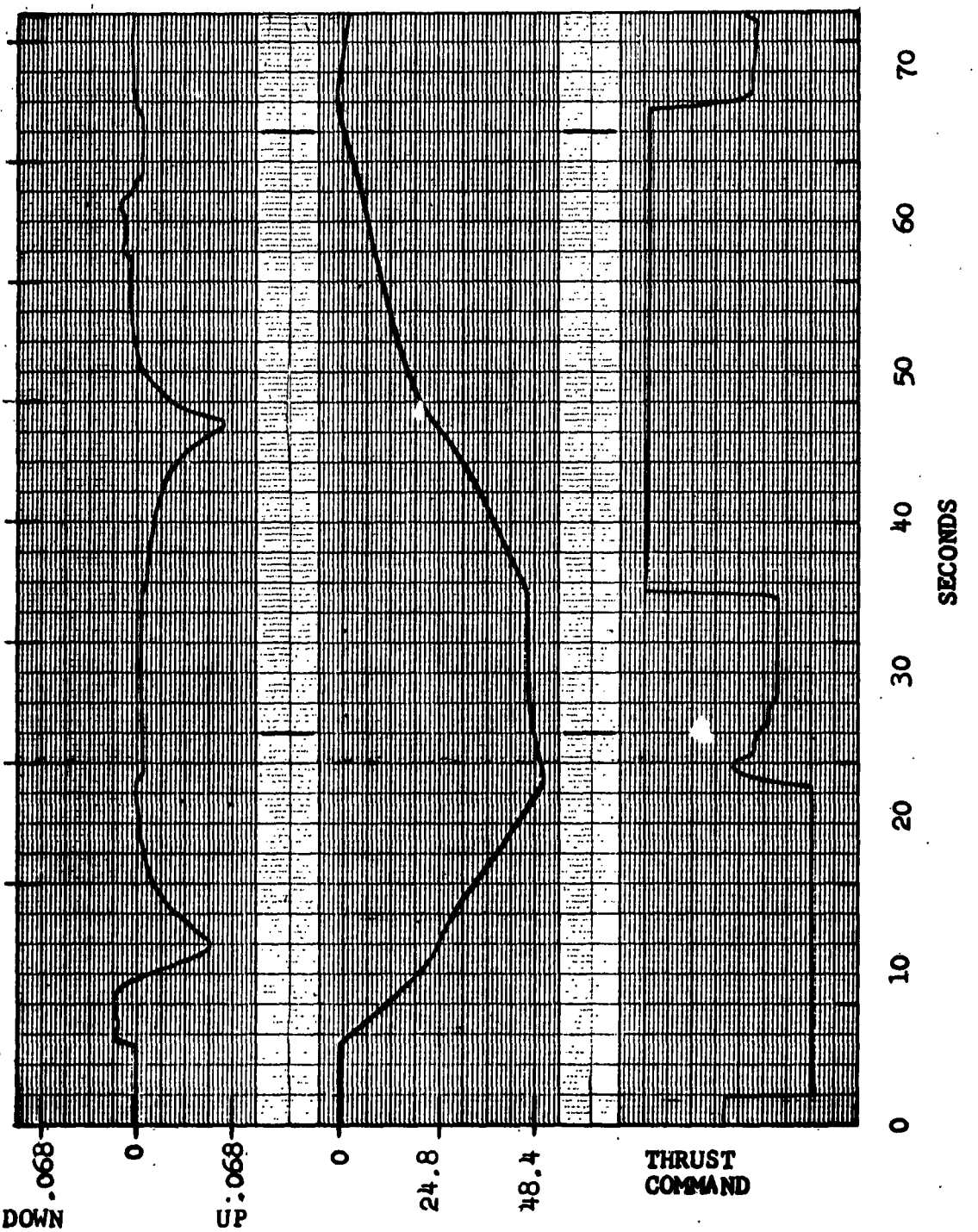

FIGURE 4-5 ACCELERATION AND BRAKING

4.2.2 Side Motions

Side velocity is controlled only by rolling the GEM. The roll angle attainable is determined by the maximum excursion of the inlet guide vanes and is about 0.03 radian or 1.72 degrees. At this roll angle the GEM was accelerated sideways at various forward velocities. The results are summarized in Table 4-2.

U_x (fps)	ϕ (rad)	U_y Range (fps)	Time (sec.)	a_{AV} G-Units	a_{AV}/ϕ
0	0.030	0 to +10	12.5	0.025	0.83
		+10 to -10	21.8	0.0285	0.95
		0 to +20	31.8	0.0195	0.65
		+20 to 0	15.6	0.040	1.33
40	0.022	0 to +10	18	0.0173	0.79
		+20 to 0	25	0.025	1.14
60	0.019	0 to +10	13.5	0.023	1.21
		+20 to 0	28.5	0.022	1.16
80	0.022	+20 to 0	27.5	0.023	1.05

SIDE MOTIONS
TABLE 4-2

The data in Table 4-2 shows several characteristics of side motions. The zero forward-velocity data shows that more acceleration is available for reducing than for increasing velocities. This is the expected result due to aerodynamic drag. It shows also that acceleration decreases as velocity increases. The maximum attainable side velocity is about 20 feet per second. This appears to be about the hump speed. However, it actually is the result of a balance between side force due to roll and side aerodynamic drag, because the water surface response due to side motions was not included in the analog computer simulation.

The variation of side acceleration with speed appears to be somewhat erratic. The traces indicate that side velocity has a somewhat oscillatory character when forward velocity is present. Figure 4-6 has been included to show this. The reason for this somewhat erratic side velocity is that the center of pressure for side drag is aft of the center of gravity, causing the craft to yaw, and yawing causes an additional side acceleration due to coupling with forward velocity. The operator attempted to hold yaw rate zero during this test and succeeded in causing it to oscillate about the zero yaw rate point. The result is that the side accelerations due to roll only could not be separated from the coupling effects. Therefore, the data in Table 4-2 at forward velocities can, at best, show trends only. It appears that side acceleration is not much affected by forward speed except through yaw.

Although pilot opinions will be discussed in Section 6, it is worth mentioning here that most pilots would prefer to have more side force available for maneuvering purposes.

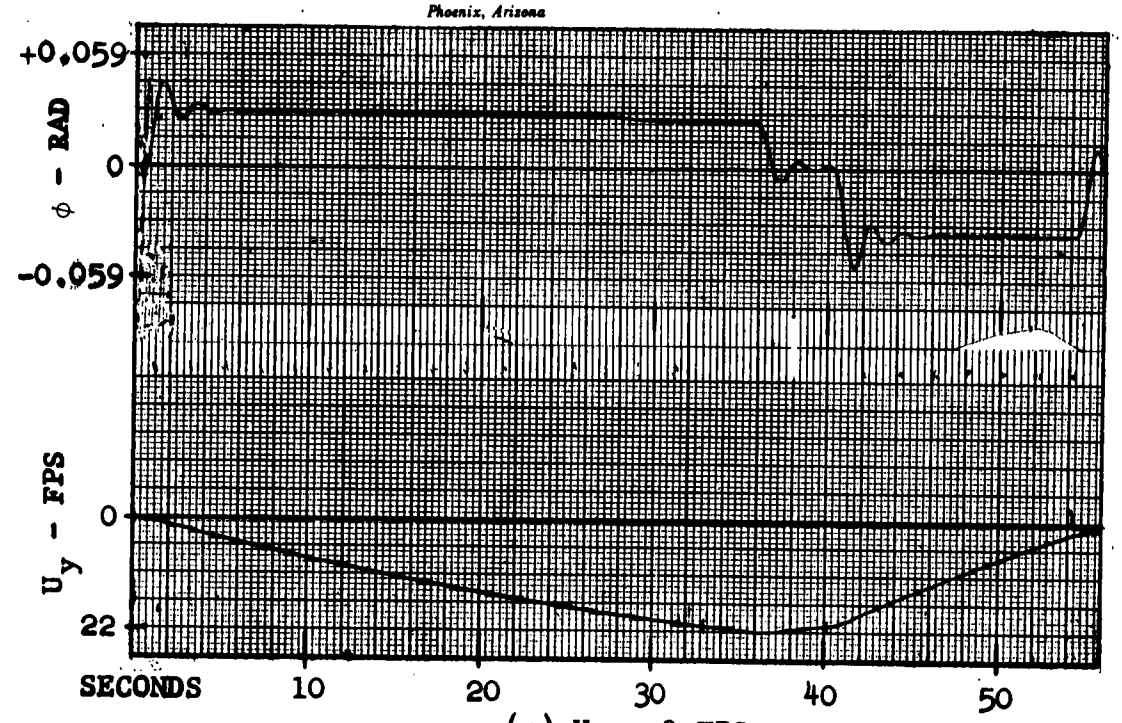

(a) U_x = 0 FPS

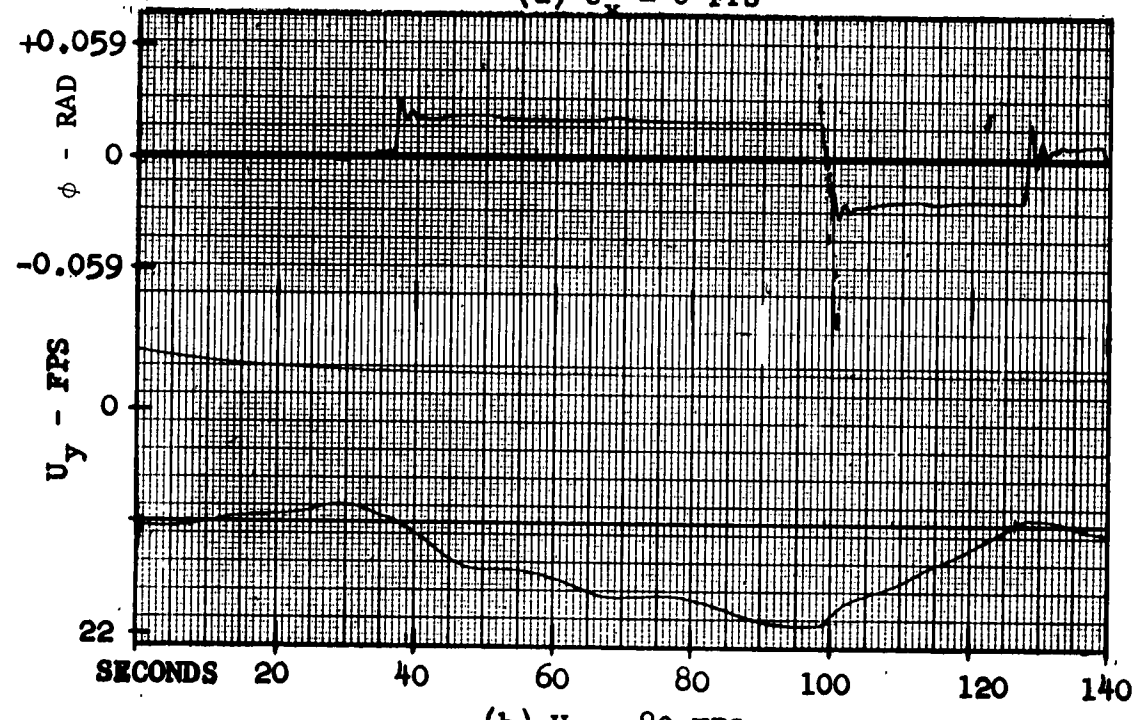

(b) U_x = 80 FPS

SIDE ACCELERATIONS AT 0 AND 80 FPS

FIGURE 4-6

4.2.3 Holding Course in a Wind

Since the GEM has no solid connection with the surface, it is very susceptible to being blown off course by surface winds. Two means are available for coping with undesirable wind effects. The first is to roll into the wind so that the side force due to base pressure equals the side drag. The second is to yaw the GEM into the wind so that a component of the thrust vector balances the side aerodynamic force.

The main forces involved in rolling into the wind are illustrated in Figure 4-7.

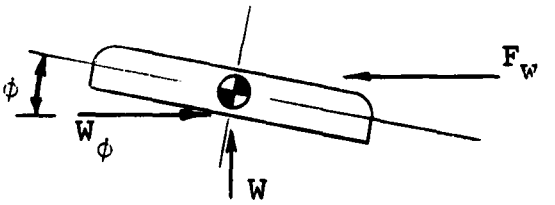

ROLLING INTO A WIND

FIGURE 4-7

In performing this maneuver it was found, as expected, that the pilot had no particular difficulty holding zero side speed relative to the ground in side winds of 10 and 20 feet per second (fps). This test was run at 0, 10 fps, and 20 fps forward velocities. In some cases the pilot held zero side velocity from the start; in others the GEM was allowed to drift with the wind velocity. It was then rolled into the wind to reduce the

velocity to zero, much as in the side acceleration runs mentioned previously. The traces, in fact, closely resemble those shown in Figure 4-6 if they are interpreted in terms of air speed rather than ground speed. Another effect that should be noted here is that a small differential thrust is needed to prevent yaw due to the aerodynamic moment. This again is similar to the "side acceleration" runs in that the pilot tends to generate slow oscillations in finding the proper yaw command.

The main forces involved in yawing into the wind are illustrated in Figure 4-8.

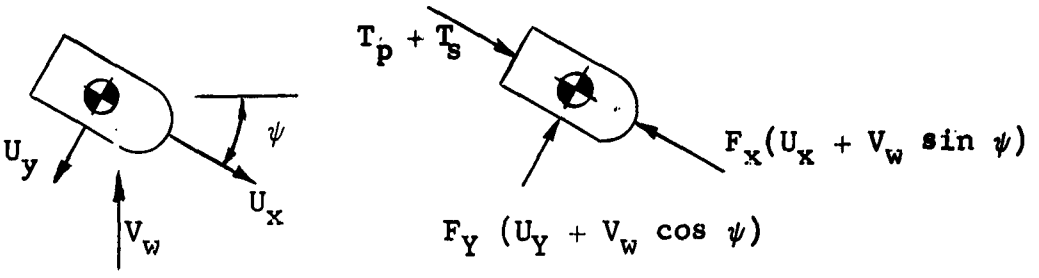

a) VOLOCITIES b) FORCES

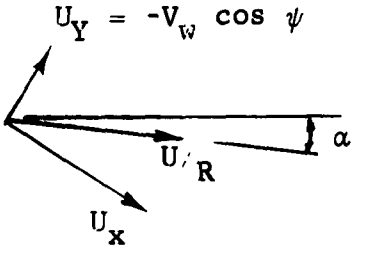

c) RESULTANT VOLOCITIES

YAWING INTO A WIND
FIGURE 4-8

Figure 4-8(b) shows the forces as they are simulated on the computer. Since the drag force F_x is colinear with the thrust, $T_p + T_s$, these two forces must be equal for constant velocity U_x. That is

$$\text{If } U_x = \text{const} \qquad \text{then} \quad T_p + T_s = F_x$$

Furthermore, since there is only one force in the Y direction it must be zero for constant velocity. This means that

$$U_y = -V_w \cos\psi \quad \text{if} \quad U_y = \text{constant}$$

The result of these two conditions is that the resultant velocity will also be constant but may not be in the desired direction. In any case,

$$U_R = \sqrt{U_x^2 + V_w^2 \cos^2\psi}$$

$$\alpha = \psi - \tan^{-1} \frac{V_w \cos\psi}{U_x}$$

The conditions that U_R have a prescribed value U and be directed perpendicular to the wind are the following:

(a) $\alpha = 0$ or $U_x \tan\psi = V_w \cos\psi$

(b) $U_R = V_w \cos\psi \quad \dfrac{\cos^2\psi + \sin^2\psi}{\sin^2\psi} = \dfrac{V_w}{\tan\psi}$

That is $\tan\psi = \dfrac{V_w}{U_R}$

$$(c) \quad T_p + T_s = F_x \left(U \cos\psi + V_w \sin\psi\right)$$

Attempts to fly a straight course in a wind without rolling indicate that it can be done but that it takes several minutes to find the proper control setting because of the slow yaw transients. It was considered a commendable feat when a pilot succeeded in holding a fixed position in space by yawing the craft 90 degrees into a 40-fps wind. Subsequent experience in flying prescribed courses further pointed out the difficulty of controlling yawing position with the long transient times involved. It is suggested at this point that greater yaw stability be built into future designs. Physically, this means more vertical stabilizer area. Analytically, it means moving the center of pressure farther aft. It was located 6 feet behind the center of gravity (about 10 percent of the vehicle length) in the simulation discussed here.

4.2.4 Turning

Turning is done for the purpose of altering the vehicle heading or course. Vehicle heading is controlled by yawing. However, unlike an automobile, a GEM can yaw while moving in a given direction without noticeably changing its course. The strong tendency to sideslip requires that side force as well as yaw moment be used in turning. The yaw capability built into the simulation was limited to a maximum rate of 10 degrees per second. This is not realistic for a real vehicle because the limiting yaw rate will vary with forward speed due to aerodynamic changes and changing thrust gain. The changing gains, however, were realistically simulated. The required pilot input at zero

propeller thrust is high due to low propeller gain. The required pilot input at high velocities is high due to increased yaw stability. At moderate speeds the yaw gain in response to pilot commands is maximum.

Three turning situations were used to demonstrate turning capability. The first was yawing in place (zero linear velocities). The second was coordinated turning (zero sideslip). The third was a sideslipping turn with U_x approximately equal to U_y. Yawing in place is governed by the built-in yaw rate limit of 10 degrees per second. Therefore the minimum time to turn 180 degrees is 18 seconds. With a yaw rate meter the pilot can readily hold any desired steady yaw rate.

A coordinated turn is illustrated in Figure 4-9.

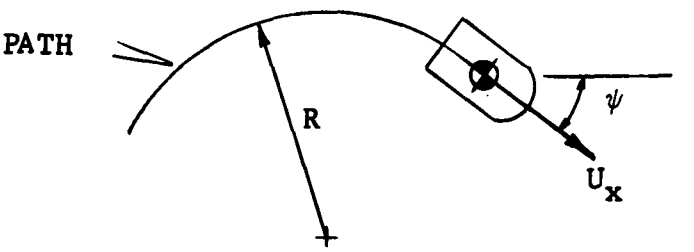

FIGURE 4-9. COORDINATED TURN

In this turn, $U_y = 0$ and the yaw rate is related to forward velocity and radius of curvature by

$$\frac{d\psi}{dt} = \Omega = \frac{U_x}{R}$$

In order to perform such a turn, a centripetal force must be applied to the vehicle. The magnitude of this force is

$$F_y = \frac{W_c}{g} R\Omega^2 = \frac{W_c}{g} \frac{U_x^2}{R}$$

Since there is no sideslip, F_y must be supplied by roll only. From Section 4.2.2 the maximum side acceleration is 0.03 g. Therefore, the minimum radius of curvature for coordinated turns should be

$$R = \frac{U_x^2}{0.03\ g} = 1.036\ U_x^2 \quad \text{feet.}$$

The computer runs show a slightly smaller radius than this. These are shown in Table 4-3.

FORWARD SPEED	TURNING RADIUS	
	COMPUTER	EQUATION
12 FPS	145 FT	149 FT
20 FPS	405 FT	414 FT

TABLE 4-3. COORDINATED TURN RADIUS WITH MAXIMUM ROLL COMMAND

The computer traces from which the data in Table 4-3 were taken are reproduced in Figure 4-10.

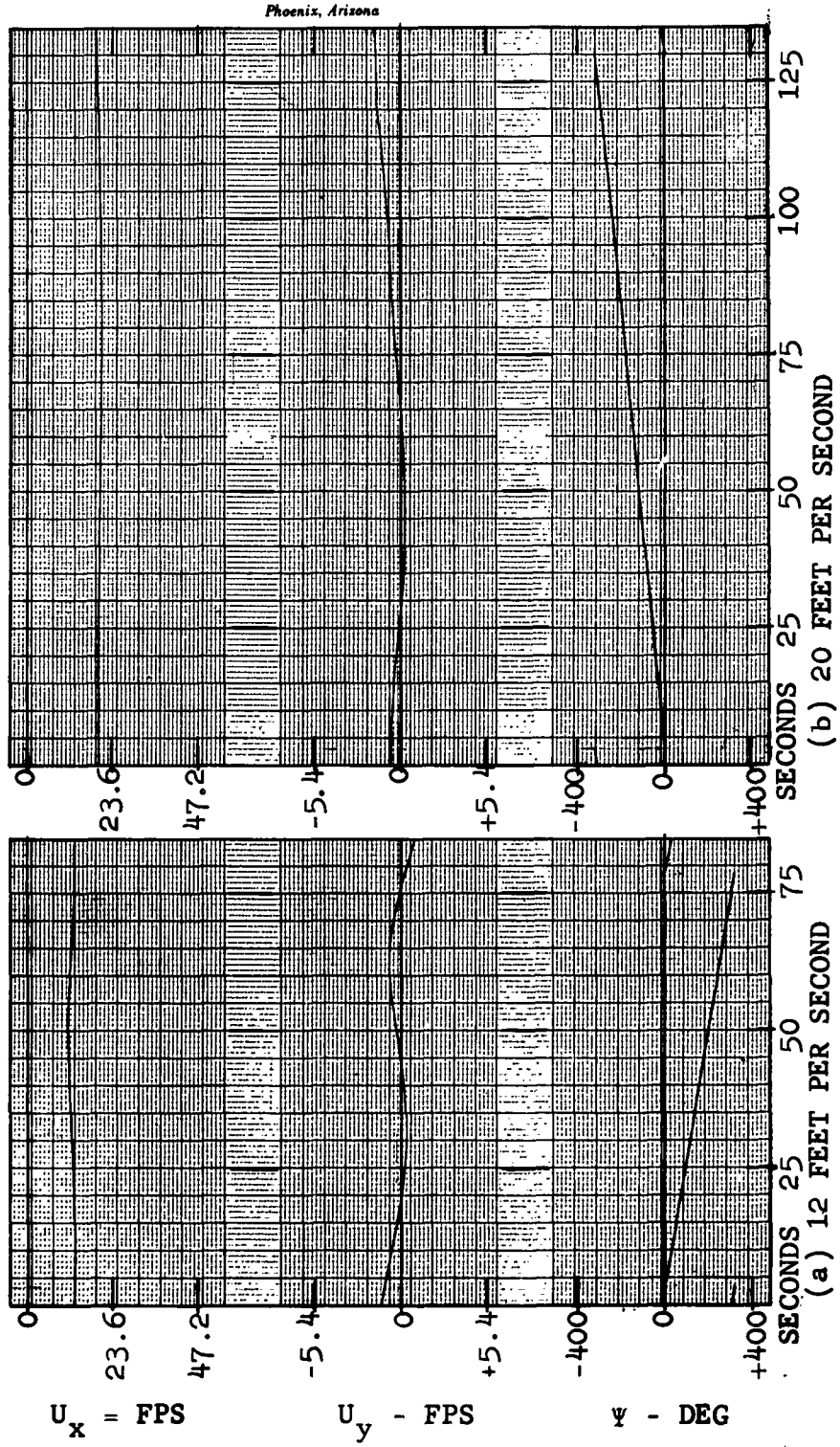

FIGURE 4-10. COORDINATED TURNS

A sideslipping turn is illustrated in Figure 4-11.

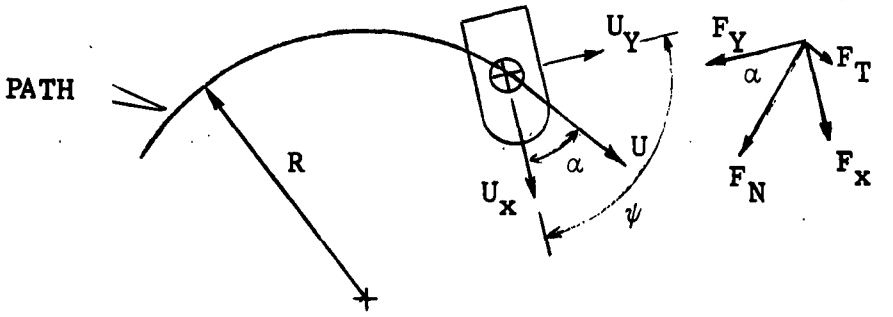

FIGURE 4-11. SIDESLIPPING TURN

In this turn, there is side force due to roll and sideslip. The centripetal force, which is normal to the resultant velocity U, is given by

$$F_N = F_x \sin \alpha + F_y \text{ Cos } \alpha$$

The tangential force is

$$F_T = F_x \text{ Cos } \alpha - F_y \sin \alpha$$

If the magnitudes of the velocities are constant, then F_T must be zero, giving $F_x = F_y \tan \alpha$ and

$$F_N = F_y \sec \alpha$$

The resulting radius of curvature will be

$$R = \frac{W_c}{g} \frac{U^2}{F_N}$$

Numerous constant U and Ω sideslipping turns were executed. It was found quite difficult to control sideslip angle. Velocity, sideslip angle, and turning radius for several of these turns are listed in Table 4-4.

TANGENTIAL VELOCITY	SIDESLIP ANGLE	TURNING RADIUS	F_N/W_c
18.2 fps	57°	130 ft	0.0792
20.9	57°	167	0.0813
22.2	54°	195	0.0786
23.3	55°	215	0.0785
25.3	51°	254	0.0783
27.3	49°	298	0.0777
30.3	46°	374	0.0763
33.6	45°	472	0.0743

TABLE 4-4. SIDESLIPPING TURNS

In Table 4-4 it is seen that a 20.9-fps turn can be made with a radius of 167 feet. The minimum coordinated turn radius at 20 fps was 405 feet. A sideslipping turn with this radius can be made at a speed in excess of 30 feet per second. Table 4-4 also shows an effective centripetal force equal to 0.075 to 0.080 W_c for sideslipping turns, whereas the value for coordinated turns is only 0.03 W_c. It is apparent that over half of this is due to the centripetal component of propulsion. Figure 4-12 shows the computer trace from which the 20.9 and 22.2-fps points were taken.

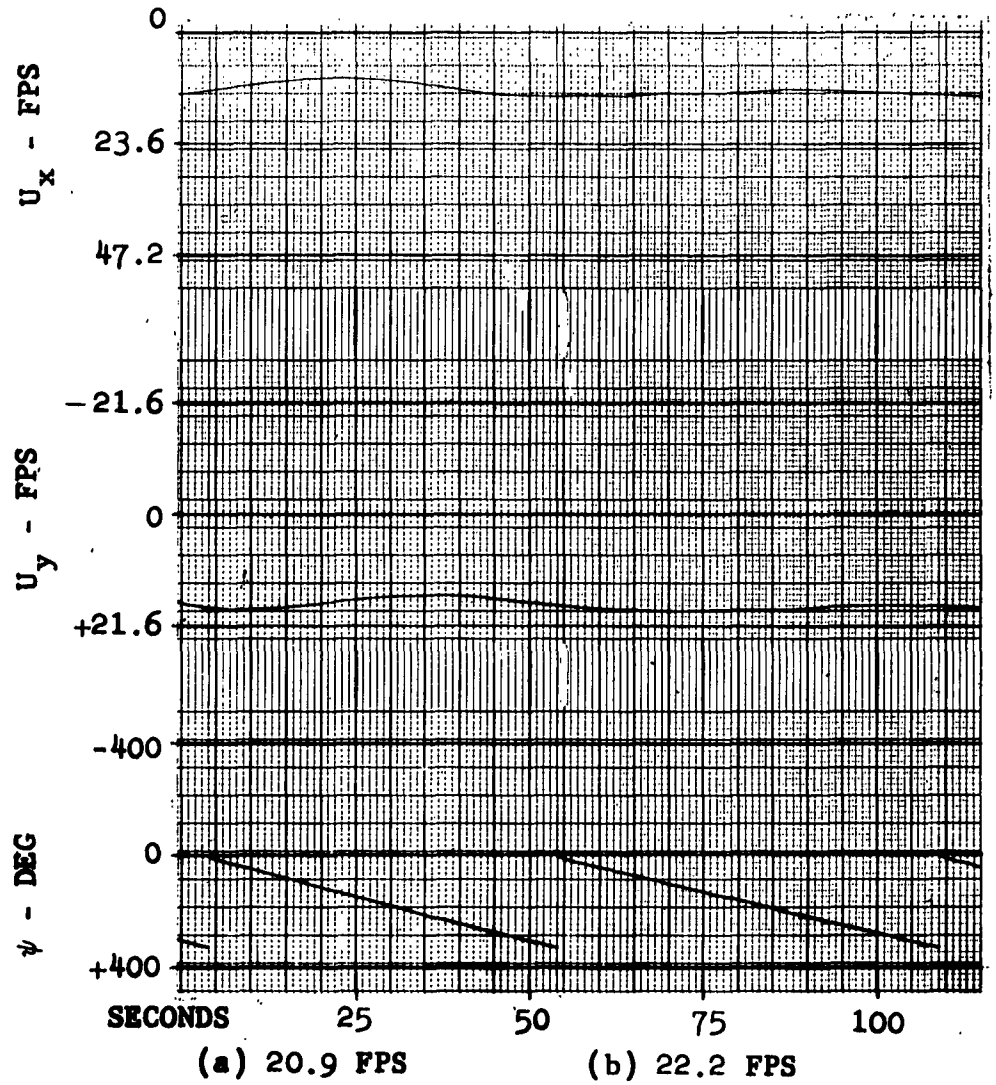

FIGURE 4-12. SIDESLIPPING TURNS

4.3 Controllability

4.3.1 Introduction

The attempt has been made to evaluate seriously a vehicle being controlled by a human operator. However excellent the simulation may be in reproducing or predicting natural vehicle motions, response to winds and waves, or reaction to a control command, it falls short insofar as it fails to give some answers to the obvious question, "Can a man really pilot this vehicle into a harbor and dock it without endangering other small craft in the area?" If the simulation can give answers to such basic questions, it will be of real value in evaluating proposed vehicles and proposed control systems. It is felt that the results described in this section show:

(a) That the present simulation gives considerable insight into the practical aspects of designing controllable GEM's and

(b) That additional work is needed in giving the pilot an immediate realistic feeling for vehicle motions as they occur.

Several problems are encountered in trying to put a human operator in command of a vehicle.

(a) The vehicle must be controllable.

For the reference GEM an analysis was performed to determine the most feasible means of providing pitch control, side force, propulsion, braking, and yaw moments.

(b) The pilot must have, at his control station, physical hardware with which he commands the various vehicle inputs.

A rudimentary control station was constructed as described in Section 3. It has been called a "universal control station" because most of the pilot motions that are normally found in vehicles have been included without designating the particular pilot motion that controls each vehicle input.

(c) The pilot must be continuously informed of vehicle motions, attitudes, locations, etc.

Initial trial runs, which were made to check out the program, used a standard X-Y plotter for course plotting, a Sanborn 8-channel recorder for speeds, heading, etc., and one or two dial meters. During these initial runs it was found difficult to keep track of heading and yaw rate, so that the GEM tended to spin in rather tight loops. It was found that a yaw rate meter helped the operator very much. The final pilot display employed six meters, showing pitch angle, roll angle, forward velocity, side velocity, heading (ψ) and yaw rate, and an X-Y plotter to show the vehicle path relative to surface coordinates.

4.3.2 Control Modes

Basically the pilot controls four inputs to the vehicle. These are thrust (acceleration and braking), roll moment (producing roll angle and, thus, side force), pitch moment (producing pitch angle and thrust), and yaw moment. With the flexibility of a computer simulation, it was possible to use any of the pilot motions to control a given vehicle motion. In the actual runs, four control modes were used to show their relative merits and the ability of a pilot to learn new control modes.

4.3.2.1 Control Mode 1

Parameter	Pilot Motion
Thrust	Left-hand hand lever
Roll	Wheel-base rotation
Pitch	Push-pull wheel
Yaw	Wheel rotation

4.3.2.2 Control Mode 2

Parameter	Pilot Motion
Thrust	Foot pedals
Roll	Wheel-base rotation
Pitch	Push-pull wheel
Yaw	Wheel rotation

4.3.2.3 Control Mode 3

Parameter	Pilot Motion
Thrust	Push-pull wheel
Roll	Wheel rotation
Pitch	Righ-hand hand lever
Yaw	Foot pedals

4.3.2.4 Control Mode 4

Parameter	Pilot Motion
Thrust	Left-hand hand lever
Roll	Wheel rotation
Pitch	Right-hand hand lever
Yaw	Foot pedals

4.3.2.5 Discussion

Rotation of the wheel base and push-pull motion of the wheel were centered by springs. For this reason these motions required a continuous force by the pilot. The other motions (wheel rotation, hand levers, and pedals) can be moved to a desired setting and left unattended until a change is desired. In Control Modes 3 and 4, the wheel base rotation was locked out.

4.3.3 Evaluation Courses

Evaluations of vehicle controllability were divided into low-speed and high-speed maneuvers. For this purpose low speed is defined as speeds below 20 feet per second--below hump speed. High speed is above hump speed. The high-speed runs were generally made above 40 feet per second, and speeds in the 80- to 100-feet-per-second range were not uncommon.

Three basic maneuvers were used to demonstrate controllability. These are:

(a) Flying a straight course and stopping in a prescribed area.

(b) Flying a simple 90-degree turn and stopping in a prescribed area.

(c) Flying from point A to point B in the presence of obstacles, including going through a relatively narrow passage.

Reduced reproductions of the four plates used on the X-Y plotter are shown in Figures 4-13, 4-14, 4-15, and 4-16. The actual size of the plates used was 11 by 17 inches, with a 10 x 15-inch area of grid lines. The low-speed courses (1a, 1b, and 1c) shown in Figures 4-13 and 4-14 used a scale of 200 feet to the inch. The small craft shown on these plates are 30 by 60 feet, which is approximately the size of the reference design. The high-speed courses shown in Figures 4-15 and 4-16 used a scale of 1000 feet to the inch. Note that the dotted rectangular area

at the bottom of Figure 4-16 is a reduced drawing of the low-speed harbor course in Figure 4-14. These two courses taken together represent a high-speed approach to the coast line through a straight followed by a low speed course through a breakwater and harbor.

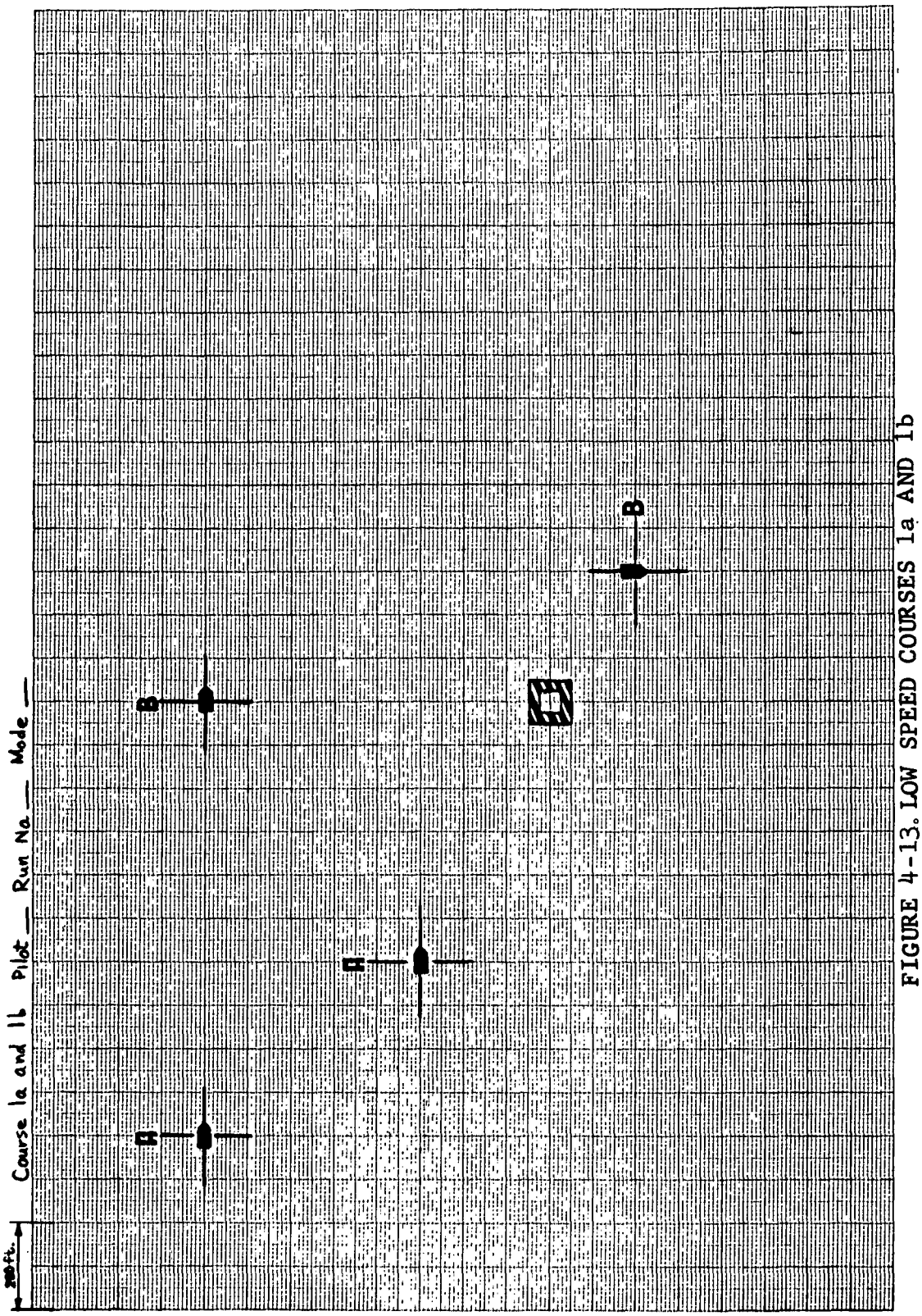

FIGURE 4-13. LOW SPEED COURSES 1a AND 1b

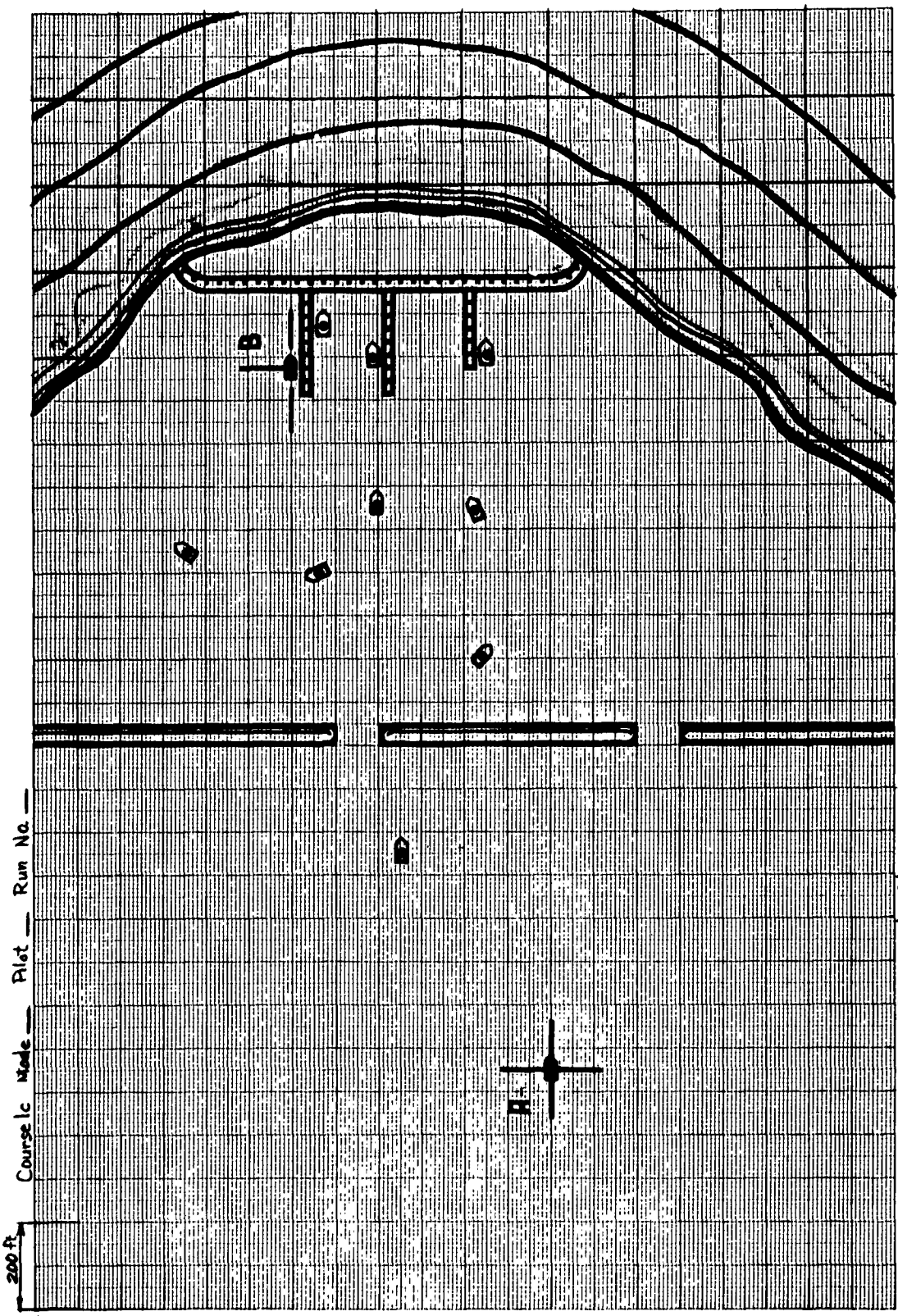

FIGURE 4-14. LOW SPEED HARBOR MANEUVERING COURSE 1c

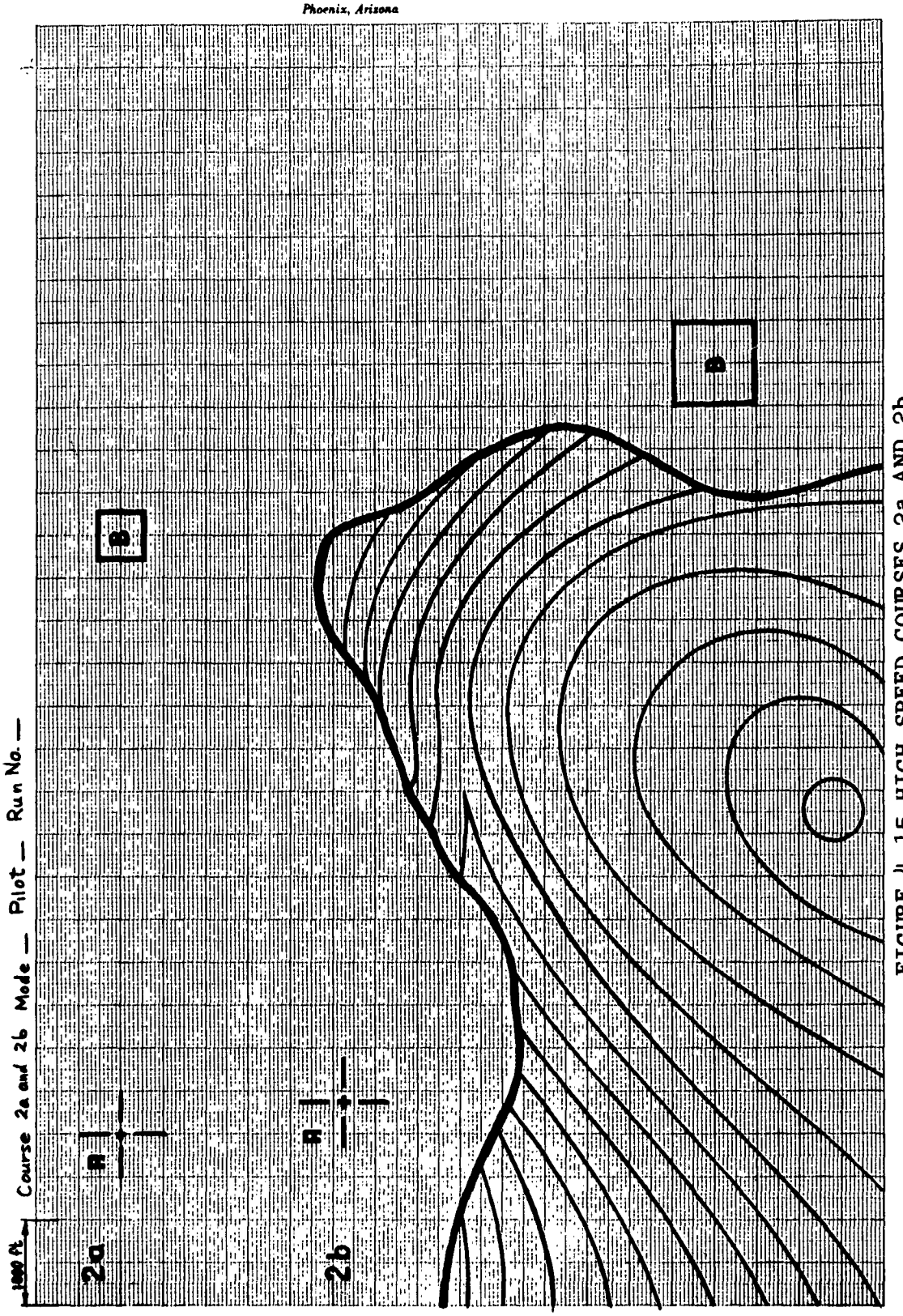

FIGURE 4-15 HIGH SPEED COURSES 2a AND 2b

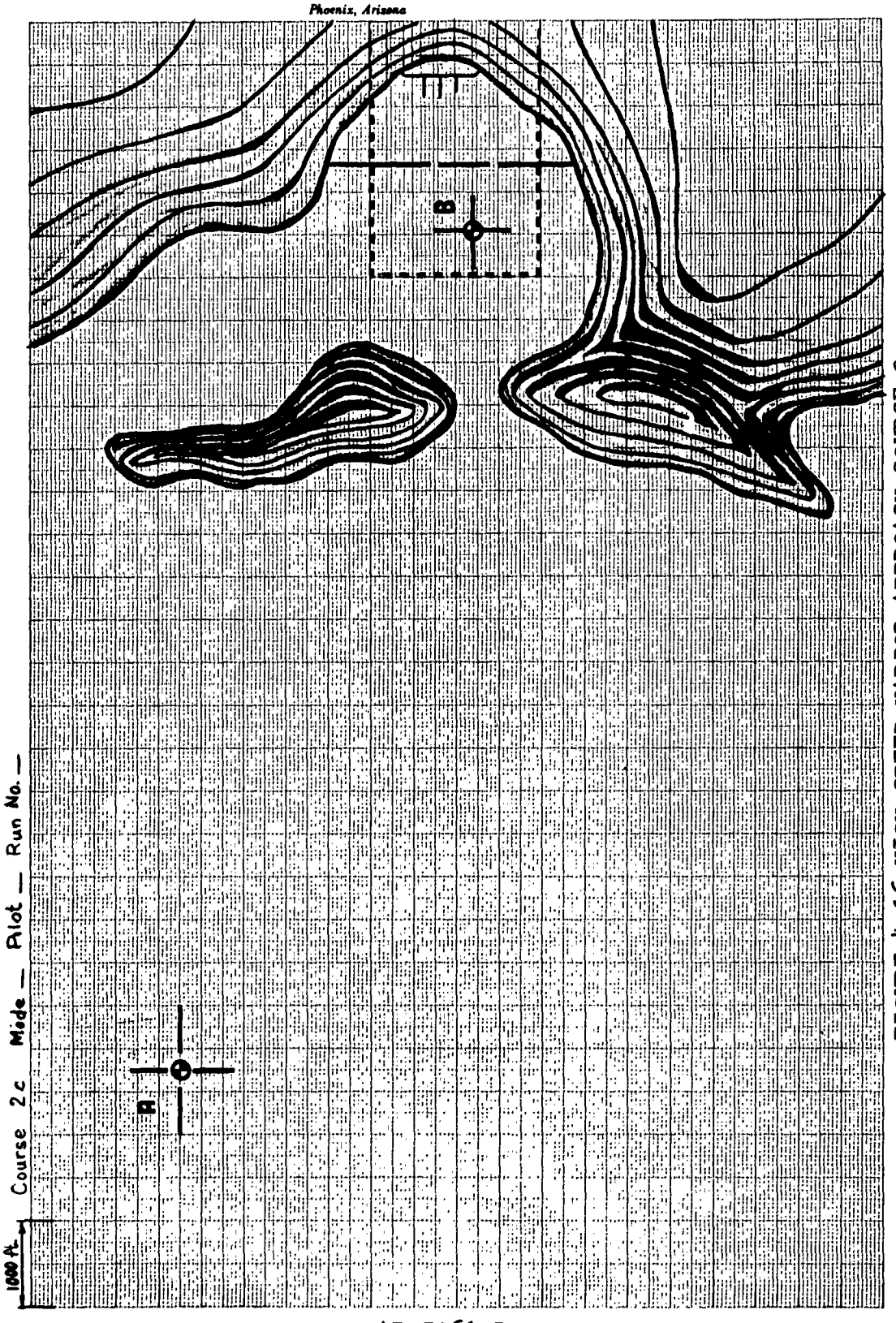

FIGURE 4-16 HIGH SPEED HARBOR APPROACH COURSE 2c

4.3.3 Results of Controllability Runs

4.3.3.1 Procedure

The general procedure for flying the courses was to allow the pilots some practice time to become familiar with the control mode and then to fly all six courses in that mode. Three pilots were used throughout the test runs. Usually, all three pilots performed the low-speed runs before any started the high-speed runs. In all cases, the pilot was allowed reruns at his own discretion. It should also be noted that all of the preliminary familiarization with vehicle characteristics was done in Mode 1. Each pilot had several hours of flying time in Mode 1 before any runs were made for the record. Following a change in control mode, the pilots generally made runs for the record beginning with their third or fourth trial run.

During the test runs continuous recordings of forward velocity, side velocity, yaw angle, roll angle, pitch angle, and hovering height variation were made. To correlate these traces with the X-Y plotter course record, both the Sanborn trace and the X-Y plotter pen were blipped at 10-second intervals.

The low-speed runs were made in Modes 1 and 3 only. The reason is that all of the pilots preferred to use pitch only for low-speed propulsion. Therefore, since Modes 2 and 4 differed only in the thrust control, they were the same as Modes 1 and 3 at low speeds.

4.3.3.2 Flying a Straight Course

The tendency of the GEM to sideslip, together with the slow yaw transients, makes flying a straight course more difficult than it would at first appear. Figure 4-17 shows the low-speed runs in Control Modes 1 and 3 by each of the three pilots. The times required to traverse the 1000 feet from A to B are shown in Table 4-5.

	Pilot 1	Pilot 2	Pilot 3
Mode 1	66 Sec.	67 Sec.	62 Sec.
Mode 3	80 Sec.*	77 Sec.	150 Sec.

TABLE 4-5. Time To Fly Course 1a

As seen in Figure 4-17, all three pilots were able to hold a straight course within 15 or 20 feet, achieve an average speed near 15 feet per second, and stop within the vehicle dimensions of the preset point. This was in Mode 1, with which all pilots had had considerable flying time. It is interesting to note that an idealized run with acceleration at 0.045 g (the low-speed value due to pitch from Section 4.1.2), constant speed 20 feet per second, and deceleration at 0.045 g would require 64 seconds.

The Mode 3 tests, which were run after the Mode 1 tests, show considerably less skill on the part of the pilots. The difference lies in the change to using foot pedals for yaw control and turning the wheel for roll control. The first run of Pilot 1 shows initial inability to correct a slow

*Run 2

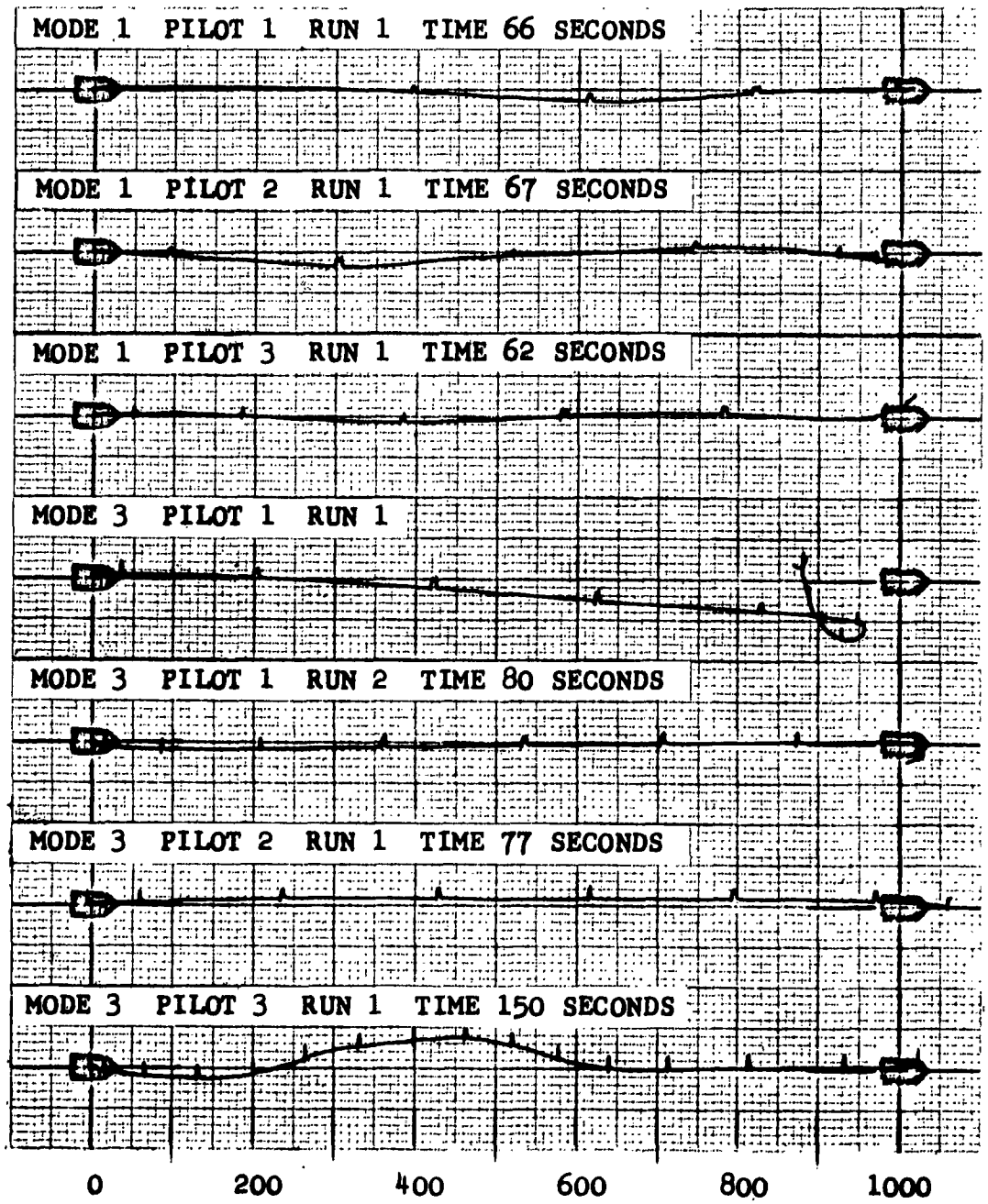

FIGURE 4-17 COURSE 1a TEST RUNS - LOW SPEED

divergence from the prescribed course, followed by a futile attempt to stop and recover. This is a situation that is neither uncommon nor difficult in car or truck driving. If the driver finds he's missing the garage door, he simply stops, backs up, and proceeds slowly onto the proper course. This would be the obvious way out for Pilot 1 in the run being considered. However, the display did not give the pilot an immediate feeling for course, heading, and the required changes. This is a pattern that recurred throughout the test runs. As a rule, when a Pilot found his course to be far enough off to require a drastic, immediate revision, he became confused as to the heading of his craft and was unable to achieve the required corrections.

The second run by Pilot 1 shows considerable improvement in holding course. However, the time increase from 66 to 80 seconds indicate the extra caution with an unfamiliar control mode. Pilot 2's run time increase shows additional caution, while that for Pilot 3 shows that he found it very difficult to make the required corrections even though his speed was less than half of that used in the Mode 1 run all three pilots had difficulty stopping in the prescribed area. The reason for this is a time delay. When the Mode 3 runs were made, several days had elapsed since the previous low-speed runs and the pilots had forgotten the required stopping distance (about 140 feet) which was learned by experience during the test runs.

Figure 4-18 shows the high-speed runs. The high-speed course has a length of 7000 feet. From the acceleration data in Table 4-1, an estimate can be made of the time to make this 7000-foot run. With an acceleration rate of 0.09 g from 0 to 50 fps and 0.035 g from 50 to 100 fps, the GEM would reach 3760 feet. Deceleration at 0.07 g from 100 to 50 fps and 0.045 g from 50 to 0 fps would require 57 seconds and a distance of 2530 feet. The middle 710 feet would be traversed in 7 seconds. This gives a total estimated run time of 126 seconds. Figure 4-19 shows three typical speed versus time traces for the test runs in Figure 4-18. It is seen that all pilots made their runs in less than 126 seconds. The initial accelerations in the three traces shown are 0.136 g, 0.117 g, and 0.132 g. It is apparent that the pilots were using both full propeller thrust and nose-down pitching for maximum acceleration. The braking curves likewise show that pitch was used to augment the propellers. Counting the blips in Figure 4-18 shows that most of the runs were made in about 100 seconds.

The test runs in Figure 4-18 show the results of experience. In the Mode 1 runs, all three pilots held good courses and stopped very near the center of the target area (a 500-foot square). In the Mode 3 runs, two pilots overshot the target area by failure to brake soon enough. However, in the Mode 4 runs, which were very similar to those of Mode 3, all three were again able to stop within the target area.

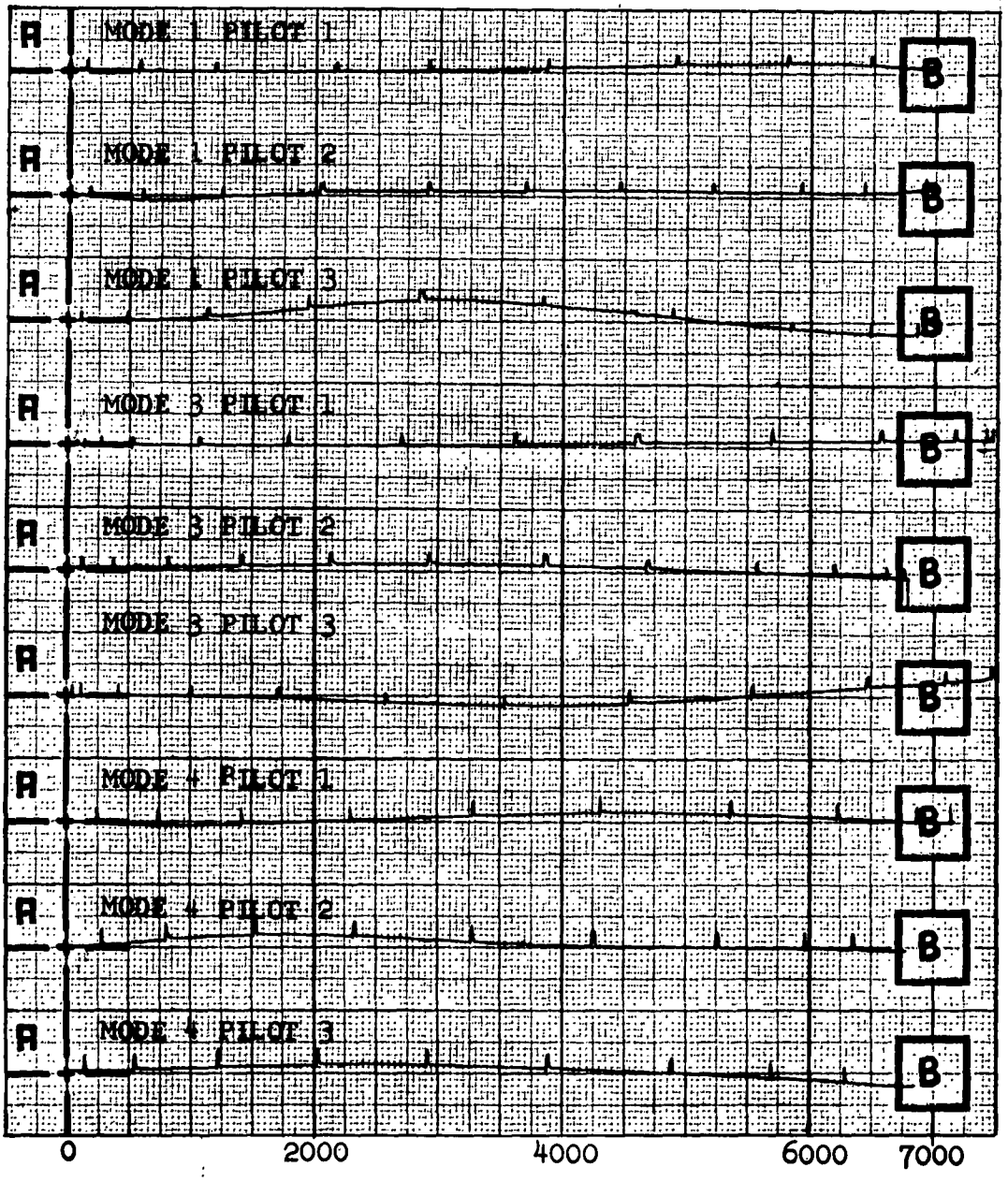

FIGURE 4-18. COURSE 2a TESTS - HIGH SPEED

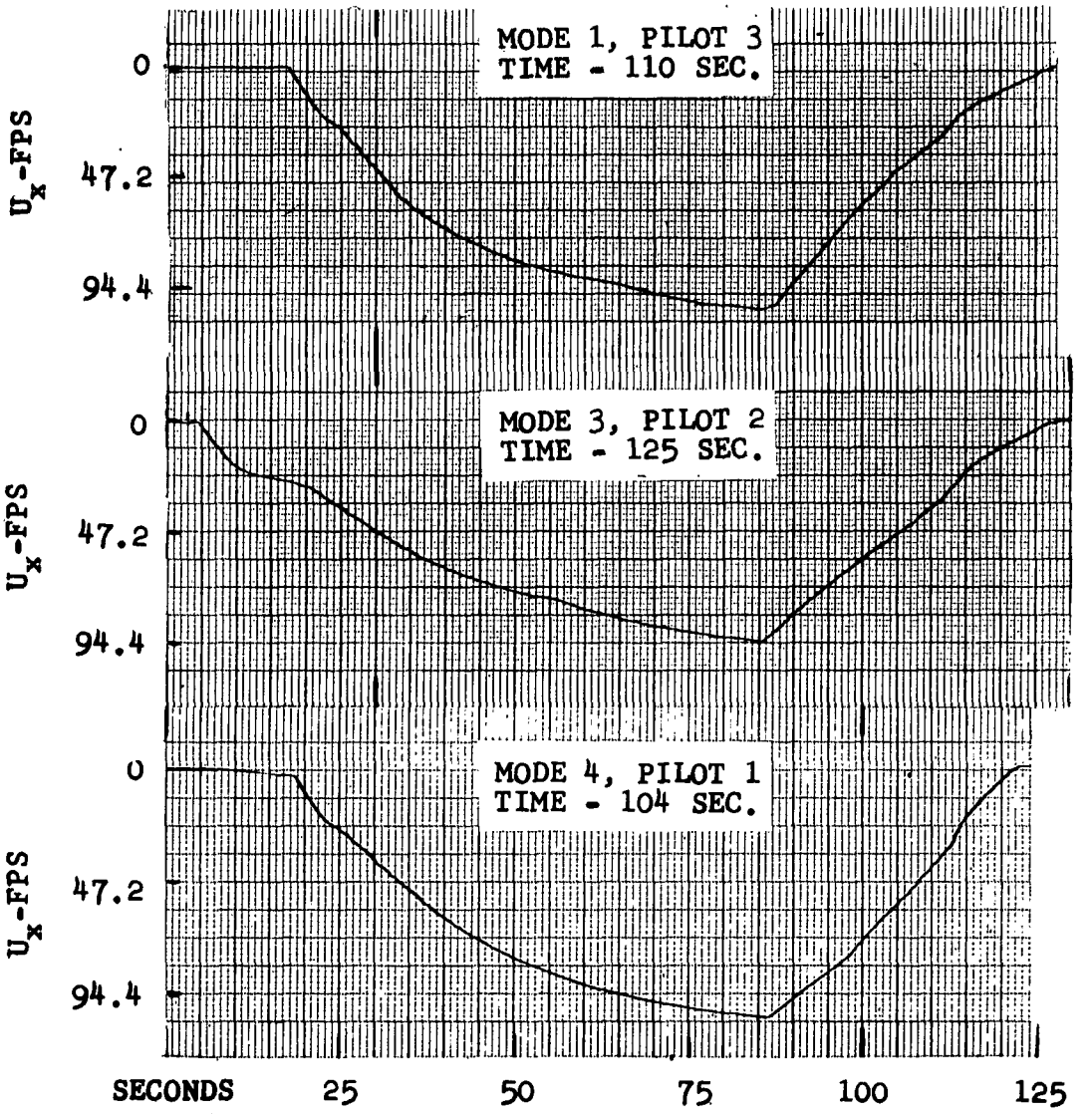

FIGURE 4-19. VELOCITY VS TIME TRACES FOR TYPICAL COURSE 2a TESTS - HIGH SPEED

4.3.3.3 Performing a Simple Turn

The low-speed, 90-degree turn tests by the three pilots in Modes 1 and 3 are shown in Figures 4-20, -22, and -24. The Sanborn traces corresponding to these tests are shown in Figures 4-21, -23, and -25. On the best run for each pilot, small arrows have been dubbed in to show the actual heading of the GEM at points along the curve.

In Figure 4-20, Mode 1, the turn was being made much too slowly. Pilot 1 slowed the vehicle--as shown between 70 and 80 seconds in Figure 4-21--until a 90-degree yaw angle was reached and then accelerated toward the target area. The Mode 1 test shows an initial zero heading, with the course drifting to the left due to sideslip. The turn toward the target area is a nearly constant velocity sideslipping turn. The final 10 seconds of the run shows an excessive yaw angle accompanied by sideslip which continued to carry the GEM away from the target area.

In Figure 4-22, Pilot 2 has a nearly perfect heading and course initially. At 40 seconds he was sideslipping into the turn. The roll angle between 30 and 40 seconds (Figure 4-23, Mode 1) is the primary cause of a turning course at this point. By 50 seconds Pilot 2 had yawed to a heading along the course, and by 60 he had developed considerable sideslip to the outside of the turn--which is normal for a minimum-radius sideslipping turn. The failure to continue on into the target area is a combination of braking which eliminated the velocity component in the direction of the heading and a reduction of roll angle to zero which failed to eliminate side velocity. It is seen in Figure 4-23 that U_x is negative at 70 seconds.

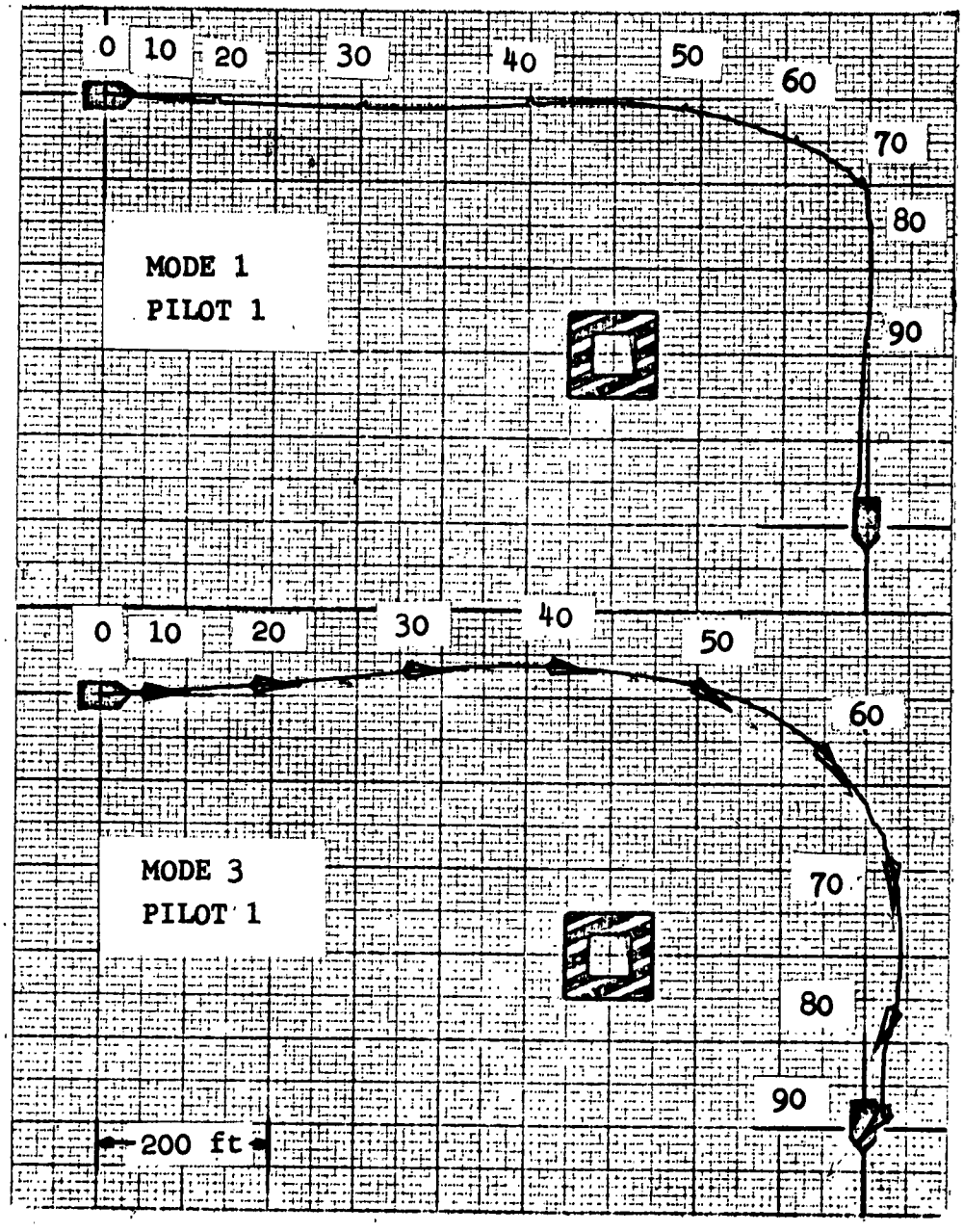

FIGURE 4-20. COURSE 1b TEST RUNS

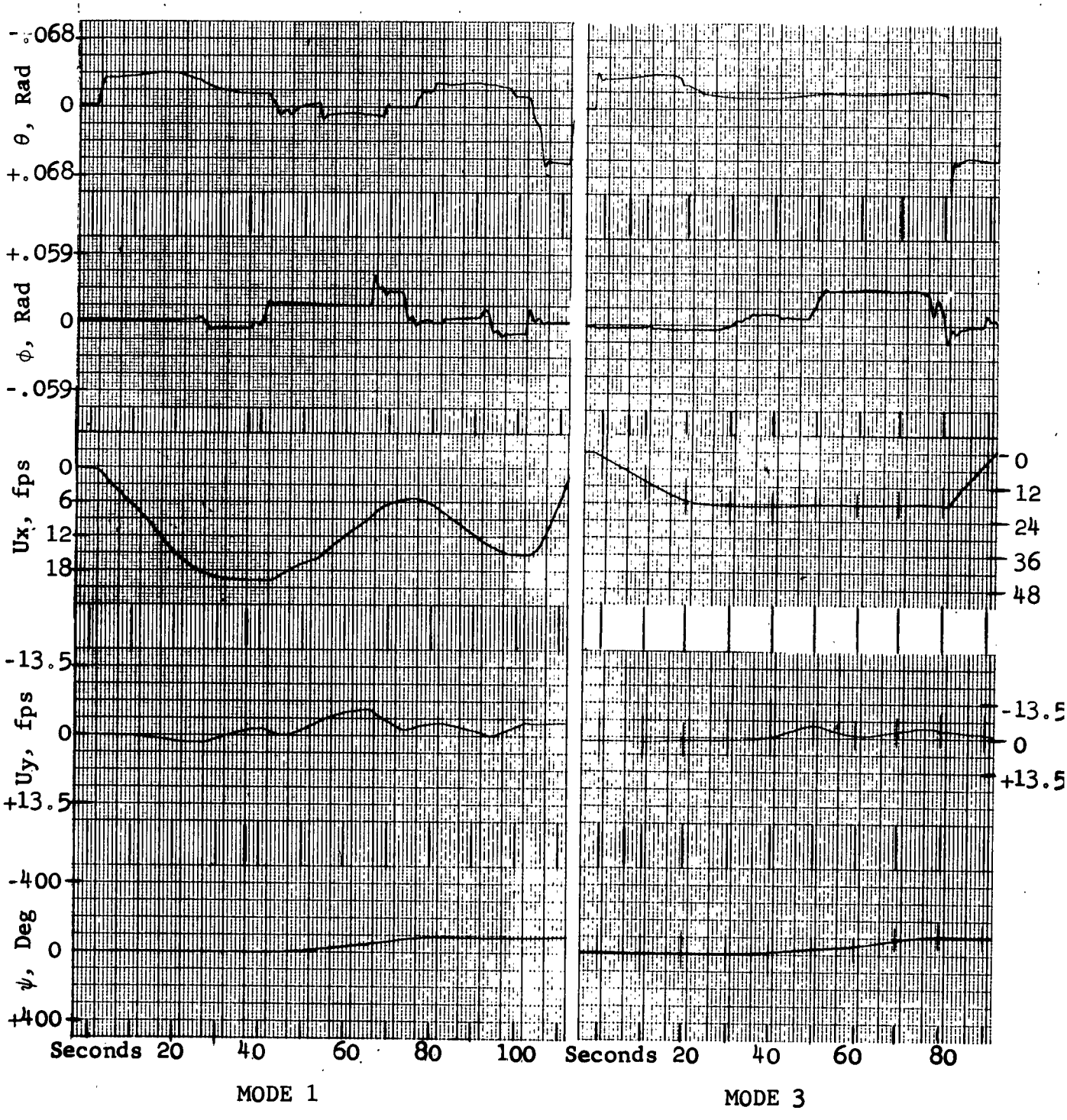

MODE 1

MODE 3

FIGURE 4-21 COURSE 1b TEST RUNS, PILOT 1

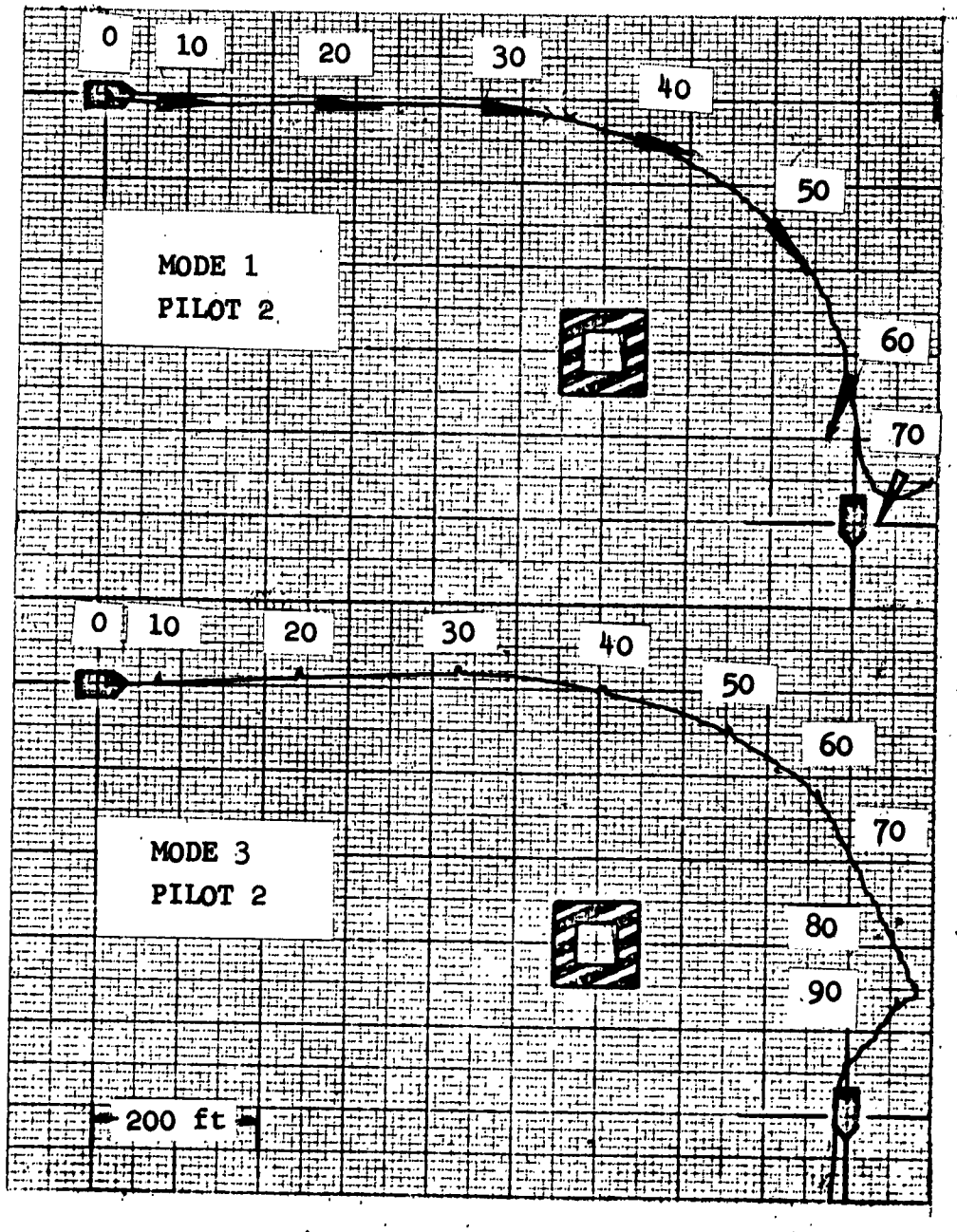

FIGURE 4-22 COURSE 1b TEST RUNS

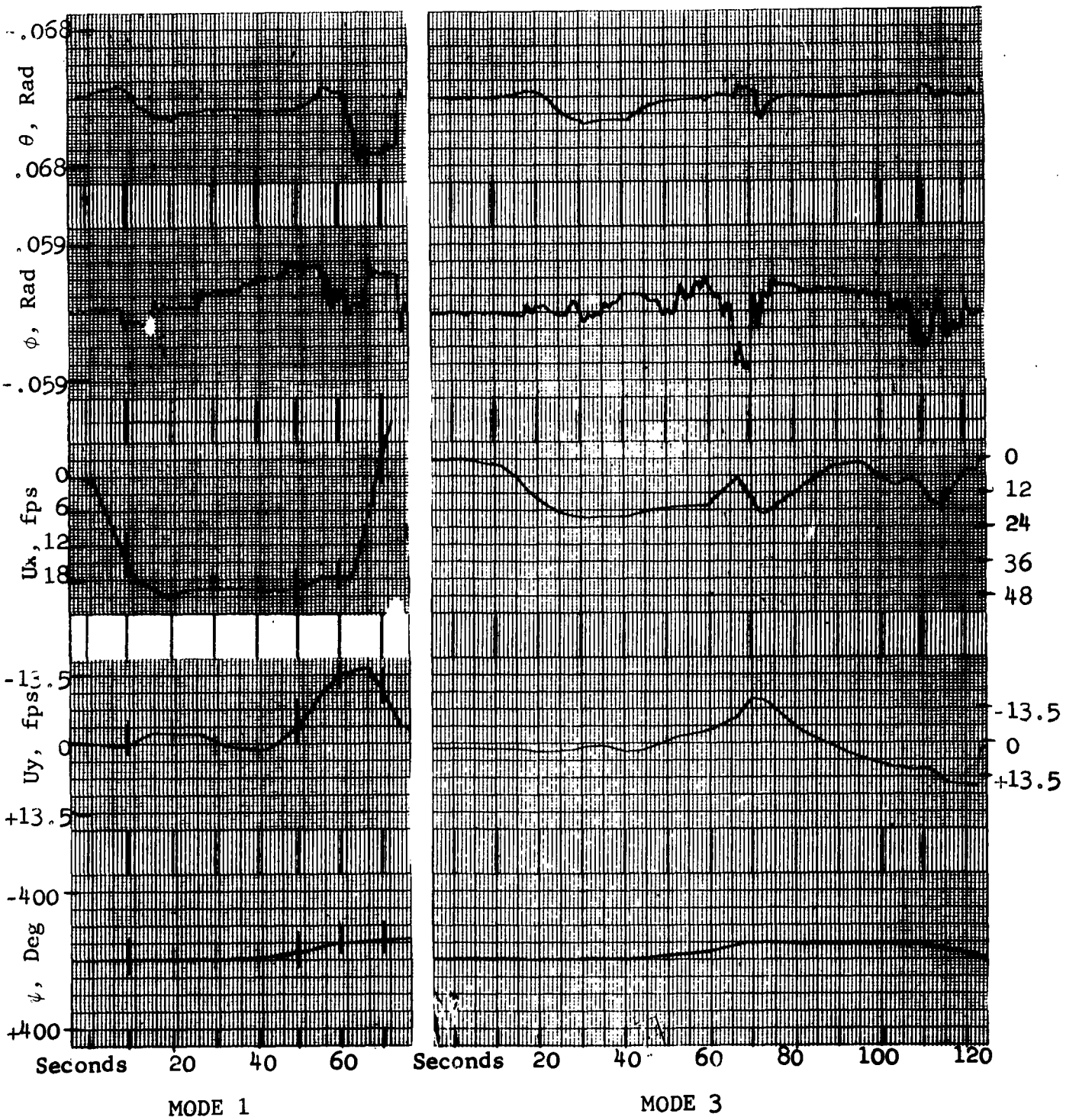

MODE 1 MODE 3

FIGURE 4-23 COURSE 1b TEST RUNS, PILOT 2

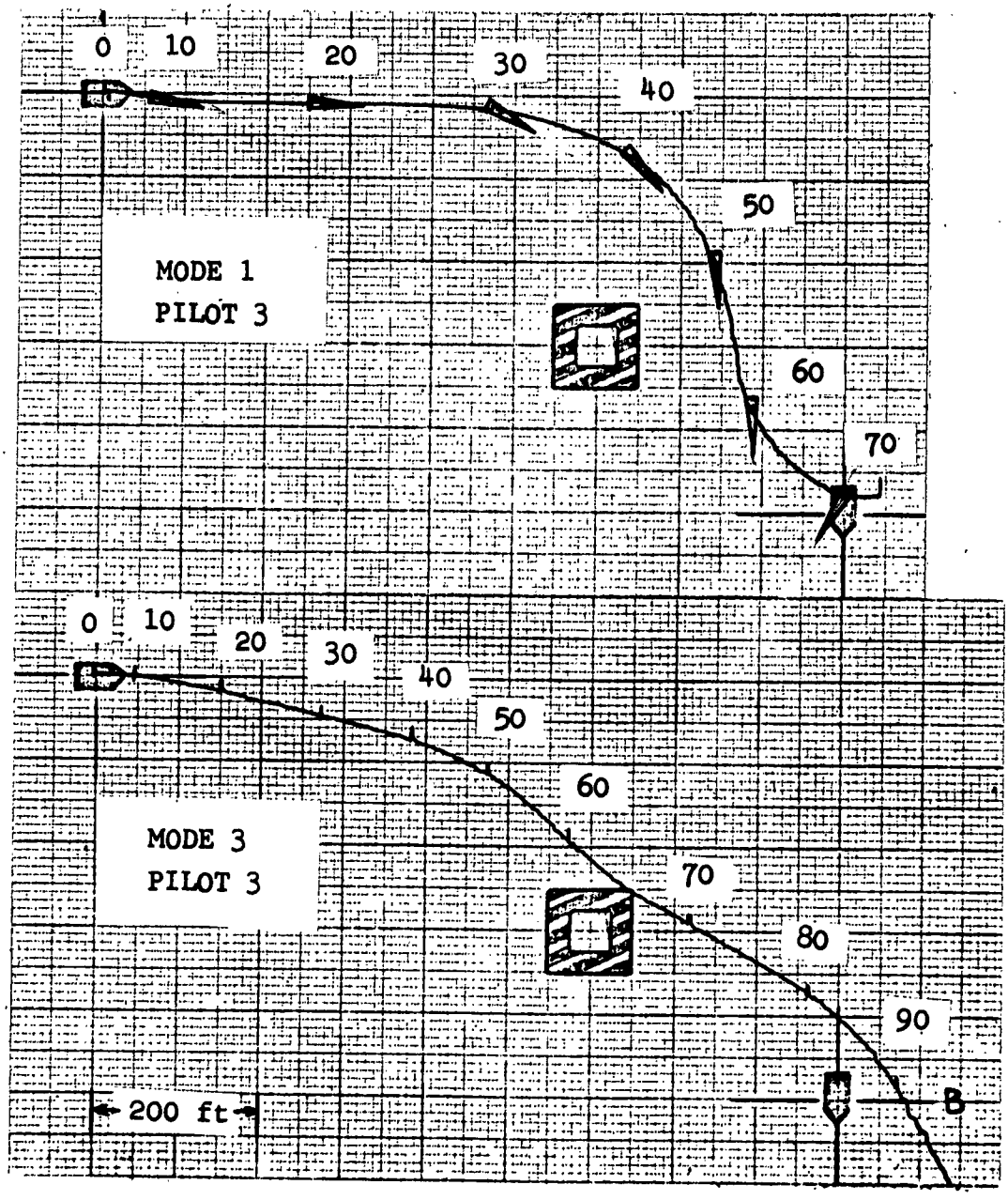

FIGURE 4-24 COURSE 1b TEST RUNS

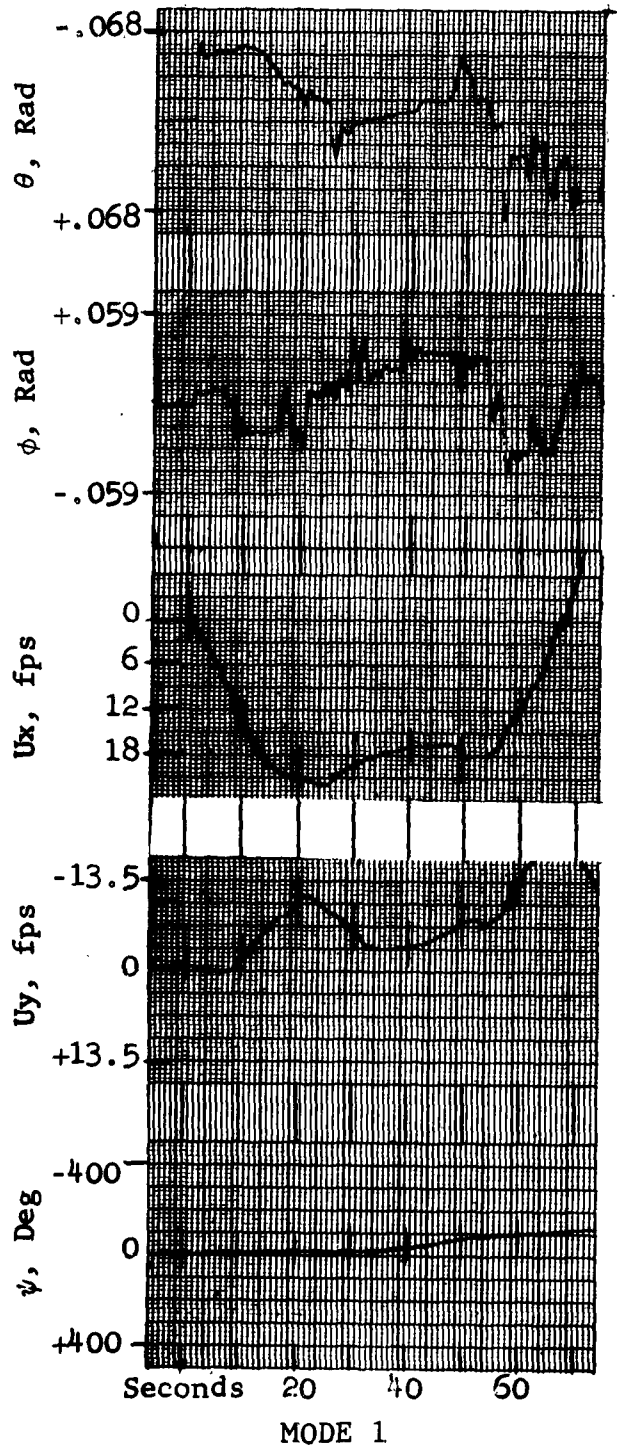

MODE 1

FIGURE 4-25 COURSE 1b TEST RUNS, PILOT 3

In Figure 4-24, Pilot 3 exhibited good control in correcting an initial drift to the right. After 20 seconds a 0-degree nonsideslipping course had been achieved. From 30 to 50 seconds, a small-radius sideslipping turn is achieved. From 50 seconds onward he controlled the course strictly by sideslip. The traces in Figure 4-25 show that the braking was accomplished by a reduction of roll angle so that sideslip carried the GEM into the target area.

Two other observations can be made regarding these tests. The first is in regard to turning radius. The smallest radius turns shown in Figures 4-20, -22, and -24 are shown in Table 4-6.

Mode	Pilot	Velocity	Radius
3	1	17.7 fps	300 ft
1	2	17.4 fps	280 ft
1	3	17.0 fps	230 ft

TABLE 4-6. Course 1b, Low-Speed Turns

From Section 4.2.4 the minimum radius of a coordinated turn at 17 fps is 299 feet. It is seen that all pilots made tighter turns than this (at 17.7 fps R = 325 feet). However, none of the pilots approached the 130-foot radius recorded at 18.2 fps in a 57-degree sideslipping turn (Table 4-4).

The second observation is that Pilots 2 and 3 tended to use roll control much more than Pilot 1 in holding a course. This can be seen by comparing roll angle traces for the three pilots.

Course 2b is a high-speed turn around a promontory and ending in a 1000-foot-square area. The flying times for the various pilots and modes are given in Table 4-7.

	Pilot 1	Pilot 2	Pilot 3
Mode 1	220 Sec.	227 Sec.	212 Sec.
Mode 2	227	266	272
Mode 3	260	258	300*
Mode 4	250	210	254

TABLE 4-7. COURSE 2b, FLYING TIMES

Mainly this table shows the added caution--hence slower speed--used with an unfamiliar control mode. The fact that Mode 4 times were all less than Mode 3 times indicates the increase of confidence with experience. The course length for these runs is about 12,500 feet. Therefore, a run time of 250 seconds indicates an average velocity of about 50 feet per second.

Figures 4-26, -27, and -28 show the test runs by Pilots 1, 2, and 3, respectively, using Control Modes 1 and 2. The Mode 1 runs which have headings dubbed in show and interesting contrast in flying technique between Pilots 1 and 2 and Pilot 3. The relatively small sideslip angles of Pilots 1 and 2 on the straightaway and in slow turns indicate the tendency to fly by instruments. This type of run requires fairly close attention

*Did not enter the target area.

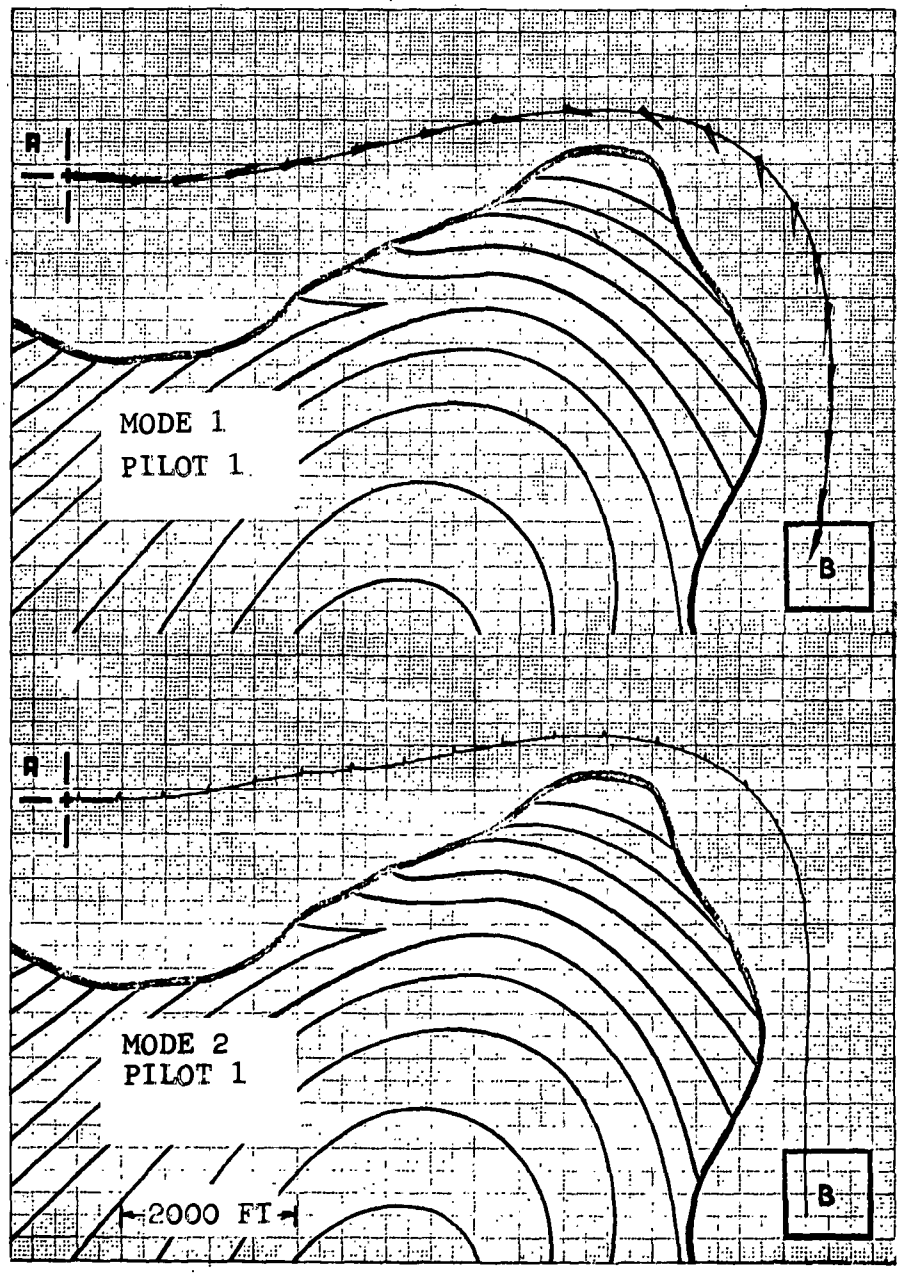

FIGURE 4-26 COURSE 2b TEST RUNS

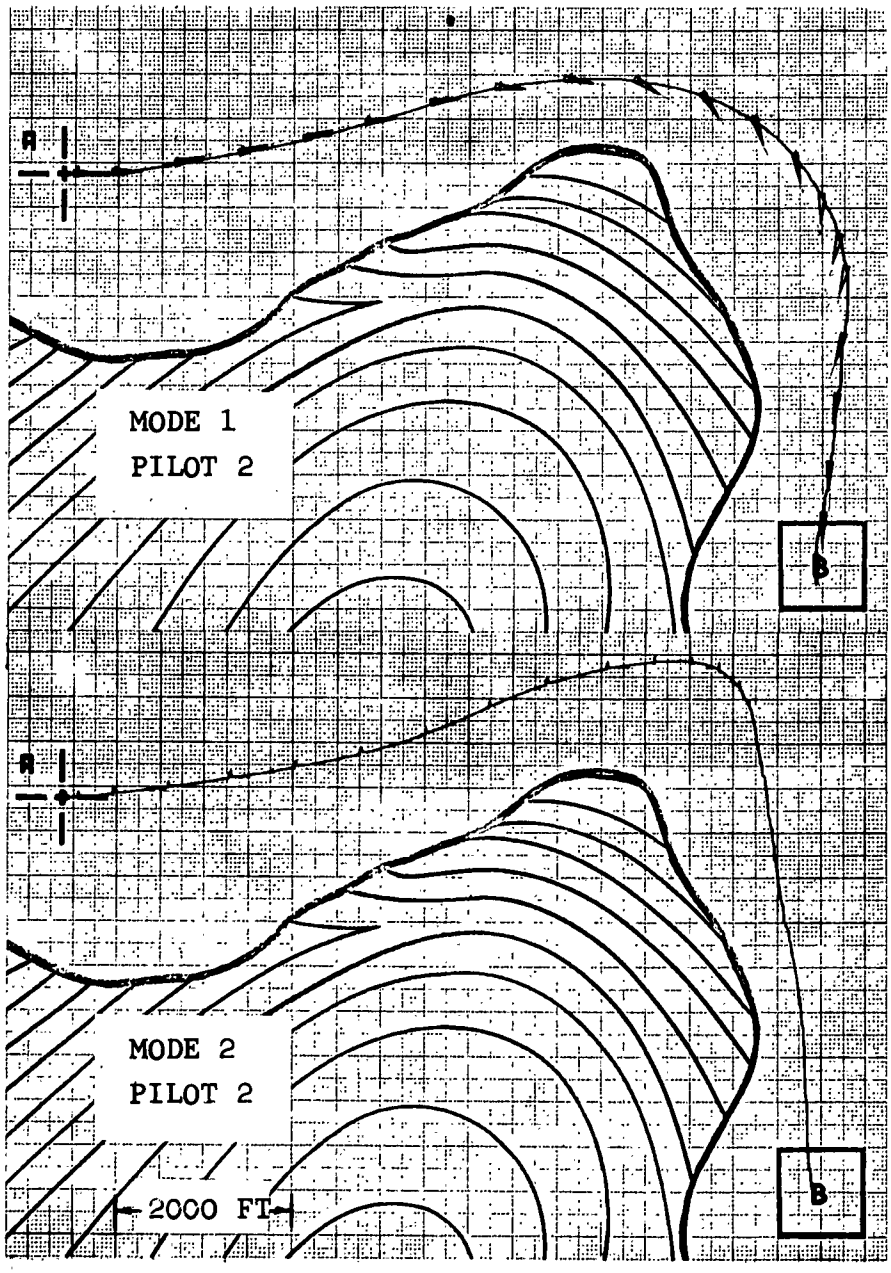

FIGURE 4-27 COURSE 2b TEST RUNS

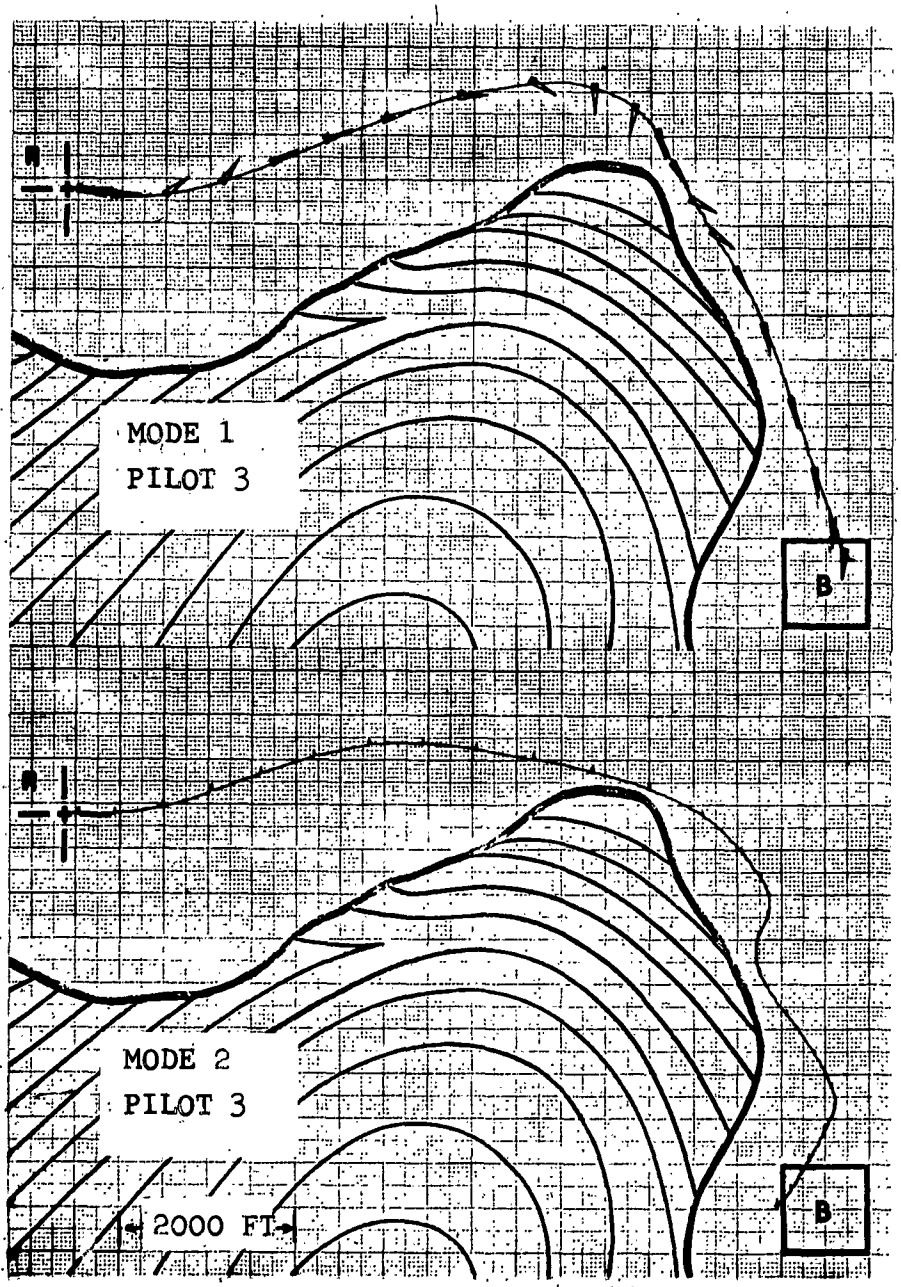

FIGURE 4-28 COURSE 2b TEST RUNS

to keeping yaw rate and side velocity small. The smooth curves are the result of uniform yaw rate and continuous side force (due to roll). The rather large sideslip angles produced by Pilot 3 show a tendency to fly by "feel"--that is, to watch the course on the X-Y plotter and control drastically when a change is required. The relatively slow vehicle response results in rather large sideslip angles before a course change is is noticed.

It should be noted that all three pilots were able to produce test runs as good as those shown in Modes 1 and 2 at the time these runs were made.

Figure 4-29 shows two Mode 4 runs by Pilot 1. The first run shows what can happen to an instrument pilot when an instrument is misread. The yaw angle meter has two scales--one reading from minus 180° to plus 180°, the other from minus 360° to plus 360°. This is useful in that it premits full 360-degree turns without saturating the meter and yet allows the pilot to read smaller angles accurately by a flip of the switch. In Run 1, the switch was on the 360-degree scale and the pilot was reading the 180-degree scale. When he thought he was approaching a 90-degree heading as he rounded the promontory, he actually was approaching a 180-degree heading. The result is obvious. Run 2 was made immediately to show (the witnesses) that he was able to control yaw as well with the yaw pedals as in the Mode 1 run with the wheel.

Figure 4-30 shows the "fly by feel" pilot first in an aborted run which resulted from instinctively doing the wrong thing with an unfamiliar control and their successfully bringing his craft into the target area.

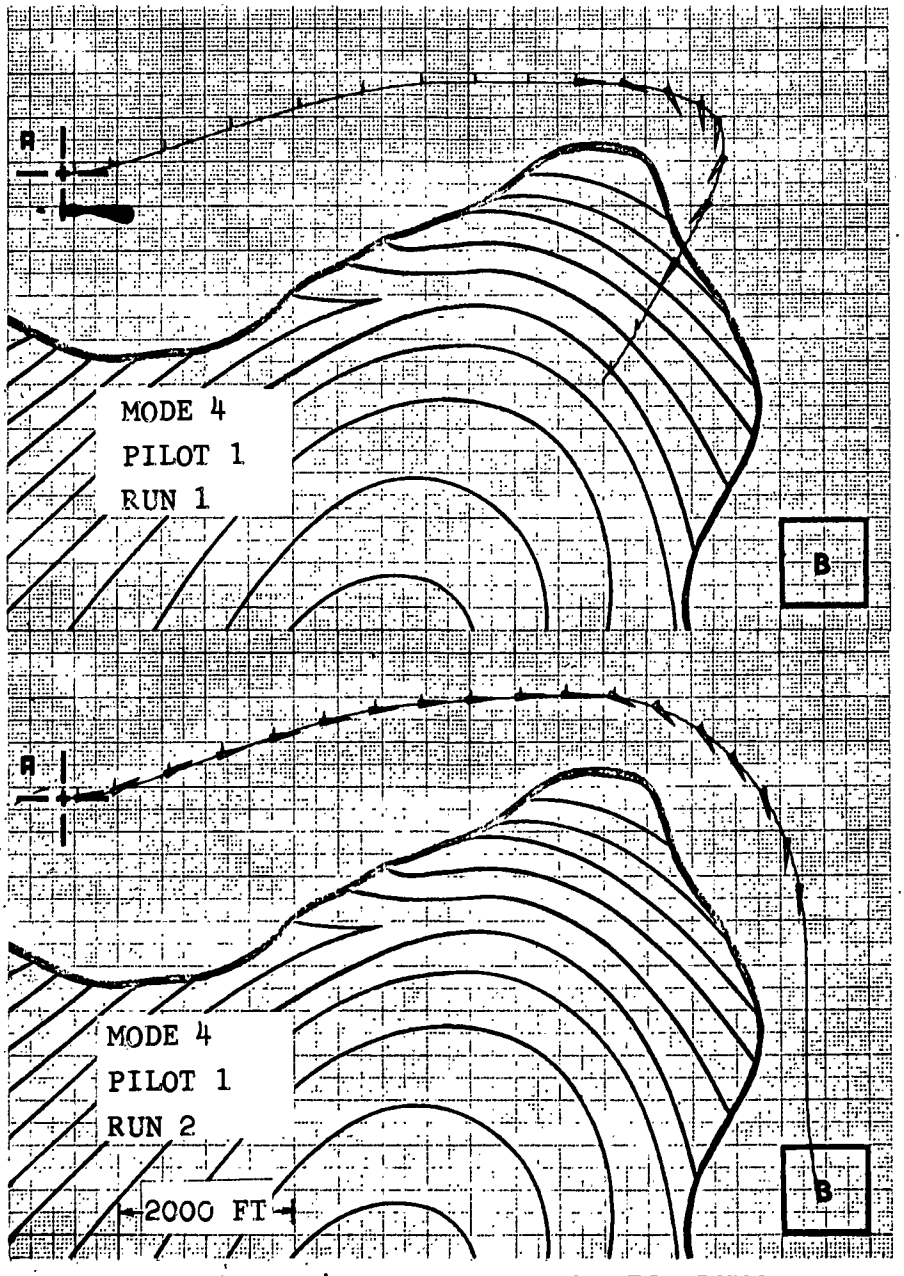

FIGURE 4-29 COURSE 2b TEST RUNS

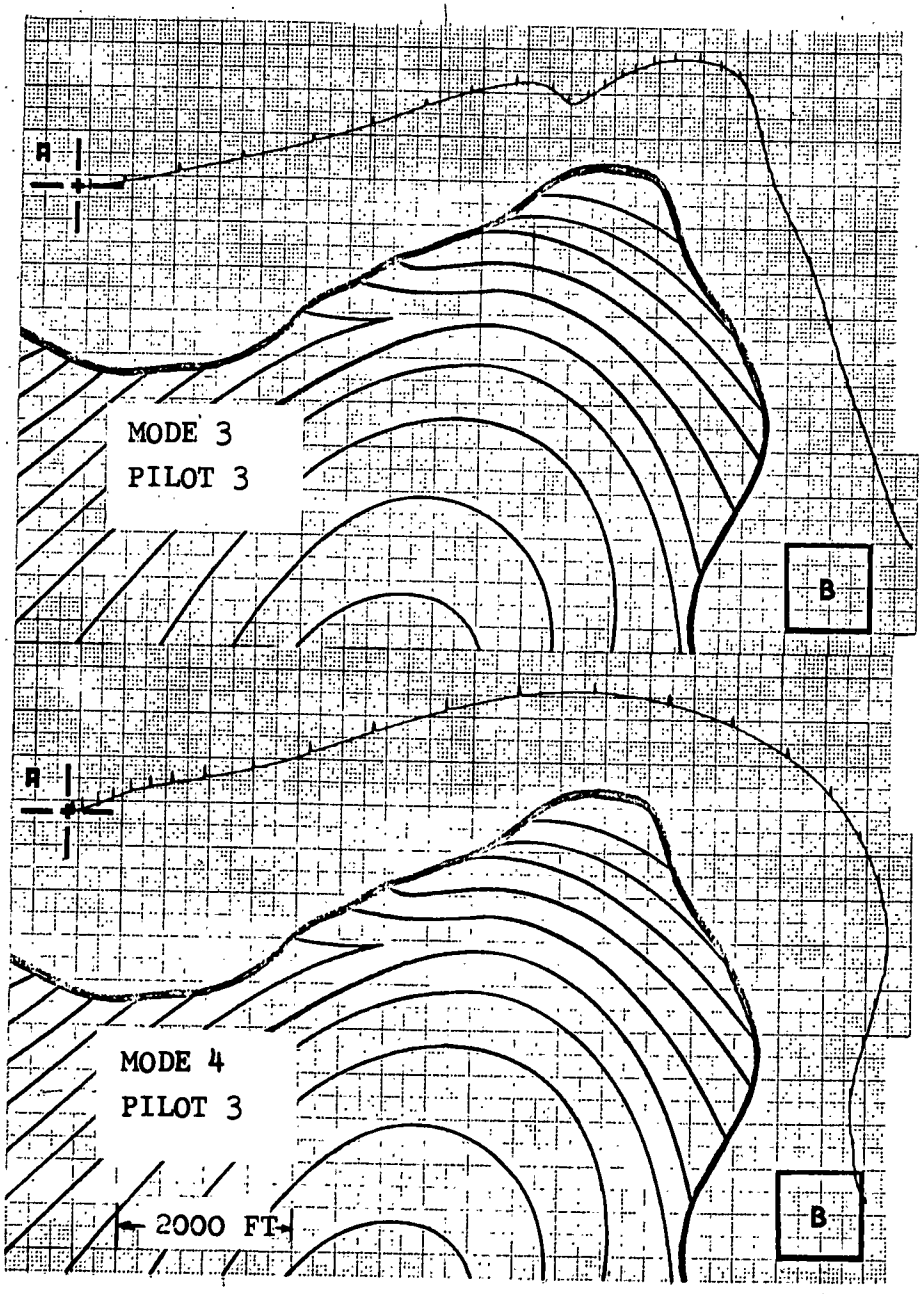

FIGURE 4-30 COURSE 2b TEST RUNS

4.3.3.4 Obstacle Courses

Courses 1c and 2c were designed to test the pilot's ability to fly to a prescribed point through narrow passages and in the presence of obstacles. Figures 4-31, -32, and -33 show the Mode 1 and 3 runs by Pilots 1, 2, and 3, respectively. As seen in the traces, the course offered considerable flexibility in choosing a path to the dock. It is apparent also that each pilot had his own idea as to the best approach. However, only Pilot 2 was able to consistently fly this course without a mishap. It is suggested that in future test runs Pilot 2 be appointed harbor pilot so that he can specialize in getting the open-sea men through the 100-foot gaps in the breakwater. One general observation may be made concerning low-speed maneuvering and that is that the pilots generally were traveling too fast for the congested harbor conditions. At speeds below 10 feet per second most pilots were able to negotiate the turns or at least stop in time to avert disasters. An estimate of speed is readily obtained by measuring the distance between 10-second blips. In this way it is seen that in his first run Pilot 1 traversed 140 to 150 feet in 10 seconds as he passed through the breakwater. Pilot 2 consistently went 15 to 20 feet per second outside the harbor and 10 to 11 feet per second inside the harbor. Pilot 3 achieved his best runs at speeds of 8 to 10 feet per second.

Another general observation which is probably very realistic for real GEM's is that a harbor is no place for daydreaming on the part of a pilot. Many preliminary practice runs by the three pilots included and others ended much worse than the first and third runs shown for Pilot 1. It was generally conceded that only by complete and continuous attention to the controls, dials, and flight path could a pilot successfully negotiate this course.

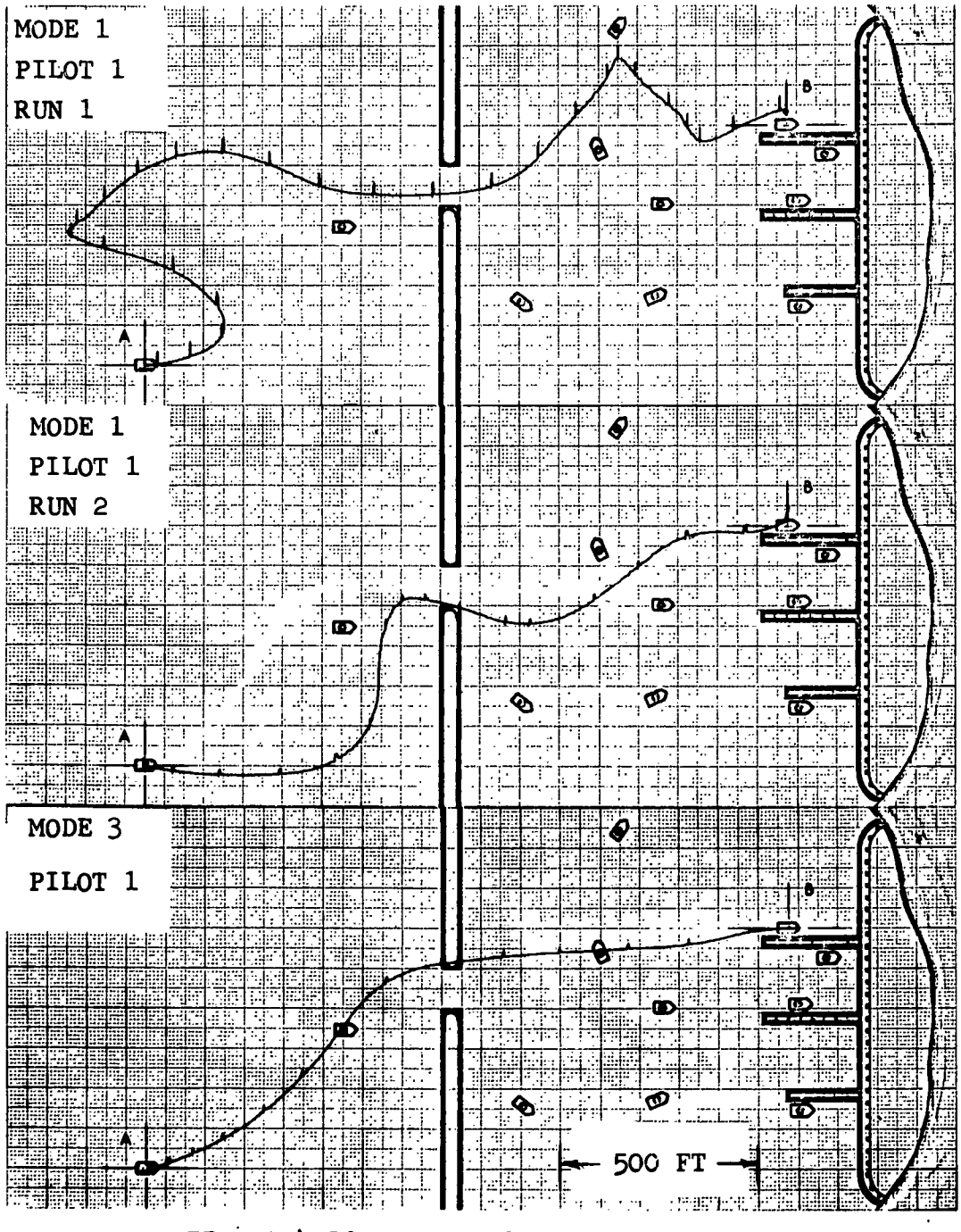

FIGURE 4-31 COURSE 1c TEST RUNS

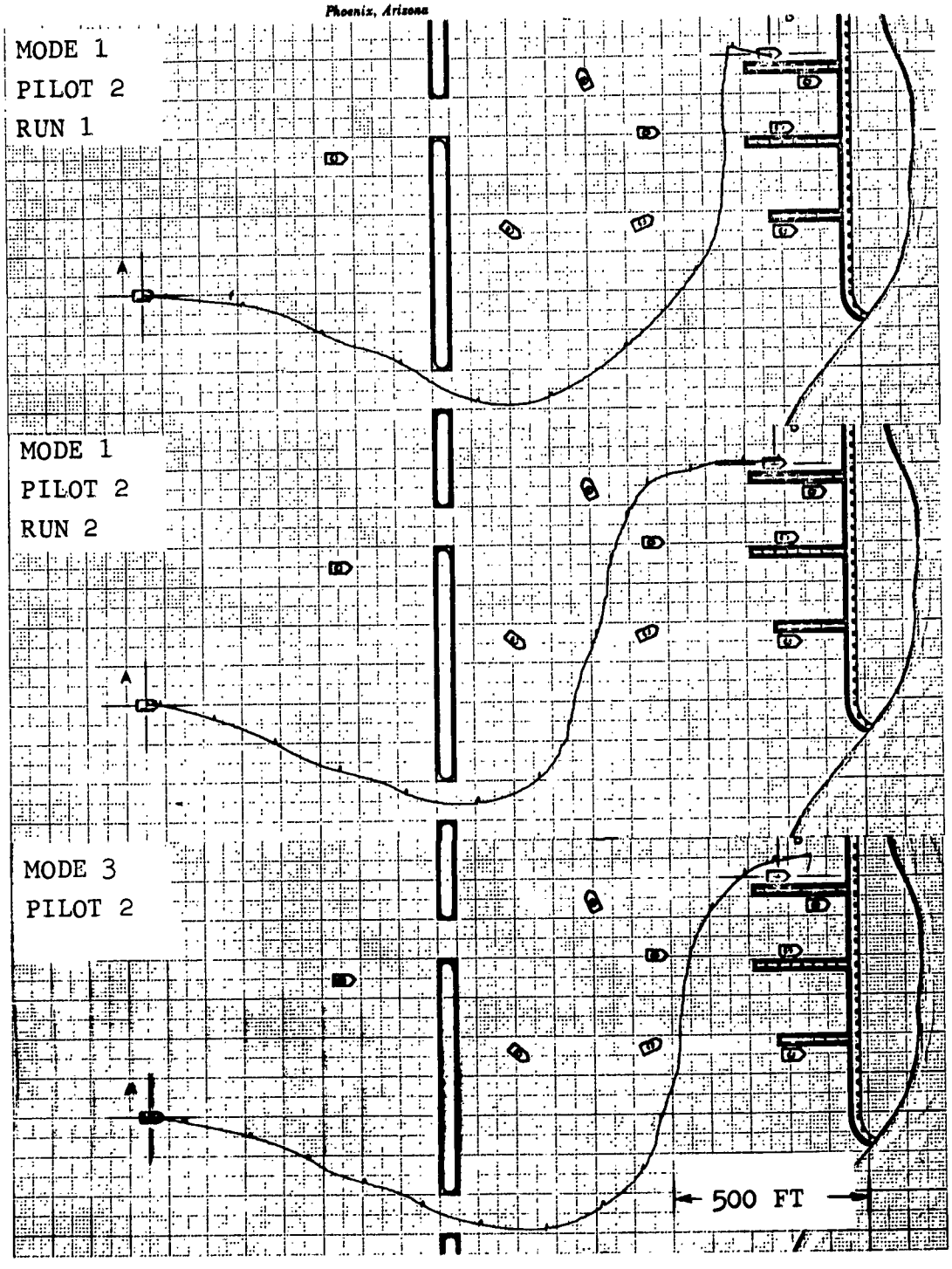

FIGURE 4-32 COURSE 1c TEST RUNS

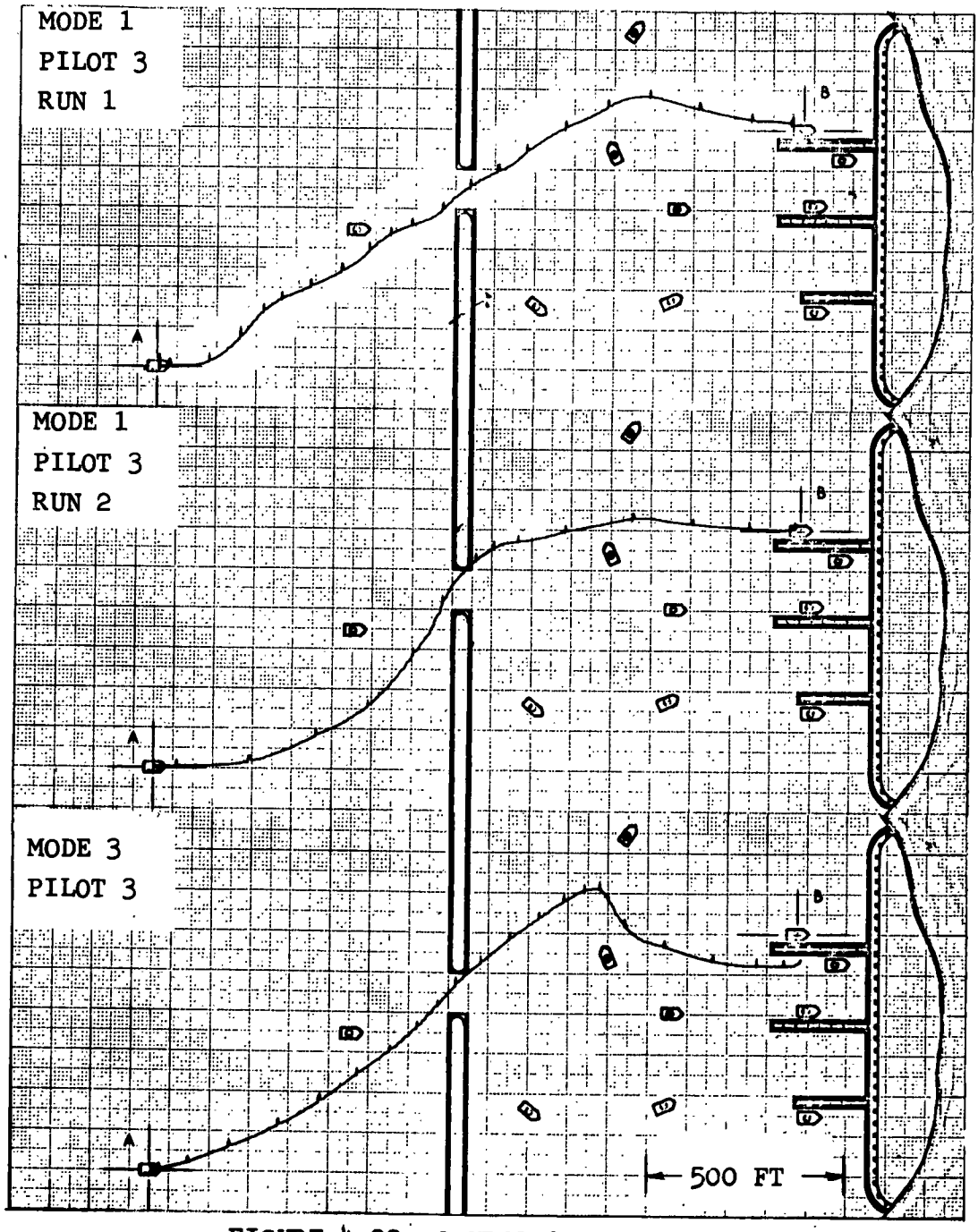

FIGURE 4-33 COURSE 1c TEST RUNS

Figures 4-34 through 4-39 show high-speed test runs in each of the four modes by each of the three pilots. The pilots were instructed to fly at speeds in excess of 40 feet per second in all high-speed runs except, of course, when starting or stopping. Despite the higher speed this was a considerably easier course than the low-speed course. The strait has a width of 500 feet and is the only obstacle. The open sea ahead of the strait afforded ample room for maneuvering into a proper approach course provided that the pilot did not attain too much speed before starting his approach. The tendency of novice pilots on this course was to accelerate first and begin maneuvering afterward. This often resulted in speeds too high for successful entry to the harbor area. It is seen, however, that all three pilots were able to get through the strait reasonably well in all four control modes.

It is seen in Figures 4-34 and 4-35 that Pilot 1 consistently made this run at 60 to 70 feet per second. Figures 4-36 and 4-37 show that Pilot 2 made his best runs at 60 to 70 feet per second also. However, in Mode 3 he passed the strait going 100 feet per second and in Mode 4 achieved a similar speed before braking drastically in order to make his turn. Figure 4-38 shows that Pilot 3 had some difficulty in negotiating the strait at speeds over 60 feet per second. His more cautious turns at 20 to 40 feet per second were more successful but were in violation of the minimum speed instruction.

THE GARRETT CORPORATION
AiResearch Manufacturing Division
Phoenix, Arizona

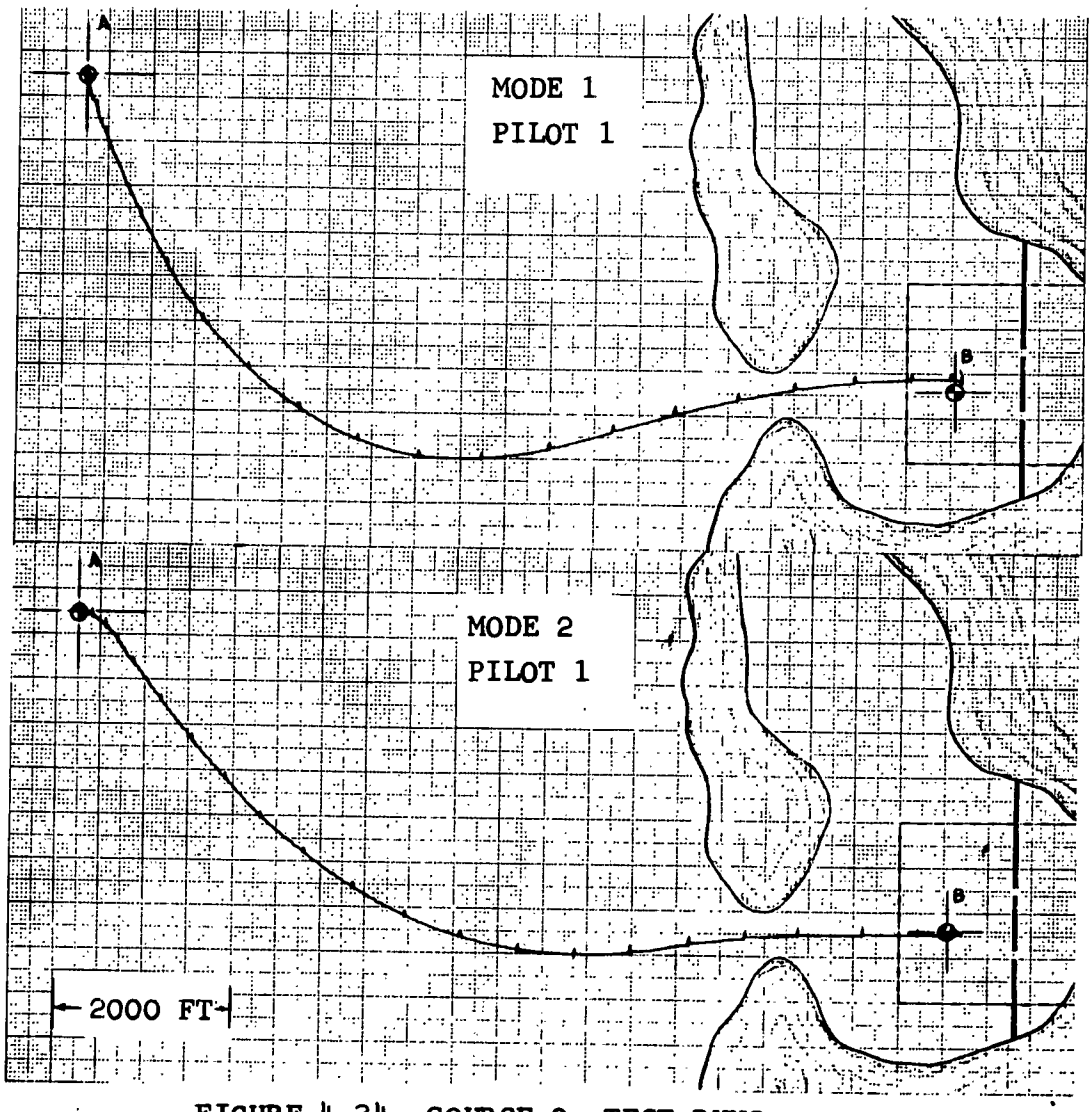

FIGURE 4-34 COURSE 2c TEST RUNS

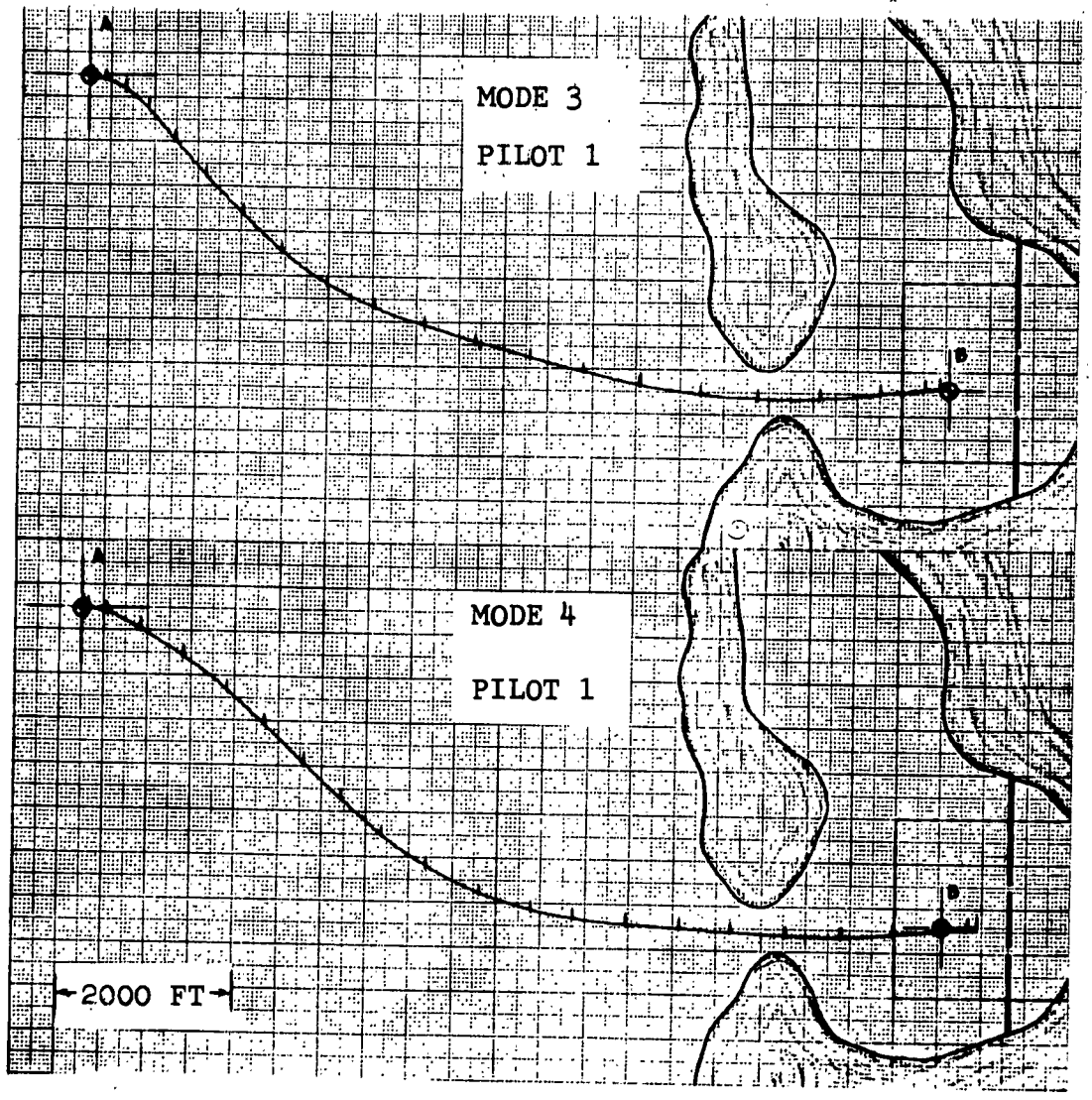

FIGURE 4-35 COURSE 2c TEST RUNS

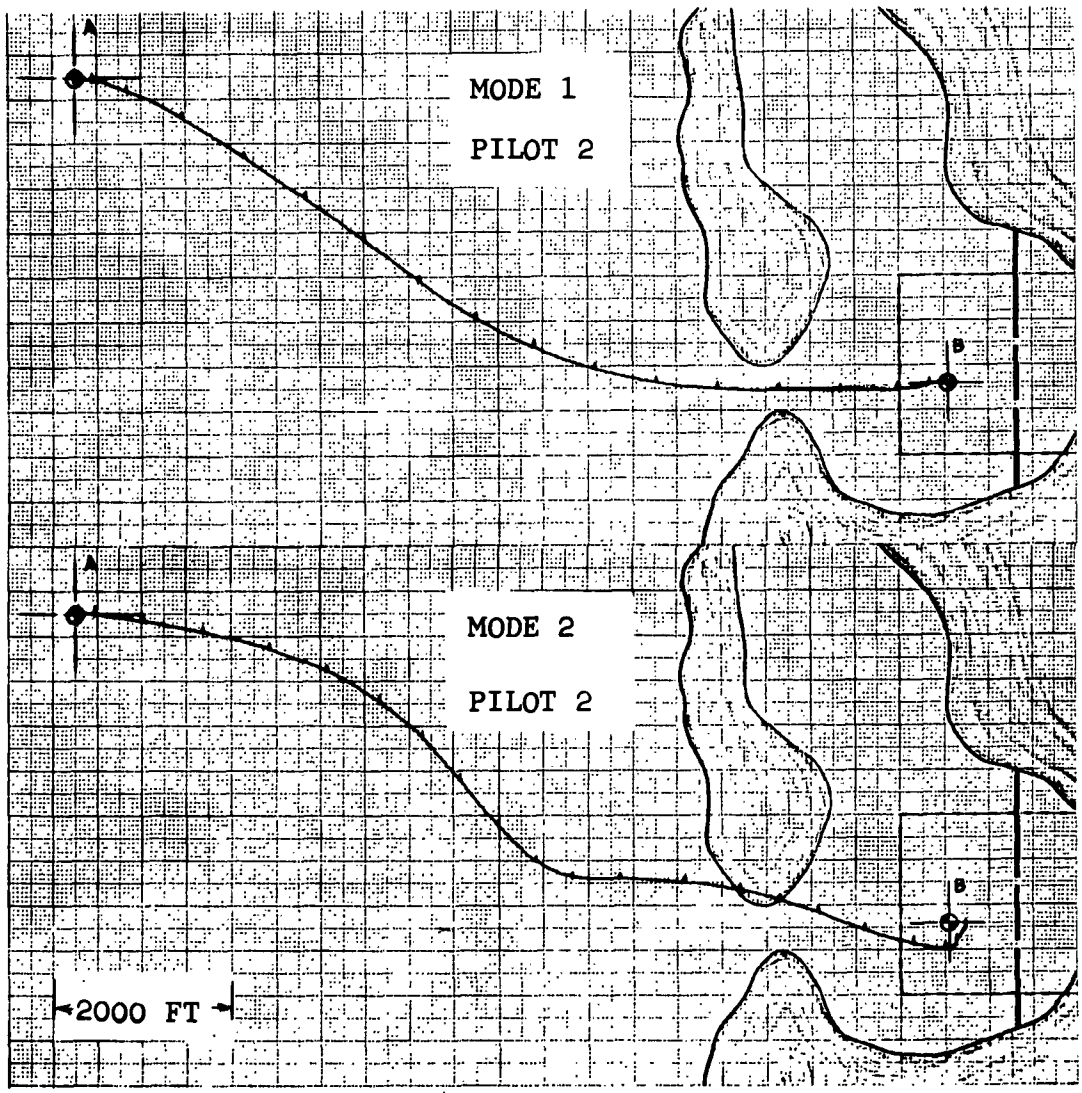

FIGURE 4-36 COURSE 2c TEST RUNS

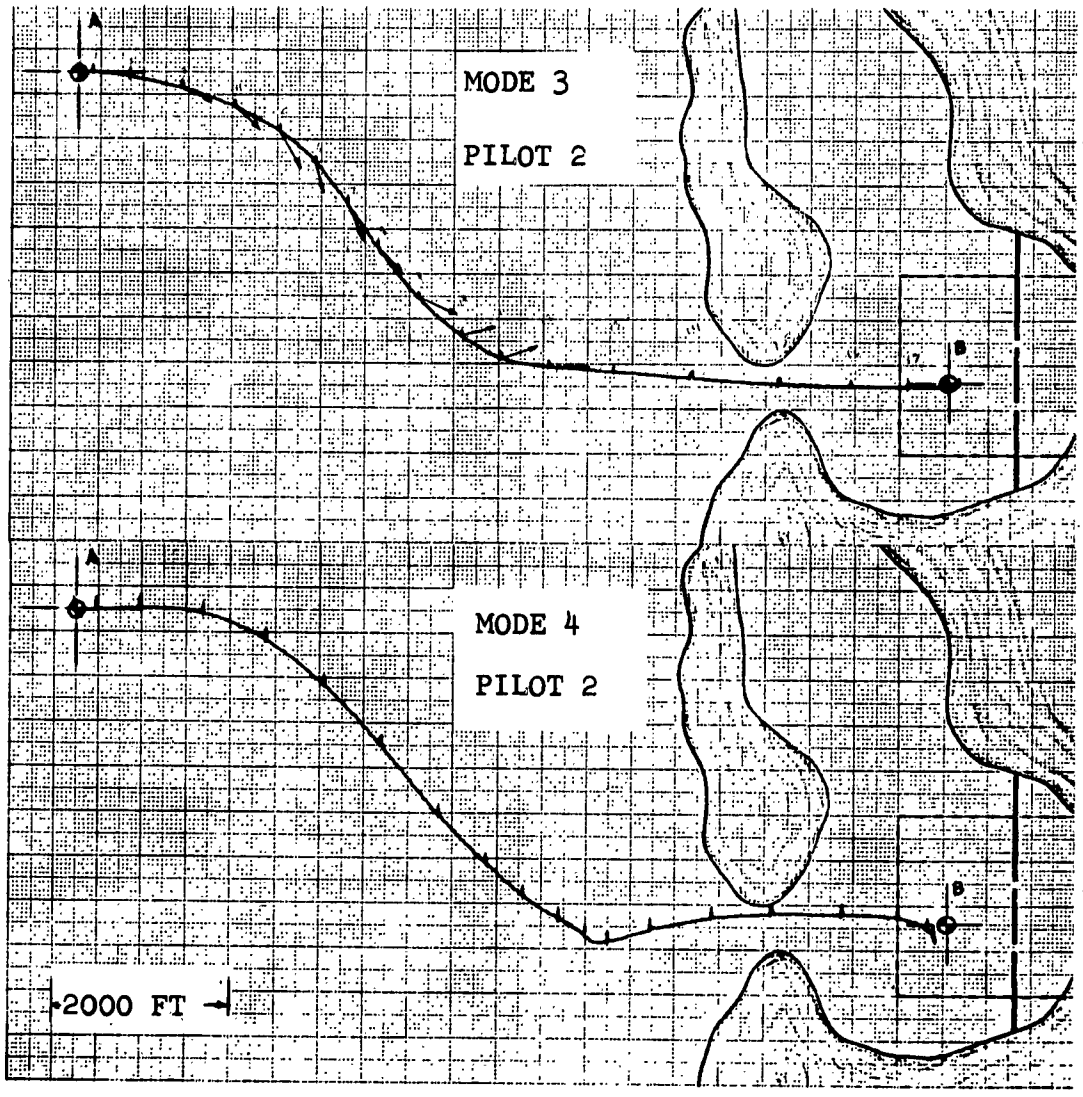

FIGURE 4-37 COURSE 2c TEST RUNS

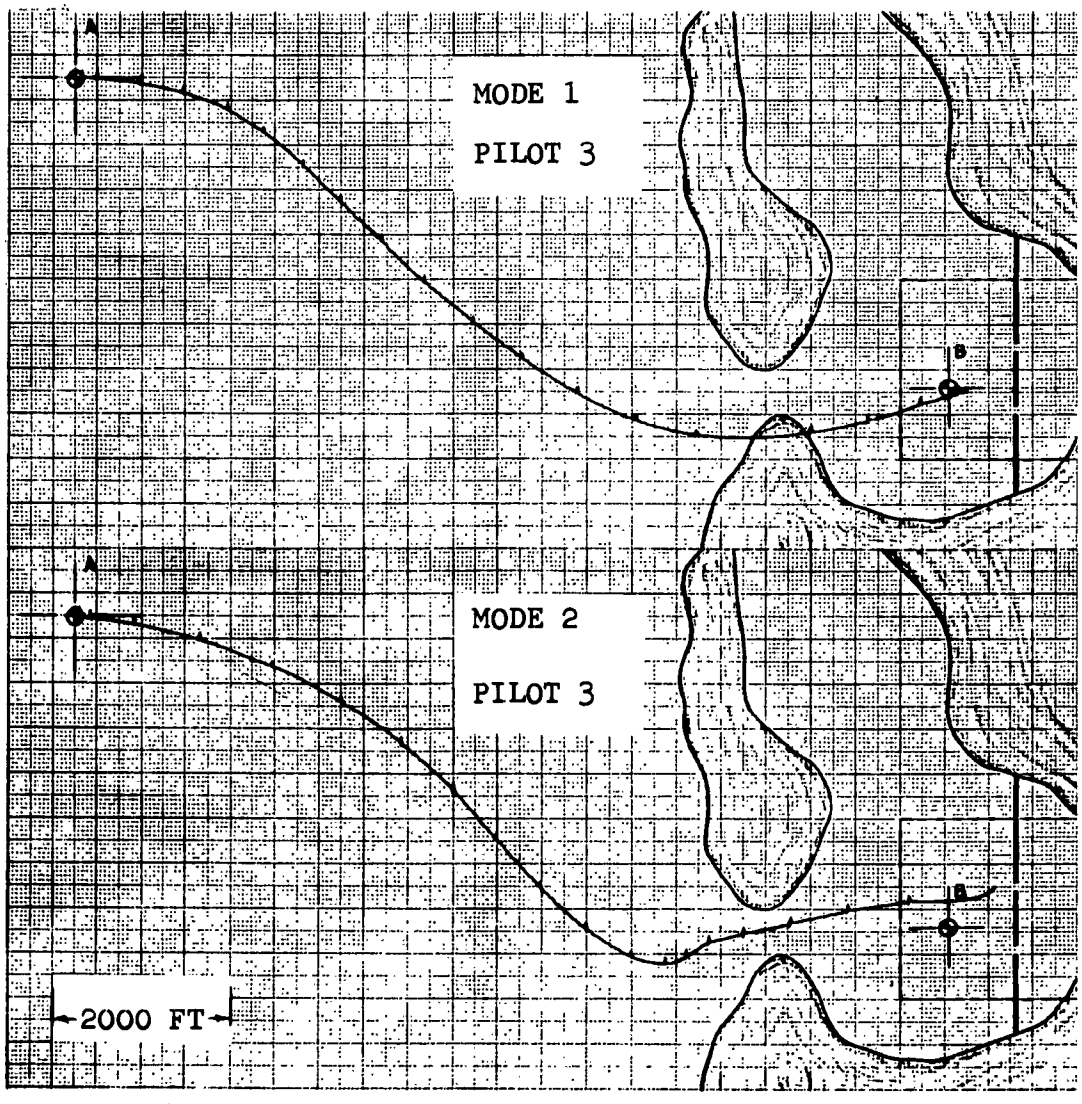

FIGURE 4-38 COURSE 2c TEST RUNS

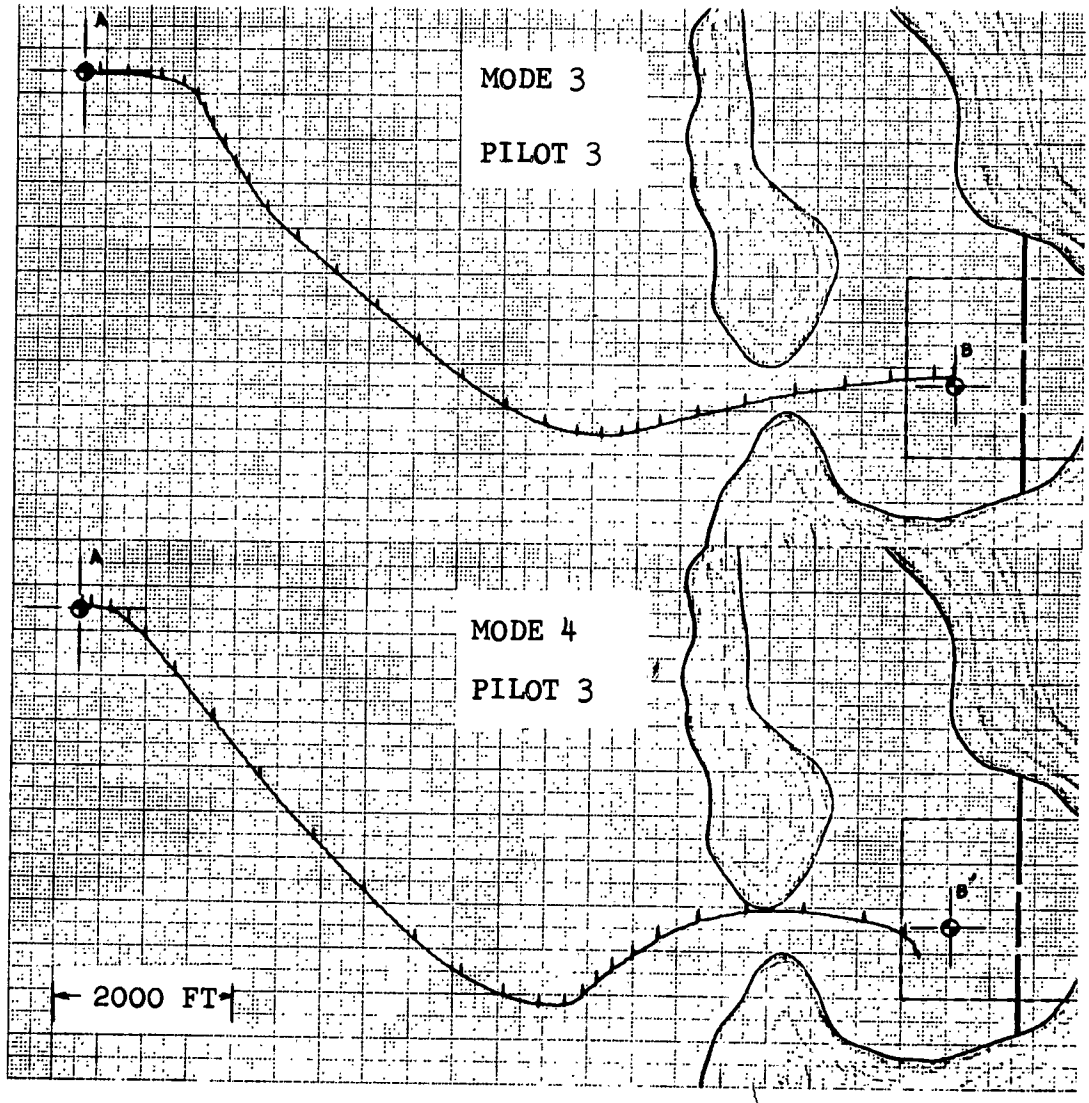

FIGURE 4-39 COURSE 2c TEST RUNS

5.0 CONTROL SYSTEM DESIGN CONSIDERATIONS

5.1 Introduction

The main objective in designing the control system of the GEM vehicle is to achieve optimum performance of the vehicle. Also of great importance are reliability considerations which often lead to giving preference to a simple rather than an elaborate system. Reliability can be given more consideration if control performance is not critical.

The analysis of the inherent GEM response characteristics indicate a rather sluggish behavior with respect to heave, pitch, roll, and yaw modes. For this reason the requirements on the corresponding control components are insofar as frequency response is concerned, easily satisfied. In fact, it can be shown that no combination of fast-responding devices like electric transducers, transmissions, and actuators with hydraulic assist are needed to comply with the GEM performance characteristics.

5.2 General Concept of Control Arrangement

The present GEM design concept considers two independent power plants, one on either side of the vehicle. The power plants are gas turbines, and either one drives via a gear train, two fans and one thrust propeller. The fans deliver the air flow to the jets, while the propeller provides the thrust forces necessary for forward, back, and yaw motions. The four fans supply the air for each of the four base compartments and thus enable the vehicle to pitch and roll by changing the flow to the respective compartments. In order to prevent severe

interaction of the controls, a modification of the turbine speed cannot be basically utilized since the power level of the fans and propellers would be changed simultaneously. The thrust control is therefore brought about mainly by a pitch modification of the propellers (slanting the vehicle by pitch or roll actuation will also contribute to the propulsion of the GEM vehicle).

The flow change to the compartments is accomplished by adjusting the inlet guide vanes (IGV) to the respective fans.

The hover height may be selected by resetting the operation point of the centrifugal-force/speed sensor of the turbines. Since a change of hover height is not required very often, it is felt that the disturbance to the other controls may be tolerated.

5.3 Control of Roll, Pitch, and Heave Motion

As outlined above, these control functions are brought about by setting the IGV to obtain the desired flow to the respective base compartment. The actuation of the IGV requires positive positioning and represents (due to a prevailing high level of static friction) a severe control problem. Any modulating actuator would therefore require rather high input signals to develop sufficient breaking force to get control motion starter. Excessive overshoot and undue position error may be the result. To cope with this situation, it is intended to utilize either a step actuation system (Proposal AP-5059-R*) or an air motor with a self-locking screw drive. To reduce the effects of high static friction, a surplus of actuation force would have to be provided.

*Ref. 4

In this application where, in view of the sluggish behavior of the vehicle, response is not a major problem, it seems possible to select the gear ratio in such a manner as to provide (1) sufficient force surplus (to overcome the effects of static friction), (2) self-locking action, and (3) sufficient frequency response with a motor of relatively small size.

5.4 Control of Fore, Back, and Yaw Motion

All of these control functions are executed according to the present design concept by modifying the propeller pitch angle. To attain fore and back motion as well as braking action, the pitch of both propellers located in the rear of the vehicle will be altered simultaneously.

The yaw control serves to change the heading of the vehicle. For this purpose a differential thrust condition is established by increasing the propeller pitch angle on one side and decreasing the pitch angle of the propeller located on the other side of the vehicle. At steady state, the yaw moment is counter balanced by the drag moment. Because this moment is a function of speed, the response of the vehicle to yaw input is also speed-dependent. At zero speed the drag moment diminishes and the yaw control approaches an unstable condition. The vehicle has a tendency to drift out of heading position.

5.5 Description of the Proposed Pneumatic Control System

Figure 5.1 shows a schematic diagram of the entire system. Compressor bleed air being used for signal modulation and transmission is first filtered and regulated in a common section

for all branches (pressure regulation is, however, not required to assure control accuracy). Each control branch represents a pneumatic bridge circuit (see sketch) consisting of two fixed orifices (1 and 2), one input modified orifice (3), and one orifice (4) adjusted by the position of the actuator. Steady-state balance is attained when $A_1/A_2 = A_3/A_4$. Thus, since $A_1/A_1 = \text{Const}$, A_4 and, therefore, the actuator position is proportional to the input, represented by orifice area A_3. The error sensor may be a zero rate diaphragm and the actuator a piston or air motor. Note that the signal transmission line in this all-pneumatic system is tubing just big enough to supply orifices of very small size (approximately 0.010 inch diameter).

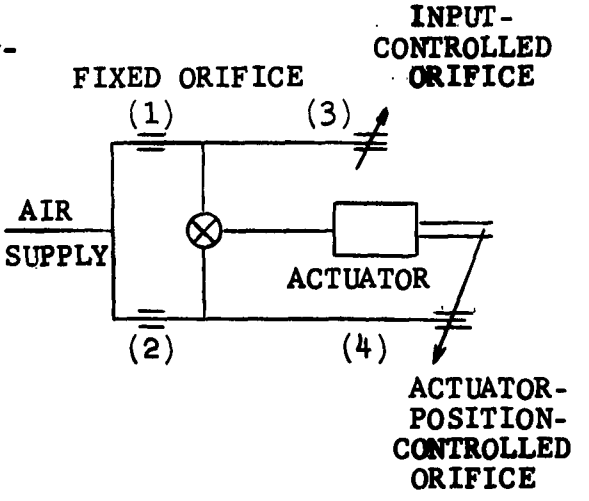

A rather interesting component of this all-pneumatic control system is the automatic trim control as shown in Figure 5.2. The error sensor is here a pendulum, free to rotate in the X and Y plane. A disc is attached to the pendulum modifying the flow area of four orifices. Each orifice affects the equilibrium condition of the control to the IGV of one of the four fans in such a manner as to correct the flow to the respective compartments until horizontal orientation of the vehicle platform is attained. To establish a horizontal orientation initially, a level instrument is required. This instrument will be placed on

SCHEMATIC OF AN ALL PNEUMATIC CONTROL SYSTEM

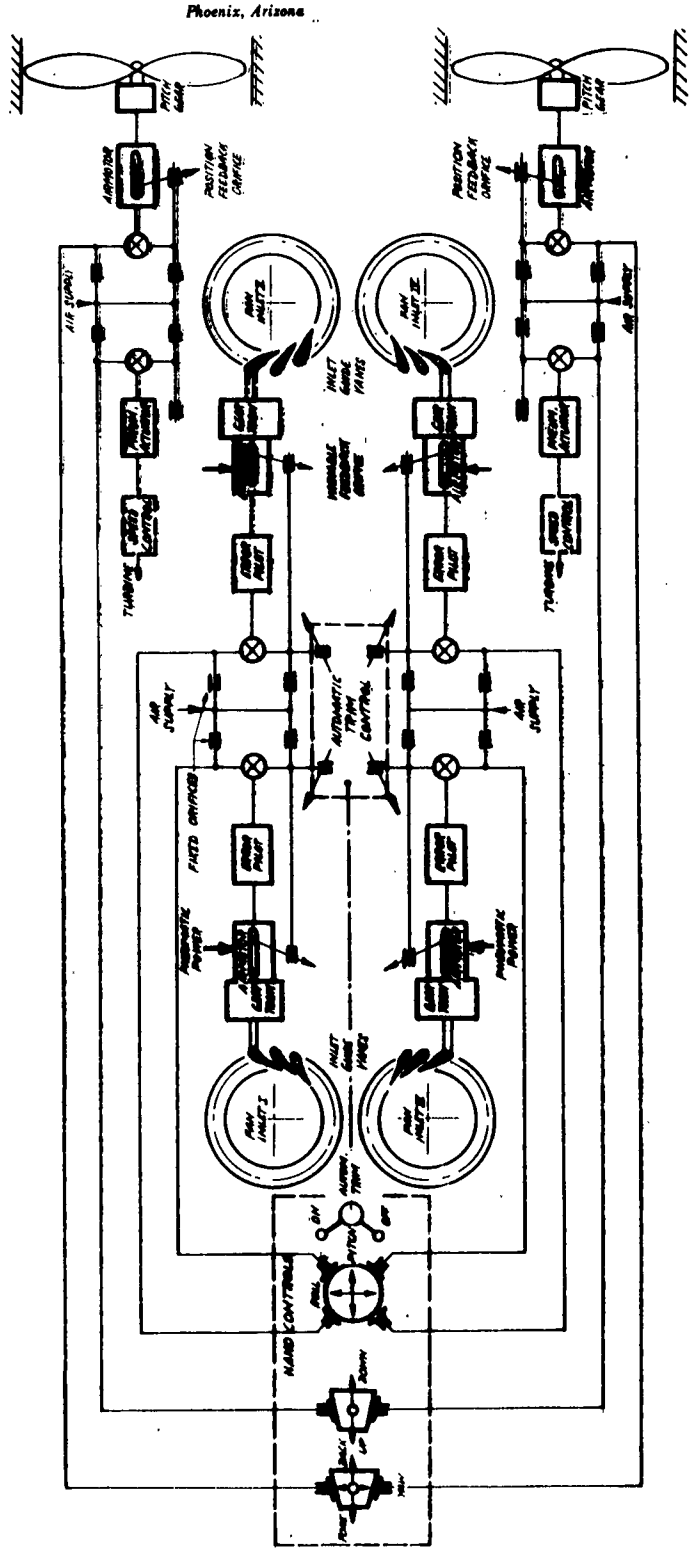

FIGURE 5-1 CONTROL SCHEMATIC

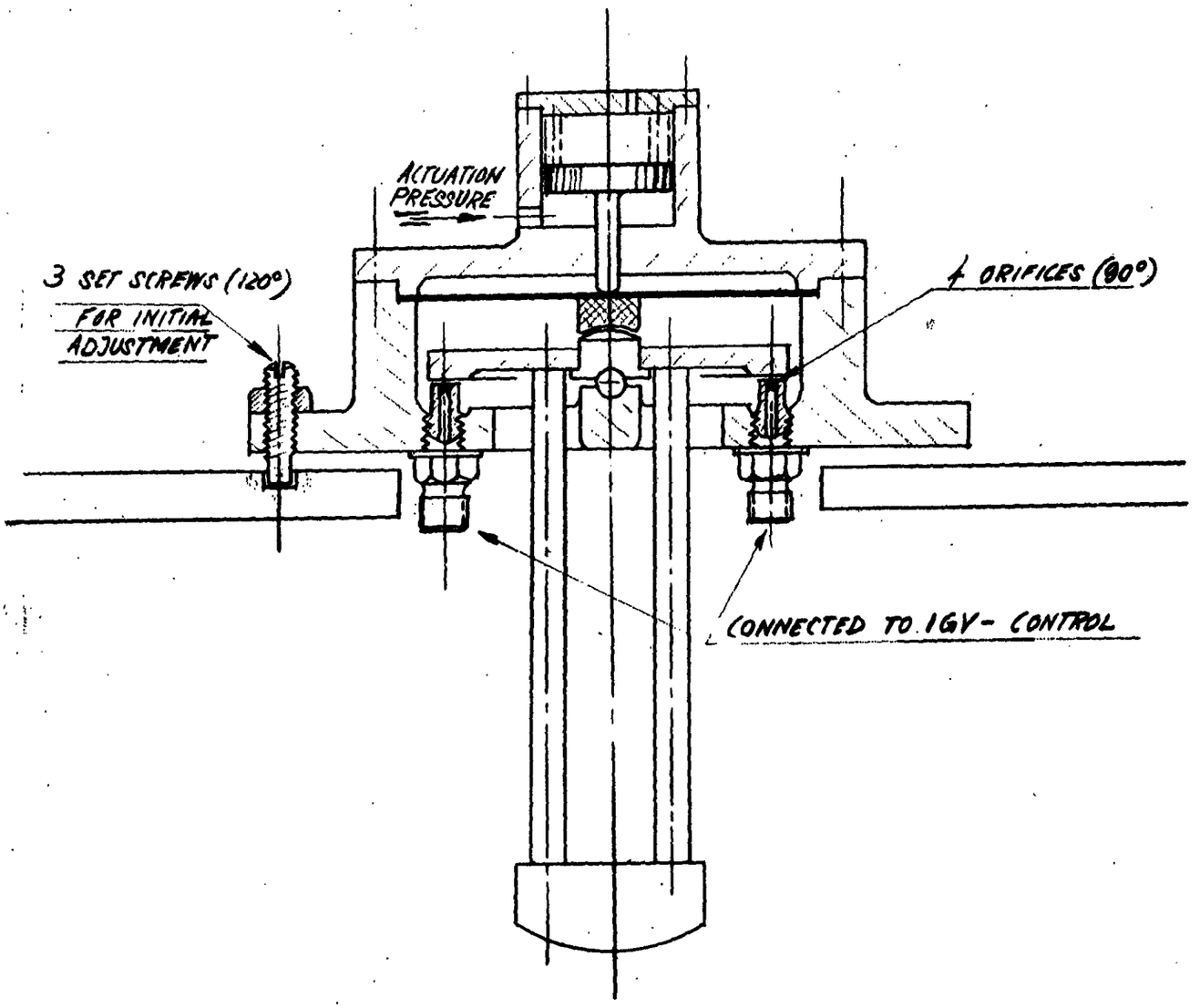

FIGURE 5-2
SEMI-AUTOMATIC TRIM PENDULUM

the platform of the hovering vehicle. The hand controls for pitch and roll will be brought into neutral position, and then the three set screws of the automatic trim control will be adjusted until the reading of the level instrument indicates perfect horizontal orientation of the GEM platform. After this initial calibration the trim control will always readjust the vehicle to horizontal orientation whenever the automatic trim control is actuated. During flight the trim control will be inactive. In case a new trim adjustment is required, the vehicle must stop or drift with pitch and roll at neutral. A short duration with automatic trim on will then readjust the level orientation.

In the inactive condition, the pendulum is held in trim position by a spring-loaded braking device. Actuation of the automatic trim is accomplished by a pneumatically controlled brake release (see Figure 5.2).

6.0 CONCLUSIONS AND RECOMMENDATIONS

The various areas of interest involved in the studies reported here necessitate classifying the principal results and conclusions. Section 6.1 deals with the simulation itself. This is further divided into subsections dealing with actual vehicle characteristics, the control station simulation, and the pilot display simulation. Section 6.3 deals with the control modes. Section 6.4 deals with the test runs that were used to evaluate the vehicle, the control mode, and the pilot.

6.1 The Simulation

6.1.1 Vehicle Dynamics

The simplified 6-degree-of-freedom vehicle simulation used here has been evolved over a period of 2 years. It has been shown in past reports that the fundamental analysis used successfully predicts the dynamic characteristics of both models and full-scale vehicles. The test results in Section 4.1 further verify that pitch, heave, and roll motions conform to those found in model tests. Beyond this, the representations of fore and aft motions, side motions, and yaw motions give reasonable results. It is concluded that the formulation used here--including coupling between the various motions--reliably reproduces the response of these three vehicle motions to external forces. This means that the program can now be used to evaluate any peripheral jet vehicle for which the basic design is known.

The representations of external forces are less well established than are the equations of motion. The effect of surface waves was established in an earlier progress report. However, waves were not simulated in this study because of limited computer capacity. The response of the water surface and formation of a wake is very reasonably represented for forward motions. However, it is felt that a more sophisticated three-dimensional representation can be made which will show the effect of rolling as well as pitching due to the standing wave. Such other surface conditions as a sudden change in surface height, a sloping surface, or a transition from overland to over-water operation have not been simulated--although it would not be difficult to include any or all of these to show how they affect vehicle motions.

The external aerodynamic forces are reasonably represented. The lift, drag, and moment coefficients were based upon model test results where possible and were otherwise obtained analytically. The conclusion here is that it would be well to have aerodynamic model data to verify the numbers obtained by analysis. Two parameters that are not well known are the moment coefficient in sideslip and the interaction of side force and drag during sideslip.

The characteristics of the air-moving equipment (engines, fans, ducts, and propellers) are well established. The only significant transient in this system is the engine response to speed-change commands. This command is seldom used in practice. The steady-state gains can be easily obtained from either experimental or analytical performance maps. The forces applied to the vehicle due to fan-flow and propeller-flow changes are well represented in the simulation.

The control components, which are intermediate between the pilot's control and the force-producing components, may be designed to have whatever gains are required for control of the vehicle. During the test runs a gain change was made in any control that appeared too sensitive or too unresponsive. Initially, the yaw control yielded large yaw rates for very small pilot inputs. The initially selected gain was reduced by a factor of 5 before the Mode 1 runs were made. After several trial runs in Mode 3, the gain of yaw moment to pedal motion was further reduced. The conclusion is that the control simulation was reasonable and that the gains arrived at through studies similar to this may be specified for the design of control components.

To summarize the conclusion of this subsection:

(1) The six equations of vehicle motion are valid and can apply to any peripheral jet vehicle.

(2) The surface effects of normal waves and two-dimensional wake are well represented, but a three-dimensional wake representation and possible variations from a flat surface could improve the surface simulation.

(3) Wind tunnel data may improve the simulation of external aerodynamics. However, the simulation is quite reasonable in this respect.

(4) The air-moving equipment is well simulated. Evaluation of any particular vehicle will require performance maps and engine dynamics.

(5) Since the control system can be designed to perform as desired, the simulation should be used to specify rather than evaluate the control gains.

6.1.2 Control Station

The control station used was very successful in giving the pilot control of basic vehicle motions. The ease with which various modes of control--e.g., the manner in which the pilot commands a particular vehicle motion--could be simulated is an outstanding feature. In general, the human engineering of the particular hardware used is good. However, several limitations were noted by the pilots during test runs:

(1) Prolonged application of a control that is spring-centered is very tiring. This applied to the push-pull wheel motion and to the wheel base rotation.

(2) Controls that are not spring centered should have a detent or other indication of the neutral position. This applied particularly to the yaw and roll controls.

The pilot read-out was probably the weakest part of the simulation in duplicating actual flying conditions. Aside from the absence of engine noise, salt spray, and wind noises, the pilot has no feeling of motion and could not see where he was going. Several improvements in the pilot read-out have been proposed:

(1) A graphic display of heading would help considerably. Several possibilities have been suggested. The simplest would be to have a small model that would be continuously rotated to the proper heading as signaled by the computer. This would immediately tell the pilot when and by how much he is sideslipping. This has a limitation, which occurred when the vehicle heading reached 180°--that the pilot must reverse his thinking and yaw left to turn right. A more sophisticated suggestion is to rotate the X-Y plotter so that the pilot feels his relative rotation with respect to the ground.

(2) Mounting the entire control station on a moving platform that actually produces pitch, heave, roll, and yaw motions will give the pilot the feeling of motion and response which convey the size of the vehicle to his senses.

Aside from these limitations and recommendations, it should be pointed out that with the pilot controls and read-out used, a man can learn to fly any specified course in an hour or two of flying time. In short, with the equipment presently in use, the reference vehicle evaluated is controllable.

6.2 The Reference GEM

The vehicle evaluated during these test runs was found to be stable in pitch heave, roll, and yaw and to be controllable by means of the fans and inlet guide vanes provided. The vehicle tended to be sluggish, had a tendency to sideslip--particularly in cross winds--and is difficult to stop or turn to avoid collisions. However, the sluggishness is probably not unreasonable for a vehicle of this size (40 tons, 60 feet long). Also, it was shown that it can be controlled even in a rather stiff breeze (40 feet per second). The pilots tended to feel a need for added side force, but none of them used the full sideslipping capability in turning. Yaw stability could be increased. However, this is one of the least certain of the aerodynamic parameters used in the simulation.

In general, it can be concluded that a vehicle with the characteristics of the reference design can be safely controlled by an experienced pilot.

6.3 Control Modes

It was found in the test runs that a pilot can learn to fly the GEM with just about any reasonable control mode. However, some modes of control were found easier than others. Despite the early experience in Mode 1, the pilots agreed that Mode 4 was the most pleasant control mode. In this mode, each of the four functions were separated, and no motion against a spring was used. In his hands the pilot had only roll control. Propulsion and pitch were controlled by friction-held hand levers, and yaw was

controlled by differential foot pedals. In Mode 1, where the pilot had pitch, roll, and yaw in his hands continuously and was required to hold two of them against springs, the pilot felt busy all the time. In Mode 2, which was the same as Mode 1 except that the pilot also had continuous thrust control in his foot pedals, the pilot had trouble holding speed while maneuvering. He had a strong tendency to accelerate or brake inadvertently while yawing or rolling.

The recommendations that could be made at this point are that the various control inputs be separated as much as possible and only those really needed continuously be in the pilot's hands.

6.4 Test Runs

In general, it is felt that the test runs used give a good indication of vehicle controllability. It is suggested, however, that certain other flying conditions be used for pilot training and perhaps for evaluating the forces that will act upon a vehicle being designed. These added flying conditions are:

(1) Docking in a wind.

(2) Encountering a side gust.

(3) Beaching across waves (breakers)

THE GARRETT CORPORATION
AiResearch Manufacturing Division
Phoenix, Arizona

APPENDIX A

LINEARIZATION AND SIMPLIFICATION OF BASIC EQUATIONS

THE GARRETT CORPORATION
AiResearch Manufacturing Division
Phoenix, Arizona

APPENDIX A
LINEARIZATION AND SIMPLIFICATION OF BASIC EQUATIONS

1.0 In order to simplify future analysis of the NONR Reference Design GEM, the equations for cushion pressure, jet flow and body motions as contained in Section 2.4 of AP-5047-R, will be linearized and written in nondimensional forms.

1.1 The general nonlinear transient pressure equation (Equation 106, AP-5047-R) is:

$$\dot{P}_i = -\frac{P_{Ti}}{hA_i}\left(Q_i - \sum_{K=1}^{n} Q_{iK}\right) - \frac{P_{Ti}}{h}\left(-\dot{z} + \bar{x}_i\dot{\theta} - \bar{y}_i\dot{\phi}\right) \qquad \text{(A-1)}$$

It is assumed that if:

1. The base area (A_B) is divided into 4 equal areas (A_i); $A_i = A_B/4$
2. The projected jet length (b) in the fore-aft direction (x) is twice the length (a) in the port-starboard direction (y); $b/a = 2$
3. The quantity K_K as defined in Section 2.4 (AP-5047-R) is equal to 0.5; $K_K = 0.5$

Then it can then be seen that

$$\frac{A_B}{K_K C} = \frac{ba}{K_K\, 2\,(a+b)} = \frac{b}{3}$$

and a time constant τ_1 can then be defined as:

$$\tau_1 = \frac{bV_j}{3g\,RT} \qquad \text{(A-2)}$$

Dividing the pressure equation (Equation A-1) above by W_c/A_B and multiplying it by τ_i yields:

$$\frac{bV_j}{3g\ RT}\left(\frac{A_B}{W_c}\right)\dot{P}_i = -\frac{bV_j}{3g\ RT}\left(\frac{A_B}{W_c}\right)\frac{P_{Ti}}{hA_i}\left(Q_i - \sum_{K=1}^{n} Q_{iK}\right)$$

$$-\frac{bV_j}{3g\ RT}\left(\frac{A_B}{W_c}\right)\frac{P_{Ti}}{h}\left(-\dot{z} + \bar{x}_i\dot{\theta} - \bar{y}_i\dot{\phi}\right) \qquad \text{(A-3)}$$

From the perfect gas law, the total pressure in a compartment may be defined as:

$$P_{Ti} = \rho\ g\ RT$$

where ρ has dimensions of $\frac{\text{lb-sec.}^2}{\text{ft}^4}$

substituting P_{Ti} above and $A_i = A_B/4$ into Equation A-3 yields:

$$\frac{bV_j}{3g\ RT}\left(\frac{A_B}{W_c}\right)\dot{P}_i = -\frac{bV_j}{3}\left(\frac{4\rho}{hW_c}\right)\left(Q_i - \sum_{K=1}^{n} Q_{iK}\right)$$

$$-\frac{bV_j}{3}\left(\frac{\rho A_B}{hW_c}\right)\left(-\dot{z} + \bar{x}_i\dot{\theta} - \bar{y}_i\dot{\phi}\right) \qquad \text{(A-4)}$$

By dividing Q_i by Q_{fi} and Q_{iK} by Q_{fiK} in Equation A-4 it can now be written as:

$$\tau_i\left(\frac{A_B}{W_c}\right)\dot{P}_i = -\frac{4b\rho}{3hW_c}V_j^2\ C_iG_i\left(\frac{Q_i}{Q_{fi}} - \sum_{K=1}^{n}\frac{Q_{fiK}}{Q_{fi}}\frac{Q_{iK}}{Q_{fiK}}\right)$$

$$-\frac{b\rho V_j A_B}{3W_c}\left(-\frac{\dot{z}}{h} + \frac{\bar{x}_i\dot{\theta}}{h} - \frac{\bar{y}_i\dot{\phi}}{h}\right) \qquad \text{(A-5)}$$

Considering the effect of a wave moving beneath the vehicle as in Equation (107), AP-5047-R.

$$\tau_1 \left(\frac{A_B}{W_c}\right) \dot{P}_i = - \frac{4b\rho}{3h\,W_c} V_j^2 C_i G_i \left(\frac{Q_i}{Q_{fi}} - \sum_{K=1}^{n} \frac{Q_{fiK}}{Q_{fi}} \frac{Q_{iK}}{Q_{fiK}}\right)$$

$$- \frac{b\rho V_j A_B}{3W_c} \left[\left(- \frac{\dot{z}}{h} + \frac{\bar{x}_i \dot{\theta}}{h} - \frac{\bar{y}_i \dot{\phi}}{h}\right)\right.$$

$$\left. + \frac{\bar{E}_i}{h} \left(\frac{2\pi v}{\lambda}\right) \cos \frac{2\pi}{\lambda} (vt + \bar{x}_i)\right] \qquad (A\text{-}6)$$

Since $K_K = 0.5$

$$\frac{b}{3} = \frac{A_B}{K_K C} = \frac{2A_B}{C}$$

therefore $\frac{4C_i b}{3} = \frac{Cb}{3} = \frac{2\,(a + b)\,b}{3} = 2\,A_B$

Let $\pi_1 = \frac{2\rho V_j^2}{W_c / A_B} \frac{G}{h}$ (A-7)

above pressure equation becomes:

$$\tau_1 \left(\frac{A_B}{W_c}\right) \dot{P}_i = - \pi_1 \left(\frac{Q_i}{Q_{fi}} - \sum_{K=1}^{n} \frac{G_{iK} C_{iK}}{G_i C_i} \frac{Q_{iK}}{Q_{fiK}}\right)$$

$$- \frac{P_T A_B}{W_c} \tau_1 \left[- \frac{\dot{z}}{h} + \frac{\bar{x}_i \dot{\theta}}{h} - \frac{\bar{y}_i \dot{\phi}}{h}\right.$$

$$\left. + \frac{\bar{E}_i}{h} \left(\frac{2\pi v}{\lambda}\right) \cos \frac{2\pi}{\lambda} (vt + \bar{x}_i)\right] \qquad (A\text{-}8)$$

Appendix A of AP-5047-R contains a simplified form of the flow equations.

Equation (20) in Appendix A (AP-5047-R) is

$$\frac{Q_i}{Q_{fi}} = K_K \left[\left(\frac{h_i}{G_i} - \frac{1}{2} \sin \theta_j \right) B_i - \eta_a F_{si} B_{io} \right] \qquad (A\text{-}9)$$

$$\text{with } F_{si} = \frac{1}{\eta_a} \left(\frac{h}{G} - \frac{1}{2} \sin \theta_j \right) \qquad (A\text{-}10)$$

$$B_{io} = \frac{p_{io}}{\rho V_j^2} \qquad (A\text{-}11)$$

$$\frac{Q_i}{Q_{fi}} = K_K \left[\left(\frac{h_i}{G_i} - \frac{1}{2} \sin \theta_j \right) \frac{p_i}{\rho V_j^2} - \left(\frac{h}{G} - \frac{1}{2} \sin \theta_j \right) \frac{p_{io}}{\rho V_j^2} \right] \qquad (A\text{-}12)$$

Multiplying Equation (A-12) by π_1.

$$\pi_1 \frac{Q_i}{Q_{fi}} = \frac{2\rho V_j^2 A_B}{W_c} \frac{G}{h} K_K \left[\left(\frac{h_i}{G_i} - \frac{1}{2} \sin \theta_j \right) \frac{p_i}{\rho V_j^2} - \left(\frac{h}{G} - \frac{1}{2} \sin \theta_j \right) \frac{p_{io}}{\rho V_j^2} \right] \qquad (A\text{-}13)$$

$$\pi_1 \frac{Q_i}{Q_{fi}} = 2K_K \left[\left(\frac{h_i}{h} - \frac{1}{2} \frac{G}{h} \sin \theta_j \right) \frac{A_B}{W_c} p_i - \left(1 - \frac{1}{2} \frac{G}{h} \sin \theta_j \right) \frac{A_B}{W_c} p_{io} \right] \qquad (A\text{-}14)$$

where $h_i = h - z + x_i \theta \quad _i\phi + E_i \sin \frac{2\pi}{\lambda} (vt + x_i)$ (A-15)

h being the steady-state operating height

Equation (10) in Appendix A (AP-5047-R) is:

$$\frac{Q_{iK}}{Q_{fiK}} = 1 + F_2 \left[F_1 \frac{h_{iK}}{G_{iK}} (B_{Ki} - B_{iK}) - 1 \right]$$

$$\frac{Q_{iK}}{Q_{fiK}} = 1 - F_2 \left[1 + F_1 \frac{h_{iK}}{G_{iK}} \frac{(P_i - P_K)}{\rho V_j^2} \right] \qquad \text{(A-16)}$$

Equation (A-16) is applicable for the range of conditions given by

$$h_{iK} (P_i - P_K) \leq - \frac{\rho V_j^2 G_{iK}}{F_1}$$

The function F_1 is given by Equation 4 of Appendix A (AP-5047-R) as:

$$F_1 = \frac{2 \frac{h_{iK}}{G_{iK}}}{\sqrt{1 + 4 \left(\frac{h_{iK}}{G_{iK}}\right)^2} + 1} \qquad \text{(A-17)}$$

and F_2 (Equation 9 of Appendix A, AP-5047-R) as:

$$F_2 = \frac{1}{2} \left[\frac{1 + 4 \left(\frac{h_{iK}}{G_{iK}}\right)^2}{\sqrt{1 + 4 \left(\frac{h_{iK}}{G_{iK}}\right)^2} + 1} \right]^{1/2} \qquad \text{(A-18)}$$

Equation (3) of Appendix A, AP-5047-R, gives:

$$\frac{Q_{iK}}{Q_{fiK}} = 0.5 - \frac{0.5 F_1 h_{iK} (P_i - P_K)}{G_{iK} \rho V_j^2} \qquad \text{(A-19)}$$

Equation (A-19) is applicable for a range given by

$$\frac{-\rho V_j^2 G_{iK}}{F_1} \leq h_{iK} (P_i - P_K) \leq \frac{\rho V_j^2 G_{iK}}{F_1}$$

For the third condition on the compartment jet the following relationship holds:

$$Q_{Ki} = Q_{fiK} - Q_{iK}$$

using the value given in Equation (A-16) for Q_{iK} an expression for Q_{Ki} is obtained:

$$\frac{Q_{iK}}{Q_{fiK}} = F_2 \left[1 - F_1 \frac{h_{iK} (P_i - P_K)}{G_{iK} \rho V_j^2} \right] \qquad \text{(A-20)}$$

Equation (A-20) is applicable for the range as given by

$$\frac{\rho V_j^2 G_{iK}}{F_1} \leq h_{iK} (P_i - P_K)$$

Let $\pi_2 = \frac{G_{iK}}{G_i}$ $\pi_1 = \frac{2\rho V_j^2 A_B G_{iK}}{h W_c}$

Multiplying Equations (A-16), (A-19), and (A-20) by π_2 and redefining the boundary conditions yields:

$$\pi_2 \frac{C_{iK}}{C_i} \frac{Q_{iK}}{Q_{fiK}} = \frac{C_{iK}}{C_i} \pi_2 - F_2 \left[\frac{C_{iK}}{C_i} \pi_2 + 2F_1 \frac{C_{iK}}{C_i} \frac{h_{iK}}{h_i} \left(\frac{A_B P_i}{W_c} - \frac{A_B P_K}{W_c} \right) \right]$$

(A-21)

$$\text{when } \frac{h_{iK}}{h_i}\left(\frac{A_B P_i}{W_c} - \frac{A_B P_K}{W_c}\right) \leq -\frac{\pi_2}{2F_1}$$

$$\pi_2 \frac{C_{iK}}{C_i}\frac{Q_{iK}}{Q_{fiK}} = \frac{1}{2}\pi_2 \frac{C_{iK}}{C_i} - F_1 \frac{C_{iK}}{C_i}\frac{h_{iK}}{h_i}\left(\frac{A_B P_i}{W_c} - \frac{A_B P_K}{W_c}\right) \qquad \text{(A-22)}$$

$$\text{when } -\frac{\pi_2}{2F_1} \leq \frac{h_{iK}}{h_i}\left(\frac{A_B P_i}{W_c} - \frac{A_B P_K}{W_c}\right) \leq +\frac{\pi_2}{2F_1}$$

$$\pi_2 \frac{C_{iK}}{C_i}\frac{Q_{iK}}{Q_{fiK}} = F_2\left[\frac{C_{iK}}{C_i}\pi_2 - 2F_1 \frac{C_{iK}}{C_i}\frac{h_{iK}}{h_i}\left(\frac{A_B P_i}{W_c} - \frac{A_B P_K}{W_c}\right)\right] \qquad \text{(A-23)}$$

$$\text{when } +\frac{\pi_2}{2F_1} \leq \frac{h_{iK}}{h_i}\left(\frac{A_B P_i}{W_c} - \frac{A_B P_K}{W_c}\right)$$

$$\frac{h_{iK}}{h_i} = 1 - \bar{z} + \frac{2x_{iK}}{b}\bar{\theta} - \frac{2y_{iK}}{a}\bar{\phi} + \frac{E_{iK}}{h}\sin\frac{\pi b}{\lambda}\left(\frac{2vt}{b} + \frac{2x_{iK}}{b}\right) \qquad \text{(A-24)}$$

Equation (35), AP-5047-R, is the general, nonlinear expression for heave motions.

$$\frac{W_c}{g}\ddot{z} = -\sum_{i=1}^{n} A_i P_i - \rho\left[\sum_{i=1}^{n}\frac{Q^2_{fi}}{C_i G_i}\sin\theta_j + \sum_{i=1}^{n-1}\sum_{K=i+1}^{n}\frac{Q^2_{fiK}}{C_{iK}G_{iK}}\right] + W_c$$

At this point, if the base pressure, p_i, is thought of as being the average steady state value plus a variation, it can be seen from the above expression that at steady state conditions, i.e., $\ddot{z} = 0$, the average steady state pressure is less than the quantity W_c/A_B by an amount that is equivalent to the thrust produced by the jets, or;

$$\lambda_1 = \frac{A_B P_{AV}}{W_c} = 1 - \frac{\rho\left[\sum_{i=1}^{n} \frac{Q^2_{fi}}{C_i G_i} \sin\theta_j + \sum_{i=1}^{n-1} \sum_{K=i+1}^{n} \frac{Q^2_{fiK}}{C_{iK} G_{iK}}\right]}{W_c} \qquad \text{(A-25)}$$

Defining a dimensionless, normalized pressure, $\bar{P}_i$ as;

$$\bar{P}_i = \frac{A_B P_i}{W_c} - \lambda_1 \qquad \text{(A-26)}$$

since λ_1 is constant,

$$\dot{\bar{P}}_i = \frac{A_B \dot{P}_i}{W_c} \qquad \text{(A-27)}$$

dimensionless body motions;

$$\bar{z} = \frac{z}{h} \qquad \text{(A-28)}$$

$$\bar{\theta} = \frac{b\theta}{2h} \qquad \text{(A-29)}$$

$$\bar{\phi} = \frac{a\phi}{2h} \qquad \text{(A-30)}$$

and dimensionless flow;

$$\bar{Q} = \frac{Q}{Q_{fo}} \qquad \text{(A-31)}$$

Let $\tau_2 = \frac{P_T A_B}{W_c} \tau_1$

Equation (A-8) may now be written as:

$$\tau_1 \dot{\bar{P}}_i = - \pi_1 \bar{Q}_i + \pi_2 \sum_{K=1}^{n} \frac{C_{iK}}{C_i} \bar{Q}_{iK}$$

$$- \tau_2 \left[- \frac{\dot{\bar{z}}}{} + \frac{2\bar{x}_i}{b} \dot{\theta} - \frac{2\bar{y}_i}{a} \dot{\phi} \right.$$

$$\left. + \frac{\bar{E}_i}{h} \left(\frac{2\pi v}{\lambda_2}\right) \cos \frac{\pi b}{\lambda_2} \left(\frac{2vt}{b} + \frac{2\bar{x}_i}{b}\right) \right] \qquad \text{A-32}$$

Note here that λ in the expression for wave form is now λ_2 to differentiate it from the pressure expression λ_1.

Dividing Equation (A-14) by the steady-state fan flow (Q_{fio}) yields:

$$\pi_1 \bar{Q}_i = 2K_K \left[\left(\frac{h_i}{h} - \frac{1}{2} \frac{G}{h} \sin \theta_j\right) \frac{A_B}{W_c} p_i - \left(1 - \frac{1}{2} \frac{G}{h} \sin \theta_j\right) \frac{A_B}{W_c} p_{io} \right] \bar{Q}_{fi}$$

where $\bar{Q}_i = \dfrac{Q_i}{Q_{fio}}$

and $\bar{Q}_{fi} = \dfrac{Q_{fi}}{Q_{fio}}$

Linearizing on the basis that

1. $p_i = P_i + p_i$ (steady state plus a variation)

2. Fan flow consists of a steady state plus a variation.

From Equation (A-15)

$$h_i = h - z + x_i\theta - y_i\phi + E_i \sin \frac{2\pi}{\lambda_2} (vt + x_i)$$

$$\pi \bar{Q}_i = 2K_K \Bigg\{ \left[1 - \bar{z} + \frac{2x_i}{b} \bar{\theta} - \frac{2y_i}{a} \bar{\phi} + \frac{E_i}{h} \sin \frac{\pi b}{\lambda_z} \left(\frac{2vt}{b} + \frac{2x_i}{b} \right) - \frac{1}{2} \frac{G}{h} \sin \theta_j \right] \frac{A_B}{W_c} (P_i + p_i) - (1 - \frac{1}{2} \frac{G}{h} \sin \theta_j) \frac{A_B}{W_c} P_{io} \Bigg\} \bar{Q}_{fio} + \frac{\partial \pi \bar{Q}_i}{\partial \bar{Q}_{fi}} \bar{q}_{fi} \qquad \text{(A-33)}$$

From Equation (41) (AP-5047-R)

$$\frac{\partial Q_i}{\partial Q_{fi}} = \frac{Q_i - 2p_i \frac{\partial Q_i}{\partial P_i}}{Q_{fi}}$$

therefore

$$\frac{\partial \pi \bar{Q}_i}{\partial \bar{Q}_{fi}} = \frac{\pi \bar{Q}_i - 2p_i \frac{\partial \pi \bar{Q}_i}{\partial P_i}}{\bar{Q}_{fi}}$$

$$= -2K_K \left[\left(\frac{h_i}{h} - \frac{1}{2} \frac{G}{h} \sin \theta_j \right) \frac{A_B}{W_c} p_i + \left(1 - \frac{1}{2} \frac{G}{h} \sin \theta_j \right) \frac{A_B}{W_c} P_{io} \right] \qquad \text{(A-34)}$$

Equation (A-33) then becomes:

$$\pi_1 \bar{Q}_i = 2K_K \left\{ \left[1 - \bar{z} + \frac{2x_i}{b} \bar{\theta} - \frac{2y_i}{a} \bar{\phi} + \frac{E_i}{h} \sin \frac{\pi b}{\lambda_2} \left(\frac{2vt}{b} + \frac{2x_i}{b} \right) \right. \right.$$

$$\left. - \frac{1}{2} \frac{G}{h} \sin \theta_j \right] \frac{A_B}{W_c} (P_i + p_i) - \left(1 - \frac{1}{2} \frac{G}{h} \sin \theta_j\right) \frac{A_B}{W_c} P_{i_o}$$

$$- \left[1 - \bar{z} + \frac{2x_i}{b} \bar{\theta} - \frac{2y_i}{a} \bar{\phi} + \frac{E_i}{h} \sin \frac{\pi b}{\lambda_2} \left(\frac{2vt}{b} + \frac{2x_i}{b} \right) \right.$$

$$\left. \left. - \frac{1}{2} \frac{G}{h} \sin \theta_j \right] \frac{A_B}{W_c} (P_i + p_i) \bar{q}_{fi} - \left(1 - \frac{1}{2} \frac{G}{h} \sin \theta_j\right) \frac{A_B}{W_c} P_{i_o} \bar{q}_{fi} \right\}$$

(A-35)

Let the steady-state pressure terms,

$$P_i \left(\frac{A_B}{W_c} \right) = \lambda_1$$

and variations in pressure,

$$P_i \left(\frac{A_B}{W_c} \right) = \bar{p}_i$$

Equation (A-35) may be written:

$$\pi_1 \bar{Q}_i = 2K_K \left\{ \left(1 - \frac{1}{2}\frac{G}{h}\sin\theta_j\right)\left(\lambda_1 - \frac{A_B P_{i_o}}{W_c}\right) - \left[\left(1 - \frac{1}{2}\frac{G}{h}\sin\theta_j\right)\cdot \left[\left(\lambda_1 + \frac{A_B P_{i_o}}{W_c}\right)\right]\bar{q}_{fi}\right.\right.$$

$$+ \lambda_1\left[-\bar{z} + \frac{2x_i}{b}\bar{\theta} - \frac{2y_i}{a}\bar{\phi} + \frac{E_i}{h}\sin\frac{\pi b}{\lambda_2}\left(\frac{2vt}{b} + \frac{2x_i}{b}\right)\right]$$

$$+ \left(1 - \frac{1}{2}\frac{G}{h}\sin\theta_j\right)\bar{P}_i$$

$$+ \left[\bar{P}_i\left(1 + \bar{q}_{fi}\right) + \bar{q}_{fi}\lambda_1\right]\cdot$$

$$\left.\left.\cdot\left[-\bar{z} + \frac{2x_i}{b}\bar{\theta} - \frac{2y_i}{a}\bar{\phi} + \frac{E_i}{h}\sin\frac{\pi b}{\lambda_2}\left(\frac{2vt}{b} + \frac{2x_i}{b}\right)\right]\right\} \qquad \text{(A-36)}$$

It is noted here that:

$$K_K = K_{KA} \quad \text{when } 0 \le \pi_1 \bar{Q}_i \qquad \text{(positive)}$$

$$= K_{KB} \quad \text{when } \pi_1 \bar{Q}_i \le 0 \qquad \text{(negative)}$$

Equations (A-21), (A-22), and (A-23) may be rewritten by setting

$$\frac{A_B P_i}{W_c} = \bar{P}_i + \lambda_1$$

$$\frac{A_B P_K}{W_c} = \bar{P}_K + \lambda_1$$

$$\frac{C_{iK}}{C_i}\,\pi_2\bar{Q}_{ik} = K_{Lik} - K_{Pik}\left[1 - \bar{z} + \frac{2x_{ik}}{b}\,\bar{\theta} - \frac{2y_{ik}}{a}\,\bar{\phi} + \frac{E_{ik}}{h}\sin\frac{\pi b}{\lambda_2}\left(\frac{2vt}{b} + \frac{2x_{ik}}{b}\right)\right](\bar{p}_i - \bar{p}_k)$$

(A-37)

Boundary conditions for Equation (A-37)

$$\left.\begin{aligned} K_{Lik} &= (1 - F_2)\,\pi_2\,\frac{C_{ik}}{C_i} \\ K_{Pik} &= 2F_2F_1\,\frac{C_{ik}}{C_i} \end{aligned}\right\} \quad \text{when } F_1\frac{h_{ik}}{h_i}(\bar{p}_i - \bar{p}_k) \le \frac{1}{2}\,\pi_2$$

$$\left.\begin{aligned} K_{Lik} &= \frac{1}{2}\,\pi_2\,\frac{C_{ik}}{C_i} \\ K_{Pik} &= F_1\,\frac{C_{ik}}{C_i} \end{aligned}\right\} \quad \text{when } -\frac{1}{2}\,\pi_2 \le F_1\frac{h_{ik}}{h_i}(\bar{p}_i - \bar{p}_k) \le +\frac{1}{2}\,\pi_2$$

$$\left.\begin{aligned} K_{Lik} &= F_2\,\pi_2\,\frac{C_{ik}}{C_i} \\ K_{Pik} &= 2F_2F_1\,\frac{C_{ik}}{C_i} \end{aligned}\right\} \quad \text{when } \frac{1}{2}\,\pi_2 \le F_1\frac{h_{ik}}{h_i}(\bar{p}_i - \bar{p}_k)$$

1.2 Equations (35), (36), and (37) of AP-5047-R present the equations of motion.

Heave

$$\frac{W_c}{g}\ddot{z} = -\sum_{i=1}^{n} A_i P_i - \rho\left[\sum_{i=1}^{n} \frac{Q^2_{fi}}{C_i G_i} \sin\theta_j + \sum_{i=1}^{n-1}\sum_{k=i+1}^{n} \frac{Q^2_{fik}}{C_{ik} G_{ik}}\right] + W_c$$

Rewritting the above equation using the notation as expressed in Equations (A-25) and (A-26)

$$\ddot{\bar{z}} = -\omega^2_H \left(\frac{\bar{P}_1 + \bar{P}_2 + \bar{P}_3 + \bar{P}_4}{4}\right) \qquad \text{(A-38)}$$

where $\omega_H = \sqrt{g/h}$

Roll

$$\frac{I_x}{g}\ddot{\phi} = -\sum_{i=1}^{n} \bar{y}_i A_i P_i - \rho\left[\sum_{i=1}^{n} \frac{y_i Q^2_{fi}}{C_i G_i} \sin\theta_j + \sum_{i=1}^{n-1}\sum_{k=i+1}^{n} \frac{y_{ik} Q^2_{fik}}{C_{ik} G_{ik}}\right]$$

With Equations (A-25) and (A-26) the above equation may be written as follows:

$$\ddot{\bar{\phi}} = -\omega^2_H \left(\frac{a}{4r_y}\right)^2 \sum_{i=1}^{4} \frac{2\bar{y}_i}{a} \bar{P}_i \qquad \text{(A-39)}$$

where $r_y = \sqrt{I_x/W_c}$

Pitch

$$\frac{I_y}{g}\ddot{\theta} = \sum_{i=1}^{n} \bar{x}_i A_i p_i + \rho \left[\sum_{i=1}^{n} \frac{x_i Q^2 f_i}{C_i G_i} \sin \theta_j + \sum_{i=1}^{n-1} \sum_{k=i+1}^{n} \frac{x_{ik} Q^2 f_{ik}}{C_{ik} G_{ik}} \right]$$

Equations (A-25) and (A-26) into above equation yields:

$$\ddot{\theta} = \omega^2_H \left(\frac{b}{4r_x}\right)^2 \sum_{i=1}^{4} \frac{2\bar{x}_i}{b} \bar{p}_i \qquad \text{(A-40)}$$

where $r_x = \sqrt{I_y/W_c}$

2.0 PARTICULAR EQUATIONS FOR REFERENCE DESIGN GEM

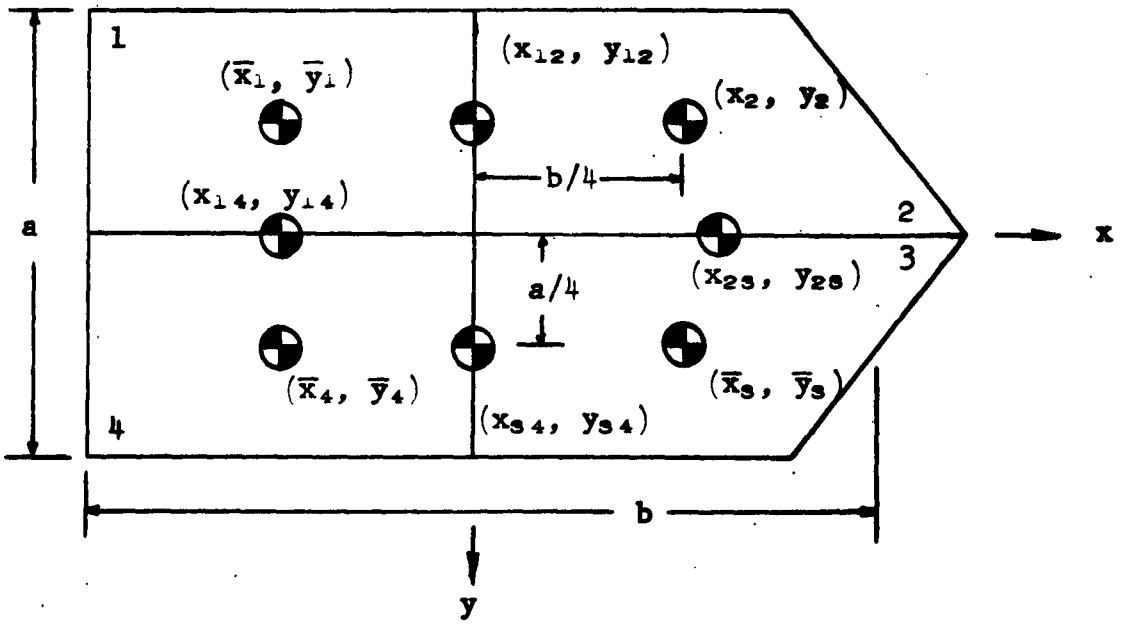

FIGURE A-1. REFERENCE DESIGN SCHEMATIC

$$x_3 = \frac{b + 2a}{b + a}\left(\frac{b}{4}\right); \quad y_3 = \frac{2b + a}{b + a}\left(\frac{a}{4}\right)$$

2.1 Pressure Equations

Applying Equation (A-32) to each sector:

$$\tau_1 \dot{\bar{p}}_1 = -\pi_1 \bar{Q}_1 + \pi_2 \left(\frac{C_{12}}{C_1} \bar{Q}_{12} + \frac{C_{14}}{C_1} \bar{Q}_{14}\right) - \tau_2 \left[-\dot{\bar{z}} - \frac{1}{2}\dot{\bar{\theta}} + \frac{1}{2}\dot{\bar{\phi}} + \frac{\bar{E}}{h}\left(\frac{2\pi v}{\lambda_2}\right) \cos\frac{\pi b}{\lambda_2}\left(\frac{2vt}{b} - \frac{1}{2}\right)\right] \quad (41)$$

$$\tau_1 \dot{\bar{p}}_2 = -\pi_1 \bar{Q}_2 + \pi_2 \left(\frac{C_{21}}{C_2} \bar{Q}_{21} + \frac{C_{23}}{C_2} \bar{Q}_{23}\right) - \tau_2 \left[-\dot{\bar{z}} + \frac{1}{2}\dot{\bar{\theta}} + \frac{1}{2}\dot{\bar{\phi}} + \frac{\bar{E}}{h}\left(\frac{2\pi v}{\lambda_2}\right) \cos\frac{\pi b}{\lambda_2}\left(\frac{2vt}{b} + \frac{1}{2}\right)\right] \quad (42)$$

$$\tau_1 \dot{\bar{p}}_3 = -\pi_1 \bar{Q}_3 + \pi_2 \left(\frac{C_{23}}{C_3} \bar{Q}_{32} + \frac{C_{34}}{C_3} \bar{Q}_{34}\right)$$

$$- \tau_2 \left[-\dot{\bar{z}} + \frac{1}{2}\dot{\bar{\theta}} - \frac{1}{2}\dot{\bar{\phi}} + \frac{\bar{E}}{h}\left(\frac{2\pi v}{\lambda_2}\right) \cos\frac{\pi b}{\lambda_2}\left(\frac{2vt}{b} + \frac{1}{2}\right)\right] \qquad (A\text{-}43)$$

$$\tau_1 \dot{\bar{p}}_4 = -\pi_1 \bar{Q}_4 + \pi_2 \left(\frac{C_{43}}{C_4} \bar{Q}_{43} + \frac{C_{41}}{C_4} \bar{Q}_{41}\right)$$

$$- \tau_2 \left[-\dot{\bar{z}} - \frac{1}{2}\dot{\bar{\theta}} - \frac{1}{2}\dot{\bar{\phi}} + \frac{\bar{E}}{h}\left(\frac{2\pi v}{\lambda_2}\right) \cos\frac{\pi b}{\lambda_2}\left(\frac{2vt}{b} - \frac{1}{2}\right)\right] \qquad (A\text{-}44)$$

2.2 Flow Equations (Peripheral Jets)

Applying Equation (A-36) to each sector, neglecting the products of the variations, $\bar{p}_i$, $\bar{z}$, etc. Reasons for, and proof of validity of this linearization will be given in Section 2.5.

$$\pi_1 \bar{Q}_1 = 2K_{K_1}\Big\{ \left(1 - \frac{1}{2}\frac{G}{h}\sin\theta_j\right)\bar{p}_1$$

$$+ \lambda_1\left[-\bar{z} - \frac{2x_3}{b}\bar{\theta} + \frac{2y_3}{a}\bar{\phi} + \frac{E_1}{h}\sin\frac{\pi b}{\lambda_2}\left(\frac{2vt}{b} - \frac{2x_3}{b}\right)\right]$$

$$- \left(1 - \frac{1}{2}\frac{G}{h}\sin\theta_j\right)\left(\lambda_1 + \frac{A_B P_o}{W_c}\right)\bar{q}_{f_1}\Big\}$$

$$+ 2K_{KA}\left(1 - \frac{1}{2}\frac{G}{h}\sin\theta_j\right)\left(\lambda_1 - \frac{A_B P_o}{W_c}\right) \qquad (A\text{-}45)$$

$$\pi_1 \bar{Q}_2 = 2K_{K_2}\Big\{\left(1 - \frac{1}{2}\frac{G}{h}\sin\theta_j\right)\bar{p}_2$$

$$+ \lambda_1\left[-\bar{z} + \frac{2x_3}{b}\bar{\theta} + \frac{2y_3}{a}\bar{\phi} + \frac{E_2}{h}\sin\frac{\pi b}{\lambda_2}\left(\frac{2vt}{b} + \frac{2x_3}{b}\right)\right]$$

$$- \left(1 - \frac{1}{2}\frac{G}{h}\sin\theta_j\right)\left(\lambda_1 + \frac{A_B P_o}{W_c}\right)\bar{q}_{f_2}\Big\} \qquad (A\text{-}46)$$

$$+ 2K_{KA}\left(1 - \frac{1}{2}\frac{G}{h}\sin\theta_j\right)\left(\lambda_1 - \frac{A_B P_o}{W_c}\right)$$

$$\pi_1 \bar{Q}_3 = 2K_{K_3} \left\{ \left(1 - \frac{1}{2}\frac{G}{h} \sin\theta_j\right) \bar{p}_3 \right.$$

$$+ \lambda_1 \left[-\bar{z} + \frac{2x_3}{b}\bar{\theta} - \frac{2y_3}{a}\bar{\phi} + \frac{E_3}{h} \sin\frac{\pi b}{\lambda_2}\left(\frac{2vt}{b} + \frac{2x_3}{b}\right)\right]$$

$$\left. - \left(1 - \frac{1}{2}\frac{G}{h}\sin\theta_j\right)\left(\lambda_1 + \frac{A_B P_o}{W_c}\right)\bar{q}_{f_3}\right\}$$

$$+ 2K_{KA}\left(1 - \frac{1}{2}\frac{G}{h}\sin\theta_j\right)\left(\lambda_1 - \frac{A_B P_o}{W_c}\right) \qquad (47)$$

$$\pi_1 \bar{Q}_4 = 2K_{K_4} \left\{ \left(1 - \frac{1}{2}\frac{G}{h} \sin\theta_j\right) \bar{p}_4 \right.$$

$$+ \lambda_1 \left[-\bar{z} - \frac{2x_3}{b}\bar{\theta} - \frac{2y_3}{a}\bar{\phi} + \frac{E_4}{h} \sin\frac{\pi b}{\lambda_2}\left(\frac{2vt}{b} - \frac{2x_3}{b}\right)\right]$$

$$\left. - \left(1 - \frac{1}{2}\frac{G}{h}\sin\theta_j\right)\left(\lambda_1 + \frac{A_B P_o}{W_c}\right)\bar{q}_{f_4}\right\}$$

$$+ 2K_{KA}\left(1 - \frac{1}{2}\frac{G}{h}\sin\theta_j\right)\left(\lambda_1 - \frac{A_B P_o}{W_c}\right) \qquad (48)$$

$$K_{Ki} = K_{KA} \text{ if } \pi_1 \bar{Q}_i \text{ is positive}$$

$$= K_{KB} \text{ is } \pi_1 \bar{Q}_i \text{ is negative}$$

2.3 Compartment Jets

Applying Equation (A-37) to each compartment jet, retaining the products of variations, $\bar{p}_i$, $\bar{z}$, etc.:

$$\left.\begin{aligned} \frac{C_{12}}{C_1}\,\pi_2\,\bar{Q}_{12} &= K_{L_{12}} - K_{P_{12}}\,(\bar{p}_1 - \bar{p}_2)\,\bar{h}_{12} \\ \frac{C_{12}}{C_1}\,\pi_2\,\bar{Q}_{21} &= \frac{C_{12}}{C_1}\,\pi_2 - \frac{C_{12}}{C_1}\,\pi_2\,\bar{Q}_{12} \\ \bar{h}_{12} &= 1 - \bar{z} + \frac{1}{2}\,\bar{\phi} + \frac{E_{12}}{h}\sin\frac{\pi b}{\lambda_2}\,\frac{2vt}{b} \end{aligned}\right\} \qquad \text{(A-49)}$$

$$\left.\begin{aligned} \frac{C_{23}}{C_2}\,\pi_2\,\bar{Q}_{23} &= K_{L_{23}} - K_{P_{23}}\,(\bar{p}_2 - \bar{p}_3)\,\bar{h}_{23} \\ \frac{C_{23}}{C_2}\,\pi_2\,\bar{Q}_{32} &= \frac{C_{23}}{C_2}\,\pi_2 - \frac{C_{23}}{C_2}\,\pi_2\,\bar{Q}_{23} \\ \bar{h}_{23} &= 1 - \bar{z} + \frac{1}{2}\,\bar{\theta} + \frac{E_{23}}{h}\sin\frac{\pi b}{\lambda_2}\left(\frac{2vt}{b} + \frac{1}{2}\right) \end{aligned}\right\} \qquad \text{(A-50)}$$

$$\left.\begin{aligned} \frac{C_{34}}{C_3}\,\pi_2\,\bar{Q}_{34} &= K_{L_{34}} - K_{P_{34}}\,(\bar{p}_3 - \bar{p}_4)\,\bar{h}_{34} \\ \frac{C_{34}}{C_3}\,\pi_2\,\bar{Q}_{43} &= \frac{C_{34}}{C_3}\,\pi_2 - \frac{C_{34}}{C_3}\,\pi_2\,\bar{Q}_{43} \\ \bar{h}_{34} &= 1 - \bar{z} - \frac{1}{2}\,\bar{\phi} + \frac{E_{34}}{h}\sin\frac{\pi b}{\lambda_2}\,\frac{2vt}{b} \end{aligned}\right\} \qquad \text{(A-51)}$$

$$\left.\begin{aligned} \frac{C_{41}}{C_4}\,\pi_2\,\bar{Q}_{41} &= K_{L_{41}} - K_{P_{41}}\,(\bar{p}_4 - \bar{p}_1)\,\bar{h}_{41} \\ \frac{C_{41}}{C_4}\,\pi_2\,\bar{Q}_{14} &= \frac{C_{41}}{C_4}\,\pi_2 - \frac{C_{41}}{C_4}\,\pi_2\,\bar{Q}_{41} \\ \bar{h}_{41} &= 1 - \bar{z} - \frac{1}{2}\,\bar{\theta} + \frac{E_{41}}{h}\sin\frac{\pi b}{\lambda_2}\left(\frac{2vt}{b} - \frac{1}{2}\right) \end{aligned}\right\} \qquad \text{(A-52)}$$

$$\left.\begin{aligned} K_{LiK} &= 2\,(1 - F_2)\,\frac{1}{2}\,\pi_2\,\frac{C_{iK}}{C_i} \\ K_{PiK} &= 2\,F_2\,F_1\,\frac{C_{iK}}{C_i} \end{aligned}\right\} \text{ if } F_1\,\frac{C_{iK}}{C_i}\,\bar{h}_{iK}\,(\bar{p}_i - \bar{p}_K) \le -\frac{1}{2}\,\pi_2\,\frac{C_{il}}{C_i}$$

$$\left.\begin{aligned} K_{LiK} &= \frac{1}{2}\,\pi_2\,\frac{C_{iK}}{C_i} \\ K_{PiK} &= F_1\,\frac{C_{iK}}{C_i} \end{aligned}\right\} \text{if } -\frac{1}{2}\,\pi_2\,\frac{C_{iK}}{C_i} \le F_1\,\frac{C_{iK}}{C_i}\,\bar{h}_{iK}\,(\bar{p}_i - \bar{p}_K) \le \frac{1}{2}\,\pi_2\,\frac{C_{iK}}{C_i}$$

$$\left.\begin{aligned} K_{LiK} &= 2\,F_2\,\frac{1}{2}\,\pi_2\,\frac{C_{iK}}{C_i} \\ K_{PiK} &= 2\,F_2\,F_1\,\frac{C_{iK}}{C_i} \end{aligned}\right\} \text{if } \frac{1}{2}\,\pi_2\,\frac{C_{iK}}{C_i} \le F_1\,\frac{C_{iK}}{C_i}\,\bar{h}_{iK}\,(\bar{p}_i - \bar{p}_K)$$

2.4 Body Motions

Equations (A-38), (A-39), and (A-40) become:

Heave

$$\ddot{\bar{z}} = -\frac{g}{4h}\,(\bar{p}_1 + \bar{p}_2 + \bar{p}_3 + \bar{p}_4) \qquad \text{(A-53)}$$

Roll

$$\ddot{\bar{\phi}} = -\frac{g}{4h}\,\frac{W_c a^2}{\delta I_x}\,(-\bar{p}_1 - \bar{p}_2 + \bar{p}_3 + \bar{p}_4) \qquad \text{(A-54)}$$

Pitch

$$\ddot{\bar{\theta}} = \frac{g}{4h}\,\frac{W_c b^2}{\delta I_y}\,(-\bar{p}_1 + \bar{p}_2 + \bar{p}_3 - \bar{p}_4) \qquad \text{(A-55)}$$

2.5 As previously noted, the products of the variations ($\bar{P}_i$, $\bar{q}_{fi}$, etc.) were neglected in the peripheral jet flow equations and retained in the compartmentation jet flow equations.

Consider the product of two variables X and Y, with steady-state values of X_o and Y_o. If x and y are variations from steady state, then

$$X = X_o + x$$

$$Y = Y_o + y$$

and the product $XY = (X_o + x)(Y_o + y)$

$$= X_oY_o + X_oy + Y_ox + xy$$

Let X here denote a dimensionless pressure term and Y another dimensionless variable.

2.5.1 For the peripheral jet $X_o = 1$, $x = 0.1$

$Y_o = 1$, $y = 0.1$

therefore, including the product of the variation

$$X = 1.1\ X_o$$

$$Y = 1.1\ Y_o$$

and

$$XY = (1 + .1 + .1 + .01) = 1.21$$

neglecting the product of the variation

$$(1 + .1 + .1) = 1.2$$

The error is seen to be 0.83 percent.

2.5.2 For the compartmentation jet, $X_o = 0$, $x = .1$

$Y_o = 1$, $y = .1$

Including the product of the variation

$X_oY_o + X_oy + Y_ox + xy = 0 + 0 + .1 + .01 = .11$

and neglecting the product of the variation

$X_oY_o + X_oy + Y_ox = 0 + 0 + .1 = .1$

The error is seen to be 10 percent.

Therefore, the product of the variations were retained in the compartmentation flow equations and neglected in the peripheral jet flow equations.

3.0 Completely Linear Equations

Let: $K_{KA} = K_{K1}, K_{K2}, K_{K3}, K_{K4}$

$$\bar{b} = \frac{2x_3}{b} \tag{A-56}$$

$$\bar{a} = \frac{2y_3}{a} \tag{A-57}$$

$$K_D = 2K_{KA}\left(1-1/2\,\frac{G}{h}\,\text{Sin}\,\epsilon_j\right)\left(\lambda_1+\frac{A_B P_o}{W_C}\right) \tag{A-58}$$

$$K_C = 2K_{KA}\left(1-1/2\,\frac{G}{h}\,\text{Sin}\,\theta_j\right) \tag{A-59}$$

$$K_E = 2K_{KA}\,\lambda_1 \tag{A-60}$$

$$\pi_1\,\bar{Q}_{io} = 2K_{KA}\left(1-1/2\,\frac{G}{h}\,\text{Sin}\,\theta_j\right)\left(\lambda_1-\frac{A_B P_o}{W_C}\right) \tag{A-61}$$

3.1 Peripheral Jet Flow Equations

The above substitutions into Equations (A-45), (A-46), (A-47), and (A-48) yield:

$$\pi_1 \bar{Q}_1 = \pi_1 \bar{Q}_{1o} + \left\{ K_C \bar{p}_1 - K_D \bar{q}_{f1} - K_E \left[\bar{z} + \bar{b}\,\bar{\theta} - \bar{a}\,\bar{\beta} - \frac{E_1}{h} \sin \frac{\pi b}{\lambda_2} \left(\frac{2vt}{b} - \bar{b} \right) \right] \right\} \quad \text{(A-62)}$$

$$\pi_1 \bar{Q}_2 = \pi_1 \bar{Q}_{2o} + \left\{ K_C \bar{p}_2 - K_D \bar{q}_{f2} - K_E \left[\bar{z} - \bar{b}\,\bar{\theta} - \bar{a}\,\bar{\beta} - \frac{E_2}{h} \sin \frac{\pi b}{\lambda_2} \left(\frac{2vt}{b} + \bar{b} \right) \right] \right\} \quad \text{(A-63)}$$

$$\pi_1 \bar{Q}_3 = \pi_1 \bar{Q}_{3o} + \left\{ K_C \bar{p}_3 - K_D \bar{q}_{f3} - K_E \left[\bar{z} - \bar{b}\,\bar{\theta} + \bar{a}\,\bar{\beta} - \frac{E_3}{h} \sin \frac{\pi b}{\lambda_2} \left(\frac{2vt}{b} + \bar{b} \right) \right] \right\} \quad \text{(A-64)}$$

$$\pi_1 \bar{Q}_4 = \pi_1 \bar{Q}_{4o} + \left\{ K_C \bar{p}_4 - K_D \bar{q}_{f4} - K_E \left[\bar{z} + \bar{b}\,\bar{\theta} + \bar{a}\,\bar{\beta} - \frac{E_4}{h} \sin \frac{\pi b}{\lambda_2} \left(\frac{2vt}{b} - \bar{b} \right) \right] \right\} \quad \text{(A-65)}$$

3.2 Compartmentation Jet Flow Equations

Neglecting the effects of pitching, rolling, heaving and surface irregularities, that is $\bar{h}_{ik} = 1$, equations (A-49), (A-50), (A-51) and (A-52) become:

$$\left.\begin{aligned} \frac{C_{12}}{C_1}\,\pi_2\,\bar{Q}_{12} &= \frac{1}{2}\,\pi_2\,\frac{C_{12}}{C_1} - F_1\,\frac{C_{12}}{C_1}\,(\bar{p}_1 - \bar{p}_2) \\ \frac{C_{21}}{C_2}\,\pi_2\,\bar{Q}_{21} &= \frac{1}{2}\,\pi_2\,\frac{C_{21}}{C_1} - F_1\,\frac{C_{21}}{C_2}\,(\bar{p}_2 - \bar{p}_1) \end{aligned}\right\} \quad \text{(A-66)}$$

$$\left.\begin{aligned} \frac{C_{23}}{C_2}\,\pi_2\,\bar{Q}_{23} &= \frac{1}{2}\,\pi_2\,\frac{C_{23}}{C_2} - F_1\,\frac{C_{23}}{C_2}\,(\bar{p}_2 - \bar{p}_3) \\ \frac{C_{32}}{C_3}\,\pi_2\,\bar{Q}_{32} &= \frac{1}{2}\,\pi_2\,\frac{C_{32}}{C_3} - F_1\,\frac{C_{32}}{C_3}\,(\bar{p}_3 - \bar{p}_2) \end{aligned}\right\} \quad \text{(A-67)}$$

$$\left.\begin{aligned} \frac{C_{34}}{C_3}\,\pi_2\,\bar{Q}_{34} &= \frac{1}{2}\,\pi_2\,\frac{C_{34}}{C_3} - F_1\,\frac{C_{34}}{C_3}\,(\bar{p}_3 - \bar{p}_4) \\ \frac{C_{43}}{C_4}\,\pi_2\,\bar{Q}_{43} &= \frac{1}{2}\,\pi_2\,\frac{C_{43}}{C_4} - F_1\,\frac{C_{43}}{C_4}\,(\bar{p}_4 - \bar{p}_3) \end{aligned}\right\} \quad \text{(A-68)}$$

$$\left.\begin{aligned} \frac{C_{14}}{C_1}\,\pi_2\,\bar{Q}_{14} &= \frac{1}{2}\,\pi_2\,\frac{C_{14}}{C_1} - F_1\,\frac{C_{14}}{C_1}\,(\bar{p}_1 - \bar{p}_4) \\ \frac{C_{41}}{C_4}\,\pi_2\,\bar{Q}_{41} &= \frac{1}{2}\,\pi_2\,\frac{C_{41}}{C_4} - F_1\,\frac{C_{41}}{C_4}\,(\bar{p}_4 - \bar{p}_1) \end{aligned}\right\} \quad \text{(A-69)}$$

LET: $\frac{1}{2}\,\pi_2\,\frac{C_{12}}{C_1} = \frac{1}{2}\,\pi_2\,\frac{C_{34}}{C_3} = K_F$

$\frac{1}{2}\,\pi_2\,\frac{C_{14}}{C_1} = \frac{1}{2}\,\pi_2\,\frac{C_{23}}{C_2} = K_G$

$F_1\,\frac{C_{12}}{C_1} = F_1\,\frac{C_{34}}{C_3} = K_Y$

$F_1\,\frac{C_{14}}{C_1} = F_1\,\frac{C_{23}}{C_2} = K_X$

In Equations (A-41), (A-42), (A-43), and (A-44), let $\dot{\bar{p}}_i = 0$ and in the peripherial jet flow equations let $\bar{q}_{fi} = \bar{q}_{fi} + \frac{\partial \bar{Q}_{fi}}{\partial \bar{p}_i}\,\bar{p}_i = \bar{q}_{fi} + \frac{W_c}{A_B\,Q_{fi}}\,\frac{\partial Q_{fi}}{\partial \bar{p}_i}\,\bar{p}_i$.

Substitution of the appropriate flow terms from equations (A-62) through (A-69) into each pressure equation yields after cancellation of steady state terms ($\pi_1\,\bar{Q}_{io} = K_F + K_G$)

$$(K_c + K_x + K_y - K_D\,\frac{\partial \bar{Q}_{f_1}}{\partial P_1})\,\bar{p}_1 - K_y\,\bar{p}_2 - K_x\,\bar{p}_4$$

$$= K_E\left[\bar{z} + b\,\bar{\theta} - \bar{a}\,\bar{\phi} - \frac{E}{h}\,\mathrm{Sin}\,\frac{\pi b}{\lambda_2}\left(\frac{2vt}{b} - b\right)\right] + K_D\,\bar{q}_{f_1}$$

$$+ \tau_2\left[\dot{\bar{z}} + \frac{1}{2}\,\dot{\bar{\theta}} - \frac{1}{2}\,\dot{\bar{\phi}} - \frac{E}{h}\left(\frac{2\pi v}{\lambda_2}\right)\cos\frac{\pi b}{\lambda_2}\left(\frac{2vt}{b} - \frac{1}{2}\right)\right] \qquad \text{(A-70)}$$

$$\left(K_c + K_x + K_y - K_D \frac{\partial \bar{Q}_{f2}}{\partial \bar{P}_2}\right) \bar{P}_2 - K_y \bar{P}_1 - K_x \bar{P}_3$$

$$= K_E\left[\bar{z} - \bar{b}\,\bar{\theta} - \bar{a}\,\bar{\phi} - \frac{E}{h} \sin \frac{\pi b}{\lambda_2}\left(\frac{2vt}{b} + \bar{b}\right)\right] + K_D \bar{q}_{f2}$$

$$+ \tau_2\left[\dot{\bar{z}} - \frac{1}{2}\dot{\bar{\theta}} - \frac{1}{2}\dot{\bar{\phi}} - \frac{E}{h}\left(\frac{2\pi v}{\lambda_2}\right) \cos \frac{\pi b}{\lambda_2}\left(\frac{2vt}{b} + \frac{1}{2}\right)\right] \quad \text{(A-71)}$$

$$\left(K_c + K_x + K_y - K_D \frac{\partial \bar{Q}_{f3}}{\partial \bar{P}_3}\right) \bar{P}_3 - K_x \bar{P}_2 - K_y \bar{P}_4$$

$$= K_E\left[\bar{z} - \bar{b}\,\bar{\theta} + \bar{a}\,\bar{\phi} - \frac{E}{h} \sin \frac{\pi b}{\lambda_2}\left(\frac{2vt}{b} + \bar{b}\right)\right] + K_D \bar{q}_{f3}$$

$$= \tau_2\left[\dot{\bar{z}} - \frac{1}{2}\dot{\bar{\theta}} + \frac{1}{2}\dot{\bar{\phi}} - \frac{E}{h}\left(\frac{2\pi v}{\lambda_2}\right) \cos \frac{\pi b}{\lambda_2}\left(\frac{2vt}{b} + \frac{1}{2}\right)\right] \quad \text{(A-72)}$$

$$\left(K_c + K_x + K_y - K_D \frac{\partial \bar{Q}_{f4}}{\partial \bar{P}_4}\right) \bar{P}_4 - K_x \bar{P}_1 - K_y \bar{P}_3$$

$$= K_E\left[\bar{z} + \bar{b}\,\bar{\theta} + \bar{a}\,\bar{\phi} - \frac{E}{h} \sin \frac{\pi b}{\lambda_2}\left(\frac{2vt}{b} - \bar{b}\right)\right] + K_D \bar{q}_{f4}$$

$$= \tau_2\left[\dot{\bar{z}} + \frac{1}{2}\dot{\bar{\theta}} + \frac{1}{2}\dot{\bar{\phi}} - \frac{E}{h}\left(\frac{2\pi v}{\lambda_2}\right) \cos \frac{\pi b}{\lambda_2}\left(\frac{2vt}{b} - \frac{1}{2}\right)\right] \quad \text{(A-73)}$$

3.3 Solution of Pressure Equations

3.3.1 Dividing each pressure equation by the coefficient of $\bar{P}_i$, $(K_c + K_x + K_y - K_d \frac{\partial \bar{Q}_{fi}}{\partial \bar{P}_i})$, and denoting the right sides as $\left[C_i\right]$, Equations (A-70), (A-71), (A-72), and (A-73) are now written in matrix form.

$$\begin{bmatrix} 1 & -B & 0 & -A \\ -B & 1 & -A & 0 \\ 0 & -A & 1 & -B \\ -A & 0 & -B & 1 \end{bmatrix} \cdot \begin{bmatrix} \bar{P}_1 \\ \bar{P}_2 \\ \bar{P}_3 \\ \bar{P}_4 \end{bmatrix} = \begin{bmatrix} C_1 \\ C_2 \\ C_3 \\ C_4 \end{bmatrix} \qquad \text{(A-74)}$$

where

$$A = \frac{K_x}{K_c + K_x + K_y - K_d \frac{\partial \bar{Q}_{fi}}{\partial \bar{P}_i}}$$

$$B = \frac{K_y}{K_c + K_x + K_y - K_d \frac{\partial \bar{Q}_{fi}}{\partial \bar{P}_i}}$$

The general solution of Equation (A-74) is:

$$\begin{bmatrix} \bar{P}_1 \\ \bar{P}_2 \\ \bar{P}_3 \\ \bar{P}_4 \end{bmatrix} = \frac{1}{1-2(A^2+B^2)+(A^2-B^2)^2} \begin{bmatrix} (1-A^2-B^2) & B(1+A^2-B^2) & 2AB & A(1+B^2-A^2) \\ B(1+A^2-B^2) & (1-A^2-B^2) & A(1+B^2-A^2) & 2AB \\ 2AB & A(1+B^2-A^2) & (1-A^2-B^2) & B(1+A^2-B^2) \\ A(1+B^2-A^2) & 2AB & B(1+A^2-B^2) & (1-A^2-B^2) \end{bmatrix} \cdot \begin{bmatrix} C_1 \\ C_2 \\ C_3 \\ C_4 \end{bmatrix} \quad \text{(A-75)}$$

$\left[C_i\right]$'s from Equations (A-70), (A-71), (A-72), and (A-73), can be written in the general form;

$$K_E \left[\bar{z} \pm \bar{b}\,\bar{\theta} \pm \bar{a}\,\bar{\phi} - \frac{E}{h} \sin \frac{\pi b}{\lambda_2} \left(\frac{2vt}{b} \pm \bar{b} \right) \right] + K_D \bar{q}_{fi}$$

$$+ \tau_2 \left[\dot{\bar{z}} \pm \frac{1}{2} \dot{\bar{\phi}} \pm \frac{1}{2} - \frac{\bar{E}}{h} \left(\frac{2\pi v}{\lambda_2}\right) \cos \frac{\pi b}{\lambda_2} \left(\frac{\pi b}{\lambda_2} \left(\frac{2vt}{b}\right) \pm \frac{1}{2} \right) \right]$$

where the signs of the $\bar{\theta}$, $\bar{\phi}$, and b terms depend upon which pressure equation is being expanded.

Completing the solution of the pressure equations now proceeds with the substitution of the proper terms in the $\left[C_i\right]$ matrix.

3.3.2 Flow Terms

The $\bar{q}_{fi}$ terms can be written as

$$\left[C_i\right] = \frac{K_d}{K_c + K_x + K_y - K_d \dfrac{\partial \bar{Q}_{fi}}{\partial \bar{P}_i}} \cdot \left[\bar{q}_{fi}\right] \quad \text{(A-76)}$$

3.3.3 Heave Terms

The pitch terms in $\left[C_i\right]$ may be written (denoting $\frac{s}{\bar{z}}$ as $s\bar{z}$):

$$\left[C_i\right] = \frac{K_E\left(1 + \frac{\tau_2}{K_E}s\right)}{K_c + K_x + K_y - K_D\frac{\partial \bar{Q}_{fi}}{\partial \bar{P}_i}}\begin{bmatrix}1\\1\\1\\1\end{bmatrix}\bar{z} \qquad \text{(A-77)}$$

since all of the $\bar{z}$ terms are positive and the matrix in Equation (A-75) is symmetrical, the coefficient becomes:

$$1 - A^2 - B^2 + B + BA^2 - B^3 + 2AB + A + AB^2 - A^2$$

or

$$(1 + A + B)\left[1 - (A - B)^2\right]$$

$$\left[\frac{\bar{P}_i}{\bar{z}}\right] = \frac{(1+A+B)\left[1-(A-B)^2\right]}{1-2(A^2+B^2) + (A^2-B^2)^2}\frac{K_E}{K_c + K_x + K_y - K_D\frac{\partial \bar{Q}_{fi}}{\partial \bar{P}_i}}\begin{bmatrix}1\\1\\1\\1\end{bmatrix}\left(1 + \frac{\tau_2}{K_E}s\right) \qquad \text{(A-78)}$$

3.3.4 Pitch Terms

The pitch terms in C_i may be written as (denoting $\dot{\bar{\theta}}$ as $s\bar{\theta}$):

$$\left[C_i\right] = \frac{K_E \bar{b}\left(1 + \frac{\tau_2}{2K_E\bar{b}}\, s\right)}{K_c + K_x + K_y - K_d \frac{\partial \bar{Q}_{fi}}{\partial \bar{P}_i}} \begin{bmatrix} +1 \\ -1 \\ -1 \\ +1 \end{bmatrix} \bar{e} \qquad \text{(A-79)}$$

Assigning the correct sign on each coefficient yields:

on $\bar{p}_1$: $(1-A^2-B^2) - B(1+A^2-B^2) - 2AB + A(1+B^2-A^2)$,

on $\bar{p}_2$: $-(1-A^2-B^2) + B(1+A^2-B^2) + 2AB - A(1+B^2-A^2)$,

on $\bar{p}_3$: $-(1-A^2-B^2) + B(1+A^2-B^2) + 2AB - A(1+B^2-A^2)$,

on $\bar{p}_4$: $(1-A^2-B^2) - B(1+A^2-B^2) - 2AB - A(1+B^2-A^2)$.

The $\bar{p}_2$ and $\bar{p}_3$ terms are of opposite sign than the $\bar{p}_1$ and $\bar{p}_4$ terms, therefore

$$1 - A^2 - B^2 - B - BA^2 + B^3 - 2AB + A + AB^2 - A^3$$

$$\text{or } (1 + A - B)\left[1 - (A + B)^2\right]$$

$$\left[\frac{\bar{P}_i}{\bar{\theta}}\right] = \frac{(1+A-B)\left[1-(A+B)^2\right]}{1-2(A^2+B^2)+(A^2-B^2)^2} \cdot \frac{K_E\bar{b}}{K_c + K_x + K_y - K_d \frac{\partial \bar{Q}_{fi}}{\partial \bar{P}_i}} \begin{bmatrix} 1 \\ -1 \\ -1 \\ 1 \end{bmatrix} \left(1 + \frac{\tau_2}{2K_E\bar{b}}\, s\right) \qquad \text{(A-80)}$$

3.3.5 Roll Terms

Using similar notation as in pitch, the roll term in $\left[C_i\right]$ may be written as:

$$\left[C_i\right] = \frac{K_E\,\bar{a}\,\left(1+\frac{\tau_2}{2K_E\,\bar{a}}\right)}{K_c+K_x+K_y - K_d\,\frac{\partial \bar{Q}_{fi}}{\partial \bar{P}_i}} \begin{bmatrix} -1 \\ -1 \\ 1 \\ 1 \end{bmatrix} \bar{\phi} \qquad \text{(A-81)}$$

Assigning the correct sign to each coefficient yields:

on $\bar{p}_1$: $-(1-A^2-B^2)\ -B(1+A^2-B^2)\ +2AB\ +A(1+B^2-A^2)$,

on $\bar{p}_2$: $-(1-A^2-B^2)\ -B(1+A^2-B^2)\ +2AB\ +A(1+B^2-A^2)$,

on $\bar{p}_3$: $+(1-A^2-B^2)\ +B(1+A^2-B^2)\ -2AB\ -A(1+B^2-A^2)$,

on $\bar{p}_4$: $+(1-A^2-B^2)\ +B(1+A^2-B^2)\ -2AB\ -A(1+B^2-A^2)$.

The $\bar{p}_1$ and $\bar{p}_2$ terms are of opposite sign than the $\bar{p}_3$ and $\bar{p}_4$ terms, therefore

$$1 - A^2 - B^2 + B + BA^2 - B^3 - 2AB - A - AB^2 + A^3$$

or $(1 - A + B)\left[1 - (A + B)^2\right]$

$$\left[\frac{\bar{P}_i}{\bar{\phi}}\right] = \frac{(1-A+B)\left[1-(A+B)^2\right]}{1-2(A^2+B^2)+(A^2-B^2)^2} \quad \frac{K_E\,\bar{a}}{K_c+K_x+K_y-K_d\frac{\partial \bar{Q}_{fi}}{\partial \bar{P}_i}} \begin{bmatrix} -1 \\ -1 \\ +1 \\ +1 \end{bmatrix} \left(1+\frac{\tau_2}{2K_E\bar{a}}\,s\right) \qquad \text{(A-82)}$$

3.3.6 Wave Motion Terms

Equations (A-70) and (A-73) contain,

$$- K_E \frac{E}{h} \sin \frac{\pi b}{\lambda_2} \left(\frac{2vt}{b} - \bar{b}\right)$$

$$- \tau_2 \frac{\bar{E}}{h} \left(\frac{2\pi v}{\lambda_2}\right) \cos \frac{\pi b}{\lambda_2} \left(\frac{2vt}{b} - \frac{1}{2}\right)$$

or

$$- K_E \frac{E}{h} \left(\sin \frac{2\pi v}{\lambda_2} t \cos \frac{\pi b \bar{b}}{\lambda_2} - \cos \frac{2\pi v}{\lambda_2} t \sin \frac{\pi b \bar{b}}{\lambda_2}\right)$$

$$- \tau_2 \frac{\bar{E}}{h} \left(\frac{2\pi v}{\lambda_2}\right)\left(\cos \frac{2\pi v}{\lambda_2} t \cos \frac{\pi b}{2\lambda_2} + \sin \frac{2\pi v}{\lambda_2} t \sin \frac{\pi b}{2\lambda_2}\right)$$

Similarly, Equations (A-71) and (A-72) contain,

$$- K_E \frac{E}{h} \left(\sin \frac{2\pi v}{\lambda_2} t \cos \frac{\pi b \bar{b}}{\lambda_2} + \cos \frac{2\pi v}{\lambda_2} t \sin \frac{\pi b \bar{b}}{\lambda_2}\right)$$

$$- \tau_2 \frac{\bar{E}}{h} \left(\frac{2\pi v}{\lambda_2}\right)\left(\cos \frac{2\pi v}{\lambda_2} t \cos \frac{\pi b}{2\lambda_2} - \sin \frac{2\pi v}{\lambda_2} t \sin \frac{\pi b}{2\lambda_2}\right)$$

The wave terms in $\left[C_i\right]$ become:

$$\left[C_i\right] = \frac{\left[-K_E \frac{E}{h} \sin \frac{2\pi v}{\lambda_2} t \cos \frac{\pi b \bar{b}}{\lambda_2} - \tau_2 \frac{\bar{E}}{h} \left(\frac{2\pi v}{\lambda_2}\right) \cos \frac{2\pi v}{\lambda_2} t \cos \frac{\pi b}{2\lambda_2}\right]}{K_C + K_X + K_Y - K_D \frac{\partial \bar{Q}_{fi}}{\partial \bar{P}_i}} \begin{bmatrix} 1 \\ 1 \\ 1 \\ 1 \end{bmatrix}$$

$$+ \frac{\left[+K_E \frac{E}{h} \cos \frac{2\pi v}{\lambda_2} t \sin \frac{\pi b \bar{b}}{\lambda_2} - \tau_2 \frac{\bar{E}}{h} \left(\frac{2\pi v}{\lambda_2}\right) \sin \frac{2\pi v}{\lambda_2} t \sin \frac{\pi b}{2\lambda_2}\right]}{K_C + K_X + K_Y - K_D \frac{\partial \bar{Q}_{fi}}{\partial \bar{P}_i}} \begin{bmatrix} 1 \\ -1 \\ -1 \\ 1 \end{bmatrix} \quad \text{(A-83)}$$

Assigning the proper sign to the coefficients yields:

$$\left[\bar{P}_i\right] = \frac{(1+A+B)\left[1-(A-B)^2\right]}{1-2(A^2+B^2)+(A^2-B^2)^2} \cdot \frac{\left[-K_E \frac{E}{h} \sin \frac{2\pi v}{\lambda_2} t \cos \frac{\pi b \bar{b}}{\lambda_2} - \frac{2\pi v \tau_2 \bar{E}}{h\lambda_2} \cos \frac{2\pi v}{\lambda_2} t \cos \frac{\pi b}{2\lambda_2}\right]}{K_C + K_X + K_Y - K_D \frac{\partial \bar{Q}_{fi}}{\partial \bar{P}_i}} \begin{bmatrix} 1 \\ 1 \\ 1 \\ 1 \end{bmatrix}$$

$$+ \frac{(1+A-B)\left[1-(A+B)^2\right]}{1-2(A^2+B^2)+(A^2-B^2)^2} \cdot \frac{\left[K_E \frac{E}{h} \cos \frac{2\pi v}{\lambda_2} t \sin \frac{\pi b \bar{b}}{\lambda_2} - \frac{2\pi v \tau_2 \bar{E}}{h\lambda_2} \sin \frac{2\pi v}{\lambda_2} t \sin \frac{\pi b}{2\lambda_2}\right]}{K_C + K_X + K_Y - K_D \frac{\partial \bar{Q}_{fi}}{\partial \bar{P}_i}} \begin{bmatrix} +1 \\ -1 \\ -1 \\ +1 \end{bmatrix} \quad \text{(A-84)}$$

4.0 Equations of Motion

To complete the linearization, the expressions for the transient pressure in each compartment, Equations (A-70), (A-71), (A-72), and (A-73) will be combined with the equations of motion, Equations (A-53), (A-54), and (A-55).

4.1 Heave

From Equation (A-53)

$$\ddot{z} = - \omega_H^2 \left(\frac{\bar{P}_1 + \bar{P}_2 + \bar{P}_3 + \bar{P}_4}{4} \right)$$

where $\omega_H = \sqrt{g/h}$

Substitution of the pressure terms, as given in general form in Equation (A-75), into the above equation involves inclusion of the terms defined as the $\left[C_i \right]$ matrix which have an effect on the heave motion. This formulation, which deals with a symmetrical platform will therefore exclude pitch and roll terms in the heave mode equations.

The applicable terms are:

$\bar{q}_{fi}$ Equation (A-76)

$\bar{z}$ Equation (A-78)

Wave form Equation (A-84)

Denoting $\ddot{\bar{z}}$ as $s^2\bar{z}$ and making the above substitutions yields:

$$\frac{s^2}{\omega_H^2}\bar{z} = \frac{-(1+A+B)\left[1-(A-B)^2\right]K_E}{\left[1-2(A^2+B^2)+(A^2-B^2)^2\right]\left[K_c+K_x+K_y-K_D\frac{\partial Q_{fi}}{\partial P_i}\right]}$$

$$\left\{(1+\frac{\tau_2}{K_E}s)\,\bar{z}+\frac{K_D}{4K_E}(\bar{q}_{f_1}+\bar{q}_{f_2}+\bar{q}_{f_3}+\bar{q}_{f_4})\right.$$

$$\left.-(\frac{E}{h}\sin\frac{2\pi v}{\lambda_2}t\cos\frac{\pi b\bar{b}}{\lambda_2}+\frac{2\pi v\tau_2 E}{K_E h\lambda_2}\cos\frac{2\pi v}{\lambda_2}t\cos\frac{\pi b}{2\lambda_2}\right\} \qquad \text{(A-85)}$$

Note that:

$$1-2(A^2+B^2)+(A^2-B^2)^2=(1+A+B)(1+A-B)(1-A+B)(1-A-B)$$

and

$$(1+A+B)\left[1-(A-B)^2\right]=(1+A+B)\left[1-(A+B)\right]\left[1+(A+B)\right]$$

Therefore, the coefficient becomes:

$$\frac{K_E}{(1-A-B)\left(K_c+K_x+K_y-K_D\frac{\partial\bar{Q}_{fi}}{\partial\bar{P}_i}\right)}$$

$$(1 - A - B) = 1 - (A + B)$$

$$= 1 - \frac{K_x + K_y}{K_c + K_x + K_y - K_D \frac{\partial \bar{Q}_{fi}}{\partial \bar{P}_i}}$$

$$= \frac{K_c + K_x + K_y - K_D \frac{\partial \bar{Q}_{fi}}{\partial \bar{P}_i} - K_x - K_y}{K_c + K_x + K_y - K_D \frac{\partial \bar{Q}_{fi}}{\partial \bar{P}_i}}$$

$$= \frac{K_c - K_D \frac{\partial \bar{Q}_{fi}}{\partial \bar{P}_i}}{K_c + K_x + K_y - K_D \frac{\partial \bar{Q}_{fi}}{\partial \bar{P}_i}}$$

therefore:

$$\frac{K_E}{(1-A-B)(K_c+K_x+K_y-K_D\frac{\partial \bar{Q}_{fi}}{\partial \bar{P}_i})} = \frac{K_E}{K_c - K_D \frac{\partial \bar{Q}_{fi}}{\partial \bar{P}_i}}$$

$$= \frac{2K_{KA}\,\lambda_1}{2K_{KA}\,(1 - \frac{1}{2}\frac{G}{h}\sin\theta_j)\left[1 - (\lambda_1 + \frac{A_B P_o}{W_c})\frac{\partial \bar{Q}_{fi}}{\partial \bar{P}_i}\right]}$$

$$= \frac{\lambda_1}{(1 - \frac{1}{2}\frac{G}{h}\sin\theta_j)\left[1 - (\lambda_1 + \frac{A_B P_o}{W_c})\frac{\partial \bar{Q}_{fi}}{\partial \bar{P}_i}\right]}$$

Equation (A-85) becomes:

$$\left(\frac{s^2}{\omega_H^2}\right)\bar{z} = -\frac{\lambda_1\left(1+\frac{\tau_2}{2K_{KA}\lambda_1}s\right)}{\left(1-\frac{1}{2}\frac{G}{h}\sin\theta_j\right)\left[1-\left(\lambda_1+\frac{A_B P_o}{W_c}\right)\frac{\partial\bar{Q}_{fi}}{\partial\bar{P}_i}\right]}\bar{z}$$

$$-\frac{\left(\lambda_1+\frac{A_B P_o}{W_c}\right)}{4\left[1-\left(\lambda_1+\frac{A_B P_o}{W_c}\right)\frac{\partial\bar{Q}_{fi}}{\partial\bar{P}_i}\right]}\left(\bar{q}_{f_1}+\bar{q}_{f_2}+\bar{q}_{f_3}+\bar{q}_{f_4}\right)$$

$$+\frac{\frac{\lambda_1 E}{\left(1-\frac{1}{2}\frac{G}{h}\sin\theta_j\right)h}}{\left[1-\left(\lambda_1+\frac{A_B P_o}{W_c}\right)\frac{\partial\bar{Q}_{fi}}{\partial\bar{P}_i}\right]}\left\{\sin\frac{2\pi v}{\lambda_2}\,t\cos\frac{\pi b\bar{b}}{\lambda_2}\right.$$

$$\left.+\frac{2\pi v\tau_2}{\lambda_2}\;\frac{E}{2K_{KA}\lambda_1 E}\cos\frac{2\pi v}{\lambda_2}\,t\cos\frac{\pi b}{2\tau_2}\right\} \qquad \text{(A-86)}$$

4.2 Pitch

From Equation (A-55)

$$\ddot{\bar{\theta}} = \omega_H^2 \left(\frac{W_c b^2}{8I_y}\right) \left(\frac{-\bar{P}_1 + \bar{P}_2 + \bar{P}_3 - \bar{P}_4}{4}\right)$$

$$\left(\frac{8I_y}{W_c b^2}\right) \frac{s^2}{\omega_H^2} \bar{\theta} = - \frac{(1 + A - B)\left[1 - (A+B)^2\right]}{1 - 2(A^2+B^2) + (A^2-B^2)^2} \cdot \frac{K_E \bar{b}}{K_c + K_x + K_y - K_D \frac{\partial Q_{fi}}{\partial P_i}} \cdot$$

$$\cdot (1 + \frac{\tau_2}{2K_E b} s)\, \bar{\theta} + \frac{(1 - A - B)\left[1 - (A+B)^2\right]}{1 - 2(A^2+B^2) + (A^2-B^2)^2} \cdot$$

$$\cdot \frac{K_D}{K_c + K_x + K_y - K_D \frac{\partial Q_{fi}}{\partial P_i}} \frac{(-\bar{q}_{f_1} + \bar{q}_{f_2} + \bar{q}_{f_3} - \bar{q}_{f_4})}{4}$$

$$- \frac{(1+A-B)\left[1-(A+B)^2\right]}{1 - 2(A^2+B^2) + (A^2-B^2)^2} \cdot \frac{1}{K_c + K_x + K_y - K_D \frac{\partial Q_{fi}}{\partial P_i}} \cdot$$

$$\cdot \left\{ \frac{K_E E}{h} \cos \frac{2\pi v}{\lambda_2} t \sin \frac{\pi b \bar{b}}{\lambda_2} \right.$$

$$\left. - \frac{2\pi v \tau_2 E}{h \lambda_2} \sin \frac{2\pi v}{\lambda_2} t \sin \frac{\pi b}{2\lambda_2} \right\} \qquad \text{(A-87)}$$

The term $\dfrac{(1 + A-B)\left[1 - A+B)^2\right]}{1-2(A^2+B^2) + (A^2-B^2)^2} = \dfrac{1}{1 - A+B}$

$$1 - A+B = \frac{K_c + K_x + K_y - K_D \dfrac{\partial \bar{Q}_{fi}}{\partial \bar{P}_i} - K_x + K_y}{K_c + K_x + K_y - K_D \dfrac{\partial \bar{Q}_{fi}}{\partial \bar{P}_i}}$$

$$= \frac{K_c - K_D \dfrac{\partial \bar{Q}_{fi}}{\partial \bar{P}_i} + 2K_y}{K_c + K_x + K_y - K_D \dfrac{\partial \bar{Q}_{fi}}{\partial \bar{P}_i}}$$

Equation (A-87) becomes:

$$\left(\frac{8I_y}{W_c b^2}\right)\frac{s^2}{W_H^2}\,\bar{\theta} = \frac{K_c+K_x+K_y-K_D \dfrac{\partial \bar{Q}_{fi}}{\partial \bar{P}_i}}{K_c - K_D \dfrac{\partial \bar{Q}_{fi}}{\partial \bar{P}_i} + 2K_y}\left\{\frac{-K_E\bar{b}}{K_c+K_x+K_y-K_D \dfrac{\partial \bar{Q}_{fi}}{\partial \bar{P}_i}}\cdot\right.$$

$$\left.\cdot\left(1 + \frac{\tau_2}{2K_E\bar{b}}s\right)\bar{\theta} + \frac{K_D}{K_c+K_x+K_y-K_D \dfrac{\partial \bar{Q}_{fi}}{\partial \bar{P}_i}} - \frac{\bar{q}_{f_1} + \bar{q}_{f_2} + \bar{q}_{f_3} - \bar{q}_{f_4}}{4}\right\}$$

$$- \frac{1}{K_c + K_x + K_y - K_D \dfrac{\partial \bar{Q}_{fi}}{\partial \bar{P}_i}}\left[\frac{K_E E}{h}\cos\frac{2\pi v}{\lambda_2}\,t\,\sin\frac{\pi b\bar{b}}{\lambda_2}\right.$$

$$\left.-\frac{2\pi v\tau_2 E}{h\lambda_2}\sin\frac{2\pi v}{\lambda_2}\,t\,\sin\frac{\pi b}{2\lambda_2}\right] \qquad \text{(A-88)}$$

Coefficient of $\bar{\theta}$ terms:

$$\frac{-K_E\bar{b}}{K_c - K_D\frac{\partial\bar{Q}_{fi}}{\partial\bar{P}_i} + 2K_y} = \frac{-2K_{KA}\lambda_1\bar{b}}{2K_{KA}\left(1-\frac{1}{2}\frac{G}{h}\sin\theta_j\right)\left[1-\left(\lambda_1+\frac{A_B P_o}{W_c}\right)\frac{\partial\bar{Q}_{fi}}{\partial\bar{P}_i}\right]+2F_1\frac{C_{s4}}{C_s}}$$

$$= -\frac{\lambda_1\bar{b}}{\left(1-\frac{1}{2}\frac{G}{h}\sin\theta_j\right)\left[1-\left(\lambda_1+\frac{A_B P_o}{W_c}\right)\frac{\partial\bar{Q}_{fi}}{\partial\bar{P}_i}\right]+\frac{a}{a+b}\frac{F_1}{K_{KA}}}$$

Coefficient of $\bar{q}_{fi}$ terms:

$$\frac{K_D}{K_c - K_D \frac{\partial \bar{Q}_{fi}}{\partial \bar{P}_i} + 2K_y}$$

$$= \frac{2K_{KA}\left(1 - \frac{1}{2}\frac{G}{h}\sin\theta_j\right)\left(\lambda_1 + \frac{A_B P_o}{W_c}\right)}{2K_{KA}\left(1 - \frac{1}{2}\frac{G}{h}\sin\theta_j\right)\left[1 - \left(\lambda_1 + \frac{A_B P_o}{W_c}\right)\frac{\partial \bar{Q}_{fi}}{\partial \bar{P}_i}\right] + 2F_1\frac{C_{s4}}{C_s}}$$

$$= \frac{\left(1 - \frac{1}{2}\frac{G}{h}\sin\theta_j\right)\left(\lambda_1 + \frac{A_B P_o}{W_c}\right)}{\left(1 - \frac{1}{2}\frac{G}{h}\sin\theta_j\right)\left[1 - \left(\lambda_1 + \frac{A_B P_o}{W_c}\right)\frac{\partial \bar{Q}_{fi}}{\partial \bar{P}_i}\right] + \frac{a}{a+b}\frac{F_1}{K_{KA}}}$$

Coefficient of wave terms:

$$\frac{K_E \frac{E}{h}}{K_c - K_D \frac{\partial \bar{Q}_{fi}}{\partial \bar{P}_i} + 2K_y}$$

$$= \frac{2K_{KA}\lambda_1\left(\frac{E}{h}\right)}{2K_{KA}\left(1 - \frac{1}{2}\frac{G}{h}\sin\theta_j\right)\left[1 - \left(\lambda_1 + \frac{A_B P_o}{W_c}\right)\frac{\partial \bar{Q}_{fi}}{\partial \bar{P}_i}\right] + 2F_1\frac{C_{s4}}{C_s}}$$

$$= \frac{\lambda_1\left(\frac{E}{h}\right)}{\left(1 - \frac{1}{2}\frac{G}{h}\sin\theta_j\right)\left[1 - \left(\lambda_1 + \frac{A_B P_o}{W_c}\right)\frac{\partial \bar{Q}_{fi}}{\partial \bar{P}_i}\right] + \frac{a}{a+b}\frac{F_1}{K_{KA}}}$$

Equation (A-88) becomes:

$$\left(\frac{8I_y}{W_c b^2}\right)\frac{s^2}{W_H^2}\,\bar{\theta}$$

$$= -\frac{\lambda_1 \bar{b}\left(1+\frac{\tau_2}{4K_{KA}\lambda_1 \bar{b}}s\right)\bar{\theta}}{\left(1-\frac{1}{2}\frac{G}{h}\sin\theta_j\right)\left[1-\left(\lambda_1+\frac{A_B P_o}{W_c}\right)\frac{\partial \bar{Q}_{fi}}{\partial \bar{P}_i}\right]+\left(\frac{a}{a+b}\right)\frac{F_1}{K_{KA}}}$$

$$-\frac{\left(1-\frac{1}{2}\frac{G}{h}\sin\theta_j\right)\left(\lambda_1+\frac{A_B P_o}{W_c}\right)}{\left(1-\frac{1}{2}\frac{G}{h}\sin\theta_j\right)\left[1-\left(\lambda_1+\frac{A_B P_o}{W_c}\right)\frac{\partial \bar{Q}_{fi}}{\partial \bar{P}_i}\right]+\left(\frac{a}{a+b}\right)\frac{F_1}{K_{KA}}}\cdot$$

$$\cdot\frac{1}{4}\left(\bar{q}_{f_1}-\bar{q}_{f_2}-\bar{q}_{f_3}+\bar{q}_{f_4}\right)$$

$$-\frac{\lambda_1\left(\frac{E}{h}\right)}{\left(1-\frac{1}{2}\frac{G}{h}\sin\theta_j\right)\left[1-\left(\lambda_1+\frac{A_B P_o}{W_c}\right)\frac{\partial \bar{Q}_{fi}}{\partial \bar{P}_i}\right]+\left(\frac{a}{a+b}\right)\frac{F_1}{K_{KA}}}\cdot$$

$$\cdot\left\{\cos\frac{2\pi v}{\lambda_2}t\,\sin\frac{\pi b\bar{b}}{\lambda_2}-\frac{2\pi v\tau_2}{\lambda_2}\frac{\bar{E}}{2K_{KA}\lambda_1 E}\sin\frac{2\pi v}{\lambda_2}t\,\sin\frac{\pi b}{2\lambda_2}\right\}$$

(A-89)

4.3 Roll

From Equation (A-54)

$$\ddot{\bar{\phi}} = -\omega_H^2 \left(\frac{W_c a^2}{8 I_x}\right)\frac{(-\bar{p}_1 - \bar{p}_2 + \bar{p}_3 + \bar{p}_4)}{4}$$

$$\left(\frac{8 I_x}{W_c a^2}\right)\frac{s^2}{\omega_H^2}\bar{\phi}$$

$$= -\frac{(1-A+B)\left[1-(A+B)^2\right]}{1-2(A^2+B^2)+(A^2-B^2)^2}\cdot\frac{K_E\,\bar{a}}{K_c + K_x + K_y - K_D\dfrac{\partial \bar{Q}_{fi}}{\partial \bar{P}_i}}\left(1+\frac{\tau_2}{2K_E}s\right)\bar{\phi}$$

$$+\frac{(1-A+B)\left[1-(A+B)^2\right]}{1-2(A^2+B^2)+(A^2-B^2)^2}\cdot\frac{K_D}{K_c + K_x + K_y - K_D\dfrac{\partial \bar{Q}_{fi}}{\partial \bar{P}_i}}\left(\frac{\bar{q}_{f_1}+\bar{q}_{f_2}-\bar{q}_{f_3}-\bar{q}_{f_4}}{4}\right) \qquad (A\text{-}90)$$

Coefficient of $\bar{\phi}$ terms:

$$-\frac{K_E\,\bar{a}}{K_c - K_D\dfrac{\partial \bar{Q}_{fi}}{\partial \bar{P}_i} + 2K_x}$$

$$=\frac{-2K_{KA}\,\lambda_1\,\bar{a}}{2K_{KA}\left(1-\frac{1}{2}\frac{G}{h}\sin\theta_j\right)\left[1-\left(\lambda_1+\frac{A_B P_o}{W_c}\right)\dfrac{\partial \bar{Q}_{fi}}{\partial \bar{P}_i}\right]+2F_1\dfrac{C_{14}}{C_1}}$$

$$=-\frac{\lambda_1\,\bar{a}}{\left(1-\frac{1}{2}\frac{G}{h}\sin\theta_j\right)\left[1-\left(\lambda_1+\frac{A_B P_o}{W_c}\right)\dfrac{\partial \bar{Q}_{fi}}{\partial \bar{P}_i}\right]+\left(\frac{b}{a+b}\right)\dfrac{F_1}{K_{KA}}}$$

Coefficient of $\bar{q}_{fi}$ terms:

$$\frac{K_D}{K_c - K_D \frac{\partial \bar{Q}_{fi}}{\partial \bar{P}_i} + 2K_x}$$

$$= \frac{2K_{KA}\left(1 - \frac{1}{2}\frac{G}{h}\sin\theta_j\right)\left(\lambda_1 + \frac{A_B P_o}{W_c}\right)}{2K_{KA}\left(1 - \frac{1}{2}\frac{G}{h}\sin\theta_j\right)\left[1 - \left(\lambda_1 + \frac{A_B P_o}{W_c}\right)\frac{\partial \bar{Q}_{fi}}{\partial \bar{P}_i}\right] + 2F_1\frac{C_{14}}{C_1}}$$

$$= \frac{\left(1 - \frac{1}{2}\frac{G}{h}\sin\theta_j\right)\left(\lambda_1 + \frac{A_B P_o}{W_c}\right)}{\left(1 - \frac{1}{2}\frac{G}{h}\sin\theta_j\right)\left[1 - \left(\lambda_1 + \frac{A_B P_o}{W_c}\right)\frac{\partial \bar{Q}_{fi}}{\partial \bar{P}_i}\right] + \left(\frac{b}{a+b}\right)\frac{F_1}{K_{KA}}}$$

Equation (A-90) becomes:

$$\left(\frac{8I_x}{W_c a^2}\right)\frac{s^2}{\omega_H^2}\bar{\phi}$$

$$= \frac{-\lambda_1 \bar{a}\left(1 + \frac{\tau_2}{4K_{KA}\lambda_1 \bar{a}}s\right)}{\left(1 - \frac{1}{2}\frac{G}{h}\sin\theta_j\right)\left[1 - \left(\lambda_1 + \frac{A_B P_o}{W_c}\right)\frac{\partial \bar{Q}_{fi}}{\partial \bar{P}_i}\right] + \left(\frac{b}{a+b}\right)\frac{F_1}{K_{KA}}}\bar{\phi}$$

$$+ \frac{\left(1 - \frac{1}{2}\frac{G}{h}\sin\theta_j\right)\left(\lambda_1 + \frac{A_B P_o}{W_c}\right)}{\left(1 - \frac{1}{2}\frac{G}{H}\sin\theta_j\right)\left[1 - \left(\lambda_1 + \frac{A_B P_o}{W_c}\right)\frac{\partial \bar{Q}_{fi}}{\partial \bar{P}_i}\right] + \left(\frac{b}{a+b}\right)\frac{F_1}{K_{KA}}} \cdot$$

$$\cdot \frac{1}{4}\left(\bar{q}_{f_1} + \bar{q}_{f_2} - \bar{q}_{f_3} - \bar{q}_{f_4}\right) \qquad \text{(A-91)}$$

5.0 Recapitulation of Equations of Motion

5.1 Heave

Equation (A-86) may be written:

$$\left[s^2 + 2\zeta_Z \omega_Z s + \omega_Z^2\right] \bar{z} = -\omega_Z^2 \frac{\partial \bar{Z}}{\partial \bar{Q}_{f_1}} (\bar{q}_{f_1} + \bar{q}_{f_2} + \bar{q}_{f_3} + \bar{q}_{f_4})$$

$$+ \omega_Z^2 \left[\frac{E}{h} \sin \frac{2\pi v}{\lambda_2} t \cos \frac{\pi b \bar{b}}{\lambda_2} + \frac{2\pi v \tau_2}{\lambda_2 h} \frac{\bar{E}}{2K_{KA}\lambda_1} \cos \frac{2\pi v}{\lambda_1} t \cos \frac{\pi b}{2\lambda_2}\right] \quad \text{(A-92)}$$

In Equation (A-92)

$$\omega_Z = \sqrt{\frac{\lambda_1 \frac{g}{h}}{(1 - \frac{1}{2}\frac{G}{h} \sin \theta_j)\left[1 - (\lambda_1 + \frac{A_B P_o}{W_c}) \frac{\partial \bar{Q}_{fi}}{\partial \bar{P}_i}\right]}} \quad \text{(A-93)}$$

$$\zeta_Z = \frac{\tau_2 \omega_Z}{4\lambda_1 K_{KA}} \quad \text{(A-94)}$$

$$\frac{\partial \bar{Z}}{\partial \bar{Q}_{fi}} = \frac{(1 - \frac{1}{2}\frac{G}{h} \sin \theta_j)(\lambda_1 + \frac{A_B P_o}{W_c})}{4\lambda_1} \quad \text{(A-95)}$$

5.2 Pitch

Equation (A-89) may be written:

$$\left[s^2 + 2\zeta_\theta \omega_\theta s + \omega_\theta^2\right] \bar{\theta} = -\omega_\theta^2 \frac{\partial \bar{\theta}}{\partial \bar{Q}_{fi}} \left(\bar{q}_{f_1} - \bar{q}_{f_2} - \bar{q}_{f_3} + \bar{q}_{f_4}\right)$$

$$-\omega_\theta^2 \left[\frac{E}{h\bar{b}} \cos \frac{2\pi v}{\lambda_2} t \sin \frac{\pi b \bar{b}}{2} - \frac{2\pi v \zeta_2}{\bar{b}\, \lambda_2 h} \frac{E}{2K_{KA}\, \lambda_1} \sin \frac{2\pi v}{\lambda_2} t \sin \frac{\pi b}{2\lambda_2}\right] \tag{A-96}$$

In Equation (A-96)

$$\omega_\theta = \sqrt{\frac{\lambda_1 \bar{b} \left(\frac{W_c b^2}{8 I_y}\right) \frac{g}{h}}{\left(1 - \frac{1}{2}\frac{G}{h} \sin \theta_j\right)\left[1 - \left(\lambda_1 + \frac{A_B P_o}{W_c}\right) \frac{\partial \bar{Q}_{fi}}{\partial \bar{P}_i}\right] + \left(\frac{a}{a+b}\right) \frac{F_1}{K_{KA}}}} \tag{A-97}$$

$$\zeta_\theta = \frac{\tau_2\, \omega_\theta}{8 K_{kA}\, \lambda_1\, \bar{b}} \tag{A-98}$$

$$\frac{\partial \bar{\theta}}{\partial \bar{Q}_{fi}} = \frac{\left(1 - \frac{1}{2}\frac{G}{H} \sin \theta_j\right)\left(\lambda_1 + \frac{A_B P_o}{W_c}\right)}{4 \lambda_1 \bar{b}} \tag{A-99}$$

5.3 Roll

Equation (A-91) may be written:

$$\left[s^2 + 2\zeta_\phi \omega_\phi s + \omega_\phi^2\right] \bar{\phi} = + \omega_\phi^2 \frac{\partial \bar{\phi}}{\partial \bar{Q}_{fi}} (\bar{q}_{f_1} + \bar{q}_{f_2} - \bar{q}_{f_3} - \bar{q}_{f_4}) \qquad \text{(A-100)}$$

In Equation (A-100):

$$\omega_\phi = \sqrt{\frac{\lambda_1 \bar{a} \left(\frac{W_c a^2}{\partial I_x}\right) \frac{g}{h}}{(1 - \frac{1}{2}\frac{G}{h} \sin \theta_j)\left[1 - (\lambda_1 + \frac{A_B P_o}{W_c}) \frac{\partial \bar{Q}_{fi}}{\partial P_i}\right] + \left(\frac{b}{a+b}\right) \frac{F_1}{K_{KA}}}} \qquad \text{(A-101)}$$

$$\zeta_\phi = \frac{\tau_2 \omega_\phi}{\partial K_{KA} \lambda_1 \bar{a}} \qquad \text{(A-102)}$$

$$\frac{\partial \bar{\phi}}{\partial \bar{Q}_{f_1}} = \frac{(1 - \frac{1}{2}\frac{G}{h} \sin \theta_j)(\lambda_1 + \frac{A_B P_o}{W_c})}{4\lambda_1 \bar{a}} \qquad \text{(A-103)}$$

THE GARRETT CORPORATION
AiResearch Manufacturing Division
Phoenix, Arizona

APPENDIX B

FORMULATION OF GEM-SIX DEGREE FREEDOM-BODY MOTION EQUATIONS

APPENDIX B

FORMULATION OF GEM SIX DEGREE FREEDOM BODY MOTIONS

1.0 GENERAL EQUATIONS OF VEHICLE MOTION WITH SIX DEGREES OF FREEDOM

1.1 Velocity

Consider a body with mass (m), body fixed axes xyz, inertial system XYZ and rotating with angular velocity $\bar{\omega}$. Thomson (Ref. 2) shows that the absolute velocity of any point on the body is:

$$\bar{V}_i = \bar{V}_o + \bar{V}_{REL} + \bar{\omega} \times \bar{r}_i \qquad \text{(B-1)}$$

where

$\bar{V}_o$ = velocity of origin of xyz relative to XYZ

$\bar{V}_{REL}$ = velocity of point relative to xyz

$\bar{\omega} \times \bar{r}$ = velocity of point due to the rotation of body

Since xyz is a body-fixed axes, it is apparent that there can be no velocity of the body relative to xyz. Therefore, Equation (B-1) becomes:

$$\bar{V}_i = \bar{V}_o + \bar{\omega} \times \bar{r}_i \qquad \text{(B-2)}$$

1.2 Momentum

Since linear momentum is the product of the mass of the body and its instantaneous velocity and angular momentum is defined as the moment of the linear momentum, it can be shown that the angular momentum of the body is given by:

$$\bar{h}_o = \sum_i \bar{r}_i \times m_i \bar{V}_i$$

$$= \sum_i \bar{r}_i \times m_i (\bar{V}_o + \bar{\omega} \times \bar{r}_i)$$

$$= \sum_i \bar{r}_i \times m_i (\bar{\omega} \times \bar{r}_i) - \bar{V}_o \times \sum_i m_i \bar{r}_i \qquad \text{(B-3)}$$

Integrating over the body and noting that if the origin of xyz coincides with the center of mass

$$\sum_i \bar{r}_i m_i = 0 \qquad \text{(B-4)}$$

Therefore, the angular momentum written as components in xyz become:

$$\bar{h}_o = h_x \bar{I} + h_y \bar{J} + h_z \bar{K} \qquad \text{(B-5)}$$

Defining the moments of inertia about the xyz axes as:

$$\left.\begin{aligned} I_x &= \int (y^2 + z^2)\, dm \\ I_y &= \int (x^2 + z^2)\, dm \\ I_z &= \int (x^2 + y^2)\, dm \end{aligned}\right\} \qquad \text{(B-6)}$$

and the products of inertia as:

$$\left.\begin{aligned} I_{xy} &= \int xy\, dm \\ I_{xz} &= \int xz\, dm \\ I_{yz} &= \int yz\, dm \end{aligned}\right\} \qquad \text{(B-7)}$$

It can be shown that the angular momentum components about xyz become:

$$\left.\begin{aligned} h_x &= I_x\omega_x - I_{xy}\omega_y - I_{xz}\omega_z \\ h_y &= I_y\omega_y - I_{xy}\omega_x - I_{yz}\omega_z \\ h_z &= I_z\omega_z - I_{xz}\omega_z - I_{yz}\omega_y \end{aligned}\right\} \qquad \text{(B-8)}$$

Assuming that the xyz axes are the principal axes (those axes about which the products of inertia go to zero) the angular momentum becomes:

$$\bar{h}_o = I_x\omega_x\bar{I} + I_y\omega_y\bar{J} + I_z\omega_z\bar{k} \qquad \text{(B-9)}$$

1.3 Moments

Thomson shows that the moment about the mass center of a body is equal to the time derivative of the moment of momentum about this point.

$$\bar{M}_o = \dot{\bar{h}}_o + \bar{\omega} \times \bar{h}_o$$

$$= (\dot{h}_x\bar{I} + \dot{h}_y\bar{J} + h_z\bar{k}) + \bar{\omega} \times \bar{h}_o \qquad \text{(B-10)}$$

The cross product $\bar{\omega} \times \bar{h}_o$ is shown to be the rotation of vectors $h_x\bar{I}$, $h_y\bar{J}$, and $h_z\bar{k}$ due to ω_x, ω_y and ω_z

or

$$\bar{\omega} \times \bar{H}_o = (\omega_y h_z - \omega_z h_y)\bar{I} + (\omega_z h_x - \omega_x h_z)\bar{J} + (\omega_x h_y - \omega_y h_x)\bar{K} \quad \text{(B-11)}$$

Equation (B-10) then becomes:

$$\bar{M}_o = M_x\bar{I} + M_y\bar{J} + M_z\bar{K} \quad \text{(B-12)}$$

where

$$\left.\begin{aligned} M_x &= \dot{h}_x + \omega_y h_z - \omega_z h_y \\ M_y &= \dot{h}_y + \omega_z h_x - \omega_x h_z \\ M_z &= \dot{h}_z + \omega_x h_y - \omega_y h_x \end{aligned}\right\} \quad \text{(B-13)}$$

Equation (B-8) substituted into Equation (B-13) neglecting the products of inertia yields:

$$\left.\begin{aligned} M_x &= I_x\dot{\omega}_x + I_z\omega_z\omega_y - I_y\omega_y\omega_z \\ M_y &= I_y\dot{\omega}_y + I_x\omega_x\omega_z - I_z\omega_z\omega_x \\ M_z &= I_z\dot{\omega}_z + I_y\omega_y\omega_x - I_x\omega_x\omega_y \end{aligned}\right\} \quad \text{(B-14)}$$

1.4 Forces

Thomson also denotes the force acting on the mass as:

$$\bar{F} = F_x\bar{I} + F_y\bar{J} + F_z\bar{K} \qquad \text{(B-15)}$$

With the xyz axes system being body fixed and rotating with the mass, the force components in the x, y and z directions may be determined from:

$$\bar{F} = m\frac{d\bar{v}}{dt} + \bar{\omega} \times m\bar{v} \qquad \text{(B-16)}$$

These components are seen to be:

$$\left.\begin{aligned} F_x &= m(\dot{v}_x + v_z\omega_y - v_y\omega_z) \\ F_y &= m(\dot{v}_y + v_x\omega_z - v_z\omega_x) \\ F_z &= m(\dot{v}_z + v_y\omega_x - v_x\omega_y) \end{aligned}\right\} \qquad \text{(B-17)}$$

1.5 Recapitulation of Motion Equations

The general equations of motion, written in GEM terminology become:

$$\left.\begin{aligned} F_x &= \frac{W_c}{g}\left[\ddot{x} + \dot{\theta}\dot{z} - \dot{\psi}\dot{y}\right] \\ F_y &= \frac{W_c}{g}\left[\ddot{y} + \dot{\psi}\dot{x} - \dot{\phi}\dot{z}\right] \\ F_z &= \frac{W_c}{g}\left[\ddot{z} + \dot{\phi}\dot{y} - \dot{\theta}\dot{x}\right] \end{aligned}\right\} \qquad \text{(B-18)}$$

and

$$\left.\begin{aligned} M_x &= I_x\ddot{\phi} + (I_z - I_y)\,\dot{\psi}\dot{\theta} \\ M_y &= I_y\ddot{\theta} + (I_x - I_z)\,\dot{\phi}\dot{\psi} \\ M_z &= I_z\ddot{\psi} + (I_y - I_x)\,\dot{\theta}\dot{\phi} \end{aligned}\right\} \qquad \text{(B-19)}$$

The forces and moments comprising the left sides of Equations (B-18) and (B-19) will be shown to include such quantities as propulsive forces, aerodynamic forces, ground effect forces and the moments resulting from these forces.

Let the left sides of Equations (B-18) and (B-19) be expressed as:

$$F_x = \Sigma F_x, \qquad M_x = \Sigma M_x$$
$$F_y = \Sigma F_y, \qquad M_y = \Sigma M_y$$
$$F_z = \Sigma F_z, \qquad M_z = \Sigma M_z$$

2.0 PARTICULAR "SIX-DEGREE FREEDOM" EQUATIONS

The terms comprising the six equations will be given as "full range" parameters, i.e., they will not be perturbated about a steady-state point, as were the equations for pitch, roll and heave in Appendix A. The terms will also be normalized in such a manner as to give dimensionless equations.

2.1 Forward Velocity

Propeller Thrust

$$f_x = (T_p + T_s)$$

let

$$T = \frac{T}{W_c}$$

and thrust term becomes

$$f_x = W_c (T_p + T_s) \qquad \text{(B-20)}$$

Parasite Drag

At this point it will be well to define "relative wind" as the combination of vehicle velocity and wind.

Let the vehicle have a heading ψ relative to XYZ inertial system and let there be a wind at an angle β with the inertial system. The relative wind can then be expressed by:

$$U_{xr} = U_x + V_w \cos(\beta - \psi)$$

and

$$U_{yr} = U_y + V_w \sin(\beta - \psi)$$

Expanding the sine and cosine terms and letting

$$\bar{U}_x = \frac{U_x}{b}$$

$$\bar{U}_y = \frac{U_y}{a}$$

$$\bar{V}_w = \frac{V_w}{b}$$

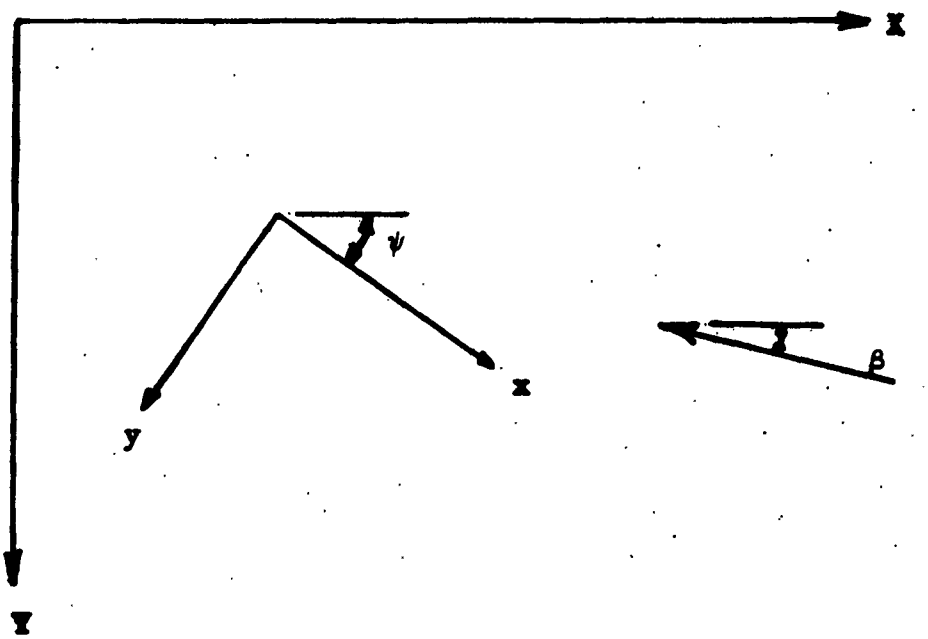

FIGURE B-1

$$U_{xr} = b\left[\bar{U}_x + \bar{V}_w\,(\cos\beta\cos\psi + \sin\beta\sin\psi)\right] \qquad \text{(B-21)}$$

$$U_{yr} = a\left[\bar{U}_y + \frac{b}{a}\,\bar{V}_w\,(\sin\beta\cos\psi - \cos\beta\sin\psi)\right] \qquad \text{(B-22)}$$

The relative wind will be used primarily as a drag force and will therefore appear in the equation as U^2_{xr} and U^2_{yr}. As the square destroys the sign of the terms, they will henceforth be written as follows:

$$U^2_{xr} = b^2\left|\bar{U}_x + \bar{V}_w(\cos\beta\cos\psi + \sin\beta\sin\psi)\right|\left[\bar{U}_x + \bar{V}_w(\cos\beta\cos\psi + \sin\beta\sin\psi)\right] \qquad \text{(B-23)}$$

$$U^2_{yr} = a^2\left|\bar{U}_y + \frac{b}{a}\,\bar{V}_w(\sin\beta\cos\psi - \cos\beta\sin\psi)\right|\left[\bar{U}_y + \frac{b}{a}\,\bar{V}_w(\sin\beta\cos\psi - \cos\beta\sin\psi)\right] \qquad \text{(B-24)}$$

The parasite drag can then be defined as:

$$f_x = -c_D q A_B$$

drag coefficient (c_D) here is related to base area rather than frontal area.

$$q = \frac{1}{2}\rho\,U^2_{xr}$$

and U^2_{xr} from Equation (B-23) yields:

$$f_x = -\frac{C_D \rho A_B b^2}{2} \left| \overline{U}_x + \overline{V}_w(\cos\beta\cos\psi + \sin\beta\sin\psi) \right| \left[\overline{U}_x + \overline{V}_w(\cos\beta\cos\psi + \sin\beta\sin\psi) \right] \quad \text{(B-25)}$$

Positive Pitch Angle

$$f_x = -P_B A_B \sin\theta$$

It is noted that in the steady-state, $P_B A_B$ is very nearly equal to the vehicle weight (W_c). It is therefore assumed that the force due to a positive pitch angle (nose up):

$$f_x = -W_c \theta$$

Since θ is small, $\sin\theta = \theta$ (radians)

Let $\overline{\theta} = \frac{b}{2h}\theta$

The force due to positive pitch angle becomes:

$$f_x = -\frac{2hW_c}{b}\overline{\theta} \quad \text{(B-26)}$$

Momentum Drag

$$f_x = -Q_f U_x \rho$$

where

Q_f = total volume flow to fans

and

$$U_x = b\left[\bar{U}_x + \bar{V}_w\,(\cos\beta\cos\psi + \sin\beta\sin\psi)\right]$$

$$f_x = -Q_f\rho b\left[\bar{U}_x + \bar{V}_w\,(\cos\beta\cos\psi + \sin\beta\sin\psi)\right] \qquad \text{(B-27)}$$

The summation of forces in the x direction equated to the x component of Equation (B-18) yields:

$$\frac{W_c}{g}\left[\ddot{x} + \ddot{\theta z} - \ddot{\psi y}\right] = W_c\,(T_p + T_s)$$

$$- \frac{C_D\rho A_B b^2}{2}\left|\bar{U}_x + \bar{V}_w(\cos\beta\cos\psi + \sin\beta\sin\psi)\right|\left[\bar{U}_x + \bar{V}_w(\cos\beta\cos\psi + \sin\beta\sin\psi)\right]$$

$$- \frac{2hW_c}{b}\,\bar{\theta} - Q_f\rho b\left[\bar{U}_x + \bar{V}_w\,(\cos\beta\cos\psi + \sin\beta\sin\psi)\right]$$

Let $\ddot{x} = \dfrac{d\bar{U}_x}{dt}$, $\dot{y} = \bar{U}_y$

where

$$\bar{U}_x = \frac{U_x}{b}, \qquad \bar{U}_y = \frac{U_y}{a}$$

and neglect $\ddot{\theta z}$ because of relative magnitude,

$$\frac{d\bar{U}_x}{dt} = \frac{g}{b}(T_p + T_s) + \frac{a}{b}\dot{\psi}\bar{U}_y$$

$$- \frac{c_D \rho g A_B b}{2W_c} \left|\bar{U}_x + \bar{V}_w(\cos\beta\cos\psi + \sin\beta\sin\psi)\right|\left[\bar{U}_x + \bar{V}_w(\cos\beta\cos\psi + \sin\beta\sin\psi)\right]$$

$$- \frac{2hg}{b^2}\bar{\theta} - \frac{Q_f \rho g}{W_c}\left[\bar{U}_x + \bar{V}_w(\cos\beta\cos\psi + \sin\beta\sin\psi)\right] \qquad \text{(B-28)}$$

2.2 Side Velocity

Parasite Drag

The relative wind is given in Equation (B-24) as

$$U^2_{yr} = a^2\left[\bar{U}_y + \frac{b}{a}\bar{V}_w(\sin\beta\cos\psi - \cos\beta\sin\psi)\right]\left[\bar{U}_y + \frac{b}{a}\bar{V}_w(\sin\beta\cos\psi - \cos\beta\sin\psi)\right]$$

The parasite drag then becomes:

$$f_y = -\frac{c_D \rho A_B b}{2a} U_{yr}$$

$$= -\frac{c_D \rho A_B ab}{2}\left|\bar{U}_y + \frac{b}{a}\bar{V}_w(\sin\beta\cos\psi - \cos\beta\sin\psi)\right|\left[\bar{U}_y + \frac{b}{a}\bar{V}_w(\sin\beta\cos\psi - \cos\beta\sin\psi)\right] \qquad \text{(B-29)}$$

It is noted that this term contains the same drag coefficient as the equivalent term in the forward velocity equation. It is therefore modified by the ratio of planform length to width (b/a).

Positive Roll

$$f_y = P_B A_B \sin\phi = W_c \phi = \frac{2hW_c}{a} \bar{\phi} \qquad \text{(B-30)}$$

where

$$\bar{\phi} = \frac{a}{2h} \phi$$

Momentum Drag

$$f_y = - Q_f \rho U_y = - Q_f \rho a \left[\bar{U}_y + \frac{b}{a} \bar{V}_w \left(\sin\beta\cos\psi - \cos\beta\sin\psi \right) \right] \qquad \text{(B-31)}$$

The summation of forces in the y direction equated to the y component of Equation (B-18) yields:

$$\frac{W_c}{g}\left[\ddot{y} + \dot{\psi}\dot{x} - \dot{\phi}\dot{z} \right] = - Q_f \rho a \left[\bar{U}_y + \frac{b}{a} \bar{V}_w \left(\sin\beta\cos\psi - \cos\beta\sin\psi \right) \right]$$

$$+ \frac{2hW_c}{a} \bar{\phi} - \frac{C_D \rho A_B ab}{2} \left| \bar{U}_y + \frac{b}{a} \bar{V}_w (\sin\beta\cos\psi - \cos\beta\sin\psi) \right| \left[\bar{U}_y + \frac{b}{a} \bar{V}_w (\sin\beta\cos\psi - \cos\beta\sin\psi) \right]$$

Let $\ddot{y} = \frac{d\bar{U}_y}{dt}$, $\dot{x} = \bar{U}_x$

where

$$\bar{U}_y = \frac{U_y}{a}, \qquad \bar{U}_x = \frac{U_x}{b}$$

and neglect $\ddot{\phi}z$ because of relative magnitude,

$$\frac{d\bar{U}_y}{dt} = -\frac{Q_f \rho g}{W_c}\left[\bar{U}_y + \frac{b}{a}\bar{V}_w(\sin\beta\cos\psi - \cos\beta\sin\psi)\right] + \frac{2hg}{a^2}\bar{\phi}$$

$$-\frac{c_D \rho g A_B b}{2W_c}\left|\bar{U}_y + \frac{b}{a}\bar{V}_w(\sin\beta\cos\psi - \cos\beta\sin\psi)\right|\left[\bar{U}_y + \frac{b}{a}\bar{V}_w(\sin\beta\cos\psi - \cos\beta\sin\psi)\right] - \frac{b}{a}\dot{\psi}\bar{U}_x \qquad \text{(B-32)}$$

2.3 Yaw

The yaw component of Equation (B-19) is:

$$M_z = I_z \ddot{\psi} + (I_y - I_x)\dot{\theta}\dot{\phi}$$

The external moments that constitute the left side of the above equation will include the differential thrust on the propellers and aerodynamic forces due to side velocity (relative wind).

Differential Thrust

Let a_p be the moment arm of the propellers and the moment about z due to propeller thrust becomes:

$$m_z = W_c a_p (T_p - T_s) \qquad \text{(B-33)}$$

It is reasonable to assume that any properly designed vehicle will have a certain amount of yaw stability. This will arise from aerodynamic forces due to a side velocity (side-slip) which produces a moment opposite to the angle of yaw. It is quite obvious that this "weather vane" effect must be built in the vehicle, lest the operator be continually "riding" the yaw control.

If this force is defined as a drag force due to a side velocity it is seen that:

$$m_z = c_D \left(\frac{1}{2} \rho U^2_{yr}\right) A_B \frac{b}{a} b_w \qquad \text{(B-34)}$$

where

b_w = "moment arm" of relative wind (aft of vehicle c.g.)

and

U_{yr} = relative wind given in Equation (B-22)

These external moments equated to Equation (B-19) yield:

$$\frac{d^2\psi}{dt^2} = \frac{a_p g W_c}{I_z} (T_p - T_s)$$

$$+ \frac{c_D \rho g A_B b b_w a}{2 I_z} \left| \bar{U}_y + \frac{b}{a} \bar{V}_w (\sin\beta\cos\psi - \cos\beta\sin\psi) \right| \left[\bar{U}_y + \frac{b}{a} \bar{V}_w (\sin\beta\cos\psi - \cos\beta\sin\psi) \right] \quad \text{(B-35)}$$

2.4 Pitch

Equation (A-96) of Appendix A gives the normalized, linearized equation for pitching motion due to variations in fan flow and wave disturbance. Neglecting, for the present, the wave disturbances, the equation is:

$$\left[s^2 + 2\zeta_\theta \omega_\theta s + \omega_\theta^2 \right] \bar{\theta} = -\omega^2{}_\theta \frac{\partial \bar{\theta}}{\partial \bar{\theta}_{fi}} (\bar{q}_{f_1} - \bar{q}_{f_2} - \bar{q}_{f_3} + \bar{q}_{f_4})$$

From which

$$\frac{d^2\bar{\theta}}{dt^2} = -2\zeta_\theta \omega_\theta \frac{d\bar{\theta}}{dt} - \omega^2{}_\theta \bar{\theta}$$

$$- \omega^2{}_\theta \frac{\partial \bar{\theta}}{\partial \bar{\theta}_{fi}} (\bar{q}_{f_1} - \bar{q}_{f_2} - \bar{q}_{f_3} + \bar{q}_{f_4}) \quad \text{(B-36)}$$

The external moments indicated by M_y in Equation (B-19) and which will apply also to the above equation will be shown to include moments arising from aerodynamic forces, propulsive forces and surface displacements.

Up to this point in the formulation it has been assumed that the surface over which the vehicle was "flying" was rigid, that is, there has been no allowance for the surface to deflect due to a change in surface pressure as will occur when a vehicle "flies" over water. This characteristic, which will be analytically described in detail in Appendix C, is a necessary parameter in a complete formulation.

It is shown in Appendix C, Equation (C-52) that the mean slope of the water surface as a function of forward velocity is:

$$\theta_w = \frac{12}{b} \frac{\sin \alpha}{\alpha} \left(\frac{\sin \alpha}{\alpha} - \cos \alpha\right)$$

where

$$\alpha = \frac{bg}{2U_x^2}$$

It can be seen that as a vehicle "flies" over the water surface at some forward velocity (U_x) it will tend to follow the shape of the surface deflection, that is, as forward speed

increases, the vehicle will tend to nose up due to the formation of an uphill slope beneath it. It will continue to pitch up until the "hump" speed* is reached at which time the vehicle will return to a near horizontal altitude.

As this water slope (θ_w) can be thought of as a disturbance, it can be included in Equation (B-35). Normalized to Equation (B-36) the disturbance becomes:

$$\frac{\omega^2_\theta W_c b}{2\rho_w A_B h} \left[\frac{12}{b} \frac{\sin\alpha}{\alpha} \left(\frac{\sin\alpha}{\alpha} - \cos\alpha\right)\right] \qquad \text{(B-37)}$$

In addition to the above description of water surface behavior, it will be well at this point to include the term which describes the transient behavior of the surface due to pitching motions. This term, as fully described in Appendix C, is seen to modify the ω^2_θ term of Equation (B-36) by

$$(1 - \bar{K}_\theta)\ \omega^2_\theta$$

*"Hump speed" is defined as the speed at which the slope of the water is a maximum.

where

$$\bar{K}_\theta = \frac{\omega^2_\theta \frac{16\, I_y}{\rho_w A_B b^2 g} \left(1 + \epsilon - \frac{2 \sin\alpha}{\alpha} \cos\alpha\right)}{1 + \omega^2_\theta \frac{16\, I_y}{\rho_w A_B b^2 g}} \qquad \text{(B-38)}$$

Pitching Moment due to Propeller Thrust

$$M_\theta = -Z_p (T_p + T_s)$$

Z_p = moment arm of propellers

Normalized to Equation (B-36) the above term becomes:

$$M_\theta = -\frac{Z_p W_c b g}{2h I_y} (\bar{T}_p + \bar{T}_s) \qquad \text{(B-39)}$$

Pitching Moment due to Aerodynamic Lift

If the aerodynamic lift does not act through the vehicle c.g. and it can be shown that it does not, there will occur a pitching moment due to forward velocity.

Defining the aerodynamic lift as

$$f_Z = c_L \left(\tfrac{1}{2} \rho U^2\right) A_B$$

For the pitch mode, only the forward velocity will be considered.

With the relative wind from Equation (B-23) and normalizing to Equation (B-36), the aerodynamic pitching moment becomes:

$$M_\theta = \frac{c_L \rho g A_B b^3 x_a}{4h\, I_y} \left|\bar{U}_x + \bar{V}_w(\cos\beta\cos\psi + \sin\beta\sin\psi)\right|\left[\bar{U}_x + \bar{V}_w(\cos\beta\cos\psi + \sin\beta\sin\psi)\right] \quad \text{(B-40)}$$

Appendix C shows the variation of base pressure due to forward and side velocity. This term which produces an increase in base pressure in the forward compartments and a decrease in pressure in the aft compartments, produces a nose up ($+\theta$) moment.

The variation in base pressure depends upon the relative wind as do the aerodynamic forces. Normalizing to Equation (B-36) this moment becomes:

$$M_\theta = -\frac{\rho g A_B b^4\ (.29a)}{4h I_y 4(a+b+2aF_1)} \left|\bar{U}_x + \bar{V}_w(\cos\beta\cos\psi + \sin\beta\sin\psi)\right|\left[\bar{U}_x + \bar{V}_w(\cos\beta\cos\psi + \sin\beta\sin\psi)\right] \quad \text{(B-41)}$$

The summation of the above outlined pitching moments when substituted into Equation (B-36) yields:

$$\frac{d^2\bar{\theta}}{dt^2} = -2\zeta_\theta \omega_\theta \frac{d\bar{\theta}}{dt} - (1 - \bar{K}_\theta)\ \omega^2{}_\theta\ \bar{\theta}$$

$$- \omega^2{}_\theta \frac{\partial\bar{\theta}}{\partial\bar{Q}_{f_1}} (\bar{q}_{f_1} - \bar{q}_{f_2} - \bar{q}_{f_3} + \bar{q}_{f_4})$$

$$+ \omega^2{}_\theta \frac{6W_c}{\rho_w A_B h} \frac{\sin\alpha}{\alpha} \left(\frac{\sin\alpha}{\alpha} - \cos\alpha\right) - \frac{Z_p g b W_c}{4hI_y} (T_p + T_s)$$

$$+ \frac{\rho g A_B b^4}{4hI_y} \left(\frac{c_L x_a}{b} + \frac{0.29a}{4(a+b+2aF_1)}\right) \left|\bar{U}_x + \bar{V}_w(\cos\beta\cos\psi + \sin\beta\sin\psi)\right| \left[\bar{U}_x + \bar{V}_w(\cos\beta\cos\psi + \sin\beta\sin\psi)\right] \quad \text{(B-42)}$$

2.5 Roll

Equation (A-100) of Appendix A shows the normalized, linearized equation for rolling motions as a function of fan flow variations. Rewriting this equation:

$$\frac{d^2\bar{\phi}}{dt^2} = -2\zeta_\phi \omega_\phi \frac{d\bar{\phi}}{dt} - \omega^2{}_\phi\ \bar{\phi}$$

$$+ \omega^2{}_\phi \frac{\partial\bar{\phi}}{\partial\bar{Q}_{f_1}} (\bar{q}_{f_1} + \bar{q}_{f_2} - \bar{q}_{f_3} - \bar{q}_{f_4}) \quad \text{(B-43)}$$

The external rolling moments indicated in Equation (B-19) are assumed to arise only from aerodynamic forces.

The change in water surface slope is neglected because it is not anticipated the vehicle will travel at high speeds in the side direction. It is further assumed that "side slipping" at high forward speeds will occur above the hump speed. The transient behavior of the surface due to rolling motions will be included however.

As there might exist crosswinds of appreciable magnitude the aerodynamic moment due to relative wind will be included as well as the moments due to an increase in base pressure at forward velocity.

As in pitch the term which describes the transient behavior can be shown to modify the ω^2_ϕ term of Equation (B-43) by:

$$(1 - \bar{K}_\phi)\, \omega^2_\phi \quad \bar{\phi}$$

where

$$\bar{K}_\phi = \frac{\omega^2_\phi \quad \frac{16\, I_x}{\rho_w A_B a^2 g} \quad \left(1 + \epsilon - \frac{2 \sin \alpha}{\alpha} \cos \alpha\right)}{1 + \omega^2_\phi \quad \frac{16\, I_y}{\rho_w A_B a^2 g}} \qquad \text{(B-44)}$$

This term is more fully described in Appendix C.

With the relative wind from Equation (B-24) and normalizing to Equation (B-43), the aerodynamic rolling moment becomes:

$$M_\phi = - \frac{c_L \rho g A_B a^2 b y_a}{4h\, I_x} \left| \bar{U}_y + \frac{b}{a} \bar{V}_w (\sin\beta\cos\psi - \cos\beta\sin\psi) \right| \left[\bar{U}_y + \frac{b}{a} \bar{V}_w (\sin\beta\cos\psi - \cos\beta\sin\psi) \right] \tag{B-45}$$

As shown in Appendix C the variation of base pressure due to velocity produces a rolling moment as:

$$M_\phi = \frac{- \rho g A_B a^3 b (0.365a)}{4h I_x 4(a+b+2b\bar{F}_1)} \left| \bar{U}_y + \frac{b}{a} \bar{V}_w (\sin\beta\cos\psi - \cos\beta\sin\psi) \right| \left[\bar{U}_y + \frac{b}{a} \bar{V}_w (\sin\beta\cos\psi - \cos\beta\sin\psi) \right] \tag{B-46}$$

Equation (B-43) then becomes:

$$\frac{d^2\bar{\phi}}{dt^2} = - 2\zeta_\phi \omega_\phi \frac{d\bar{\phi}}{dt} - (1 - \bar{K}_\phi) \omega_\phi \bar{\phi} + \omega^2_\phi \frac{\partial \bar{\phi}}{\partial \bar{q}_{fi}} (\bar{q}_{f_1} + \bar{q}_{f_2} - \bar{q}_{f_3} - \bar{q}_{f_4})$$

$$- \frac{\rho g A_B a^3 b}{4h\, I_x} \left(\frac{c_L y_a}{a} + \frac{0.365a}{4(a+b+2b\bar{F}_1)} \right) \left| \bar{U}_y + \frac{b}{a} \bar{V}_w (\sin\beta\cos\psi - \cos\beta\sin\psi) \right| \left[\bar{U}_y + \frac{b}{a} \bar{V}_w (\sin\beta\cos\psi - \cos\beta\sin\psi) \right] \tag{B-47}$$

It is noted that the products $\dot{\psi}\dot{\theta}$ and $\dot{\psi}\dot{\phi}$ were neglected because of their relative magnitude in the pitch and roll equations.

2.6 Heave

The normalized, linearized equation of motion in the heave mode from Equation (A-92) (neglecting wave disturbance) is:

$$\frac{d^2\bar{Z}}{dt^2} = -2\zeta_z \omega_z \frac{d\bar{Z}}{dt} - \omega^2_z \bar{Z} - \omega^2_z \frac{\partial Z}{\partial \bar{q}_{fi}} (\bar{q}_{f_1} + \bar{q}_{f_2} + \bar{q}_{f_3} + \bar{q}_{f_4})$$

As shown in Appendix C, the frequency term in the above equation will be modified by a term that shows the transient behavior of the water surface due to heaving motions.

The $\omega^2_z \bar{Z}$ term becomes $(1 - K_z)\, \omega^2_z \bar{Z}$

where

$$K_z = \frac{\omega^2_z \frac{W_c}{\rho g A_B} \left(1 + \epsilon - \frac{2 \sin \alpha}{\alpha} \cos \alpha\right)}{1 + \omega^2_z \frac{W_c}{\rho g A_B}} \qquad \text{(B-48)}$$

As stated previously, the lift due to the trapped pressure is augmented by an aerodynamic lift arising with velocity. It is assumed that the lift due to side velocity is small and may be neglected. Hence, only the forward velocity will be considered. It is further assumed that the variation of base pressure due to forward velocity is nearly balanced fore and aft and may be neglected.

The aerodynamic lift term is:

$$F_z = - \frac{c_L \rho A_B g}{2 W_c h} U^2_{xr}$$

or with U_{xr} from Equation (B-23)

$$F_z = - \frac{c_L \rho A_B g b^2}{2 W_c h} \left| \bar{U}_x + \bar{V}_w \left(\cos\beta\cos\psi + \sin\beta\sin\psi\right) \right| \left[\bar{U}_x + \bar{V}_w \left(\cos\beta\cos\psi + \sin\beta\sin\psi\right) \right] \quad \text{(B-49)}$$

The equation for heave motion then becomes:
(with additional terms from Equation (B-18))

$$\frac{d^2\bar{Z}}{dt^2} = -2\zeta_z \omega_z \frac{d\bar{Z}}{dt} - (1 - K_z)\omega^2_z \bar{Z} - 2(\dot{\theta}\bar{U}_x - \dot{\phi}\bar{U}_y)$$

$$- \omega^2_z \frac{\partial \bar{Z}}{\partial \bar{Q}_{fi}} (\bar{q}_{f_1} + \bar{q}_{f_2} + \bar{q}_{f_3} + \bar{q}_{f_4})$$

$$\frac{c_L \rho A_B g b^2}{2 W_c h} \left| \bar{U}_x + \bar{V}_w(\cos\beta\cos\psi + \sin\beta\sin\psi) \right| \left[\bar{U}_x + \bar{V}_w(\cos\beta\cos\psi + \sin\beta\sin\psi) \right] \qquad (B\text{-}50)$$

THE GARRETT CORPORATION
AiResearch Manufacturing Division
Phoenix, Arizona

APPENDIX C

SURFACE DEFLECTIONS AND BASE PRESSURE VARIATIONS DUE TO FORWARD VELOCITY

SURFACE DEFLECTIONS AND BASE PRESSURE VARIATIONS DUE TO FORWARD VELOCITY

1.0 Surface Deflections

To more fully describe the behavior of a vehicle hovering and maneuvering over water it was necessary to investigate the behavior of the water surface when subjected to a uniform pressure over the surface. The following then, presents a two dimensional problem solution of standing waves in a stream of infinite depth due to a uniform pressure distribution over a finite length of the surface.

The general solution of the problem is given by J. J. Stoker* in his book Water Waves in the form of an integral of an analytic function.

List of Symbols (used in this appendix only)

x	-	horizontal space coordinate
y	-	vertical space coordinate
t	-	time
$\eta(x,t)$	-	surface displacement (from y = 0)
U	-	free stream velocity
Po	-	pressure on the surface

*Reference 3

List of Symbols (Cont'd)

ρ - water density

g - gravity

ϕ - velocity potential

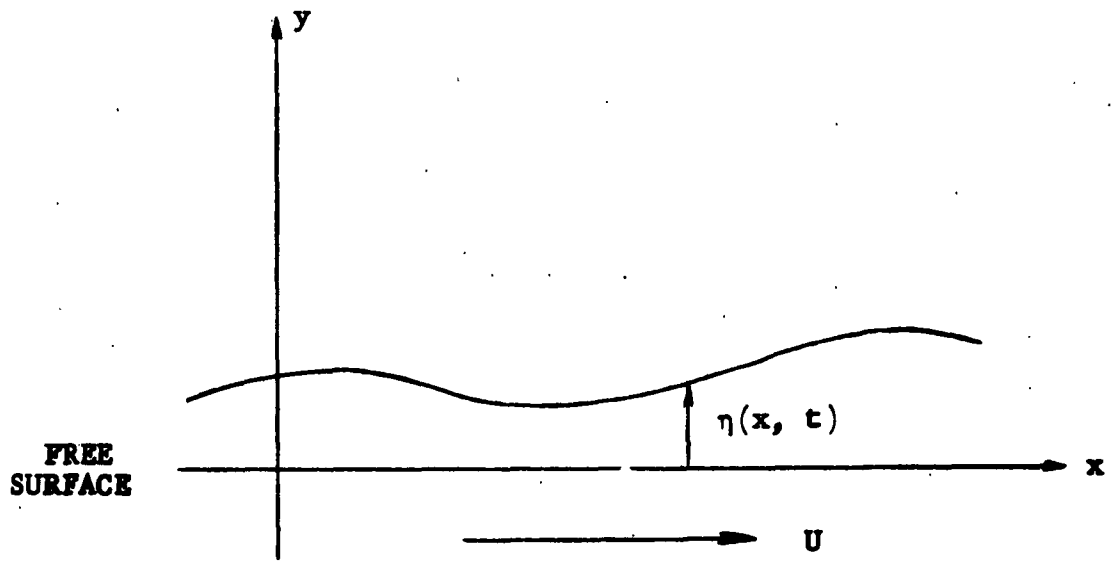

FIGURE C-1, POSITIVE SENSE OF COORDINATES

In brief, the problem is formulated as follows: (See Chapter 7 of Reference 3).

The velocity potential must satisfy the LaPlace Equation.

$$\nabla^2\phi = \phi_{xx} + \phi_{yy} = 0 \qquad \text{(C-1)}$$

For the general case where η is a function of time, the surface conditions are given by:

$$\left.\begin{aligned} \frac{p}{\rho} + g\eta + \phi_t + U\phi_x + \frac{1}{2}U^2 &= 0 \\ \eta_t + U\eta_x - \phi_y &= 0 \end{aligned}\right\} \text{ at } y = 0 \qquad \text{(C-2)}$$

Note that the letter subscripts denote partial differentiation.

For deep water, ϕ and its derivatives must be bounded at $y = -\infty$. Also, to obtain a unique solution, Stoker uses the condition that upstream waves die out (at $x = -\infty$).

Assuming a steady wave form, i.e., independent of time, and introducing the analytic function f(Z) of the complex variable x + iy whose real part is ϕ, Stoker finds the solution

$$f(Z) = -\frac{p_o i}{U\rho\pi} e^{-\frac{ig}{U^2}Z} \int_{+i\infty}^{Z} e^{\frac{ig}{U^2}t} \log\frac{t-a}{t+a}\,dt \qquad \text{(C-3)}$$

where

$$f(Z) = \phi(x, y) + i\,\psi(x, y) \qquad \text{(C-4)}$$

The value of ϕ obtained from Equations (C-3) and (C-4) satisfies the boundary conditions mentioned as well as the condition that the surface pressure is p_o over the region from -a to +a.

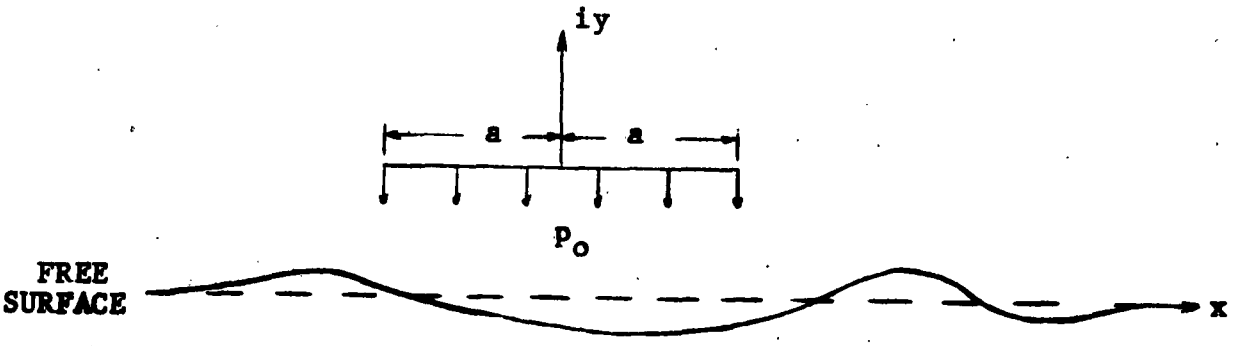

FIGURE C-2

Stoker states that Equation (C-3) must be integrated from $+ i\infty$ (positive imaginary axis) to any point (Z) in the lower half plane (negative y).* Interest here is the surface shape which will be obtained by evaluating η from the first of Equation (C-2). Noting that ϕ and η are independent of time we obtain

$$\eta = -\frac{p_o}{\rho g}\left(1 + \frac{\rho U^2}{2p_o} + \frac{\rho U \phi_x}{p_o}\right) \qquad \text{(C-5)}$$

*The path of integration must incircle the origin and the points (-a, o) and (+a, o) in a counterclockwise fashion.

Since the equation for η contains not ϕ but its derivative with respect to x, it will be convenient to differentiate f(Z) with respect to x.

Equation (C-4) then yields

$$f_x = \phi_x + i\,\psi_x \tag{C-6}$$

It is noted that partial differentiation of a function of Z with respect to x is the same as total differentiation with respect to Z because:

$$\frac{\partial Z}{\partial x} = \frac{\partial}{\partial x}(x + iy) = 1 \tag{C-7}$$

Differentiation of Equation (C-3) yields:

$$f_x = \frac{df}{dZ} = -\frac{p_{oi}}{U\rho\pi}\left[-\frac{ig}{U^2}\, e^{-\frac{ig}{U^2}Z} \int_{i\infty}^{Z} e^{\frac{ig}{U^2}t} \log\frac{t-a}{t+a}\, dt + e^{-\frac{ig}{U^2}Z}\, e^{+\frac{ig}{U^2}Z} \log\frac{Z-a}{Z+a}\right] \tag{C-8}$$

$$f_x = -\frac{p_o g}{U^3 \rho \pi} e^{-\frac{ig}{U^2} Z} \int_{i\infty}^{Z} e^{\frac{ig}{U^2} t} \log \frac{t-a}{t+a} \, dt$$

$$- \frac{p_o i}{U \rho \pi} \log \frac{Z-a}{Z+a} \qquad \text{(C-9)}$$

Integrating the first term by parts gives:

$$+ \int_{i\infty}^{Z} e^{\frac{ig}{U^2} t} \log \frac{t-a}{t+a} \, dt = -i \frac{U^2}{g} e^{\frac{ig}{U^2} Z} \log \frac{Z-a}{Z+a}$$

$$+ i \frac{U^2}{g} \int_{i\infty}^{Z} e^{\frac{ig}{U^2} t} \left(\frac{1}{t-a} - \frac{1}{t+a} \right) dt$$

(C-10)

Substituting Equation (C-10) into (C-9) yields:

$$f_x = -\frac{p_o i}{U \rho \pi} e^{-\frac{ig}{U^2} Z} \int_{i\infty}^{Z} e^{\frac{ig}{U^2} t} \left(\frac{1}{t-a} - \frac{1}{t+a} \right) dt$$

$$+ \frac{p_o i}{U \rho \pi} \log \frac{Z-a}{Z+a} - \frac{p_o i}{U \rho \pi} \log \frac{Z-a}{Z+a} \qquad \text{(C-11)}$$

It is seen that the latter two terms will cancel. The term remaining to be integrated does not yield elementary functions but rather yields an infinite power series upon successive integration by parts. Therefore, to obtain numerical solutions, Equation (C-11) will be integrated numerically. Letting b denote a particular point on x, Figure C-3 shows the four regions of interest.

Also, define:

$$\alpha = \frac{ag}{U^2} \qquad \text{(C-12)}$$

$$\beta = \frac{b}{a} \qquad \text{(C-13)}$$

$$\eta = \frac{y}{a} \qquad \text{(C-14)}$$

$$\epsilon = \frac{x}{a} \qquad \text{(C-15)}$$

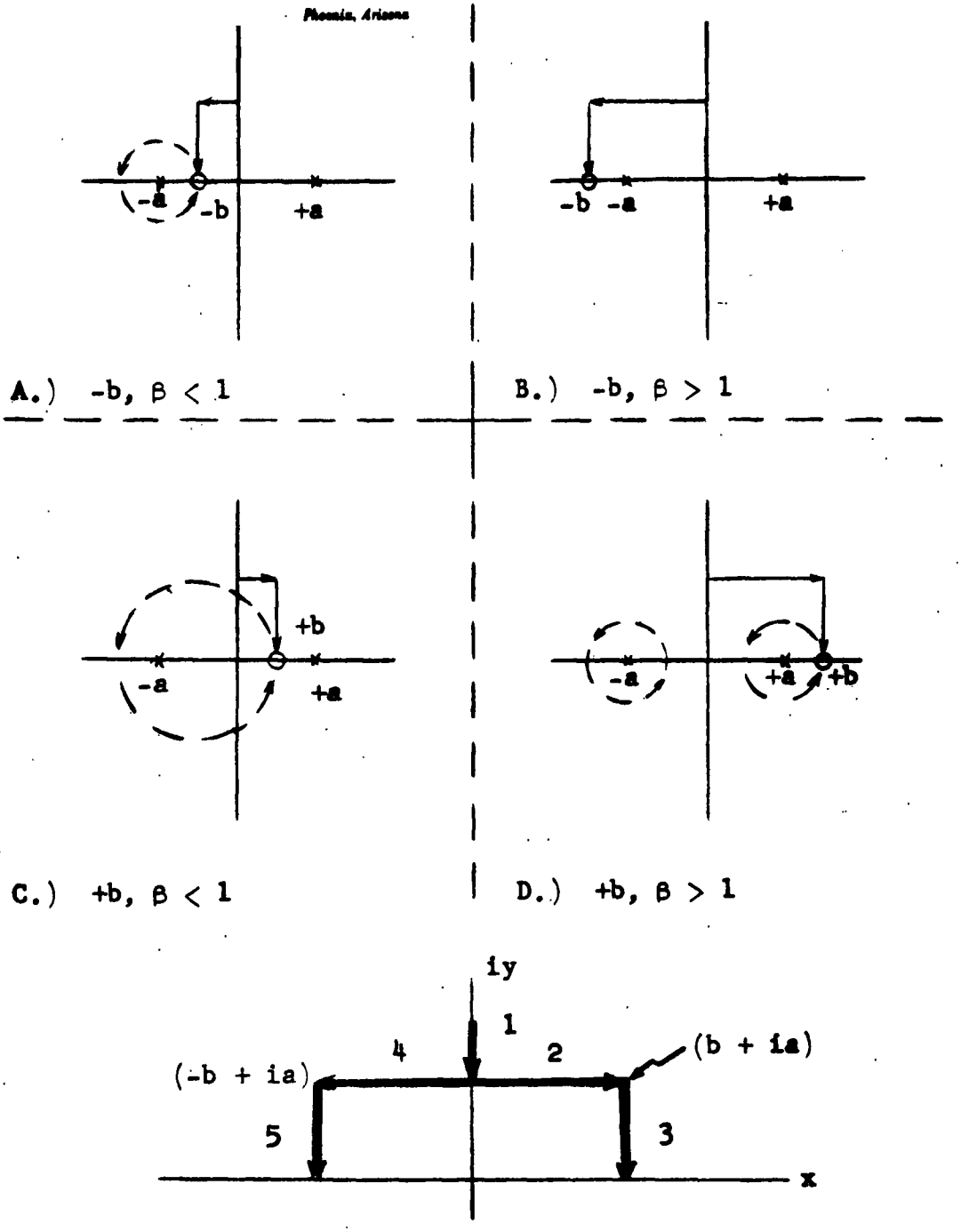

FIGURE C-3, FOUR REGIONS OF INTEREST AND INTEGRATION PATHS

Define five paths of integration:

(1) Let $t = iy$, $dt = idy$

$\infty \geq y \geq a$

(2) Let $t = x + ia$, $dt = dx$

$0 \leq x \leq b$

(3) Let $t = b + iy$, $dt = idy$

$a \geq y \geq 0$

(4) Let $t = x + ia$, $dt = dx$

$0 \geq x \geq -b$

(5) Let $t = -b + iy$, $dt = idy$

$a \geq y \geq 0$

Figure C-3 shows the possible paths of integration. Paths (1), (4) and (5) will determine ϕ_x for -b, $\beta > 1$. Paths (1), (2), (3), (4) and (5) will determine ϕ_x for -b, $\beta < 1$; +b, $\beta > 1$ and +b, $\beta < 1$ <u>provided</u> the dashed (closed) paths shown are added to (1), (2), (3), (4), and (5).

In view of Equations (C-5) and (C-11) the function to be integrated is:

$$\bar{f}_x = \frac{\rho U f_x}{p_o} = -\frac{i}{\pi} e^{-i\alpha\frac{Z}{a}} \int_{+1\infty}^{\frac{Z}{a}} e^{i\alpha\frac{t}{a}} \left(\frac{1}{\frac{t}{a} - 1} - \frac{1}{\frac{t}{a} + 1} \right) d\left(\frac{t}{a}\right) \qquad (C\text{-}16)$$

The five integrals now become:

Path (1)

$$I_{(1)} = -\frac{i}{\pi} \int_{\infty}^{1} e^{-\alpha\eta} \left(\frac{1}{i\eta_1 - 1} - \frac{1}{i\eta + 1} \right) i\,d\eta$$

$$= -\frac{i}{\pi} \int_{1}^{\infty} e^{-\alpha\eta} \left(\frac{-i\eta - 1}{\eta^2 + 1} - \frac{-i\eta + 1}{\eta^2 + 1} \right) d\eta$$

$$= +\frac{2}{\pi} \int_{1}^{\infty} \frac{1}{\eta^2 + 1} e^{-\alpha\eta} \, d\eta$$

$$I_{(1)} = \frac{2}{\pi} \int_0^1 e^{-\frac{\alpha}{\eta}} \frac{d\eta}{\eta^2 + 1} \qquad \text{(C-17)}$$

Path (2)

$$I_{(2)} = -\frac{i}{\pi} \int_0^\beta e^{i\alpha(\epsilon + i)} \left(\frac{1}{\epsilon + i - 1} - \frac{1}{\epsilon + i + 1} \right) d\epsilon$$

$$= -\frac{i}{\pi} e^{-\alpha} \int_0^\beta (\cos\alpha\epsilon + i \sin\alpha\epsilon) \left(\frac{\epsilon - 1 - i}{(\epsilon - 1)^2 + 1} - \frac{\epsilon + 1 - i}{(\epsilon + 1)^2 + 1} \right) d\epsilon$$

$$= -\frac{i}{\pi} e^{-\alpha} \int_0^\beta (\cos\alpha\epsilon + i \sin\alpha\epsilon) \left[\frac{\epsilon - 1}{(\epsilon - 1)^2 + 1} - \frac{\epsilon + 1}{(\epsilon + 1)^2 + 1} \right.$$

$$\left. - i \left(\frac{1}{(\epsilon - 1)^2 + 1} - \frac{1}{(\epsilon + 1)^2 + 1} \right) \right] d\epsilon$$

$$I_{(2)} = \frac{e^{-\alpha}}{\pi} \left\{ \int_0^\beta \left[\left(\frac{\epsilon - 1}{(\epsilon-1)^2+1} - \frac{\epsilon + 1}{(\epsilon+1)^2+1} \right) \sin \alpha\epsilon - \left(\frac{1}{(\epsilon-1)^2+1} - \frac{1}{(\epsilon+1)^2+1} \right) \cdot \right. \right.$$

$$\left. \cdot \cos\alpha\epsilon \right] d\epsilon$$

$$\left. -i \int_0^\beta \left[\left(\frac{\epsilon - 1}{(\epsilon-1)^2+1} - \frac{\epsilon + 1}{(\epsilon+1)^2+1} \right) \cos\alpha\epsilon + \left(\frac{1}{(\epsilon-1)^2+1} - \frac{1}{(\epsilon+1)^2+1} \right) \sin\alpha\epsilon \right] d\epsilon \right\}$$

(C-18)

Path (3)

$$I_{(3)} = -\frac{i}{\pi} \int_1^0 e^{i\alpha(\beta+i\eta)} \left(\frac{1}{\beta+i\eta-1} - \frac{1}{\beta+i\eta+1} \right) i d\eta$$

$$= \frac{e^{i\alpha b}}{\pi} \int_0^1 e^{-\alpha\eta} \left(\frac{\beta-1-i\eta}{(\beta-1)^2+\eta^2} - \frac{\beta+1-i\eta}{(\beta+1)^2+\eta^2} \right) d\eta$$

$$I_{(3)} = -\frac{1}{\pi}\left\{\left[\cos\alpha B \int_0^1 \left(\frac{\beta-1}{\eta^2+(\beta-1)^2} - \frac{\beta+1}{\eta^2+(\beta+1)^2}\right) e^{-\alpha\eta}\right.\right.$$

$$\left. + \sin\alpha b \int_0^1 \left(\frac{\eta}{\eta^2+(\beta-1)^2} - \frac{\eta}{\eta^2+(\beta+1)^2}\right) e^{-\alpha\eta}\, d\eta\right]$$

$$+ i\left[\sin\alpha\beta \int_0^1 \left(\frac{\beta-1}{\eta^2+(\beta-1)^2} - \frac{\beta-1}{\eta^2+(\beta+1)^2}\right) e^{-\alpha\eta}\, d\right.$$

$$\left.\left. - \cos\alpha\beta \int_0^1 \left(\frac{\eta}{\eta^2+(\beta-1)^2} - \frac{\eta}{\eta^2+(\beta+1)^2}\right) e^{-\alpha\eta}\, d\eta\right]\right\} \qquad \text{(C-19)}$$

Path (4)

$$I_{(4)} = -\frac{i}{\pi} \int_0^{-\beta} e^{i\alpha(\epsilon+1)} \left(\frac{1}{\epsilon+1-1} - \frac{1}{\epsilon+1+1}\right) d\epsilon$$

$$= \frac{i}{\pi} e^{-\alpha} \int_0^{\beta} (\cos\alpha\epsilon - i\sin\alpha\epsilon) \left(\frac{\epsilon-1+i}{(\epsilon-1)^2+1} - \frac{\epsilon+1+i}{(\epsilon+1)^2+1}\right) d\epsilon$$

$$I_{(4)} = \frac{e^{-\alpha}}{\pi}\left\{\int_0^{\beta}\left[\left(\frac{\epsilon-1}{(\epsilon+1)^2+1}-\frac{\epsilon-1}{(\epsilon+1)^2+1}\right)\sin\alpha\epsilon-\left(\frac{1}{(\epsilon-1)^2+1}-\frac{1}{(\epsilon+1)^2+1}\right)\cos\alpha\epsilon\right]d\epsilon\right.$$

$$\left.+\,i\int_0^{\beta}\left[\left(\frac{\epsilon-1}{(\epsilon-1)^2+1}-\frac{\epsilon-1}{(\epsilon+1)^2+1}\right)\cos\alpha\epsilon+\left(\frac{1}{(\epsilon-1)^2+1}-\frac{1}{(\epsilon+1)^2+1}\right)\sin\alpha\epsilon\right]d\epsilon\right\}$$

(C-20)

Path (5)

$$I_{(5)} = -\frac{i}{\pi}\int_1^0 e^{i\alpha(-\beta+i\eta)}\left(\frac{1}{-\beta+i\eta-1}-\frac{1}{-\beta+i\eta+1}\right)i\,d\eta$$

$$= \frac{e^{-i\alpha\beta}}{\pi}\int_0^1 e^{-\alpha\eta}\left[\frac{-(\beta+1)-i\eta}{(\beta+1)^2+\eta^2}-\frac{-(\beta-1)-i\eta}{(\beta-1)^2+\eta^2}\right]d\eta$$

$$I_{(5)} = -\frac{1}{\pi}\left\{\left[\cos\alpha\beta \int_0^1 \left(\frac{\beta-1}{\eta^2+(\beta-1)^2} - \frac{\beta+1}{\eta^2+(\beta+1)^2}\right) e^{-\alpha\eta} d\eta \right.\right.$$

$$\left. + \sin\alpha\beta \int_0^1 \left(\frac{\eta}{\eta^2+(\beta-1)^2} - \frac{\eta}{\eta^2+(\beta+1)^2}\right) e^{-\eta}\, d\eta \right]$$

$$- i\left[\sin\alpha\beta \int_0^1 \left(\frac{\beta-1}{\eta^2+(\beta-1)^2} - \frac{\beta+1}{\eta^2+(\beta+1)^2}\right) e^{-\alpha\eta} d\eta \right.$$

$$\left.\left. - \cos\alpha\beta \int_0^1 \left(\frac{\eta}{\eta^2+(\beta-1)^2} - \frac{\eta}{\eta^2+(\beta+1)^2}\right) e^{-\alpha\eta} d\eta \right]\right\} \qquad \text{(C-21)}$$

In order to define the closed paths (dashed paths of Figure C-3) needed to supplement the five preceding integrals when integrating to one of the four regions of interest we will make use of Cauchy's Integral Formula.

Cauchy's Integral Formula states:

If f(Z) is regular in a region, then the formula

$$f(Z) = \frac{1}{2\pi i} \oint \frac{f(\zeta)}{\zeta - Z} \, d\zeta$$

is valid for every simple, closed, positively oriented path for every point Z in its interior.

or

$$\oint \frac{f(\zeta)}{\zeta - Z} \, d\zeta = 2\pi i f(Z) \qquad \text{(C-22)}$$

For example:

let $f(\zeta) = -e^{i\alpha t}$

$\zeta = t, \qquad d\zeta = dt$

$Z = -1$

therefore

$$\oint \frac{f(\zeta)}{\zeta - Z} \, d\zeta = \oint \frac{-e^{i\alpha t}}{t + 1} \, dt$$

$$= -\frac{i}{\pi} \oint \frac{-e^{i\alpha t}}{t + 1} \, dt = -\frac{i}{\pi} (2\pi i) (-e^{-i\alpha})$$

$$= -2e^{-i\alpha} = -2 (\cos\alpha - i \sin\alpha)$$

where $-\frac{i}{\pi}$ is an arbitrary multiplier.

In Equations (C-17) through (C-21) let:

$$
\left.
\begin{aligned}
F_1 &= \frac{1}{\pi}\int_{\alpha}^{\beta}\left(\frac{\epsilon-1}{(\epsilon-1)^2+1}-\frac{\epsilon+1}{(\epsilon+1)^2+1}\right)\sin\alpha\epsilon\ d\epsilon \\
F_2 &= \frac{1}{\pi}\int_{\alpha}^{\beta}\left(\frac{\epsilon-1}{(\epsilon-1)^2+1}-\frac{\epsilon+1}{(\epsilon+1)^2+1}\right)\cos\alpha\epsilon\ d\epsilon \\
F_3 &= \frac{1}{\pi}\int_{0}^{\beta}\left(\frac{1}{(\epsilon-1)^2+1}-\frac{1}{(\epsilon+1)^2+1}\right)\sin\alpha\epsilon\ d\epsilon \\
F_4 &= \frac{1}{\pi}\int_{0}^{\beta}\left(\frac{1}{(\epsilon-1)^2+1}-\frac{1}{(\epsilon+1)^2+1}\right)\cos\alpha\epsilon\ d\epsilon \\
G_1 &= \frac{1}{\pi}\int_{0}^{1}\left(\frac{\beta-1}{\eta^2+(\beta-1)^2}-\frac{\beta+1}{\eta^2+(\beta+1)^2}\right)e^{-\alpha\eta}\ d\eta \\
G_3 &= \frac{1}{\pi}\int_{0}^{1}\left(\frac{\eta}{\eta^2+(\beta-1)^2}-\frac{\eta}{\eta^2+(\beta+1)^2}\right)e^{-\alpha\eta}\ d\eta
\end{aligned}
\right\} \qquad \text{(C-23)}
$$

Now with the five paths of integration, the integrals themselves and the closed paths defined we may define the function $\overline{\phi}_x$ for the four regions of interest.

For the region Z = -b, $\beta > 1$ (Figure C-3B)

$$\bar{\phi}_x = e^{-\alpha\beta}\Big[I_1 + (F_1 - F_4)\, e^{-\alpha} + i\,(F_2 + F_3)\, e^{-\alpha} - G_1 \cos\alpha\beta - G_3 \sin\alpha\beta + i\,(G_1 \sin\alpha\beta - G_3 \cos\alpha\beta)\Big]$$

if $e^{i\alpha\beta} = \cos\alpha\beta + i \sin\alpha\beta$

$$\bar{\phi}_x = I_1 \cos\alpha\beta + e^{-\alpha}(F_1 - F_4)\cos\alpha\beta - e^{-\alpha}(F_2 + F_3)\sin\alpha\beta - G_3 \cos\alpha\beta \sin\alpha\beta - G_1 \cos^2\alpha\beta + G_3 \cos\alpha\beta \sin\alpha\beta - G_1 \sin^2\alpha\beta$$

$$\bar{\phi}_x = I_1 \cos\alpha\beta - G_1 + (F_1 - F_4)\, e^{-\alpha}\cos\alpha\beta - (F_2 + F_3)\, e^{-\alpha} \sin\alpha\beta \qquad \text{(C-24)}$$

For the region Z = -b, $\beta < 1$ (Figure C-3A)

Equation (C-24) will apply for this region provided the following term from Cauchy's integral is added:

$$-2e^{i\alpha\beta}\, e^{-i} = -2e^{-i\alpha(1-\beta)}$$

$$= -2\left[\cos\alpha\,(1-\beta) - i\sin\alpha\,(1-\beta)\right]$$

$$= -2\cos\alpha\,(1-\beta)$$

$$= -2\cos\alpha\cos\alpha\beta - 2\sin\alpha\sin\alpha\beta$$

$$\bar{\phi}_x = I_1\cos\alpha\beta - G_1 + (F_1 - F_4)\,e^{-\alpha}\cos\alpha\beta - (F_2 + F_3)\,e^{-\alpha}\sin\alpha\beta$$

$$- 2\cos\alpha\cos\alpha\beta - 2\sin\alpha\sin\alpha\beta \qquad \text{(C-25)}$$

<u>For the region Z = +b, $\beta < 1$ (Figure C-3C)</u>

$$\bar{\phi}_x = e^{-\alpha\beta}\Big[I_1 + (F_1 - F_4)e^{-\alpha} - i(F_2 + F_3)e^{-\alpha}$$

$$- G_1\cos\alpha\beta - G_3\sin\alpha\beta - i\,(G_1\sin\alpha\beta - G_3\cos\alpha\beta)\Big]$$

if $e^{-\alpha\beta} = \cos\alpha\beta - i\sin\alpha\beta$

$$\phi_x = I_1\cos\alpha\beta + (F_1 - F_4)e^{-\alpha}\cos\alpha\beta - (F_2 + F_3)e^{-\alpha}\sin\alpha\beta$$

$$- G_1\cos^2\alpha\beta - G_3\cos\alpha\beta\sin\alpha\beta$$

$$- G_1\sin^2\alpha\beta + G_3\cos\alpha\beta\sin\alpha\beta$$

$$\phi_x = I_1 \cos\alpha\beta - G_1 + (F_1 - F_4)e^{-\alpha} \cos\alpha\beta - (F_2 + F_3)e^{-\alpha} \sin\alpha\beta$$

The additive term due to Cauchy's integral

$$- 2e^{-\alpha\beta} e^{-i\alpha} = - 2e^{-i\alpha(1+\beta)} = - 2 \cos\alpha (1+\beta)$$

$$- i\, 2 \sin\alpha (1+\beta)$$

Therefore,

$$\bar{\phi}_x = I_1 \cos\alpha\beta - G_1 + (F_1 - F_4)e^{-\alpha} \cos\alpha\beta - (F_2 + F_3)e^{-\alpha} \sin\alpha\beta$$

$$- 2 \cos\alpha \cos\alpha\beta + 2 \sin\alpha \sin\alpha\beta \qquad \text{(C-26)}$$

For the region Z = +b, $\beta > 1$ (Figure C-3D)

The same open path as the previous region will apply here if the following closed path is added:

$$(- 2e^{-1\alpha\beta} e^{-i\alpha}) + (2e^{-i\alpha\beta} e^{i\alpha}) = + 4 \sin\alpha \sin\alpha\beta$$

Therefore,

$$\bar{\phi}_x = I_1 \cos\alpha\beta - G_1 + (F_1 - F_4)e^{-\alpha} \cos\alpha\beta - (F_2 + F_3)e^{-\alpha} \sin\alpha\beta$$

$$+ 4 \sin\alpha \sin\alpha\beta \qquad \text{(C-27)}$$

As stated previously, the integral given in Equation C-11 and hence the integrals occurring in Equations (C-24) thru (C-27) will not yield an elementary function but rather an infinite power series upon successive integration by parts.

In order to numerically integrate the functions of interest, Simpson's Rule was applied to the integrals and a digital computer program developed to evaluate the functions.

It is obvious that the expressions derived in the foregoing section are far too complex to be of any use other than as a comparison for the approximate formulation in the following section. Therefore, for purposes of comparison, several wave shapes were determined utilizing the above formulation and the Digital Computer. These surface shapes are shown graphically in Figure (C-4).

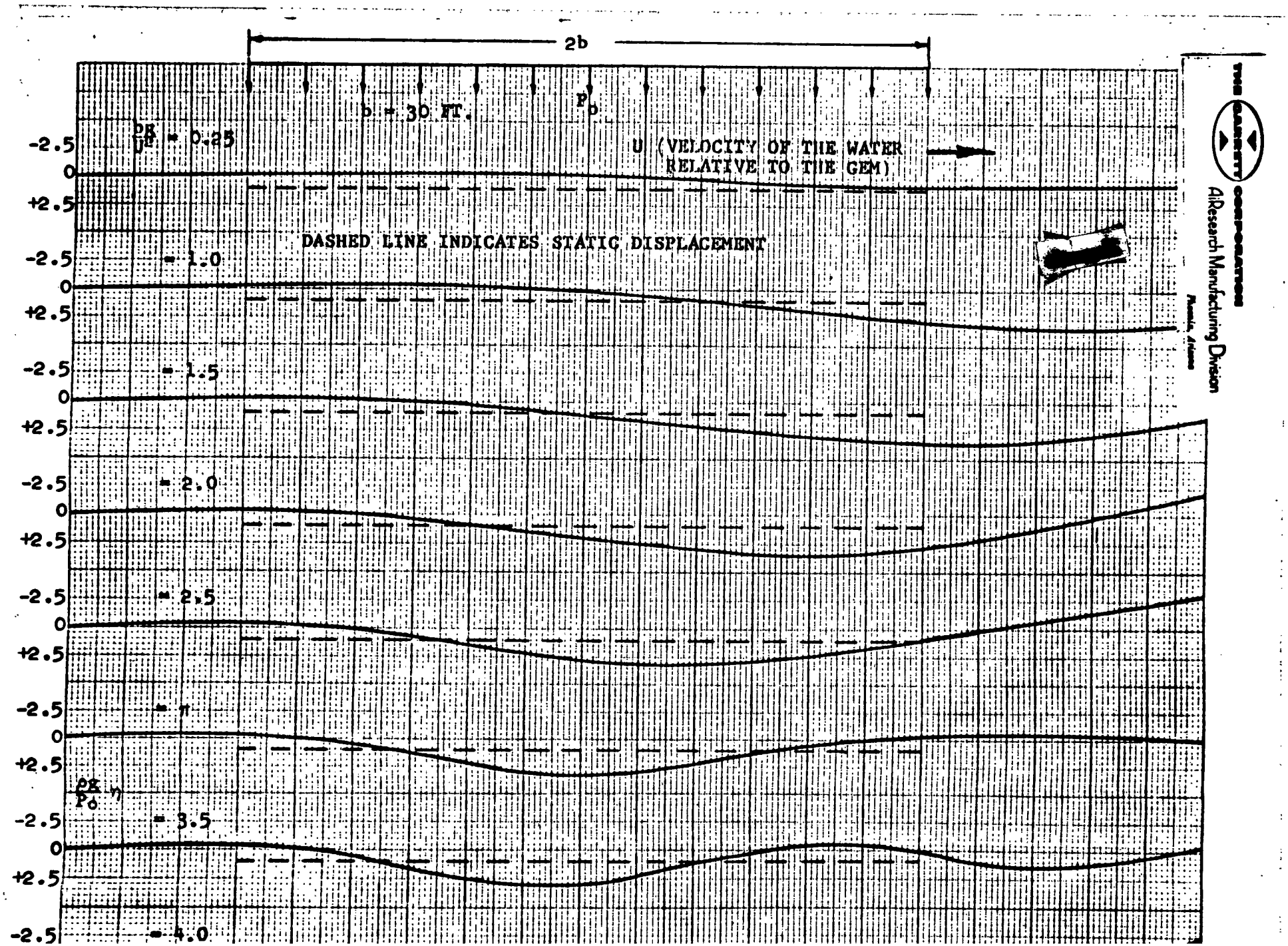
2b
b = 30 FT.
P_b
$\frac{\rho k}{\mu^2}$ = 0.25
U (VELOCITY OF THE WATER RELATIVE TO THE GEM)
DASHED LINE INDICATES STATIC DISPLACEMENT
= 1.0
= 1.5
= 2.0
= 2.5
= π
= 3.5
= 4.0
$\frac{\rho k}{P_0}\eta$
-2.5
0
+2.5
THE GARRETT CORPORATION
AiResearch Manufacturing Division
Phoenix, Arizona

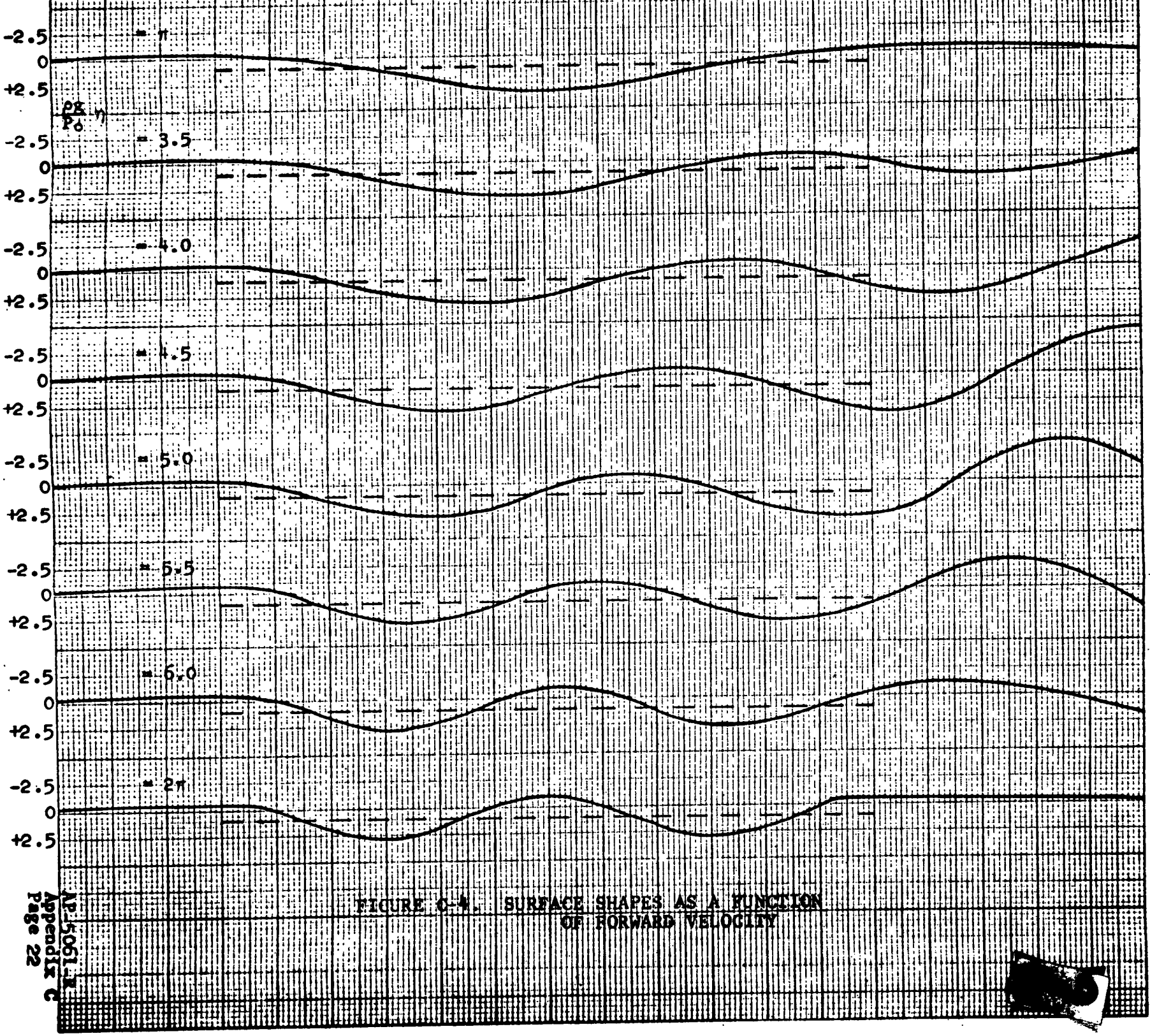

FIGURE C-4. SURFACE SHAPES AS A FUNCTION OF FORWARD VELOCITY

1.1 Simplification of Wave Shape

To obtain a more convenient expression for the wave shape, the following equation was developed which is seen to very closely approximate the shapes shown in Figure C-4.

$$Z_W = \frac{P_o}{\rho g}\left[1 + \epsilon - 2\cos\alpha\ (1 - \frac{x}{b})\right] \qquad (C\text{-}28)$$

where

$$\alpha = \frac{bg}{U^2}$$

ϵ here is a function of α (see Equation C-50)

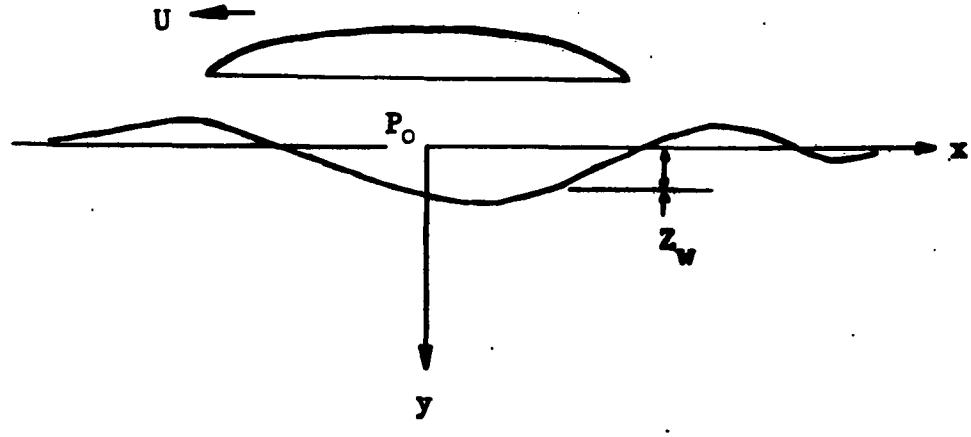

FIGURE C-5

Equation (C-28) represents a traveling wave of fixed shape moving with the craft. Note the change in coordinates in Figure C-5.

The average vertical displacement of the surface is obtained by integrating Equation (C-28) from x = -b to x = b and dividing by 2b.

$$z_o = \frac{P_o}{\rho g} \frac{1}{2b} \int_{-b}^{b} 1 + \epsilon - 2\cos\alpha \left(1 - \frac{x}{b}\right) dx$$

$$= \frac{P_o}{\rho g} \frac{(1 + \epsilon)\, 2b + 2\frac{b}{\alpha} \sin\alpha \left(1 - \frac{x}{b}\right)}{2b} \Bigg|_{-b}^{+b}$$

$$z_o = \frac{P_o}{\rho g} \left(1 + \epsilon - \frac{\sin 2\alpha}{\alpha}\right) \qquad \text{(C-29)}$$

The general slope of the water surface will be obtained by finding the slope of the best straight line approximation to Equation (C-28). This is done by making the integral of the square of the difference a minimum.

Let

$$Z_1(x) = A + Bx \quad \frac{P_o}{\rho g} \tag{C-30}$$

$$I = \int_{-b}^{+b} (Z_1 - Z_w)^2 \, dx \tag{C-31}$$

The best values of A and B will be obtained if:

$$\frac{\partial I}{\partial B} = \frac{\partial I}{\partial A} = 0$$

$$\frac{\partial I}{\partial A} = \int_{-b}^{+b} 2 (Z_1 - Z_w) \, dx = 0 \tag{C-32}$$

$$\frac{\partial I}{\partial B} = \int_{-b}^{+b} 2 (Z_1 - Z_w) \, x \, dx = 0 \tag{C-33}$$

With Equations (C-28) and (C-30), Equations (C-32) and (C-33) yield:

$$\frac{\partial I}{\partial A} = \int_{-b}^{+b} \left[(A - 1 - \epsilon) + Bx + 2 \cos\alpha \left(1 - \frac{x}{b}\right) \right] dx = 0 \tag{C-34}$$

$$\frac{\partial I}{\partial B} = \int_{-b}^{+b} \left[(A - 1 - \epsilon)x + bx^2 + 2x \cos\alpha \left(1 - \frac{x}{b}\right) \right] dx = 0 \quad \text{(C-35)}$$

$$\int_{b}^{b} dx = b - (-b) = 2b \quad \text{(C-36)}$$

$$\int_{-b}^{b} x\, dx = \frac{1}{2}(b^2 - b^2) = 0 \quad \text{(C-37)}$$

$$\int_{-b}^{b} x^2\, dx = \frac{1}{3}\, b^3 - (-b)^3 = \frac{2}{3} b^3 \quad \text{(C-38)}$$

$$\int_{-b}^{b} \cos\alpha \left(1 - \frac{x}{b}\right) dx = + \frac{b}{\alpha} \sin 2\alpha \quad \text{(C-39)}$$

$$\int_{-b}^{b} x \cos\alpha \left(1 - \frac{x}{b}\right) dx = \frac{b^2}{\alpha^2} (1 - \cos 2\alpha - 2 \sin 2\alpha) \quad \text{(C-40)}$$

Using Equations (C-36) through (C-40), Equations (C-34) and (C-35) become:

$$2b (A - 1 - \epsilon) - 2 \frac{b}{\alpha} \sin 2\alpha = 0$$

or

$$A = 1 + \epsilon - \frac{\sin 2\alpha}{\alpha} \quad \text{(C-41)}$$

and $\frac{2}{3} b^3 B + 2 \frac{b^2}{\alpha^2} (1 - \cos 2\alpha - \alpha \sin 2\alpha) = 0$

or

$$B = - \frac{3}{b\alpha^2} (1 - \cos 2\alpha - \alpha \sin 2\alpha)$$

$$B = - \frac{6}{b} \frac{\sin\alpha}{\alpha} \left(\frac{\sin\alpha}{\alpha} - \cos\alpha\right) \qquad \text{(C-42)}$$

To obtain the maximum slope Equation (C-42) is differentiated with respect to α and equated to zero.

This yields:

$$\cos\alpha = \frac{1}{3} \left[\frac{\alpha}{\sin\alpha} + 2 (1 - \alpha^2) \frac{\sin\alpha}{\alpha}\right] \qquad \text{(C-43)}$$

The lowest root of the above equation is:

$$\alpha = 1.753, \frac{\sin\alpha}{\alpha} = 0.561, \cos\alpha = -0.1812$$

The maximum value of B becomes

$$B_{max} = - \frac{6}{b} (0.561) (0.561 + 0.1812)$$

$$= - \frac{2.498}{b} \qquad \text{(C-44)}$$

Therefore, the maximum slope is:

$$\left(\frac{\partial Z_1}{\partial X}\right)_{max} = \frac{P_o}{\rho g} B_{max} = \frac{2.498\ P_o}{\rho g b} \qquad \text{(C-45)}$$

Numerical value of ϵ —

The parameter ϵ is a function of α and is obtained by making the approximate expression for water surface given in Equation (C-28) conform as closely as possible to the exact value given in Section 1.

Let the exact solution be defined as:

$$\eta = \frac{\rho g z}{P_o} \qquad \text{(C-46)}$$

and the approximate value be defined as in Equation (C-28)

$$\eta_1 + \epsilon \frac{\rho g\ zw}{P_o} = 1 - 2 \cos\ (1 - \frac{x}{b}) + \epsilon \qquad \text{(C-47)}$$

Define now the sum of the squares of the variation as:

$$= \sum_{i=1}^{n} (\eta_{1i} + \epsilon - \eta_i)^2 \qquad \text{(C-48)}$$

The i's represent N distinct, uniformly spaced points at which η_1 and η are evaluated. It is seen that making Σ a minimum provides the best possible value for ϵ. This is done by making the first derivating zero.

Expanding the square of Equation (C-48) yields:

$$= \sum_{i=1}^{n} (\eta_{\perp} - \eta_i)^2 + 2\epsilon (\eta_{\perp i} - \eta_i) + \epsilon^2$$

and

$$\frac{d\Sigma}{d\epsilon} = 2 \sum_{i=1}^{n} (\eta_{\perp i} - \eta_i) + 2\epsilon \sum_{i=1}^{n} 1 = 0 \qquad \text{(C-49)}$$

or

$$\epsilon = - \frac{\Sigma(\eta_{\perp i} - \eta)}{N} \qquad \text{(C-50)}$$

The values of ϵ for various values of α are determined using results of the exact solution from the Bendix Digital Computer. These values are shown graphically in Figure C-6.

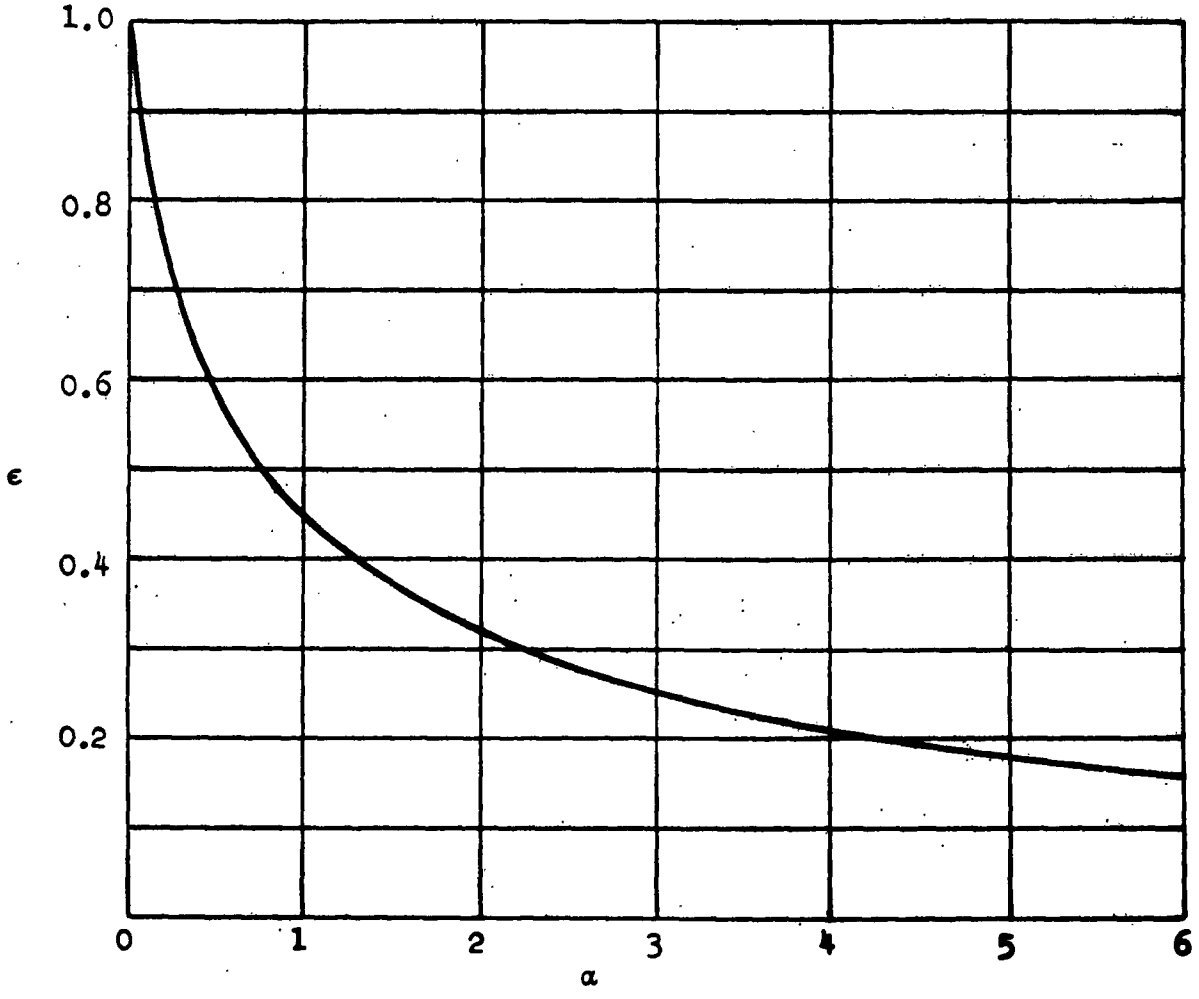

FIGURE C-6

ϵ VS. α

The mean displacement (A) and the mean slope of the water surface (B) in dimensionless equations now become:

$$A = 1 + \epsilon - 2\frac{\sin\alpha}{\alpha}\cos\alpha \qquad \text{(C-51)}$$

$$bB = 6\frac{\sin\alpha}{\alpha}\left(\frac{\sin\alpha}{\alpha} - \cos\alpha\right) \qquad \text{(C-52)}$$

2.0 Effects of Relative Wind Upon Base Pressure

To further describe the effects of forward and side velocity (relative wind) upon vehicle characteristics, the induced pressure around the vehicle due to relative wind will be investigated.

2.1 If, in Equation (1) (AP-5047-R), an ambient pressure P_{ai} is included on the right side of the equation, the end result can be seen to be the redefining of the parameter B, such that

$$B = \frac{(P_i - P_{ai})}{\rho V_j^2}$$

From Equation (A-33), the following steady-state equation can be written for the peripheral jets, in general,

$$\pi_1 \bar{Q}_i = 2K_{KA} \left(1 - \frac{1}{2}\frac{G}{h}\sin\theta\right) \bar{P}_i - \frac{A_B}{W_C}(P_o - P_{ai}) \qquad (C\text{-}53)$$

Also for compartment jets from Equation (A-37)

$$\frac{C_{ik}}{C_i}\pi_2 \bar{Q}_{ik} = K_{1ik} - K_{pik}(\bar{P}_i - \bar{P}_{ik}) \qquad (C\text{-}54)$$

In the above equations, note that

$$\bar{P}_i = \frac{P_i A_B}{W_c}$$

$$K_{1ik} = \frac{1}{2}\pi_2 \frac{C_{ik}}{C_i}$$

$$K_{pik} = F_1 \frac{C_{ik}}{C_i}$$

In the steady state

$$\bar{Q}_1 = \frac{C_{12}}{C_1} \pi_2 \bar{Q}_{12} + \frac{C_{14}}{C_1} \pi_2 \bar{Q}_{14}$$

$$\bar{Q}_2 = \frac{C_{12}}{C_1} \pi_2 \bar{Q}_{21} + \frac{C_{14}}{C_1} \pi_2 \bar{Q}_{23}$$

$$\bar{Q}_3 = \frac{C_{14}}{C_1} \pi_2 \bar{Q}_{32} + \frac{C_{12}}{C_1} \pi_2 \bar{Q}_{34} \qquad \text{(C-55)}$$

$$\bar{Q}_4 = \frac{C_{14}}{C_1} \pi_2 \bar{Q}_{41} + \frac{C_{12}}{C_1} \pi_2 \bar{Q}_{43}$$

If Equations (C-55) are expanded using Equations (C-53) and (C-54), they will yield a steady-state equation for each base sector. Assuming continuity (the net flow out of a sector is zero) when the P_{ai}'s are zero and also a $\bar{\Delta}_i$ increase on each pressure when P_{ai}'s are not zero yields the following set of equations:

$$\text{Let } \bar{F}_1 = \frac{F_1}{2K_{KA}\left(1 - \frac{1}{2}\frac{G}{h}\sin\theta\right)}$$

$$\bar{P}_{ai} = \frac{A_B P_{ai}}{W_c}$$

$$(1 + \bar{F}_1)\bar{\Delta}_1 - \bar{F}_1 \frac{C_{12}}{C_1}\bar{\Delta}_2 - \bar{F}_1 \frac{C_{14}}{C_1}\bar{\Delta}_4 = \bar{P}_{a1}$$

$$(1 + \bar{F}_1)\bar{\Delta}_2 - \bar{F}_1 \frac{C_{12}}{C_1}\bar{\Delta}_1 - \bar{F}_1 \frac{C_{14}}{C_1}\bar{\Delta}_3 = \bar{P}_{a2}$$

$$(1 + \bar{F}_1)\bar{\Delta}_3 - \bar{F}_1 \frac{C_{14}}{C_1}\bar{\Delta}_2 - \bar{F}_1 \frac{C_{12}}{C_1}\bar{\Delta}_4 = \bar{P}_{a3} \qquad \text{(C-56)}$$

$$(1 + \bar{F}_1)\bar{\Delta}_4 - \bar{F}_1 \frac{C_{14}}{C_1}\bar{\Delta}_1 - \bar{F}_1 \frac{C_{12}}{C_1}\bar{\Delta}_3 = \bar{P}_{a4}$$

Letting $$A = \frac{\bar{F}_1 C_{14}}{C_1(1 + \bar{F}_1)}$$

$$B = \frac{\bar{F}_1 C_{12}}{C_1(1 + \bar{F}_1)}$$

The solution of Δ_i written in matrix form is:

$$\begin{bmatrix}\Delta_1\\ \Delta_2\\ \Delta_3\\ \Delta_4\end{bmatrix} = \frac{\begin{bmatrix} (1-A^2-B^2) & B(1+A^2-B^2) & 2AB & A(1+B^2-A^2) \\ B(1+A^2-B^2) & (1-A^2-B^2) & A(1+B^2-A^2) & 2AB \\ 2AB & A(1+B^2-A^2) & (1-A^2-B^2) & B(1+A^2-B^2) \\ A(1+B^2-A^2) & 2AB & B(1+A^2-B^2) & (1-A^2-B^2) \end{bmatrix} \begin{bmatrix} \bar{P}_{a_1}/(1+\bar{F}_1) \\ \bar{P}_{a_2}/(1+\bar{F}_1) \\ \bar{P}_{a_3}/(1+\bar{F}_1) \\ \bar{P}_{a_4}/(1+\bar{F}_1) \end{bmatrix}}{[D]} \qquad \text{(C-57)}$$

where $[D]$ = determinant of coefficients.

Assuming that Δ_i acts at the center of the sector $\frac{C_{14}}{2}, \frac{C_{12}}{2}$ the equations for pitching and rolling moments are seen to be

$$\Delta M_g = \frac{W_c C_{14}}{8} (-\bar{\Delta}_1 + \bar{\Delta}_2 + \bar{\Delta}_3 - \bar{\Delta}_4)$$

$$= \frac{W_c}{8} \frac{C_{14}}{(1 + 2\bar{F}_1 \frac{C_{12}}{C_1})} \left[-\bar{P}_{a_1} + \bar{P}_{a_2} + \bar{P}_{a_3} - \bar{P}_{a_4}\right] \qquad \text{(C-58)}$$

and $\Delta M_x = \frac{W_c C_{12}}{8} (\bar{\Delta}_1 + \bar{\Delta}_2 - \bar{\Delta}_3 - \bar{\Delta}_4)$

$$= \frac{W_c}{8} \frac{C_{12}}{(1 + 2\bar{F}_\perp \frac{C_{14}}{C_1})} \left[\bar{P}_{a_1} + \bar{P}_{a_2} - \bar{P}_{a_3} - \bar{P}_{a_4}\right] \quad \text{(C-59)}$$

2.2 Assumed Ambient Variations Due to Forward Velocity

The assumed induced pressure coefficients are as follows:

Due to forward velocity ($+ U_x$)

front	$+ 0.35\ q_x$
sides	$- 0.23\ q_x$
rear	$- 0.23\ q_x$

(C-60)

Due to side velocity ($+ U_y$)

front	$- 0.23\ q_y$
rear	$- 0.23\ q_y$
port side	$- 0.23\ q_y$
starboard side	$+ 0.5\ q_y$

(C-61)

where $q_x = \frac{1}{2} \rho U_x^2$

$q_y = \frac{1}{2} \rho V_y^2$

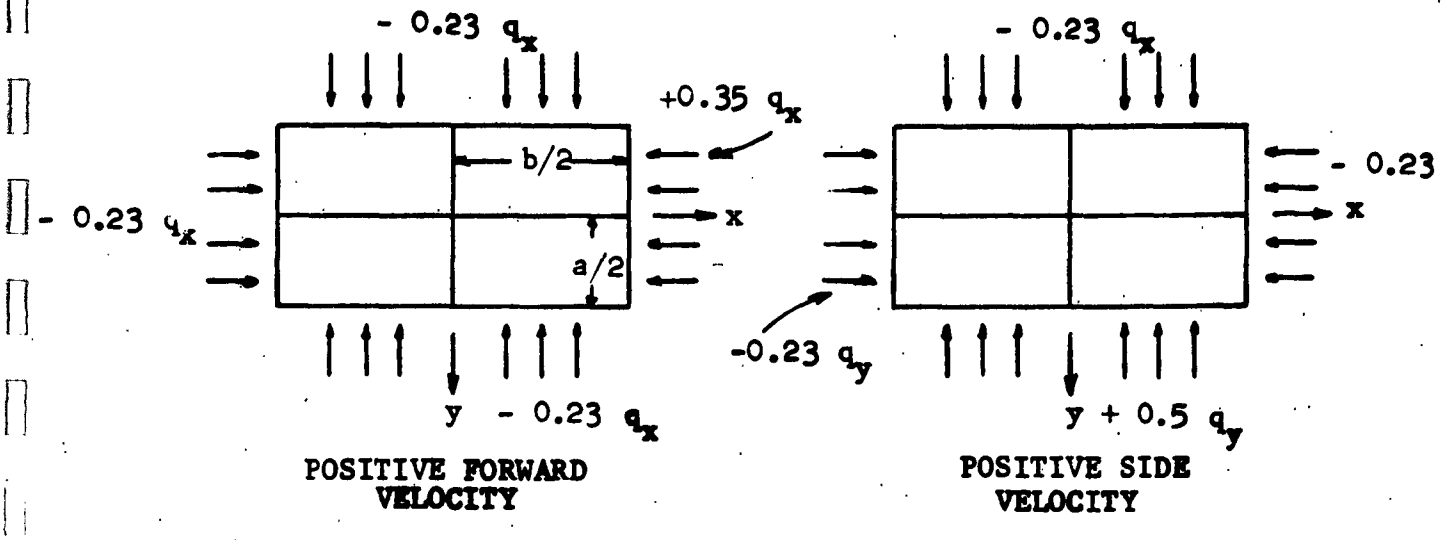

FIGURE C-7

INDUCED PRESSURE COEFFICIENTS

In pitch:

$$P_{a_1} = P_{a_4} = 0.23\, q_x$$

$$P_{a_2} = P_{a_3} = \frac{0.35\,\frac{a}{2} - 0.23\,\frac{b}{2}}{\frac{a+b}{2}}\, q_x = \frac{0.35a - 0.23b}{a+b}\, q_x$$

Equation (C-58) then becomes

$$\Delta M_y = \frac{A_B}{8} \frac{C_{l_4}}{\left(1 + 2\bar{F}_1 \frac{C_{l_2}}{C_1}\right)} \left[+ 2(0.23)\, q_x + 2 \left(\frac{0.35a - 0.23b}{a+b}\right) q_x \right]$$

recalling that $\bar{P}_1 = \frac{A_B}{W_C} P_1$

$$\Delta M_y = \frac{A_B}{4} \frac{0.29\ ab}{(1 + \frac{2a}{a+b} \bar{F}_1)(a + b)} q_x \qquad (C\text{-}62)$$

In roll:

$$P_{a_1} = P_{a_2} = - 0.23\ q_y$$

$$P_{a_3} = P_{a_4} = \frac{0.5b - 0.23a}{a + b} q_y$$

Equation (C-59) becomes:

$$\Delta M_x = \frac{A_B}{8} \frac{C_{12}}{(1 + 2\bar{F}_1 \frac{C_{14}}{C_1})} \left[- 2(0.23)\ q_y - \frac{2(0.5b - 0.23a)}{a + b} q_y \right]$$

$$\Delta M_x = \frac{A_B}{4} \frac{0.365\ ab}{(1 + \frac{2b}{a+b} \bar{F}_1)(a + b)} q_y \qquad (C\text{-}63)$$

3.0 Effect of Water Dynamics Upon Body Motion

As a vehicle pitches, rolls, or heaves there are restoring moments and forces generated. It is assumed that in the pitching mode this restoring moment is given by the following: (See Figure C-8)

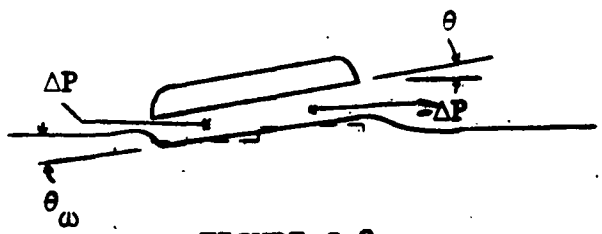

FIGURE C-8

$$M_y = - \Delta P \frac{A_B}{2} \left(\frac{b}{4}\right) - \Delta P \frac{A_B}{2} \left(\frac{b}{4}\right)$$

$$= - \frac{1}{4} \Delta P A_B b \qquad (C\text{-}64)$$

Denote this restoring moment as $K_\theta \theta$, then

$$- K_\theta \theta = - \frac{1}{4} \Delta P A_B b \qquad (C\text{-}65)$$

θ above is measured from a horizontal surface. If the vehicle is over water this angle will not be simply θ but:

$$\Delta\theta = \theta - \theta_w$$

Where $\theta_w = \frac{4\Delta P}{b\rho_w}$

Equation (C-65) becomes:

$$- K_\theta \left(\theta - \frac{4\Delta P}{b\rho_w} \right) = -\frac{1}{4} \Delta P A_B b$$

or $$\frac{1}{4} A_B b \Delta P = \frac{K_\theta \theta}{1 + \frac{16 K_\theta}{\rho_w A_B b^2}} \qquad \text{(C-66)}$$

In elementary terms the equation of motion in pitch may be written:

$$\Sigma M_y = -\frac{1}{4} \Delta P A_B b + M_y' = I_y \ddot{\theta} \qquad \text{(C-67)}$$

where M_y' are external moments

and substituting Equation (C-66) into Equation (C-67) yields:

$$\ddot{\theta} + \frac{K_\theta \theta}{I_y \left(1 + \frac{16 K_\theta}{\rho_w A_B b^2} \right)} = \frac{M_y'}{I_y}$$

or

$$\ddot{\theta} + \frac{K_\theta}{I_y}\left(1 - \frac{\frac{16\,K_\theta}{\rho_w A_B b^2}}{1 + \frac{16\,K_\theta}{\rho_w A_B b^2}}\right) = \frac{M_y'}{I_y}$$

or

$$\ddot{\theta} + \omega_\theta^2\left(1 - \frac{\frac{16\,\omega_\theta^2 I_y}{\rho_w A_B b^2}}{1 + \frac{16\,\omega_\theta^2 I_y}{\rho_w A_B b^2}}\right) = \frac{M_y'}{I_y} \qquad \text{(C-67)}$$

A similar approach will yield the equivalent terms in roll and heave motions.

Defining the modifying terms as $\bar{K}_\theta$, $\bar{K}_\phi$, and $\bar{K}_z$ we have:

$$\bar{K}_\theta = \frac{\omega_\theta^2 \frac{16\,I_y}{\rho_w A_B b^2}\left(1 + \epsilon - \frac{2\sin\alpha}{\alpha}\cos\alpha\right)}{1 + \omega_\theta^2 \frac{16\,I_y}{\rho_w A_B b^2}} \qquad \text{(C-68)}$$

$$\bar{K}_\phi = \frac{\omega_\phi^2 \frac{16\,I_x}{\rho_w A_B a^2}\left(1 + \epsilon - \frac{2\sin\alpha}{\alpha}\cos\alpha\right)}{1 + \omega_\phi^2 \frac{16\,I_x}{\rho_w A_B b^2}} \qquad \text{(C-69)}$$

$$K_z = \frac{\omega_z^2 \frac{W_c}{\rho_w A_B}\left(1 + \epsilon - \frac{2 \sin\alpha}{\alpha}\cos\alpha\right)}{1 + \omega_z^2 \frac{W_c}{\rho_w A_B}} \qquad \text{(C-70)}$$

Note that to make the terms a function of forward velocity (to die out at high speed) the term $\left(1 + \epsilon - \frac{2 \sin\alpha}{\alpha}\cos\alpha\right)$ is added to the above terms.

This takes into account the time response of the water surface. At high speed the GEM base is above a given point on the water for such a short time that the surface may deflect only a small amount (compared with its static deflection) before the GEM has passed by.

FORM 2787A-1

THE GARRETT CORPORATION
AiResearch Manufacturing Division
Phoenix, Arizona

APPENDIX D

ANALOG COMPUTER DIAGRAM

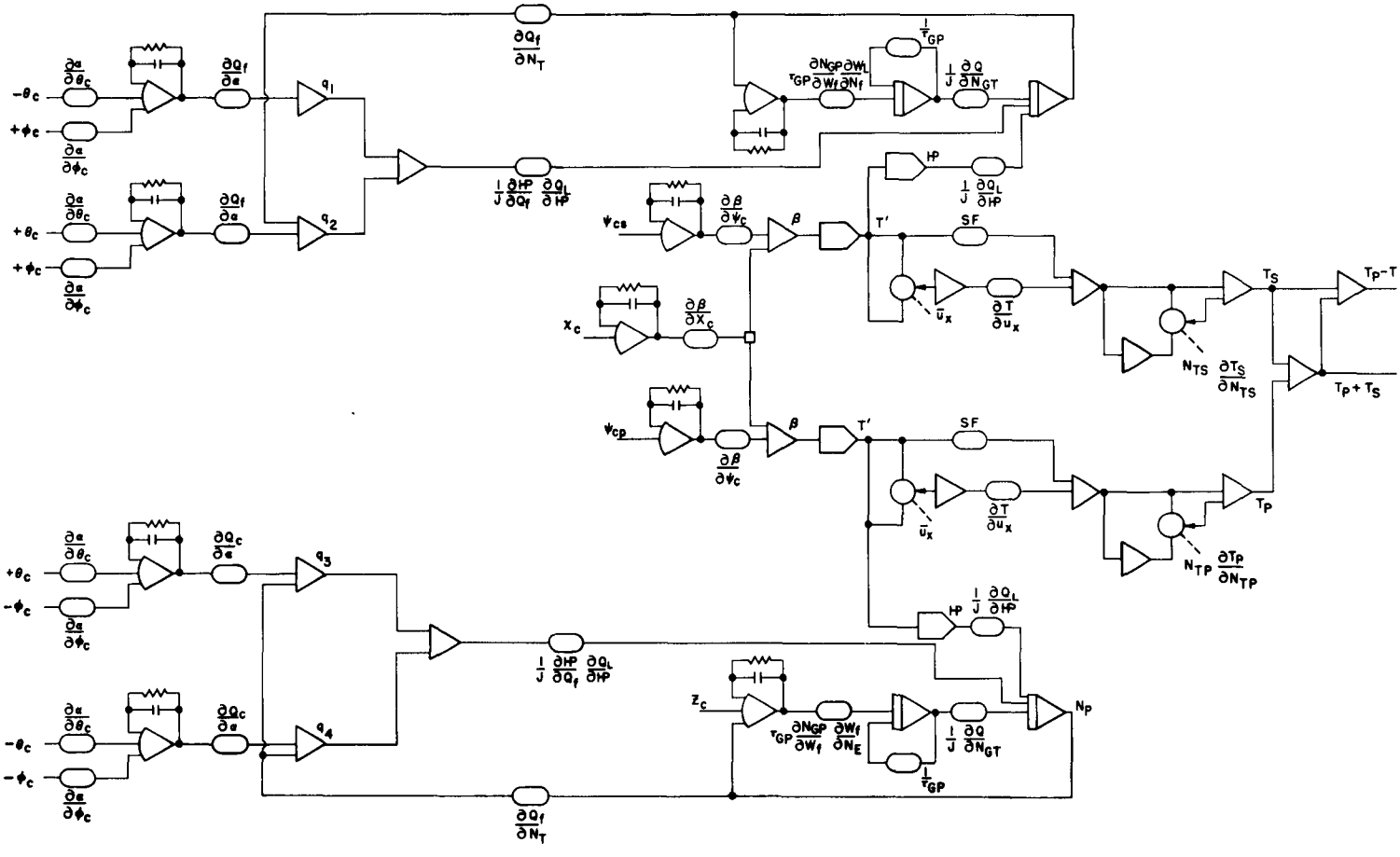
$-\theta_c$
$+\phi_c$
$+\theta_c$
$+\phi_c$
$+\theta_c$
$-\phi_c$
$-\theta_c$
$-\phi_c$
$\frac{\partial Q_f}{\partial N_T}$
q_1
q_2
q_3
q_4
$\frac{1}{J}\frac{\partial HP}{\partial Q_f}\frac{\partial Q_L}{\partial HP}$
$\frac{1}{\tau_{GP}}$
$\frac{\partial N_{GP}}{\partial W_f}\frac{\partial W_f}{\partial N_f}$
$\frac{1}{J}\frac{\partial Q}{\partial N_{GT}}$
HP
$\frac{1}{J}\frac{\partial Q_L}{\partial HP}$
ψ_{cs}
$\frac{\partial \beta}{\partial \psi_c}$
β
T'
SF
X_c
$\frac{\partial \beta}{\partial X_c}$
$\bar{u}_x$
$\frac{\partial T}{\partial u_x}$
T_S
$T_P - T$
$N_{TS}\frac{\partial T_S}{\partial N_{TS}}$
$T_P + T_S$
ψ_{cp}
T_P
$N_{TP}\frac{\partial T_P}{\partial N_{TP}}$
Z_c
N_P
A
$A\cos\psi$
$A\sin\psi$
$-A\cos\psi$
$+A\cos\psi$
$+A\sin\psi$
$-A\cos\psi$
X
$-A\sin\psi$
$+A\sin\psi$
$-A\cos\psi$
$+A\cos\psi$
$\bar{u}_y$

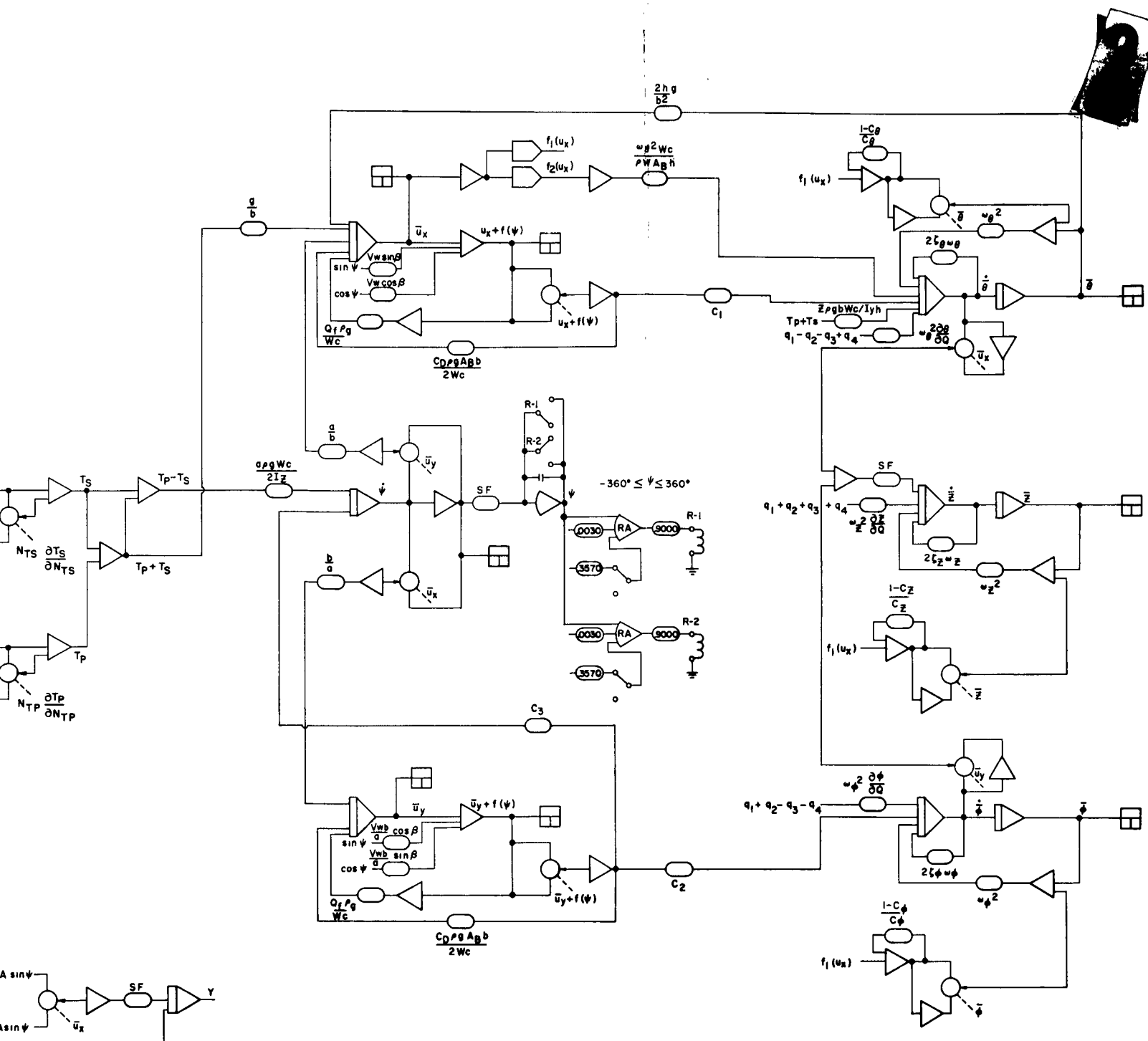

AP-5061-R
Appendix D
Page 1

THE GARRETT CORPORATION
AiResearch Manufacturing Division
Phoenix, Arizona

REFERENCES

1. Andersen, B. W. and Boyle, R. V., "Progress Report of Contract NONR 3173 GEM Control Systems Study." AiResearch Report AP-5047-R; April 6, 1962.

2. Thomson, W. T., "Introduction to Space Dynamics"; John Wiley and Sons, New York; 1961.

3. Stoker, J. J., "Water Waves." Interscience Publishers, New York; 1957.

4. Becker, O. A., Norgren, W. and Senoo, Y., "Technical Proposal To Investigate GEM Duct-Jet Systems." AiResearch Report AP-5059-R; September 17, 1962.